



Multiscale study of stone decay by salt crystallization in porous networks

Matthieu Angeli

► To cite this version:

Matthieu Angeli. Multiscale study of stone decay by salt crystallization in porous networks. Applied geology. Université de Cergy Pontoise, 2007. English. <tel-00239456>

HAL Id: tel-00239456

<https://tel.archives-ouvertes.fr/tel-00239456>

Submitted on 5 Feb 2008

HAL is a multi-disciplinary open access archive for the deposit and dissemination of scientific research documents, whether they are published or not. The documents may come from teaching and research institutions in France or abroad, or from public or private research centers.

L'archive ouverte pluridisciplinaire **HAL**, est destinée au dépôt et à la diffusion de documents scientifiques de niveau recherche, publiés ou non, émanant des établissements d'enseignement et de recherche français ou étrangers, des laboratoires publics ou privés.



ECOLE DOCTORALE SCIENCES ET INGENIERIE
de l'université de Cergy-Pontoise

THESE

Présentée pour obtenir le grade de docteur d'université
Spécialité : Géologie - Sciences de la Terre

Multiscale study of stone decay by salt crystallization in porous networks

Etude multiéchelle de la dégradation des roches par la cristallisation de sels
dans les réseaux poreux

Matthieu Angeli

*Université de Cergy-Pontoise
Département des Sciences de la Terre et Environnement
Laboratoire de tectonique UMR 7072*

Soutenue le 16 novembre 2007

Devant le jury composé de :

Pr. François Renard (Université Joseph Fourier, Grenoble)
Pr. Carlos Rodriguez-Navarro (Universidad de Granada)
Pr. Christian David (Université de Cergy-Pontoise)
Dr. Beatriz Menéndez (Université de Cergy-Pontoise)
Dr. Jean-Philippe Bigas (Chryso, Sermaises)
Pr. Albert Noumowe (Université de Cergy-Pontoise)
Dr. Jean-Didier Mertz (LRMH, Champs sur Marne)
Dr. Michael Steiger (Universität Hamburg)

Rapporteur
Rapporteur
Directeur de thèse
Co-directeur de thèse
Co-directeur de thèse
Président du jury
Examinateur
Examinateur

ACKNOWLEDGEMENTS

First I would like to thank my PhD directors, Christian David, Beatriz Menéndez and Jean-Philippe Bigas, who helped me during the three years and gave me the opportunity to choose the direction of my work. The beginning of the thesis was quite difficult and they helped me find a topic that would make me work during these three years.

I also would like to thank the other members of the laboratory who have worked with me during these years: Ronan Hébert mainly, Philippe Robion and also Laurent Louis during the final year. Their knowledge in the microstructure analysis of the stones greatly helped me to understand what the point of my work was.

During the beginning of my thesis, the visit of two laboratories allowed me to discover what was an experimental laboratory working on the weathering of the stone: the LISA in the University Créteil-Paris XII (Laboratoire Inter-universitaire des Systèmes Atmosphériques) and the LRMH in Champs-sur-Marne (Laboratoire de Recherche sur les Monuments Historiques). I would like to thank all the people that have welcomed me in these laboratories and kindly explained me what their research was about: Roger Lefèvre, Anne Chabas, Patrick Ausset and Tiziana Lombardo from the LISA, Jean-Didier Mertz from the LRMH.

During these three years I have met many people working in the field of stone weathering. I had very interesting discussions with some of these researchers, discussions which helped me to take a step backwards and see how my work could fit in the general research about stone weathering. I am very grateful for this to David Benavente from Alicante; Muzahim Al-Mukhtar, Kevin Beck and Thua Tri Van from the CRMD in Orléans (Centre de Recherche sur la Matière Divisée); and Michael Steiger from Hamburg.

I would like to thank Carlos Rodriguez-Navarro (University of Granada) and François Renard (University of Grenoble) for accepting to review my work, Albert Noumowe from the Civil Engineering department in the University of Cergy-Pontoise for accepting to be the president of the jury, and also again Jean-Didier Mertz and Michael Steiger for accepting to be in my jury.

I always had a lot of support from all the people from my laboratory, during good and bad times. The general atmosphere was very friendly and favourable to a good work. For this I would like to thank: Siegfried, Bertrand, Jean-Marc, Jean-Christian, Béatrice, Charly, Danielle, Pascale, Paul-Emile and Dominique.

This thesis would not have been the same without the support of other PhD students or former PhD students, especially during the hard time of the final redaction: Yves, Nicolas and Fabien in Cergy, and also Matteo and Virginie during the first year; William, Cédric, Thomas and Pipo (les professeurs); Martin, Elo, Béné, Laetitia, Ben, Louise, Kristell, Agnès and many others in Paris.

And finally, I would like to thank my parents, my sister and especially Alex.

<i>General introduction on salt decay</i>	3
---	---

<i>Outline of thesis</i>	4
--------------------------	---

<i>Chapter I: Decay of natural stones</i>	7
---	---

1. Weathering agents	9
-----------------------------	---

1.1.Salt decay	9
-----------------------	---

1.1.1.Efflorescences	10
----------------------	----

1.1.2.Contour scaling	10
-----------------------	----

1.1.3.Granular disintegration	11
-------------------------------	----

1.1.4.Honeycomb weathering (also called alvéolisation)	11
--	----

1.2.Freeze and thaw	11
----------------------------	----

1.3.Thermal shock	13
--------------------------	----

1.4.Water streaming	13
----------------------------	----

1.5.Atmospheric pollution	14
----------------------------------	----

1.5.1.Soiling	14
---------------	----

1.5.2.Gypsum crusts	14
---------------------	----

1.5.3.Acid rains	15
------------------	----

1.6.Biological colonisation	15
------------------------------------	----

2. Influence of the stone characteristics on weathering	16
--	----

2.1.Mineral composition	16
--------------------------------	----

2.2.Hydrlic properties	17
-------------------------------	----

2.2.1.Fluid flow	17
------------------	----

2.2.2.Hydrlic dilation	17
------------------------	----

2.3.Strength contrast	18
------------------------------	----

2.4.Stone-stone and stone-mortar compatibility	19
---	----

3. Building characteristics	20
3.1.Location of stones	20
3.2.Sheltered zones	21
3.3.Mechanical load	22
4. Human causes	22
Chapter II: Materials and methods	25
1. Overview of the studied stones	27
1.1.Lutetian limestones	27
1.2.Pierre de Souppes	30
1.3.Fontainebleau sandstones	31
1.4.Chinese sandstone	32
1.5.Agra sandstones	32
2. Microstructural studies	33
2.1.Characterization of the studied stones	34
2.1.1.Optical microscopy	34
2.1.2.Porosity	40
2.1.3.Mercury porosimetry	41
2.1.4.Helium pyknometry	46
2.1.5.Discussion about porosity	47
2.1.6.Specific surface area	49
2.2.Geophysical properties	49
2.2.1.P-waves velocity	50
2.2.2.Magnetic Susceptibility	51
2.2.3.Analysis of results	53
3. Hydromechanical properties	55

3.1.Hydric tests	55
3.1.1.Water Absorption Capacity	55
3.1.2.Capillarity	56
3.1.3.Evaporation	57
3.2.Mechanical tests	60
4. Accelerated ageing by salt decay	60
Chapter III: Salt crystallization	63
1. Experimental results	65
2. Theories of salt damage	66
3. Sodium sulphate	68
3.1.Mechanism of damage	68
3.2.Thermal recording during experimental weathering of limestones: the role of imbibition on salt crystallization and rock decay (article1; Journal of crystal growth)	69
Chapter IV: Salt damage	97
1. Macroscopic experiments	99
1.1.Durability estimation	99
1.2.Crystallization of salts in pores: quantification and estimation of damage (article 2; Environmental geology)	100
1.3.Effects on mechanical strength	121
2. Microscale experiment:Modification of the porous network by salt crystallization of experimentally weathered sedimentary stones (article 3; Materials and structures)	122
Chapter V: Influence of environmental parameters	161
1.Influence of capillary properties and evaporation on salt weathering of sedimentary rocks (article 4 ; HWC 2006)	163

*2.Influence of temperature and salt content on the salt weathering of sedimentary rocks
(article 5; GSL special publication)* _____ 185

Conclusion _____ 207

Perspectives _____ 209

References _____ 215

General introduction on salt decay

GENERAL INTRODUCTION ON SALT DECAY

General introduction on salt decay

General introduction on salt decay

Crystallization of soluble salts in porous networks is a major source of decay for natural stones (Goudie and Viles 1997). It is known as a major cause of erosion that shapes the landscapes from polar valleys (Prebble 1967) to arid regions (Beaumont 1968) and coastal areas (Mottershead 1982). It is responsible for the development of many geomorphological features like honeycombs, tafoni or pedestal rocks (Rodriguez-Navarro and Doehne 1999). It has even been proposed as the cause of erosion on martian landscape (Malin 1974; Rodriguez-Navarro 1998). But its effect is not limited to natural environments: natural building stone used in recent or historical buildings also suffer heavily from salt decay (Goudie and Viles 1997; Winkler 1997; Rodriguez-Navarro and Doehne 1999; Ruiz-Agudo et al 2007). This phenomenon is known since antiquity: Herodotus (about 440BC, translation from 1972) has reported it in the Nile Valley in his book “The histories”: “salt exudes from the soil to such an extent it affects even the pyramids”. Although this problem has been seriously studied since the 19th century (Turner 1833), the mechanism at stake is yet only partially understood. A reason for this lack of knowledge could be that this mechanism comes into the field of several sciences: rock physics and mechanics, civil engineering, geochemistry and thermodynamics.

The importance of this topic comes from the fact that it has applications in various topics, from the conservation of historical monuments (the basis for this study) to the study of reservoir rocks, without forgetting geotechnics or CO₂ storage. The presence of cracks and salt crystals in the porous networks has a direct influence on the fluid flow in sedimentary stones, as well as on their mechanical strength. For instance a good understanding of the crystallization processes could help to improve oil recovery rate in reservoir rocks, or help finding stone treatments to prevent damage from crystallization of salts in cultural heritage.

The aim of this PhD is to understand the decay from a rock mechanics and rock physics point of view. Numerous theoretical studies have been led on the thermodynamics of salt crystallization under stress (Correns 1949; Wellman and Wilson 1965; Benavente et al. 1999, 2004a; Scherer 1999, 2004; Flatt 2002; Steiger 2005a,b). Nevertheless, there exist very few experimental attempts at confirming these theories. Sometimes, the theoretical results do not explain some facts that are observed on site or during accelerated ageing tests. For instance, the theory cannot explain why sometimes sodium sulphate is more destructive for

some tests, while for other tests other salts like magnesium sulphate or sodium carbonate are the more destructive (Goudie and Viles 1997, chapter 4). It is also generally admitted that damage is more important when there are more salts in the sample (Correns 1949), and this is also contradictory to some of the datas presented in Goudie and Viles (1997). This study will thus focus mostly on the stones and their precise characterisation, with only one salt to make sure that all the differences observed between the salt decay behaviour come from the characteristics of the stone.

Outline of thesis

This thesis is presented in the form of a series of papers, which have been published, accepted or submitted for publication. These papers form the core of the different chapters

Chapter I presents an overview of the natural decay of building stones, from the noticeable patterns to the different causes for these alterations. A precise description of all the types of alteration is presented. This description shows that the alteration patterns observed on buildings and monuments are very similar to what is observed in the field on outcrops: the general decay mechanisms are the same in the same conditions (same stone, same environment).

Chapter II provides information on the stones whose alteration will be studied in this thesis. Their macroscale properties are measured with traditional standardized methods (porosity, capillary flow, mechanical strength, geophysical methods...), and their microstructures are also studied to have a complete knowledge of these stones (thin section analysis, geophysical data). Then the experimental ageing methods are exposed: first the standardized test used in the industry to assess the durability of a stone, then the modifications that were brought to this test in order to study the process of salt weathering.

Chapter III starts with a bibliographical study of salt crystallization damage. The general theories for salts are briefly exposed and the topics of interest are raised. In a second part, the particular case of sodium sulphate is presented. Its particularity is to have two stable phases at room temperature which gives it its destructive nature. The crucial point is to understand how and when these phases are stable during drying, according to the phase diagrams. A method based on temperature monitoring is explained to try to identify these

General introduction on salt decay

phase changes. It is presented in the article “**Thermal recording during experimental weathering of limestones: the role of imbibition on salt crystallization and rock decay**” (Hébert R, Angeli M, Bigas J-P and Benavente D) which has been submitted to *Journal of Crystal Growth*.

Chapter IV presents the damage caused by salt at two different scales. First, salt decay is evaluated at the scale of 7x7x7 cm³ samples. After briefly summing up the durability assessment methods in the literature, a new one is exposed in the article “**Salt crystallization in pores: quantification and estimation of damage**” (Angeli M, Bigas J-P, Benavente D, Menéndez B, Hébert R and David C) which has been published in *Environmental Geology* (2007). Then the effects of these tests on the mechanical strength of the stones are discussed. The influence of the environmental parameters is also studied. The second part of this chapter is more focused on the effects of salt decay on the microstructures of the stones. The location of the salt crystals and the size of the induced cracks are studied with the use of the mercury intrusion porosimetry method. The results are presented in “**Modification of the porous network by salt crystallization in experimentally weathered sedimentary stones**” (Angeli M, Benavente D, Bigas J-P, Menéndez B, Hébert R and David C) which has been accepted in *Materials and Structures*.

Chapter V is a study of the influence of the external parameters on salt decay. The experimental tests are now performed on only one stone to better study the variations from one environmental condition to the other. First, the influence of the evaporation possibilities is assessed by isolating some sides of the tested samples in “**Influence of capillary properties and evaporation on salt weathering of sedimentary rocks**” (Angeli M, Bigas J-P, Menéndez B, Hébert R and David C). This article has been published in the proceedings of the 2006 ‘Heritage, Weathering and Conservation’ conference which was held in Madrid. The proceedings have been edited in a book called “*Heritage, Weathering and Conservation*” edited by Taylor & Francis. Second, the influence of the temperature and the salt content in the stones has been evaluated in the article “**Influence of temperature and salt content on salt weathering of sedimentary rocks**” (Angeli M, Hébert R, Menéndez B, David C and Bigas J-P) which has been submitted to *a special bulletin of the London Geological Society*.

DECAY OF NATURAL STONES

CONTENT

1.	<i>Weathering agents</i>	9
	1.1. <i>Salt decay</i>	9
	1.2. <i>Freeze and thaw</i>	11
	1.3. <i>Thermal shock</i>	13
	1.4. <i>Water streaming</i>	13
	1.5. <i>Atmospheric pollution</i>	14
	1.6. <i>Biological colonisation</i>	15
2.	<i>Influence of the stone characteristics on weathering</i>	16
	2.1. <i>Mineral composition</i>	16
	2.2. <i>Hydric properties</i>	17
	2.3. <i>Strength contrast</i>	18
	2.4. <i>Stone-stone and stone-mortar compatibility</i>	19
3.	<i>Building characteristics</i>	20
	3.1. <i>Location of stones</i>	20
	3.2. <i>Sheltered zones</i>	21
	3.3. <i>Mechanical load</i>	22
4.	<i>Human causes</i>	22

Chapter I: Decay of natural stones

The decay of natural building stones and concrete in buildings and monuments is very similar to what happens in nature. The alteration patterns are the same on outcrops as on historical masonries. This chapter presents the different types of alteration that can occur on natural stone with a few illustrations taken from historical masonries (mainly churches) as well as outcrops.

1. Weathering agents

The causes of alteration are most of the time environmental parameters (rain, wind direction, frost, temperature contrast, soluble salts...), but can also have a human origin (bad restoration, soluble salts, atmospheric pollutants...). They are usually classified in three types: physical (or mechanical) alteration where stresses cause a cracking of the stone; chemical alteration which involves chemical reactions like crystallization or dissolution, and thus causes a mineralogical change in the stone; and biological alteration. Nevertheless, the alteration of a single building can be very different from one part of the building to the other. It depends on the exposition (sides sheltered or not from the rain, more or less exposed to the sun radiations), the height (subject to capillary rise or not), the architecture (sculptures, frontage, windows...) and eventual maintenance problems (leaking gutters...). Finally, the damage depends also on the nature of the stones (mechanical strength, porosity...).

1.1. Salt decay

Soluble salts are a major cause of building deterioration. The principle of its decay, which will be deeply detailed further in this study, is roughly that salt crystallizes in the porous networks and causes stress inside the pores. This stress is responsible for the internal cracking of the stone. This alteration is thus halfway between mechanical and chemical alteration. There are four main patterns of alteration that can be observed due to salt decay: efflorescences, granular disintegration, honeycomb weathering and contour scaling. The type of damage depends on the characteristics of the stones as well as those of the salts, and thus can be quite different from one site to the other. The stones that are the most sensitive to salt decay are generally stones with a high porosity, and rapid kinetics of imbibition and evaporation. In these stones, the filling of the pores, soluble salt supply, and their emptying, salt crystallization, occurs frequently and causes irreversible damage.

1.1.1. Efflorescences

This first type of alteration is in fact mostly harmless for the stones. Efflorescences are only salt crystals that have nucleated on the surface of the stones by evaporation. The most common salts found on efflorescences are chlorides (NaCl , KCl), sulphates (Na_2SO_4 , MgSO_4 , CaSO_4), carbonates (CaCO_3 , MgCO_3) or nitrates (KNO_3 , NaNO_3). A list of the salts that can be found in nature is provided in Goudie and Viles (1997). It is directly related to the capillary rise, and thus does not occur in buildings where this flow is either limited by non capillary stones (e.g. “meulière”) or blocked by an anticapillary barrier (e.g. clays). Efflorescences look like white-grey stains on the surfaces of the stones often on the lower part of buildings, just above the capillary fringe. They occur only when the crystallization of soluble salts takes place on the surface of the stone, because salt supply by capillary imbibition is faster than evaporation. This can be found on almost all types of stones, but they are more massive on porous stones with a quick capillary flow. It is also possible to find them inside buildings, not just on the outside walls.

1.1.2. Contour scaling

In the zone where evaporation is faster than capillary rise, on the upper part of buildings for instance, the brine cannot flow to the surface before evaporating. Evaporation, and thus the crystallization of salts, takes place inside the porous network, thus generating stresses that can be harmful for the stones. These in-depth crystallizations cause cracks below the surface, and the loss of a scale that can be several centimetres thick. This is called contour scaling, or desquamation (Fig. I-1, I-2).



Figure I-1. Contour scaling on Villiers-Adam church, Val d’Oise, France (limestone).



Figure I-2. Contour scaling on church of Objat, Corrèze, France (sandstone).

1.1.3. Granular disintegration

Granular disintegration (Fig I-3, I-4) occurs in humid places where the stone is not washed by the rain or flow of water on the surface. Soluble salts crystallize close to the surface and cause the detachment of grains. This erosion can cause the loss of several centimetres of stone on the outside surface.



Figure I-3. Granular disintegration on St Etienne church, Fécamp, Seine-Maritime, France (limestone). This church is located 300m of the sea.



Figure I-4. Granular disintegration on Stefansdom, Vienna, Austria (sandstone).

1.1.4. Honeycomb weathering (called alveolisation)

Honeycomb weathering (Fig I-5, I-6) is a particular case of granular disintegration. It happens when the erosion of grain happens differentially at the surface of the stone. The alveoli are nucleated by weakness zones that come from instance from the sedimentary bedding. Once the alveolus has started, the modification of the evaporation induced causes the decay to localize there.

1.2. Freeze and thaw

If ambient temperature reaches low values, ice starts to crystallize in the porous networks. Crystallization of ice is associated with a 9% volume raise (Prick 1995). Thus if the stone contains too much water in its porous network (the threshold is different for each stone), ice crystals do not have enough room to grow harmlessly. They start to grow in the larger pores. Since water cannot freeze in the smallest pores due to high water-solid interface energy (Remy 1993), and cryosuction drains this water in the smallest pores to the growing crystal

(Everett 1961), crystallization of ice is fed by this water in large pores (Thomachot 2002). Frost damage can cause granular disintegration (Fig I-7) and scaling (Fig I-8). Contrary to salt decay, frost decay is mostly harmful to rocks that have a high residual saturation (fast imbibition, slow drying).



Figure I-5. Honeycomb weathering on St Etienne church, Fecamp, Seine-Maritime, France (limestone). This church is located 300m of the sea



Figure I-6. Honeycomb weathering on a cliff by the seashore, Wessex, UK (eolian sandstone).



Figure I-7. Granular disintegration due to freeze and thaw on the Nidaros Domkirke, Trondheim, Norway (schists).



Figure I-8. Contour scaling due to freeze and thaw on the Nidaros Domkirke, Trondheim, Norway (schists).

1.3. Thermal shock

Thermal shock is the name given to cracking as a result of rapid temperature change. Some minerals are very sensitive to this type of damage due to their low thermal conductivity and high thermal expansion coefficients. Thermal shock occurs when a thermal gradient causes different parts of an object to expand by different amounts. This differential expansion can be understood in terms of stress or of strain. At some point, this stress overcomes the strength of the material, causing crack formation. For instance calcite has very anisotropic thermal dilation coefficient which causes intensive damage if heated too rapidly.

We can also note another type of damage due to accidental fire: the transition that occurs at approximately 573°C between quartz alpha and quartz beta. This causes severe damage that is much bigger than damage caused by simple thermal expansion (Takarli and Prince 2006).

1.4. Water streaming

This damage is due to the mechanical erosive action of water flowing on the surfaces. It is more efficient on stones with weak grain boundaries. It softens the relief for the weak stones (Fig I-9), and washes the soiled surfaces for the others (Fig I-10). It can also go along with dissolution when occurring on a carbonate substrate. This dissolution is more efficient with acid rains caused by atmospheric pollution (Morse and Arvidson 2002).



Figure I-9. Erosion by water streaming of the carved part of the soft stones exposed to rain, Hofburg, Vienna, Austria (limestone).

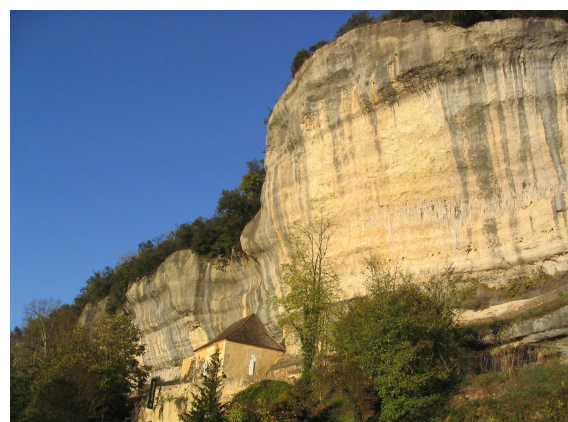


Figure I-10. Cleaning of the parts exposed to pouring rain by water streaming, Les Eyzies, Dordogne, France (limestone).

1.5. Atmospheric pollution

1.5.1. Soiling

Atmospheric pollution is responsible for numerous processes that affect directly natural stones. Some of them are harmless, e.g. soiling. Soiling is the deposition of particles (fly-ash, gas combustion waste) on the surface of stones which causes the general blackening of the stones that can be observed on most monuments in urban areas or close to roads. Besides the esthetical effect, this soiling can also have an influence on the hydraulic properties of the stones: the weaker surface tension of the particles can increase the hydrophobia of the stone, making it more waterproof.

1.5.2. Gypsum crusts

This soiling has to be clearly differentiated from the black crust that can be found in parts of monuments or sculptures isolated from water streaming (e.g. under a bridge edge or on the lower parts of statues). Although the exterior aspect is very similar to soiling, its mineralogical composition is totally different. The sulphur from the atmosphere (SO_2) reacts with calcite (CaCO_3), or with calcium provided by the atmosphere, to form gypsum ($\text{CaSO}_4 \cdot 2\text{H}_2\text{O}$) in the presence of water, releasing CO_2 in the atmosphere according to equations 1, 2 and 3 (Rodriguez-Navarro and Sebastian 1996):



These crusts thickness can reach up to 3cm. Gypsum is a translucent evaporite, but the black color comes from the atmospheric particles released by human activity (fly-ash, nanosoot). The crystallization of gypsum then damages the surface of the stone. It creates a fragile interface, between gypsum and the inner part of the stone, where both calcite and gypsum are present (Jeanette 1994). This fragile zone acts as a mechanical flaw and the crust detach periodically from the stone forming a black and white mosaic (Lefevre and Ausset 2001).

. Although this factor is related to the pollution from the industry, it is not as recent as expected. Ausset et al. (1998) have studied the composition of black crusts taken from

environments that have been preserved since the first industrial revolution. These black gypsum crusts have been exposed to the atmosphere in France and Italy mostly from the Middle Ages to the 19th century. The study of the particles trapped in gypsum showed that they were mainly wood debris and silicated or alumino-silicated spherules. Hence these cities were highly polluted by wood combustion debris as confirmed by the contemporary testimonies (books, paintings...). Nevertheless this weathering is less likely to appear since the amount of SO₂ in the atmosphere has recently fallen down due to more than 100ppb in the seventies to less than 10ppb now (Del Monte and Lefèvre 2001).

1.5.3.Acid rains

Note that the dissolution of carbonate stones by acid rains that has been explained in paragraph 1.4 takes also its origin in atmospheric pollution. The sulphur dioxide and nitrogen oxides from industrial pollution or traffic are hydrated to form sulphuric and nitric acids that cause calcite dissolution when they flow on the surface of the stones. This is not a typical problem for stones since it has destructive effects on vegetation as well. For instance, in Rouen the rain associated to industrial pollution can have a pH as low as 4.5.

1.6. Biological colonisation

Biological colonisation is usually composed of small lichens or mosses. Lichens look like coloured stains on the stones, generally white, yellow or green. They are almost harmless for the stones. They generally appear in the very humid parts of buildings or outcrops. This humidity can come from a gutter leak (Fig I-11), an exposition to the north (Fig. I-12). Figure I-12 presents an extreme biological colonisation where we can see not only mosses and lichens but also the roots and trunks of two trees in the stone wall. Figure I-13 shows an example of massive biological colonisation close to a water fall in a chalk cliff of the alabaster coast (in Normandy, France).



Figure I-11. Biological colonisation under a leaking gutter of the Neuville-sur-Oise church, Val d’Oise, France (limestone).



Figure I-12. Biological colonisation by trees on the northern side of the Villiers-Adam church, Val d’Oise, France (limestone).



Figure I-13. Biological colonisation of a waterfall near Yport, Seine-Maritime, France (chalk).

2. Influence of the stone characteristics on weathering

2.1. Mineral composition

Knowledge of the mineral composition of a stone is a decisive to understand some weathering patterns that appear to have no relationship with the environmental conditions. First, the mineral do not have the same durability towards weathering. For instance calcite is very easy to dissolve if water is in contact with it, as opposed to quartz which is almost inert. Decay could come also from the differences in the mineral properties. For instance, the decay on the block of tuffeau presented on figure I-14 is characteristic of this type of stone. This is due to pyrite nodules that are randomly present through the stone, and is not to any climatic or salt action. On the other hand, figure I-15 presents a decay which is characteristic also of old

armed concrete. The water flowing inside the porous network has corroded the armoring. The expansion due to this rust has caused the mechanical breaking of the concrete.



Figure I-14. Weathering due to a few centimetres pyrite inclusion in a very fragile stone, StCyr en Bourg, Maine-et-Loire, France (tuffeau).



Figure I-15. Salt weathering in concrete, Neuville-sur-Oise, Val d'Oise, France (concrete).

2.2. *Hydric properties*

2.2.1. *Fluid flow*

As quoted several times in the first part of this chapter, the hydric properties of the stones are decisive parameters to assess the durability of a stone. Water is the main source of alteration since it carries all the pollutants in the porous network and its drying kinetics governs the crystallization locations. Generally the stones with a very slow capillary rise are less sensitive to decay since water can barely enter the porous network. As explained in 1.1 and 1.2, the stones with a quick capillary flow can suffer mostly either from salt (fast evaporation kinetics with low residual saturation) or from frost (slow evaporation kinetics with high residual saturation).

2.2.2. *Hydric dilation*

Comparatively to what happens with thermal shock, some stones are very sensitive to pure water flowing in their porous networks. Sedimentary stones that contain small levels of hygroscopic clays (e.g. smectite) can suffer highly from this: when the clays expand all in one direction due to their assimilation of water, they can easily create inner stresses that cause defoliation along the bedding. The repetition of imbibition/drying cycles with only pure water

can also cause a weakness at the air-water interface, possibly leading to desquamation of stones that are very sensitive to it, like tuffeau for instance (Beck 2006).

2.3. Strength contrast

This is not strictly spoken a cause of alteration, but only a factor that causes a heterogeneous aspect of the stone weathering. Honeycomb weathering for instance (Fig I-5, I-6) is caused by a contrast of strength inside a stone, generally caused by sedimentary bedding. It can also cause an anisotropic decay only by alternations of weak and strong beds. It is important to notice that these beds are not necessarily visible on the fresh stone. It can be observed mostly on sandstones which, with their detritic origin, necessarily contain different sedimentation bedding. Fig I-16 and I-17 present two examples of anisotropic decay depending on the horizontal bedding of sandstones at different scales.

Nevertheless these contrasts are not necessarily horizontal. Figure I-18 and I-19 show two examples of alteration along the cross-bedding stratification of a sandstone: one on a seashore outcrop in the Wessex (Fig. I-18) and one on the frontage of a church in Göttingen (Fig. I-19).



Figure I-16. Anisotropic weathering along the bedding on Stefansdom, Vienna, Austria (sandstones).



Figure I-17. Anisotropic salt weathering of a cliff on the seashore due to strength contrast near Bridport, Wessex, UK (continental sandstones).



Figure I-18. Salt weathering along the cross-bedding stratification on seashore, Wessex, UK (continental sandstones).



Figure I-19. Weathering along the cross-bedding stratification on Johannes Kirche, Göttingen, Germany (continental sandstones).

2.4. Stone-stone and stone-mortar compatibility

In the particular case of masonries, a problem which does not have an equivalent in natural stones can occur: it concerns the stone-stone and the stone-mortar compatibility. If the materials are badly chosen, it can accelerate the weathering in a drastic way for one of the two types of stones (Beck 2006). This can be observed on figures I-20 and I-21: the stones used to replace the most altered was not compatible and accelerated the weathering of the old stones (I-18) and of the new stone (I-21). Nevertheless this contrast in the weathering can also be observed if the stone was already altered before restoration, but not enough to be changed.



Figure I-20. Alteration due to inappropriate restauration on the Nidaros Domkirke, Trondheim, Norway (schists).



Figure I-21. Alteration due to inappropriate restauration on Villiers-Adam church, Val d'Oise, France (limestones).

This damage comes generally from the incompatibility in the hydric properties of the two stones. When capillary supply is much faster in a stone than in the other, it breaks the capillary continuity in the building and causes a water accumulation in the most capillary stone, which is generally softer. This causes an acceleration of the decay of this stone (Beck 2006). This decay can be also caused by a bad choice of the mortar bounding the stones. If the chosen mortar has very different capillary properties, it causes the same problem as with two capillary-incompatible stones. It is also necessary to select one with similar mechanical strength to prevent the disjoining of the stones (Fig. I-22). The choice of the mortar is thus decisive to ensure the durability of the buildings.



Figure I-22. Disjoining around the alveolated stone due to a high strength contrast between the limestone and the lime mortar. The size of the block is 40 cm. Cormeilles-en-Vexin church, Val d'Oise, France.

3. Building characteristics

3.1. Location of stones

As it was stated in the introduction of this chapter, similar stones in the same climatic environment in the same building do not necessarily suffer from the same decay. The buildings are generally not built out of a single stone: stronger non-capillary stones are chosen for the basement or columns, soft stones are chosen for ornamentations... But even two stones of the same type do not necessarily have the same durability, depending on the location of the stones (height, building part; Figure I-23) and their exposition to the climatic conditions (wind, rain or sun). For instance we have pointed out in 1.1.1. that efflorescences occur only on the lower parts of building that are reached by capillary supply, or that subflorescences causing contour

scaling or granular disintegration occur only just above the capillary fringe. Figure I-24 gives an example of this differential weathering on a bay of the Cormeilles-en-Vexin church.



Figure I-23. Differential weathering of a buttress from the Stefansdom in Vienna Austria (sandstones). We can clearly notice that the right-hand part of the buttress is much more weathered than the left-hand part. This is certainly due to its orientation regarding the main wind direction.

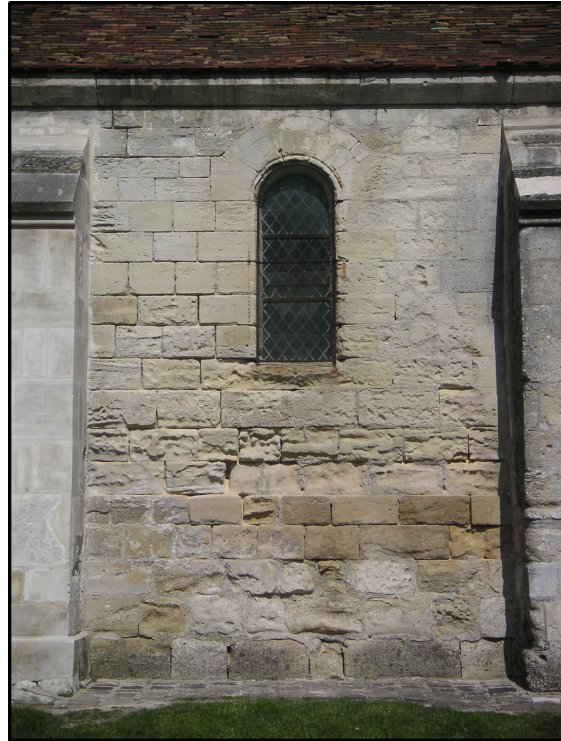


Figure I-24. Gradual weathering of a bay build with two different limestones. The decay depends on the height (capillary rise, protection by the roof), the distance to the buttress which can shelter from wind or rain... Cormeilles-en-Vexin church, Val d'Oise, France.

3.2. *Sheltered zones*

In the case of highly soiled buildings, the influence of the location of the stones is very easy to notice. Figure I-9 shows a good example of this aspect. The building is highly soiled and it is easy to notice that the top of the head is the only clean part of the sculpture. This is the only part exposed to washing rains which removes the particles that are deposited on the top of the sculpture, or erodes the surface of the stone, which in both cases gives back to the stone its original colour. The sheltered zones are also the only zones that can suffer from gypsum crusts as exposed in 1.5.2.

3.3. Mechanical load

Building stones can also simply suffer from the mechanical load related to the weight of the building itself. It causes fractures parallel to the load direction. The zones which are the most exposed to this type of damage are the zones where the most weight is concentrated in small part, like on the top of an arch (Fig. I-25) or of an alcove (Fig. I-26). It can also appear in the case of a construction built in a steep slope, or in case of differential soil depression under the basement of the building.



Figure I-25. Cracking due to mechanical load on the arch above the main door of Neuville-sur-Oise church, Val d'Oise, France.



Figure I-26. Cracking due to mechanical load on an alcove. Guiry-en-Vexin church, Val d'Oise, France.

4. Human causes

Because of an increasing interest by the public in cultural heritage, the effects of human contact upon the condition of stone, as well as all other building materials, is of growing concern. For example, stone floors are gradually worn by foot traffic, stones are damaged by people either collecting souvenirs or engraving into soft stone (Fig. I-27). These engravings are mostly found on buildings made out of limestones rather than sandstones. This

is due to the hardness of the main mineral composing these two stones. Steel, which is generally used for engraving (keys, knife...) has a Mohs hardness of around 5.5 which is higher than calcite (3), but lower than quartz (7).



Figure I-27. Engravings in the soft Lutetian limestone used in the Neuville-sur-Oise church, Val d'Oise, France.

But human effect can also have indirect or involuntary origin. Atmospheric pollution, which has a major influence on the weathering of the buildings (see paragraph 1.5), is a consequence of human industrial activity.

A badly performed building restoration can also cause a lot of damage to the stones. It generally comes from the choice, for financial reasons, of incompatible material: replacement stones or mortars. It can cause differential erosion as described in 2.4 (Figs. I-20 and I-21), but also severe desquamation or disintegration when cement mortar or plaster is used to superficially fix the stones (Fig. I-28). The phenomenon happening here is exactly the same as the one presented in I-24, except that the ions comes here from the mortar instead of the arming of the concrete.



Figure I-28. Desquamation in granite due to the cement mortar used to repair the wall. Berliner Dom, Germany.

After identifying all the alteration types that can be found on monuments or outcrops, the next chapter will focus on the characterization of the studied stones, and on the methods used to simulate stone weathering by crystallization of salts.

MATERIALS AND METHODS

CONTENT

1.	<i>Overview of the studied stones</i>	27
1.1.	<i>Lutetian limestones</i>	27
1.2.	<i>Pierre de Souppes</i>	30
1.3.	<i>Fontainebleau sandstones</i>	31
1.4.	<i>Chinese sandstone</i>	32
1.5.	<i>Agra sandstones</i>	32
2.	<i>Microstructural studies</i>	33
2.1.	<i>Characterization of the studied stones</i>	34
2.2.	<i>Geophysical properties</i>	49
3.	<i>Hydromechanical properties</i>	55
3.1.	<i>Hydric tests</i>	55
3.2.	<i>Mechanical tests</i>	60
4.	<i>Accelerated ageing by salt decay</i>	60

Chapter II: Materials and methods

Chapter II: Materials and methods

Nine sedimentary stones from different lithologies have been used in this study. The microstructures have been studied to understand the stone's general structures. This study is composed of both image analysis and geophysical techniques. Then the stones have been characterized using traditional petrophysical techniques.

1. Overview of the studied stones

Nine stones from different lithologies have been used in this study: four limestones and five sandstones. The four limestones and two sandstones come from the Parisian Basin. Two more sandstones are two commercial types of the same Indian sandstone. Finally the last stone is a Chinese sandstone. They have been chosen for their wide use in the cultural heritage in the Parisian basin (Lutetian limestones and Fontainebleau sandstones) and in the building of private housings (Agra and Chinese sandstones).

1.1. Lutetian limestones

Three of the studied stones are limestones of lutetian age (Eocene): the “roche fine” (FL), the “roche franche” (RL) and the “liais” (LL). They come from the city of Saint-Maximin-sur-Oise (Oise, France). RL (Fig. II-1) and LL (Fig. II-2) are two beige bioclastic limestone composed by mostly calcite, with traces of iron oxides. They also contain some macrofossils (bivalves, gastropods) responsible of a heterogeneous aspect. We can also notice the presence of fine irregular white bands which are diagenetic micritic cement. These two stones have a very similar aspect with a random distribution of macroporosity due to the fossils, and a much finer microporosity related to the late micritic cement. Nevertheless, the fossils appear less sharp in the “liais” than in the “roche franche” due to more dissolution and diagenetic calcite recrystallization.

The “roche fine” (Fig. II-3) is a beige detritic limestone made of calcite and quartz grains. It seems much more homogeneous than the two other lutetian limestones due to its detritic structure. It has a very rough aspect with macropores that can be seen naked-eye (size of approx. 500µm). Calcite, which represents approximately 90% of the stone, comes in the form of both calcite grains and microfossils (mainly milioles and nummulites). The detritic quartz grains represent approximately 10% of the stone. As for RL and LL, the fine white bands of diagenetic micritic cement are present. These bands are very irregularly distributed among the stone. We can also notice the presence of very few dark minerals with orange leaks

which are ferromagnetic oxides. The stone seems to have a weak bounding which suggests a very low tensile strength.



Figure II-1. Cube of 7cm side of the biodetritic cemented limestone RL (“roche franche”).



Figure II-2. Cube of 7cm side of the biodetritic cemented limestone LL (“liais”).



Figure II-3. Cube of 7cm side of the detritic limestone FL (“roche fine”).

Lutetian limestones are imposed as the restoration stones by the restoration of cultural heritage in the Vexin natural regional park. This park gathers more than 100 churches from the Middle Ages to the Renaissance that have been built using different types of lutetian limestones. More generally, lutetian limestones have been used in the Parisian basin since the antiquity (Fröhlich and Schubnel 2000).

The oldest known statue made of this stone is called the “Pilier des Nautes” (Fig; II-4; literally the pillar of the “Nautes”, a traders fellowship) dates from the 1st century AC. It is made of “Pierre de StLeu”, which is very similar to the “roche fine”. Other famous monuments in the Parisian basin are also made of lutetian limestone like Notre-Dame de Paris (Fig. II-5) or the St Denis basilica (Fig. II-6) where all the kings of France are buried. The lutetian limestone also has a worldwide repartition. Outcrops can be found in Senegal, Portugal, Italy, Hungary, Egypt... Even the Egyptian pyramids of Kheops, Kephren and Mykerinos in Gizeh are said to be built in lutetian limestones (Fig. II-7), although some authors claim that the blocks are a kind of ancient cast in place concrete (Barsoum et al. 2006).

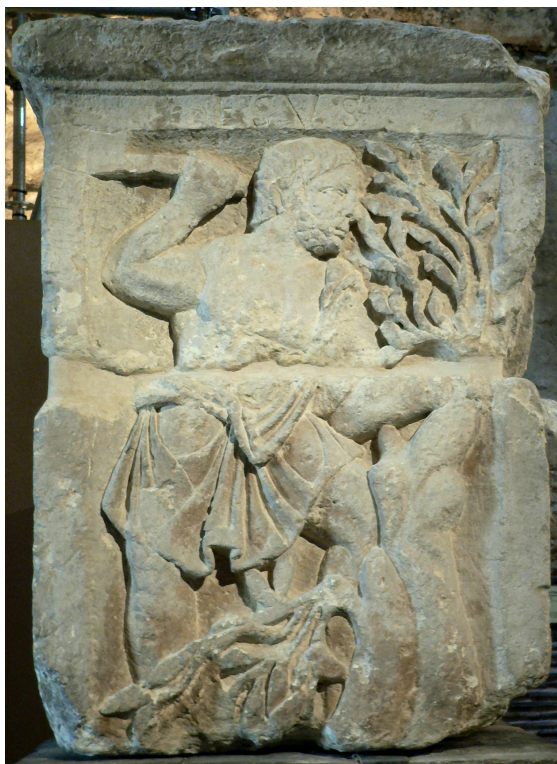


Figure II-4.Pillar of the Nautes sculpted in “Pierre de Saint-Leu”, 1st century AC (National museum of the Middle Ages of Cluny, Paris; Frohlich and Schubnel 2000).



Figure II-5.Notre-Dame de Paris Cathedral, XIIth-XIVth century, Paris, France.



Figure II-6. Basilica of Saint-Denis, XIIth-XIIIth century, Saint-Denis, France.



Figure II-7. Pyramid of Kheops, XXVIIth century BC, Gizeh, Egypt (Picture from Alexandra Cournot).

1.2. Pierre de Souppes

The fourth limestone is of bartonian age (upper Eocene): the “Pierre de Souppes” (SL), a variety of the “Calcaire de Chateau-Landon”. This stone is named after the city of “Souppes-sur-Loing” (Seine-et-Marne, France) where it comes from. It is a creamy white lacustrine limestone exclusively composed of calcite (Fig. II-8). It is very fine grained and appears quite competent with low porosity. The stone contains few inclusions of secondary translucent calcite. Due to its very pure white colour, this stone has been widely used in the Parisian architecture during the XIXth and XXth centuries. For instance, the Sacré-Coeur Basilica (Fig. II-9) and the Sorbonne University (Fig. II-10) are made of “Pierre de Souppes”.



Figure II-8. Sample of “Pierre de Souppes” (SL).



Figure II-9. Basilica of the Sacré-Coeur (Sacred Heart) in Montmartre, Paris.



Figure II-10. Frontage of the main University building of Paris I Panthéon-Sorbonne, Paris.

1.3. Fontainebleau sandstones

Two types of Fontainebleau sandstones have been used in this study. These two varieties are called hard (HF; Fig. II-11) and soft (SF; Fig. II-12). They are eolian sandstones of priabonian age (upper Eocene), but the local stage name used is Stampian. They are located just above the “Pierre de Souppes” in the stratigraphic log of south-eastern Parisian basin. The two sandstones have a very similar greyish aspect although HF looks a bit darker than SF. They have both a very homogeneous aspect and are both composed of more than 99% of quartz grains homogeneous in size. They appear to have low porosity and high tensile strength on macrosamples, although SF’s surface seems a bit more friable than HF’s. This sandstone has been used for the great horseshoe staircase of the Fontainebleau castle (Fig. II-13) as well as for pavement stones in Paris.



Figure II-11. Sample of hard Fontainebleau sandstones (HF).



Figure II-12. Sample of soft Fontainebleau sandstones (SF).



Figure II-13. Horseshoe staircase in the White Horse Yard of the Fontainebleau Castle (Seine-et-Marne, France)

1.4. Chinese sandstone

Another sandstone comes from China (CS; Fig. II-14). It is a white sandstone which seems very competent with low porosity. It is composed mainly of quartz grains of various sizes. A close look to the samples reveals a rather heterogeneous aspect of this stone, although it is not clear at first.



Figure II-14. Sample of the Chinese sandstone (CS).

1.5. Agra sandstones

The last two sandstones come from India and are two commercial varieties of Agra sandstones: the red Agra (MS; Fig. II-15) and the green Agra (VS; Fig. II-16). Both types seem to be very similar: they are fine grained, layered sandstones which seem very competent. The red Agra, the most common type, has been used in the region of Agra, India, for the building of massive monuments like the Red Fort in Delhi (Fig. II-17), a UNESCO world heritage site.



Figure II-15. Sample of the red Agra sandstone (MS).



Figure II-16. Sample of the green Agra sandstone (VS).

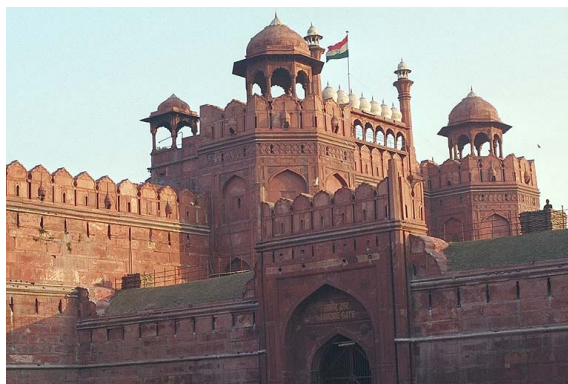


Figure II-17. Red Fort in New Delhi, India (Picture from Michael Petersen)

A simple notation with two letters for all these stones will further be used in this study. The first letter refers to the actual name of the stone: F for “roche Fine”, R for “roche fRanche”, L for “Liais”, S for “Pierre de Souppes”, H for “Hard Fontainebleau sandstone”, S for “Soft Fontainebleau sandstone”, C for “Chinese sandstone”, V for “green Agra sandstone” (“green” says “Vert” in French) and M for “red Agra sandstone” (M for “marron” in French, which means “brown”). The second letter is a reminder of its type: L for limestones (FL, RL, LL and SL), F for Fontainebleau sandstones (HF and SF) and S for other sandstones (CS, VS and MS).

2. Microstructural studies

In order to evaluate the modifications of the stone suffering from salt crystallization, it is necessary to perform a precise description of the microstructures of the studied stones. This

microstructural study will be performed in two manners: image analysis (thin sections, scanning electron microscopy) and indirect data, mainly derived from geophysical measurements (P-waves velocity, magnetic susceptibility). The numerical values are given for all the stones in Table II-1.

The aim of this part is to analyse thoroughly the stones that are used in this study. In order to properly characterize the modification of the stones due to salt decay it is important to have a precise knowledge of these stones before the tests. At first the skeleton of the stone is studied, that is to say the properties of the grains: shape, origin, size, structure... Then the general properties of the porous network are measured, both hydraulic and mechanical parameters.

2.1. Characterization of the studied stones

2.1.1. Optical microscopy

The “liais” LL (Fig. II-18) is a biodetritic limestone with a very heterogeneous porous network. It is composed of macrofossils (gastropods, bivalves) which have been totally or partially refilled with calcite crystallisation. It contains also lots of miliolids, and a few quartz grains. The porous network seems very badly connected due to secondary cement. The image analysis has not been performed on this stone because the structure is not adapted.

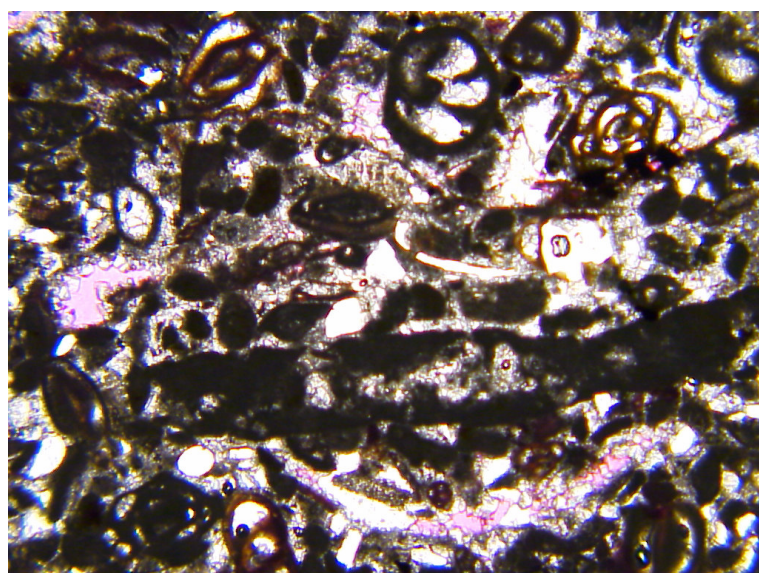


Figure II-18. Thin section of “liais” with analyzed light. The size of the picture is 4mm.

Chapter II: Materials and methods

The “roche franche” RL (Fig. II-19) has, like LL, a very complex porosity due to the heterogeneity of the matrix: it is composed mostly of gastropods, bivalves and miliolids. It contains also a few quartz grains. Nevertheless the secondary calcite recrystallization are less numerous, and this gives to the stone a more cut out aspect: the shape of the microfossils is not soften by the secondary calcite. Similarly as LL, this stone has a too chaotic structure to be studied completely with the image analysis method.

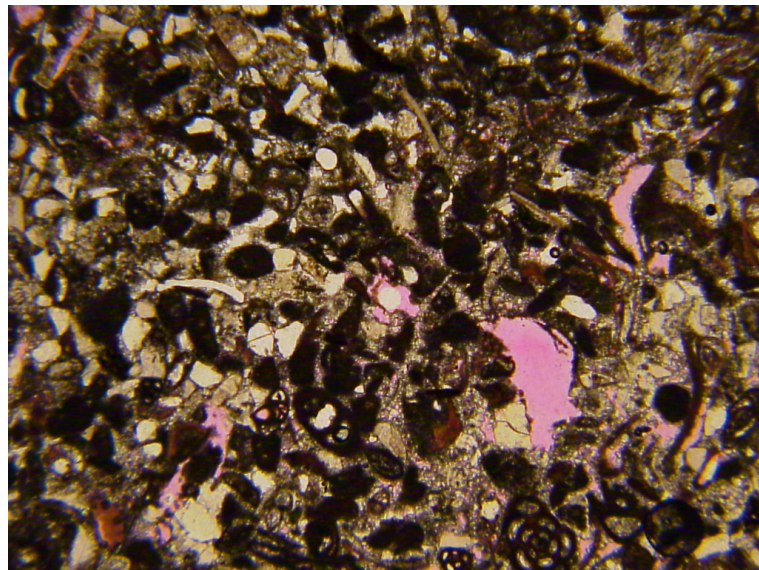


Figure II-19. Thin section of “roche franche” with analyzed light. The size of the picture is 4mm.

The “roche fine” FL (Fig. II-20) has a detritic structure. This limestone is composed mostly of miliolids and calcite grains. There are two types of porosities: one coming from the detritic structure with the intergrain distance of around $100\mu\text{m}$, and one from the micritic cement around the grains which is much smaller. The grains have a homogeneous size of approximately $100\mu\text{m}$.

The “Pierre de Souppes” SL (Fig. II-21) is a lacustrine limestone. It is very fine grained and composed only of calcite. It contains also a few holes of up to several centimetres that have been refilled with calcite recrystallization. The porosity is expected to be very fine. Since the origin of this stone is not detritic, it was not possible so study this structure with the image analysis method.

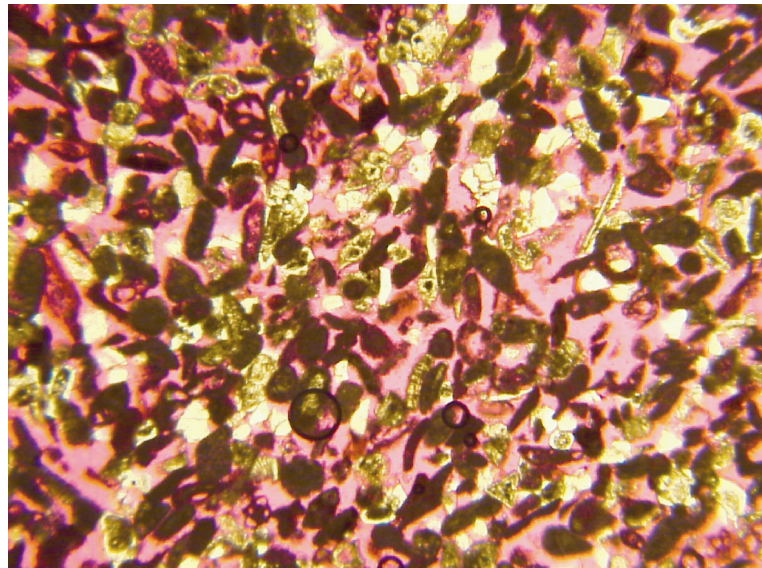


Figure II-20. Thin section of “roche fine” with non-analyzed light. The size of the picture is 4mm.

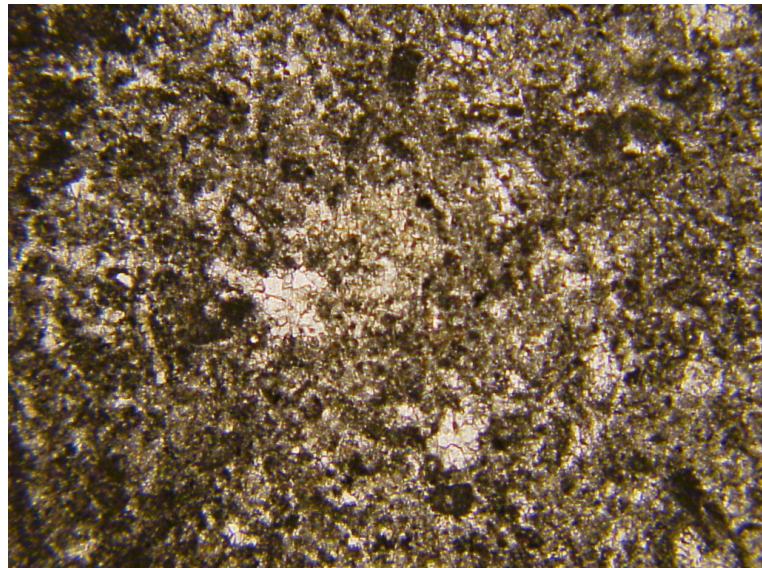


Figure II-21. Thin section of “Pierre de Souppes” SL with non-analyzed light. The size of the picture is 4mm.

The “hard Fontainebleau” sandstone HF (Fig. II-22) is almost only composed of quartz. It is very strongly cemented since almost no pore is detectable with only optical microscopy. The grains are round-shaped with a very homogeneous size around 250 μ m.

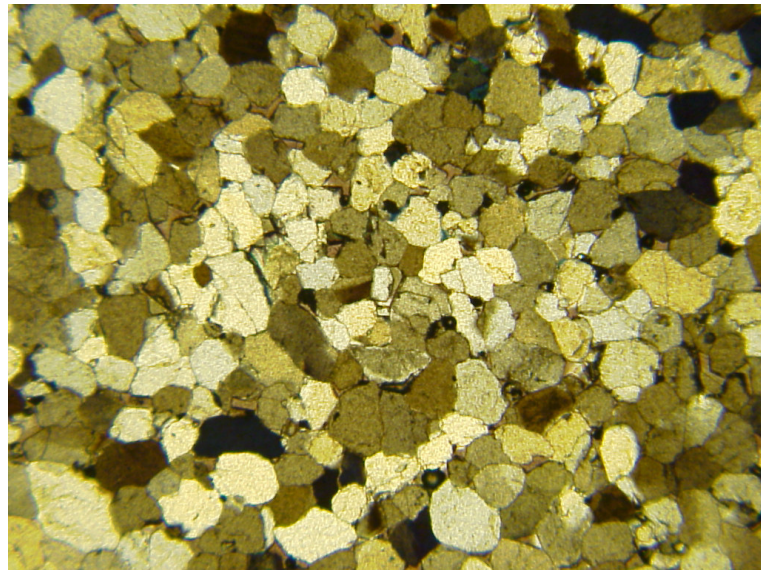


Figure II-22. Thin section of “hard Fontainebleau” sandstone HF with analyzed light.

The size of the picture is 4mm.

The “soft Fontainebleau” sandstone SF (Fig. II-23) is also almost only composed of quartz grains. The shape and size of the grains are very similar to HF. They are also homogeneous. The only difference is that they are more cracked and seem more weakly bounded. These cracks seem to have increased the connectivity of the porous network since we can notice a few pores filled with impregnation resin, which is not the case for HF.

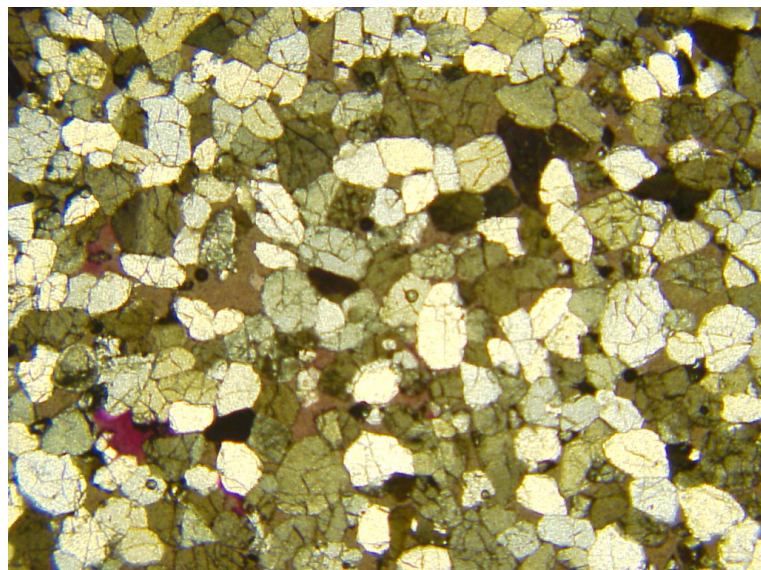


Figure II-23. Thin section of “soft Fontainebleau” sandstone SF with analyzed light.

The size of the picture is 4mm.

Chapter II: Materials and methods

The Chinese sandstone CS (Fig. II-24a,b) is a sandstone mainly composed of quartz. Nevertheless, as opposed to both Fontainebleau sandstones, the grains have very heterogeneous sizes (from 5 to 500 μm). The grains seem to be strongly bounded and there is no porosity filled with resin on the thin sections. There exists a layering in the grain sizes: figure II-24a shows a zone where the grains are quite large and cracked (up to 500 μm) and with a few crushed grains filling the big pores. On the second hand, figure II-24b shows much smaller grains which seem to be the result of the crushing of the grains due to a mechanical load.



Figure II-24a. Thin section of a big grains zone of the Chinese sandstone CS with non-analyzed light.

The size of the picture is 4mm.

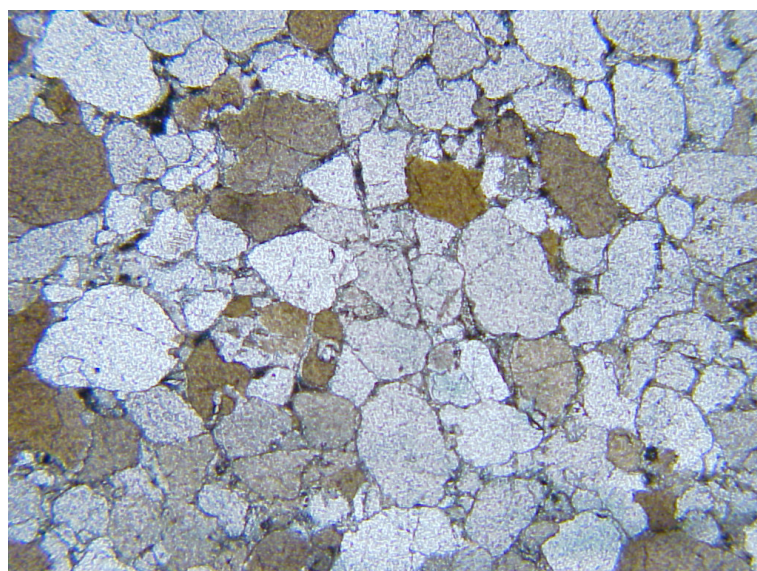


Figure II-24b. Thin section of a crushed grains zone in the chinese sandstone CS with non-analyzed light.

The size of the picture is 4mm.

Chapter II : Materials and methods

The green Agra sandstone VS (Fig. II-25) is a very strong green sandstone. A thin brown layering indicates the bedding. The grains are much smaller than in the other sandstones (homogeneous around 50-100 μm), and have an angular shape. They seem strongly bounded with very much intergrain pore space. Almost no pore has been filled with resin during impregnation. The “red Agra” sandstone MS (Fig. II-26) is very similar to the green Agra sandstone. The grains have also homogeneous sizes around 50-100 μm and irregular shapes. They are also strongly bounded leaving also very few pores noticeable at this magnification.

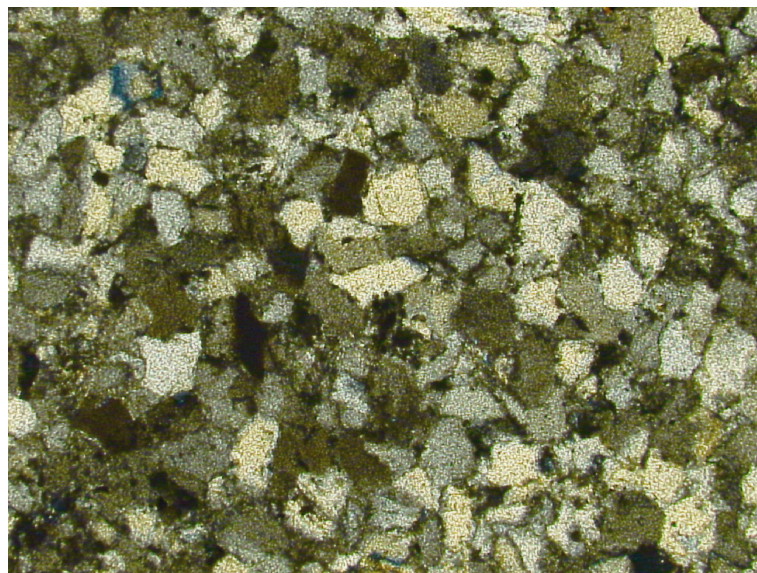


Figure II-25. Thin section of the “green Agra” sandstone VS with analyzed light.

The size of the picture is 1.5mm.

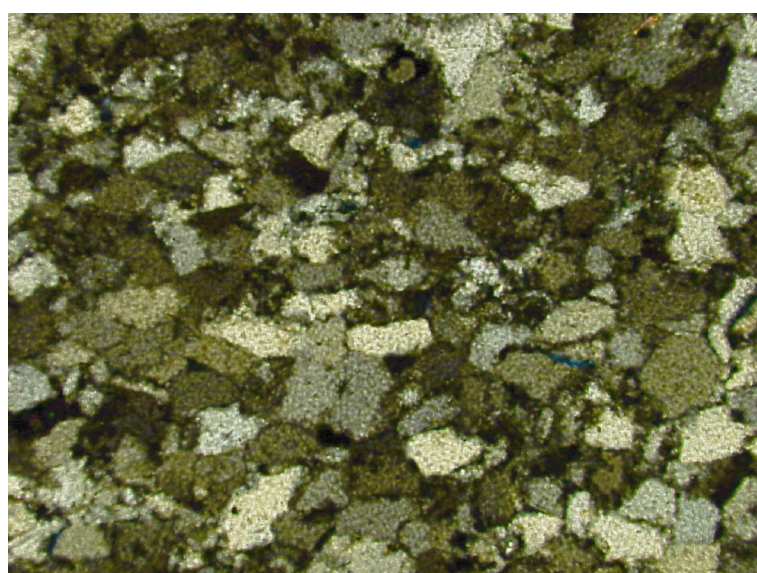


Figure II-26. Thin section of the “red Agra” sandstone MS with non-analyzed light.

The size of the picture is 1.5mm.

2.1.2.Porosity

The total open porosity is first defined as the porous space available for water under vacuum. According to the European standards (EN 1936, 1999), it is measured with the simple method of the triple weighing. A sample which is representative for the stone is weighed dry (m_{dry}), fully saturated (m_{sat}) and fully saturated and immersed (m_{imm}). The samples are saturated under vacuum with degassed deionised water. The $m_{sat} - m_{dry}$ difference gives the weight of water that has entered the porous network. The $m_{sat} - m_{imm}$ difference gives the weight of the water occupying the exact same volume as the sample. This difference comes from buoyancy. Let d_{w-RT} be the density of water at the temperature of the experiment. This gives:

$$m_{sat} - m_{dry} = d_{w-RT} \cdot V_{pores} \quad (\text{II-2})$$

$$m_{sat} - m_{imm} = d_{w-RT} \cdot V_{sample} \quad (\text{II-3})$$

The porosity open to water Φ_{wat} of a sample corresponds to the volume of pores divided by the total volume of the sample. This gives:

$$\Phi_{wat} = \frac{\frac{m_{sat} - m_{dry}}{d_{w-RT}}}{\frac{m_{sat} - m_{imm}}{d_{w-RT}}} = \frac{m_{sat} - m_{dry}}{m_{sat} - m_{imm}} \quad (\text{II-4})$$

Equation (II-4) gives the value of the porosity accessible to water under vacuum. It is also possible to obtain the bulk $d_{bulk,wat}$ and $d_{skel,wat}$ skeletal densities from this triple weighing method. They are given by equation (II-5) and (II-6) respectively:

$$d_{bulk,wat} = \frac{m_{dry}}{\frac{m_{sat} - m_{imm}}{d_{w-RT}}} \quad (\text{II-5})$$

$$d_{skel,wat} = \frac{m_{dry}}{\frac{m_{dry} - m_{imm}}{d_{w-RT}}} \quad (\text{II-6})$$

We assess that d_{w-RT} is close to 1g/cm^3 which is approximately the case, thus this gives new simple equation for the bulk and skeletal densities:

$$d_{bulk,wat} = \frac{m_{dry}}{m_{sat} - m_{imm}} \quad (\text{II-7})$$

$$d_{skel,wat} = \frac{m_{dry}}{m_{dry} - m_{imm}} \quad (\text{II-8})$$

2.1.3. Mercury porosimetry

Mercury Intrusion Porosimetry (MIP) is an indirect destructive method to obtain a distribution of the pore size entries of porous media. This technique is based on the cylindrical pore model and the Washburn equation. This equation describes capillary flow in porous media. If we consider that the pores in a stone have a cylindrical shape, the capillary pressure P_c in a cylindrical pore of radius r is defined as:

$$P_c = -\frac{2\gamma}{r} \cdot \cos(\theta) \quad (\text{II-9})$$

where θ is the Hg-solid contact angle and γ is the surface tension of mercury (0.480 N/m). Usually θ is set at 130° which is an average value for most stones (Good and Mikhail 1981). The principle is to put a small sample (up to 10cm^3) under vacuum, progressively inject mercury at increasing pressures (from 3.10^{-3} to 200 MPa) and measure the volume of mercury injected at each pressure step. This pressure is associated with a radius thanks to the Washburn equation (II-9). Thus the bigger pores are filled first with mercury, and the smaller pores are the last to be filled up. Nevertheless, a big pore with a smaller entry will be filled at the pressure corresponding to its entry size, and thus be seen on the spectrum as a smaller size. This phenomenon is known as the “ink bottle effect”, and is a disadvantage of the cylindrical pore model. The measurements have been performed on two different devices: a Micromeritics Autopore IV 9500 at the University of Alicante (Comunidad Valenciana, Spain), and a Micromeritics Autopore IV 4500 at the University of Cergy-Pontoise.

The aim of this method is to obtain a MIP spectrum with the volume of pores associated to a certain pore size entry (pore radius). It gives good information about the

distribution of pores (uni- or multimodal) but we have to take into account the fact that, as stated earlier, this method is sensitive to the pore size entry distribution and one does not obtain the actual pore size distribution. It is also possible to obtain a precise value of the bulk density, the mean pore radius, the porosity and an underestimated grain density. It must also be combined with thin section observations to understand what type of voids is detected by this technique. For each type of stone, three samples have been cut from the same original sample to ensure the reproducibility of both the measurement technique and the stone. It should be noted that since the total porosity of the samples are different from one stone to the other, the vertical scale of the spectra changes from one stone to the other.

The MIP spectra of these stones can be classified in three groups: unimodal, subunimodal and heterogeneous. First there are only two stones with a unimodal distribution of pores, HF and SF (Fig. II-27, II-28). This distribution is a characteristic of the detritic stones with homogeneous sizes of grains. The main peaks are respectively around 7 μm for HF and 20 μm for SF.

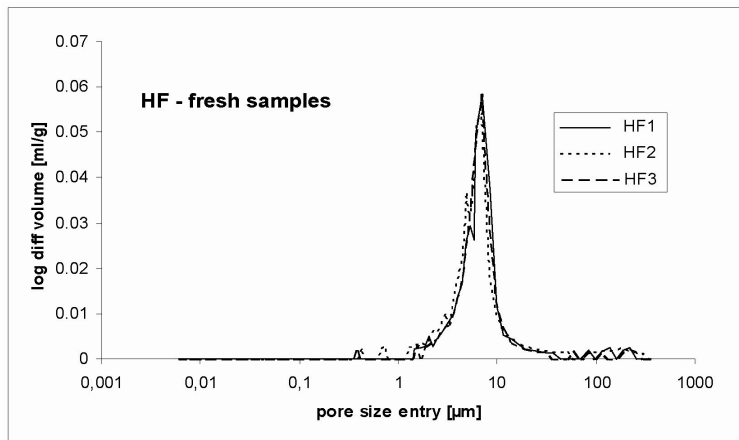


Figure II-27. MIP spectrum of three fresh samples of hard Fontainebleau sandstone (HF).

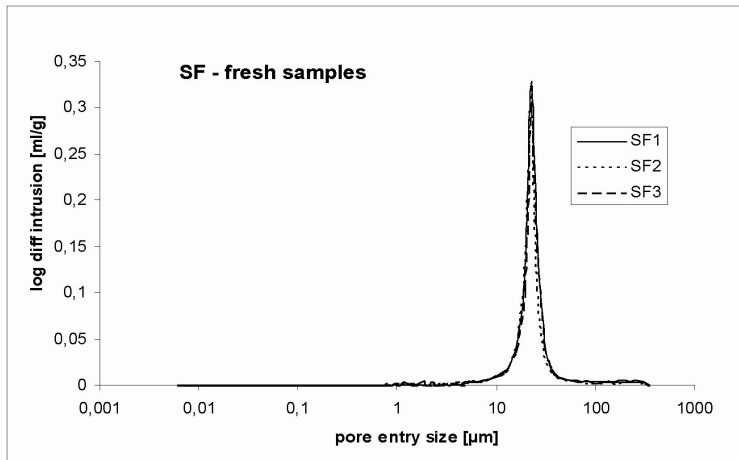


Figure II-28. MIP spectrum of three fresh samples of soft Fontainebleau sandstone (SF).

Chapter II: Materials and methods

Four stones have a subunimodal distribution of pore entry size: FL, VS, MS and CS (Figs. II-29, II-30, II-31, II-32). A subunimodal distribution of pores is defined as a distribution with a peak for a single value, but with also other pores with other entry sizes. It corresponds again to a detritic structure, but modified by some elements with a different porosity. For FL (Fig. II-29), the peak is around $20\mu\text{m}$, but we can also notice another kind of porosity with entries from 0.03 to $5\mu\text{m}$. This spectrum has a secondary peak at around 0.04ml/g for an entry size of around $0.2\mu\text{m}$. It certainly corresponds to the porosity of the secondary micritic cement.

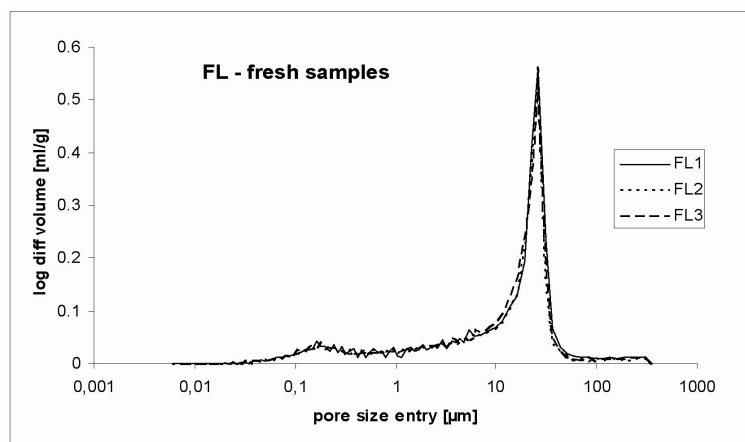


Figure II-29. MIP spectrum of three fresh samples of “roche fine” (FL).

VS and MS have both the main peak related to their detritic structure at around $0.1\mu\text{m}$ (Figs. II-30, II-31). Nevertheless, there exist some pores with smaller entries between 0.05 and $0.5\mu\text{m}$. They are certainly related to the voids between the clays contained in these two sandstones.

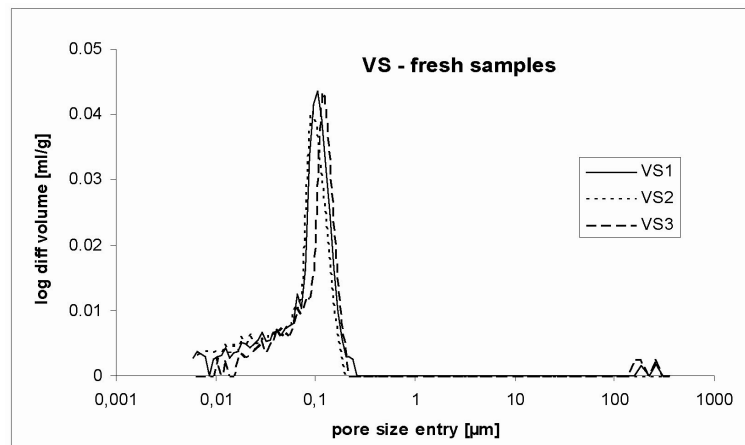


Figure II-30. MIP spectrum of three fresh samples of green Agra sandstone (VS).

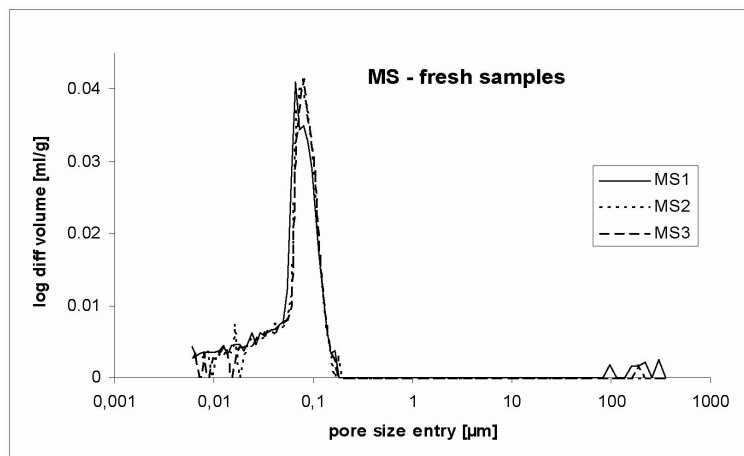


Figure II-31. MIP spectrum of three fresh samples of red Agra sandstone (MS).

CS has a slightly different pore entry size distribution (Fig. II-32). The main peak is around an entry of $2\mu\text{m}$, but the other pores are much more irregular. There is no clear reproducibility for this extra family of voids between 0.05 and $1\mu\text{m}$. This could be a reason to think that these voids are related to the numerous cracks that are observed on thin sections, or corresponds to the zones where the grains are crushed.

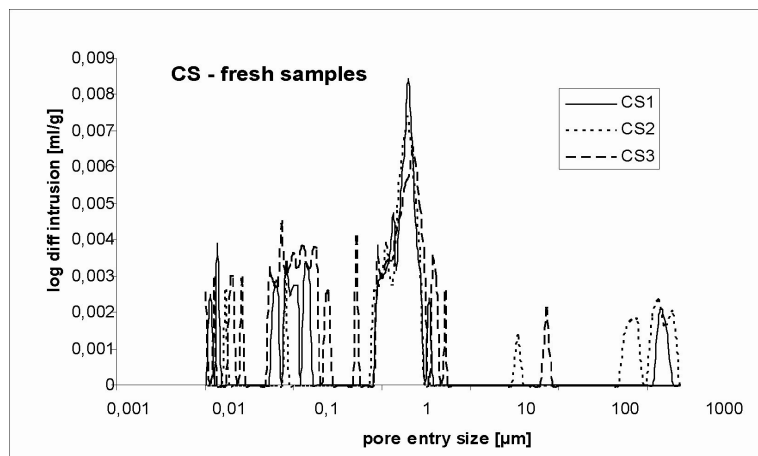


Figure II-32. MIP spectrum of three fresh samples of Chinese sandstone (CS).

The three stones with a heterogeneous distribution of pores (LL, RL and SL) are three limestones, two bidetritic and one lacustrine. The two detritic limestones have numerous similarities (Figs. II-33, II-34). LL and RL both have a range of pores between 0.01 and $1\mu\text{m}$ which is almost similar from one sample to the other. This family of pores has the exact same

Chapter II: Materials and methods

peak of 0.04mg/l for pores with entry of 0.2 μm than FL. This demonstrates that this family corresponds to a diagenetic micritic cement common to the three stones since they have been sampled in the same place. RL (Fig. II-34) also has pores with entries between 1 and 200 μm which corresponds to the macrofossils it contains. These sizes are also found in the spectrum of LL, but with lower intrusion values since they have been partially or totally filled with calcite recrystallization (Fig. II-33).

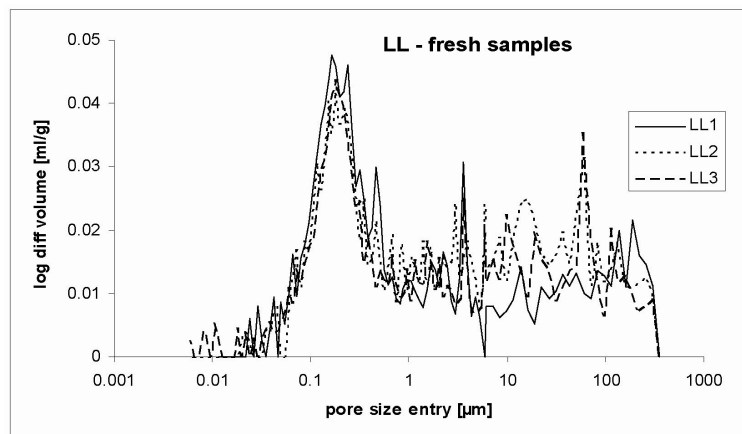


Figure II-33. MIP spectrum of three fresh samples of “liais” (LL).

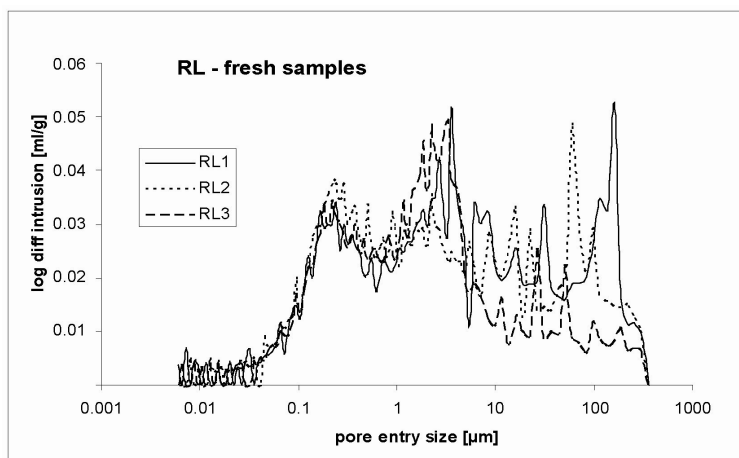


Figure II-34. MIP spectrum of three fresh samples of “roche franche” (RL).

SL has a pore entry size distribution which is halfway between unimodal and heterogeneous (Fig. II-35). It has a main peak around 0.08 μm which is not very reproducible from one sample to another. This porosity seems to come from the spaces between the calcite crystals. The other pores with larger entry sizes could result in the intrinsic heterogeneity of the limestone due to its lacustrine origin (voids than can be seen on thin sections, Fig. II-21).

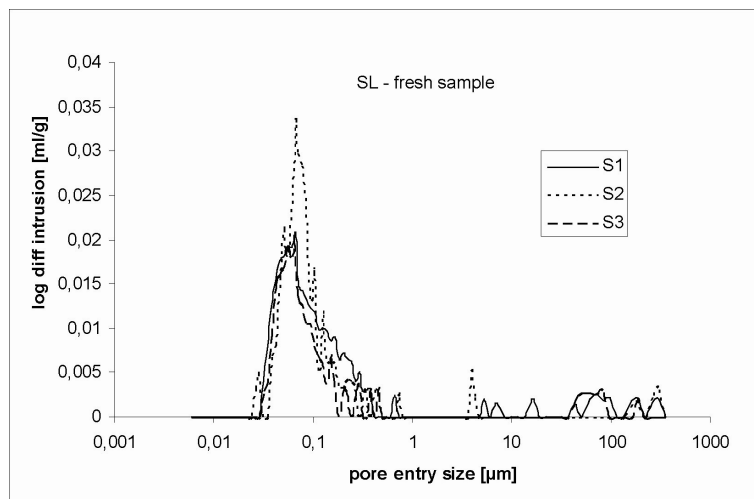


Figure II-35. MIP spectrum of three fresh samples of “Pierre de Souppes” (SL).

2.1.4. Helium pyknometry

Helium pyknometry is an intrusive non-destructive method. The principle is similar to that of mercury porosimetry: a fluid invades the porous network to measure the volume of pores in a sample. Nevertheless there are two main differences between these two techniques: since helium is a gas, the surface tension is much lower than for mercury and thus helium has access to more pores. For the same reasons, it is possible to empty the sample after measurement and perform these measurements several times on the same sample. The final value is then much more reliable since, contrary to MIP, a good reproducibility is ensured. The second difference is that it is not possible to obtain a spectrum as with MIP: since the surface tension is close to zero, as soon as helium enters the porous network it invades all the porosity. The measurements have been performed at two different locations with a Micromeritics Accupyc 1330, one at the University of Alicante (Spain) and the other at the Centre of Research on Divided Matter (CRMD, Orléans, France).

The device in fact measures the volume of a small cell by injecting helium in it. Then a small sample ($\sim 2 \text{ cm}^3$) is stored in the cell. Helium is injected in the cell with the sample. The difference between the two values gives the skeletal (or solid) volume. A precise weighing of the sample gives the mean skeletal density with a good precision. This density is generally close to 2.65 g/cm^3 (quartz density) for the sandstones and close to 2.71 g/cm^3 (calcite density) for the limestones.

2.1.5. Discussion about porosity

In order to confirm the porosity values given, other bulk and skeletal density measurements have been compared with measurements performed with mercury porosimetry and helium pyknometry (Tab. II-1). In the porosity columns, the parameters between brackets correspond to the densities used to calculate the porosity from equation (II-10): the first value corresponds to the bulk density used and the second to the skeletal density.

$$\text{Porosity}(X,Y) = \Phi_{x,y} = 1 - \frac{d_{\text{bulk},x}}{d_{\text{ske},y}} \quad (\text{II-10})$$

		bulk density (water) [g/cm ³]	bulk density (Hg) [g/cm ³]	skeletal density (water) [g/cm ³]	skeletal density (He) [g/cm ³]	skeletal density (Hg) [g/cm ³]	porosity (water) [%]	porosity (water,He) [%]	porosity (Hg,He) [%]	porosity (Hg) [%]
liais	LL	2,296	2,266	2,675	2,732	2,661	14,157	15,966	17,073	14,867
		0,019	0,007	0,016	0,025	0,020	0,696			0,690
roche franche	RL	2,129	2,117	2,673	2,692	2,610	20,340	20,902	21,367	18,901
		0,034	0,022	0,014	0,001	0,012	1,324			1,210
roche fine	FL	1,711	1,680	2,689	2,700	2,601	36,351	36,611	37,765	35,392
		0,015	0,022	0,013	0,002	0,023	0,623			0,718
soupes	SL	2,582	2,534	2,687	2,694	2,657	3,900	4,154	5,938	4,623
		0,018	0,012	0,008	0,004	0,002	0,782			0,523
hard Fontainebleau	HF	2,498	2,458	2,641	2,640	2,588	5,386	5,379	6,892	5,000
		0,020	0,013	0,008	0,002	0,031	0,809			0,641
soft Fontainebleau	SF	2,385	2,235	2,641	2,641	2,597	9,693	9,694	15,390	13,974
		0,077	0,055	0,006	0,003	0,075	2,840			1,044
chinese	CS	2,595	2,574	2,661	2,665	2,632	2,483	2,645	3,430	2,228
		0,009	0,004	0,005	0,007	0,000	0,386			0,167
green Agra	VS	2,536	2,481	2,660	2,658	2,598	4,649	4,578	6,643	4,506
		0,011	0,035	0,006	0,001	0,043	0,290			0,241
red Agra	MS	2,534	2,464	2,660	2,660	2,577	4,717	4,725	7,365	4,377
		0,005	0,025	0,005	0,002	0,027	0,223			0,067

Table II-1. Porosity and bulk and skeletal density of the nine types of stone (average value and standard deviation). Complete data can be found in annex I.

Let us focus first on the bulk densities. The values given by mercury porosimetry are always lower than the values obtained by water absorption under vacuum. This feature, although the opposite of what is expected, has been observed by Hammecker (1993) and Thomachot (2002). In fact, the only difference between the two methods is that MIP does not

Chapter II: Materials and methods

take into account the surface pores with sizes under 200 μm approximately. Thus, since it takes into account less pores than water, the bulk density should be higher with MIP (Thomachot 2002). Hammecker (1993) proposed several reasons for this contradiction, reasons which are exposed in the order of their probability: a too small sample to be representative for the entire stone; deformation of the sample due to the very high pressures reached in the porosimeter chamber; or a high amount of pores with entries under 6nm.

The skeletal densities give also good information about the meso- and micro-porosity of the samples. Helium has access to the most pores due to its gaseous state; it thus gives a very precise value of the skeletal density. For four out of the five sandstones (HF, SF, MS and VS), this value is exactly the same than the value obtained by water absorption. This comes from the fact that these stones have very few pores with entries under 50nm (IUPAC 1972). In the case of the presence of micro- and meso-pores in the samples, skeletal density obtained by pyknometry is a little higher than the one obtained with water absorption: the smallest pores are not invaded by water. This happens for instance in the case of the three lutetian limestones (LL, RL and FL) which have microporosity due to the secondary micritic cement. The porosity values in table II-1 are calculated with the equation giving porosity from bulk and skeletal densities (II-10).

The porosity which will be used and referred to in this study is the one calculated with the bulk density obtained by water and the skeletal density from helium pyknometry. This value will be considered as the most accurate for the reasons explained above. Nevertheless the variation between the different calculated porosities is still quite small.

The most porous stone of this study is the detritic limestone FL with porosity above 35%. Then the two most porous are the bidetritic cemented limestones RL and LL with porosity respectively around 20% and 15%. Nevertheless, as explained by the bidetritic nature and the heterogeneities of the grain in these two limestones, this porosity is a mean value and can vary from up to $\pm 3\%$ from one sample to the other. The soft Fontainebleau sandstone SF also has a variable porosity that can go from 4.5 to 14%. Then four stones have a mean porosity value between approximately 4 and 5%: three sandstones HF, VS and CS, and the lacustrine limestone SL. Finally, the least porous stone is the CS sandstone with a porosity of 2.5%.

2.1.6. Specific surface area

The specific surface area (SSA) is defined for a porous medium as the total surface developed on the particles forming its skeleton, and is normalized to either the volume or the weight of the sample. It is thus expressed respectively in m^{-1} or in m^2/g . It represents the surface where the adsorption of molecules or ions is possible. It depends on the pore and grain sizes: the larger SSA values are obtained with high porosity and small pore sizes. This value is obtained by measuring nitrogen adsorption-desorption at low temperature (77K). The method uses the slope of the regression line of the initial points collected at low P/P_0 . This method is named BET after Brunauer, Emett and Teller who developed it in 1938 (Brunauer et al 1938). The measurements have been performed with a Micromeritics ASAP 2010 in the University of Alicante (Spain). The SSA gives a good idea of the evaporation kinetics of a stone: the stones with a high SSA have generally a high residual saturation since more water molecules can be adsorbed by the porous network.

The stones have SSA values between 0.14 and $3.29\text{m}^2/\text{g}$. The lower values are those of the Fontainebleau sandstones (0.14 and 0.4) with big pores with entries above 5 or $6\mu\text{m}$ and low porosity. Five stones have values around $1\text{g}/\text{m}^2$: 0.73 for CS, 0.92 for LL, 1.03 for RL, 1.25 for VS and $1.48\text{g}/\text{m}^2$ for FL. All those stones show pores with minimal sizes of pore entries around 100nm on the MIP spectra. The high value for FL is explained by the very high porosity of more than 35%, and the one for VS is explained by the pore sizes around 50nm. Finally, the red Agra sandstone MS has an unexpected very high value of $3.29\text{m}^2/\text{g}$. It is all the more unexpected than its microstructural characteristics were very similar to those of the green Agra which has a SSA value of “only” $1.25\text{m}^2/\text{g}$. This high value is certainly due to the presence of clay minerals. These clay minerals can also be noticed on the mercury porosimetry spectre (fig. II-31) which indicates the presence of pores of size below the resolution of the device. No reliable data could be obtained from the adsorption-desorption curve of SL.

2.2. Geophysical properties

The objective of this part is to use geophysical methods to evaluate some physical properties at the sample scale, focusing on the anisotropic behaviour of the stones. These anisotropies are determined by the properties of both matrix and pore space distribution (Lo et al. 1986). In order to study the spatial anisotropy of the samples, it is necessary to work on

spherical samples (Vickers and Thill 1969) to avoid uncertainties due to sample heterogeneities and keep always the same contact geometry. Nevertheless it is quite difficult to shape spherical samples, thus three cylindrical cores plugged in three orthogonal directions X, Y and Z have been used (Figure II-36; Louis et al 2003). The cores have 25mm of diameter and 22.5mm length, which is the standard size for magnetic susceptibility analysis.

2.2.1. P-waves velocity

Propagation of ultrasonic waves in solids is based on the theory of elasticity. Two kinds of elastic waves polarised in two directions are commonly recorded: the longitudinal compressive wave, P-wave, and the transverse shear wave, S-wave. The P-wave velocity is obtained from the ratio of these two values. The experimental device for the elastic waves measurements includes a pulse generator Panametrics 5058 PR with a maximum voltage output up to 900V, several sets of ultrasonic P-wave transducer of 1MHz resonance frequency, and a numerical oscilloscope HP54603B. The size of the sample is precisely measured with a calliper, and the time of flight between the transducers is measured with an oscilloscope. We could not study the S-wave velocity because it was difficult to determine accurately the time of arrival of the S-wave for our samples.

The spatial variability of P-wave velocity is studied on a set of three oriented samples. For each sample, eight measurements were performed around the sample, every 22.5°. The reproducibility of the measurements from one sample to the other is ensured by the fact that each couple of samples (XY, YZ and XZ) has a measurement in common: 24 measurements are performed but only 21 are independent (Fig II-37; Louis et al 2003).

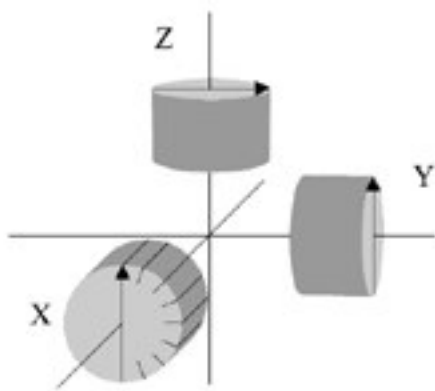


Figure II-36. Orientation of the three cylinders sampled for the geophysical study (Louis et al. 2003).

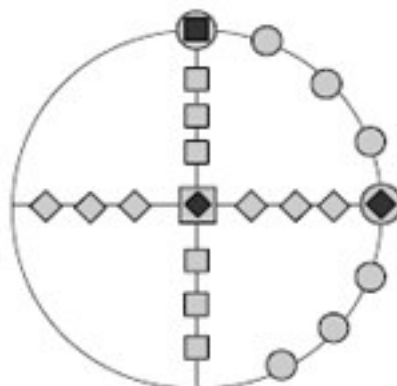


Figure II-37. 24 measurements performed on the 3 oriented cylinders (Louis et al. 2003).

The P-wave velocity is dependent of several parameters: mineral composition, porosity, presence of cracks and water content. The measured velocity in a macroscopic sample is a balanced average of the velocity in the minerals (e.g. 6060m/s in quartz, 6650m/s in calcite) and in the fluid present in the porous network (e.g. 1500m/s in water, 340m/s in air), altered by the crossing of solid-solid, fluid-fluid or solid-fluid interfaces. This means that, for several dry samples of the same stone (as is the case for the three oriented cylinders of this study), the P-waves velocity anisotropy study will depend mainly on the matrix, the porosity and the cracks. In order to try to separate the influence of these parameters, the measurements have been performed on dry and water saturated samples. The samples have been saturated under vacuum, just like in the porosity determination experiment presented earlier. The principle is based on the fact that the acoustic waves velocity is higher in water than in air. When the porous network is filled with water, the contrast between the velocity in minerals and in the pore fluid diminishes. The anisotropy of the porous network is thus diminished with saturated samples, giving more weight to the matrix anisotropy. The principal axes of the ellipsoid representing P-wave velocity variations are obtained with a numerical program written by Louis (2003) and plotted on a lower hemispheric stereogram. Two stereoplots are drawn for each set of samples: dry and water-saturated. For the reasons explained below, the two stereoplots give information respectively on the porosity and on the matrix/cracks.

2.2.2. Magnetic Susceptibility

The magnetic susceptibility χ is the degree of magnetization of a material in response to an applied magnetic field. It is thus a property of stones concerning induced magnetization, as opposed to magnetic remanence which is a remaining magnetization of a sample. Magnetic susceptibility is a dimensionless property controlled by the crystallographic directions of the minerals composing a stone (Hrouda 1982; Louis 2003). The measurements in the laboratory have been performed with an Agico KLY3S kappameter.

There are mainly three types of magnetic behaviour among the minerals: diamagnetism, paramagnetism and ferromagnetism. Diamagnetism is characterized by a negative susceptibility with low intensity ($\sim -15 \cdot 10^{-6}$). Quartz, potassic feldspar or calcite are diamagnetic minerals. Calcite is the only diamagnetic mineral with a significant anisotropic

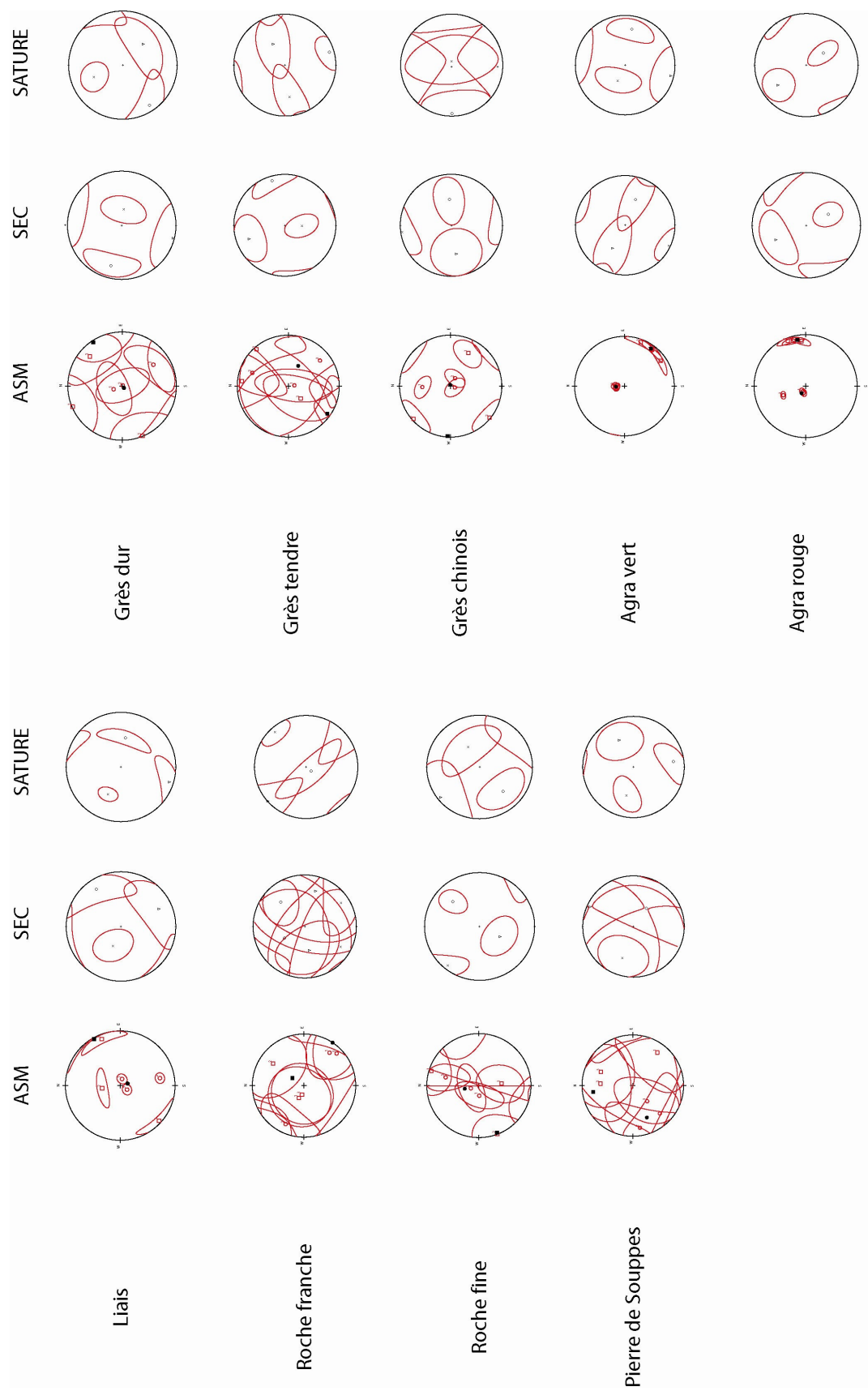


Figure II-38. Stereoplots of the principal axes of the magnetic susceptibility and P-wave velocity ellipsoids.

susceptibility ($\chi_{\max}/\chi_{\min}=1.13$; Hrouda 1982). Paramagnetism is characterized by positive values lower than 500.10^{-6} . The minerals associated with paramagnetism are phyllosilicates, mostly chlorite, biotite and muscovite. These leaf-like minerals inherit of a strong anisotropy from their crystallographic network (Tarling and Hrouda 1993). Finally, ferromagnetism is characterized by very high values of magnetic susceptibility. Main ferromagnetic minerals are hematite ($\sim 10^{-2}$) and magnetite (up to 10). Due to their very high values, a small percentage of these minerals in rocks will dominate and possibly mask the influence of other minerals of a stone.

Generally, the study of the anisotropy of magnetic susceptibility (AMS) gives information on the sedimentary fabric, detecting for instance layers that are richer in clays or ferromagnetic minerals than others. It will be performed here on the same three orthogonal cylindrical cores than before, and a similar backward method as for P-waves velocity gives a stereoplot with the three main axes for the AMS ellipsoid in each sample and their reliability zone (Figs. II-38).

2.2.3. Analysis of results

The combination of the two measurements gives good information about the general structure of the porosity and the matrix. It helps to understand the features that are inherited from the sedimentary and tectonic history of the stone, and thus explain a part of their hydromechanical behaviour. This study helps to have a very precise understanding of the microstructures of the stone, which is decisive to tackle the problem of stone weathering at this scale. For each stone, the data are presented in the form of 3 stereoplots representing the three tensors of magnetic susceptibility, the tensor of dry sample P-wave velocities and the one of water saturated sample P-wave velocities (Fig. II-38). The general anisotropy of respectively the sedimentary fabric, porosity and matrix are presented in table II-2. For each geophysical set of data, the nature of the anisotropy is reported: L for lineation, meaning that the anisotropy is defined by the maximal axis; F for foliation meaning that the anisotropy is defined by the minimal axis. The anisotropy factor is also calculated as the ratio of the difference between maximal and minimal value divided by the mean value.

	ASM (sedimentary fabric)	P waves - dry (porosity)	P waves - saturated (matrix)
LL	L $3,87\% \pm 1,71$	L 7,04%	L 9,86%
RL	L $9,3\% \pm 5,64$	F 1,16%	L 4,64%
FL	F $13,46\% \pm 10,59$	F 12,34%	F 4,42%
SL	F $0,62\% \pm 0,10$	L 9,38%	L 10,56%
HF	F $0,77\% \pm 0,18$	F 28,98%	L 7,56%
SF	F $0,96\% \pm 0,10$	L 8,84%	F 7,95%
CS	L $14,19\% \pm 3,60$	L 15,45%	F 3,89%
VS	F $1,95\% \pm 0,11$	L 10,23%	F 8,12%
MS	F $1,26\% \pm 0,09$	F 10,85%	L 6,27%

Table II-2. Nature of anisotropies and anisotropy factors
of the nine sedimentary stones.

About the magnetic susceptibility, we can notice that most of the results are difficult to analyze: most of the stones are diamagnetic, causing a very low magnetic signal. We can only notice that the two Agra sandstones (VS and MS) have a reliable direction of anisotropy which is orthogonal to the layering. The lacustrine limestone SL seems also to have a direction of anisotropy which is reproducible for the three samples, although the ellipsoids are quite large.

Concerning the P-wave velocity, we can separate the stones in three groups: those with higher anisotropy for dry measurements (FL, HF, CS and MS), those with higher anisotropy with saturated measurements (LL and RL), and those with similar anisotropy in

both cases (SL, SF and VS). A higher anisotropy factor for dry measurements suggests that this anisotropy comes mainly from the pore structure. RL and LL have a very heterogeneous and isotropic pore structure, but their detritic origin seem still to cause certain anisotropy in the matrix. Finally, the anisotropy of the three other stones (SL, SF and VS) seems to come from both the pores and the matrix. Nevertheless these results need to be considered carefully, and a thorough thin section analysis is necessary to have a more precise evaluation of the stones anisotropies and their origin.

3. Hydromechanical properties

3.1. Hydric tests

3.1.1. Water Absorption Capacity (EN 13755)

This characteristic is the part of porosity which is filled under atmospheric pressure. This test starts with a regular porosity test, with the three weighings: dry, saturated and immersed. The porosity of the samples is calculated from these three weighings as explained in 2.1.2. Afterwards the samples are dried again until constant weight. Then, they undergo capillary imbibition during the first 24 hours, and then total immersion during the last 24 hours. The final weight of the samples after 48 hours, m_{48} , is introduced in equation (II-4) and gives the value of Φ_{48} :

$$\Phi_{48} = \frac{m_{48} - m_{dry}}{m_{sat} - m_{dry}} \quad (\text{II-11})$$

Φ_{48} is always lower than global porosity. Since the imbibition is not performed under vacuum, there is always air trapped in the pores. For this purpose we define S_{48} , which the saturation of the samples reached after 48 hours. It is given by equation (II-12):

$$S_{48} = \frac{\Phi_{48}}{\Phi} \quad (\text{II-12})$$

This saturation is lower for stones with a highly heterogeneous porous network. Its value is around 1 for the three fine sandstones (CS, VS and MS) with a very homogeneous size of pores; between 0.7 and 0.8 for FL, SL and SF which have each a main family of pores but also a few pores of other sizes; 0.6 for RL and LL which have a very heterogeneous

repartition of the pore sizes; and finally only 0.4 for HF, which is due to the fact that the trapped porosity in the Fontainebleau sandstones corresponds to the macropores (50-100 μm) linked together with very fine pores corresponding to the spaces between the crystalline faces (Rousset-Tournier 2001).

3.1.2. Capillarity

The capillarity coefficient gives an idea of the imbibition kinetics of a stone by capillarity. It describes how fast a stone can be invaded by water when in contact with it. This phenomenon is due to the surface tension at the interface between two fluids, here air (non-wetting) and water (wetting). This tension moves the wetting fluid in direction of the non-wetting fluid (Rousset Tournier 2001; Thomachot 2002). Its measure has been normalized by the EN 1925 standard test. The principle is that, according to the Washburn equation and for a given surface exposed to water, the weight gain is directly proportional to the square root of time. The general aspect of the porous network can be easily deducted from the imbibition plot. There are three main types of porous imbibition kinetics (Mertz 1991, David et al. 1993) which are represented on figure II-39.

First, on figure II-39a, the weight gain shows only one breakpoint. This is characteristic for a unimodal distribution of pores which is regular in the sample. This breakpoint occurs approximately for a weight content corresponding to the water absorption capacity under atmospheric pressure of the stone. This is the case for most stones presented here (FL, SL, HF, VS and MS). But there exist two other possibilities. Figure II-39b with two breakpoints represents the weight gain for a stone with a bimodal distribution of pores, both micro- and macroporous. The filling of the pores happens successively in the two main families, the second one being generally badly connected, which seem to be the case for the soft sandstones SF and the Chinese sandstone CS. Finally, the third one (Fig. II-39c), when the weight evolution does not follow any pattern. This happens for stones with very low porosity or very low connectivity due to petrophysical heterogeneities: the liais LL, the “roche franche” RL. Nevertheless, it is sometimes difficult to make a clear difference between the last two families.

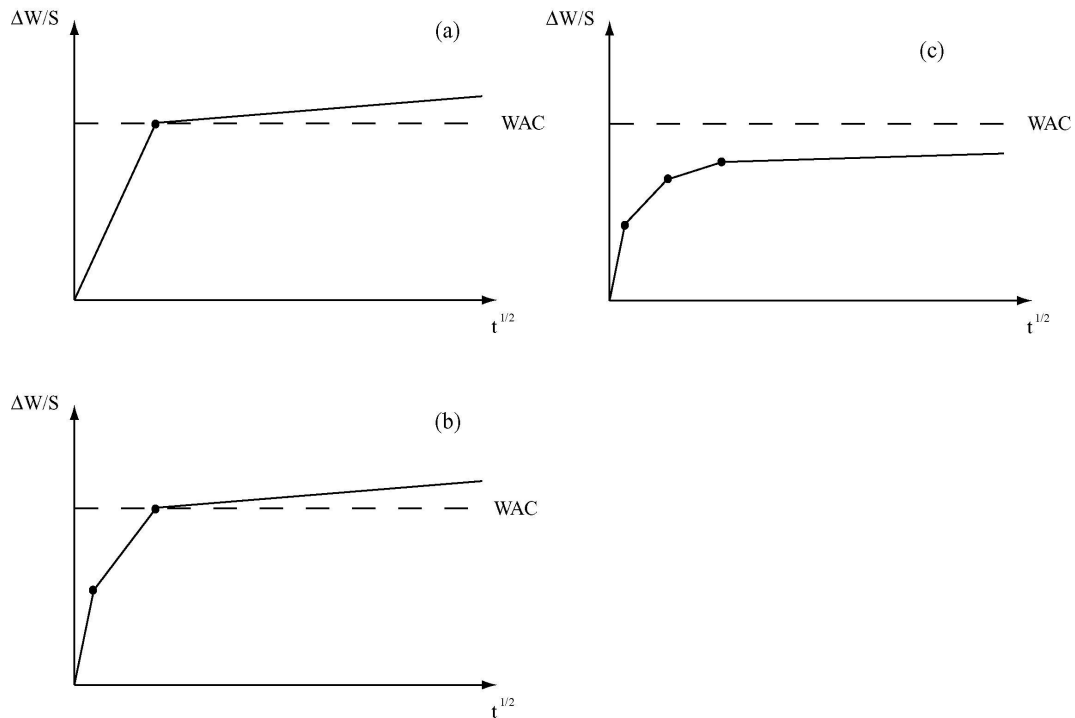


Figure II-39. Three types of capillary curves depending on the properties of the porous network. (a) unimodal pore size distribution (b) bimodal pore size distribution (c) random pore size distribution

The samples used to measure this property are cylinders of 4cm diameter and 8cm height. They have been dried in an oven until constant weight. They were put in a container with approximately 1mm of water. Weighings were performed every minute at the beginning of the test, and more spaced afterwards, depending on the capillary properties of each stone (Table II-1; complete data in annex I). The test has been stopped when the capillary front has reached the top of the sample. FL is the stone with the fastest capillary supply by far. The coefficient reaches more than $1100\text{g/m}^2/\text{s}^{1/2}$ for FL as it reaches only 80 for the second one, RL. The next two stones are LL and SF with a coefficient around $40\text{g/m}^2/\text{s}^{1/2}$ which is still quite fast. The four other sandstones (HF, MS, VS and CS) have a low capillary coefficient around $5\text{g/m}^2/\text{s}^{1/2}$. Finally, the lacustrine limestone has the lowest capillary supply with a coefficient under $1.5\text{g/m}^2/\text{s}^{1/2}$.

3.1.3. Evaporation

Evaporation is a key parameter when it comes to salt decay. The location of salt crystals is highly dependant of the evaporation rate and its correlation with capillary supply (Pel et al 2002, Ruiz-Agudo et al 2007; chapter 4 1.2 and 2.2.). It is thus very important to understand this mechanism and what are the parameters affecting this phenomenon. The

drying kinetics is dependant of numerous extrinsic parameters (relative humidity, temperature, air circulation, water content) but also of the characteristics of the porous networks (shape, size, connectivity, tortuosity) and of the surface exposed (Rousset Tournier 2001).

The water transfers in the porous networks can happen under either liquid or gaseous phase. Depending on the relative humidity, these two phases can coexist. The succession of different states is presented on figure II-40. Let us consider the sample is saturated with water. A classical evaporation plot is given in figure II-41a (Pearse et al 1949; Jouany 1981; Rousset Tournier 2001). At first, the evaporation flux is fast and depends only on the environmental parameters: relative humidity, temperature, wind velocity. Water flows in the liquid form to the evaporative surface that is always wet (Figs II-41a,b). This is possible because the capillary supply is high enough to compensate the loss of liquid water at the surface. This stage ends when the sample is not saturated any more. This is mostly due to the fact that not enough water is supplied by capillary phenomena. The water saturation in the sample at the end of this stage is called critical saturation S_C . The end of this phase is determined by the rupture of the water continuity throughout the sample.

Afterwards, during phase II, the weight loss stops to be linear as a function of time. During this period the evaporative surface dries and external parameters become less influent on the evaporation kinetics. Evaporation occurs from this moment both through capillary flow along pore walls and in the form of water vapour diffusion through the porous network (Figs. II-41c,d). The drying velocity diminishes progressively during this phase as the diffusion processes becomes more important than capillary flow. Hammecker (1993) suggested that the weight loss during this phase was linear compared to the square root of time.

Finally, phase III is characterized by a constant but very slow weight loss. There is still water in the sample but it does not flow by capillarity. The evaporative surface is totally dry and evaporation occurs only in the form of water vapour diffusion. The weight loss when the water content in the sample is in equilibrium with the relative humidity RH of the environment (Figs II-41e,f).

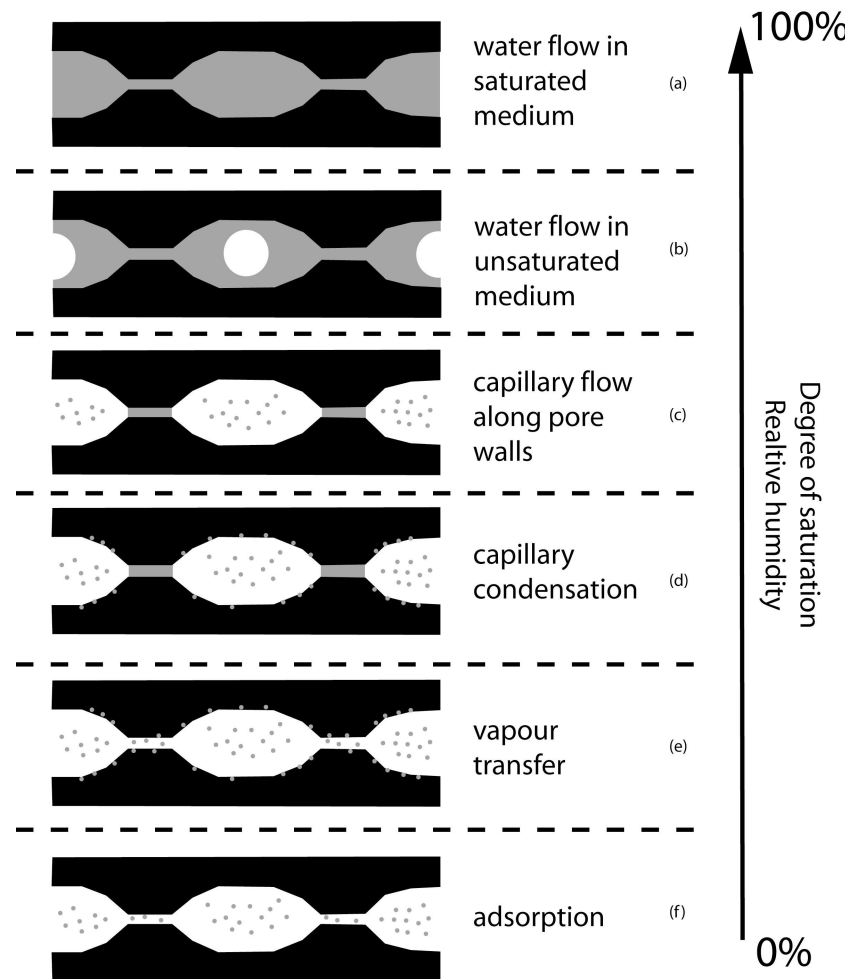


Figure II-40. Stages in the wetting of a porous system (Beck et al. 2003, after Rose 1963).

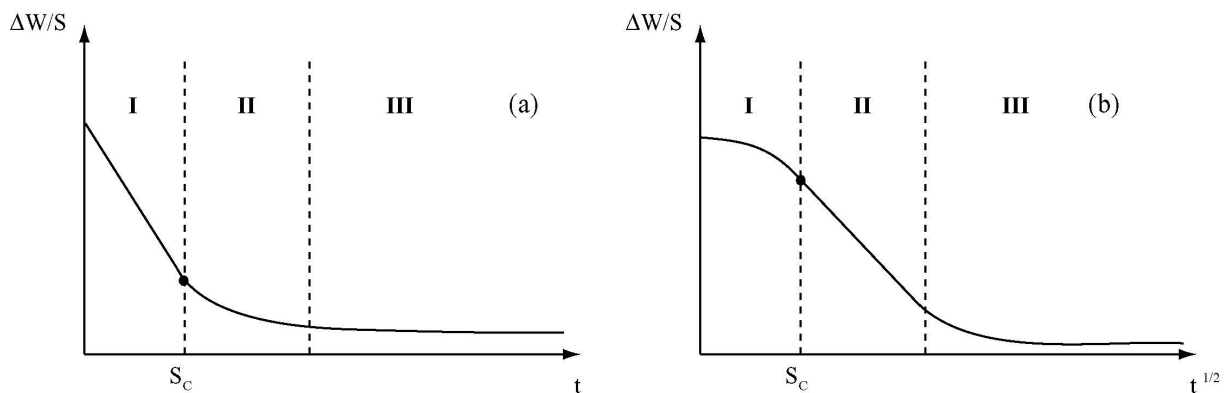


Figure II-41. General evaporation kinetics for a stone plotting the weight loss as a function of:
 (a) time (b)square root of time (Hammecker 1993).

The parameter usually chosen to quantify the evaporation properties of a stone is the weight loss rate during phase I. In this study a different parameter has been used. The usual

parameter is not only dependant of the stone, but also highly dependant of the external conditions of the test. Since we wanted a parameter depending only on the characteristics of the microstructures of a stone, the slope of the phase II of the plot representing the weight loss as a function of the square root of time (Fig. II-41b) has been chosen (Hammecker 1993).

3.2. *Mechanical tests*

Only two types of mechanical tests were performed on the samples: uniaxial compression and traction by brazilian test. The strength which has been mostly considered in this study is the tensile strength, since it is now quite unanimously considered that the stones break in traction before compression: the tensile strength is approximately 10 times lower than compressive strength.

The uniaxial compressive test is performed on cylinders of 2.5 to 4cm diameter and with length twice as long as the diameter. The axial load exerted by the press is along the main axis of the cylinder. The strain rate of the loading is 10^{-5} s^{-1} . The brazilian test which evaluates the tensile strength of the stone is an indirect measurement. It simulates tension with a compressive load in uniaxial conditions. The only difference is that the samples are cylinders of 4cm diameter and 2cm length, and they are put in the press so that the load is applied along the sample diameter. Only tensile strength measurements have been performed on all the samples since it needs much less material to perform enough measurements to ensure reproducibility. Nevertheless, a study of the evolution of mechanical strength during the weathering cycles has been performed on the detritic limestone FL (4.1.3.). In this particular study, Brazilian tests and compressive tests on 2.5cm diameter cylinders have been performed seven times along the tests.

The least resistant stones are the soft Fontainebleau SF and the detritic limestone FL with a tensile strength of approximately 1.5MPa. The other stones have all a tensile strength in the range between 3.0 and 6.0MPa, except the two Agra sandstones (VS and MS) which have a high strength of 15.0 and 16.0 MPa.

4. *Accelerated ageing by salt decay*

This work aims to understand the main processes governing salt decay of porous stones. The method chosen is to simulate decay with experimental accelerated ageing

Chapter II: Materials and methods

methods. This method has been widely used to simulate natural weathering of stone: salt (Sperling and Cooke 1985; Goudie 1986; Goudie 1993; Goudie and Viles 1997) but also frost (Thomas 1938; Remy 1993; Prick 1995; Nicholson and Nicholson 2000; Thomachot 2002), thermal shock (Kessler 1919; Widhalm et al 1996; Zeisig et al 2002;) and combination of them (Robinson and Williams 2000, Williams and Robinson 2001). All these tests have led to the elaboration of European standards for natural stone, which allow to define if a stone is durable enough or not regarding the salt (EN 12370, 1999), frost (EN 12371, 2001) or thermal shock (EN 14066 2003).

In this study, the basis for experimental work is the EN 12370 Standard test about damage by crystallization of salts. This test is performed on 4x4x4cm³ samples which have been dried until constant weight before the test. This drying consists in putting the samples in an oven at 105°C, weighing the sample every 24H. Constant weight is reached when the sample weight is exactly the same than after the latest weighing, with a precision of 0.01g. This accelerated ageing test is composed of fifteen 24h cycles with 3 stages: 2h of imbibition with a brine containing 14% of decahydrate sodium sulfate (mirabilite: Na₂SO₄.10H₂O), 16-20h of drying in an oven at 105°C, 2-6h of cooling down at room temperature. These conditions aim to match the natural conditions in the Negev desert which are those who have proven to be the most dangerous for the stones (Goudie 1993; Goudie and Viles 1997). At the end of the test, the samples are cleaned from their salt and dried until constant weight. The result of the test is the weight loss of the sample after fifteen cycles.

During this study, this test has been modified several times in order to understand the effect of some key parameters on the decay of stones. The parameters which have been modified are: evaporation possibilities (by isolating some of the faces), temperature during imbibition (5, 25 and 50°C), imbibition mode (immersion or capillary imbibition), concentration of salts in the brine (5, 12 and 25 wt.% Na₂SO₄), temperature of drying (105 and 125°C), shape and size of the samples (4cm cubes, 7cm cubes and cylinders). The details of each experiment will be given in the corresponding part.

After introducing the stones and methods used, the next chapter will focus on the problem of salt crystallization itself. The general aspects will be exposed first, followed by a detailed study of the salt used in this work, sodium sulphate.

Chapter II: Materials and methods

SALT CRYSTALLIZATION

CONTENT

1. <i>Experimental results</i> _____	65
2. <i>Theories of salt damage</i> _____	66
3. <i>Sodium sulphate</i> _____	69
3.1. <i>Mechanism of damage</i> _____	69
3.2. <i>Thermal recording during experimental weathering of limestones: the role of imbibition on salt crystallization and rock decay (article1; Journal of crystal growth)</i> _____	70

Chapter III: Salt crystallization

As stated in the introduction, salt damage has a devastating effect in various domains concerned by stone decay: archaeology, architecture, civil engineering, geomorphology, petroleum geology, environmental sciences... Crystallization of salts is a complex mechanism which depends of several different factors related to: the environment (temperature, relative humidity, wind direction...), the stone (porous network, pore size and shape, connectivity, tortuosity...) and the salt (surface energy, contact angle, hypothetic hydrated phases and their stability conditions...). This is the reason why it is necessary to separate all these aspects in order to tackle them in a simplified way.

1. Experimental results

Scientists are working on the vast problem of salt damage for more than 150 years (de Thury 1828; Turner 1833). At that time, in order to assess the durability of stones towards freeze-thaw cycles, scientists were testing them with accelerated ageing with salts. Lavalle (1853) was the first to provide experimental evidence that growing crystals exert a pressure as he observed the crystallization of salts under other crystals. The first experimental evidences of the pressure exerted by the growth of loaded crystals date from the first half of the XXth century (Becker and Day 1906, 1916; Taber 1916; Correns and Steinborn 1939). The principle of the experiment was to apply loads on crystals in a supersaturated solution. Despite this load the crystals were still growing in the solution, giving evidence that they exert a pressure against the load. Afterwards, Wellman and Wilson (1965), following a work on freezing by Everett (1961), proposed that the stones with high proportion of micropores connected to macropores are more susceptible to decay. According to them, the crystals grow in macropores for minimal energy reasons, and the solution is provided by the connected micropores. Nevertheless no experimental evidence has allowed justifying this theory.

All these global theories do not clearly explain the contrasting behaviour of different types of salts: why are some of them more destructive than others? Why the alteration patterns are different? What is the influence of external parameters such as temperature or relative humidity? What is the influence of stone parameters like porosity or tensile strength? A first answer comes from Zehnder and Arnold (1989) who showed that the pattern and degree of damage depend on the crystallographic properties of the mineral, mostly on the shape. It has been established that the crystalline network for a single salt depends on the supersaturation

of the solution and on the external parameters (Suanagawa 1981; Rodriguez-Navarro et al. 2000; Lopez-Arce and Doehne 2006). The supersaturation depends also highly on temperature, relative humidity, evaporation. Evaporation itself depends on the specific surface area of the stones, the roughness, but also on solution properties like viscosity. Other aspects also have an indirect influence on salt damage. For instance the presence of water in a porous network reduces considerably its mechanical strength. Dunning and Hulf (1983) have experimentally demonstrated that water enhances the crack propagation in a saturated stone. Beck (2006) has proven that this enhancement does not need a saturated stone, but only saturation over the critical saturation of the stone. All these various parameters thus have an influence on salt decay, which forces to consider all these aspects when studying salt damage.

2. Theories of salt damage

When water flows in a porous network, several mechanisms can cause a variation of concentration and thus supersaturation: cooling or heating, dissolution of pre-existent salt (Chatterji and Jensen 1989), evaporation (Flatt 2002, Coussy 2006). But the mechanism itself is yet poorly understood. Several mechanisms have been proposed to explain these crystallization damages: crystallization pressure, hydration pressure, thermal expansion, chemical weathering, osmotic pressure or hydraulic pressure (Rodriguez-Navarro and Doehne 1999). Although all these mechanisms certainly have an influence on salt damage, crystallization pressure has been identified as the most important.

Several crystallization mechanisms have been proposed as the origin of the damage caused by salt: Correns (1949), based on experiments of Taber (1916) with alum crystals, proposed that damage was caused by a crystal growing against a confining pressure. This pressure would be transmitted to the pore walls only if a thin supersaturated solution film exists between the two. The presence of this film is dependent of the relationship between the interfacial tensions of the stone-solution-salt triplet. Correns (1949) proposes an equation to calculate the crystallization pressure of a crystal growing from a saturated solution:

$$P = \frac{RT}{V_s} \cdot \ln\left(\frac{c}{c_s}\right) \quad (\text{III-1})$$

where R is the ideal gas constant (8.314J/K/mol), T the temperature of the solution in Kelvin, V_s the molar volume of the crystal, c is the concentration of salt in the brine and c_s the saturation concentration. Weyl (1959) proposes an extended model which considers Correns model as a special case. In this model the supersaturated film is absolutely necessary between the salt crystals and the stone to allow diffusion. Damage happens when this film is saturated, and thus causes the deposition of materials between the crystals and the pore wall. The thickness of the film was expected to be a few nanometres, which has been later experimentally observed on sodium sulphate crystals with ESEM by Rodriguez-Navarro et al. (2000).

Everett (1961) and Wellman and Wilson (1965) adopted a completely different approach in their thermodynamic studies. Note that Everett worked on freezing and that Wellman and Wilson adapted the same approach later for salt decay. They considered the problem from the side of the free energy of crystals. In order to keep this energy as low as possible, the interfaces surface area should be also kept as low as possible. The work required for the crystal growth on one face is $(P_l - P_s)dV$, P_l being the liquid pressure, P_s the solid pressure and dV the volume increase of the crystal. This quantity has to be equal to the work required to extend the surface which is σdA , where σ is the interfacial tension between the solution and the crystal, and dA the increase of surface area of the crystal. The independence of σ and V gives equation (III-2):

$$P_l - P_s = \sigma \frac{dA}{dV} \quad (\text{III-2})$$

They concluded, as stated before, that, due to this energy minimalization, damage must come from crystal in the big pores fed by solution provided by the micropores. They completed their study a few years later (Wellman and Wilson 1968) by giving an equation for the particular case of a crystal growing in a large pore of radius R connected to a small pore of radius r :

$$\Delta P = 2\sigma \cdot \left(\frac{1}{R} - \frac{1}{r} \right) \quad (\text{III-3})$$

This model explains their experimental observations about the stone with large amount of micropores connected to macropores being more sensitive to salt decay. Nevertheless, Evans (1970) and Tiller (1991) have objected that, although this model would be valid with liquid or gaseous phases, this theory is not applicable with solids.

More recently, La Iglesia et al. (1997), Benavente et al. (1999) and Scherer (1999) have developed a model about crystallization pressure exerted by crystals in equilibrium with environmental conditions. They both have derived equations from Correns model (Correns 1926, 1949; Correns and Steinborn 1939). This model considers that crystals in small pores (fewer than 100 nm) continuously exert a pressure on the pore walls. This pressure can reach 20 to 30 MPa, which is above the tensile strength of most building stones. Finally, Scherer (2004), Steiger (2005a,b) and Coussy (2006) developed, on the basis of Everett's model (1961), equations for crystallization pressure in larger pores. This model considers that the crystal growing under stress in large pores, that is to say crystals which are not in equilibrium, exert a pressure on the pore wall which is under load. The supersaturation in this case is local, close to the loaded face, and is due to the difference of saturation between the loaded and unloaded faces of the crystals. Steiger (2005a,b) demonstrated that these two approaches were in fact thermodynamically equivalent.

Nevertheless, these two theories still do not give satisfying correlation with experimental results. For instance, several authors have calculated these pressures according to different equations (Winkler and Singer 1972; Flatt 2002; Steiger 2005a). They found that sodium chloride causes crystallization pressures much higher than mirabilite (between 2 and 7 times higher), although it is widely admitted that mirabilite causes more damage than sodium chloride (Goudie and Viles 1997; Rodriguez-Navarro and Doehne 1999). This comes from the fact that high degrees of supersaturation are not easy to obtain for all different salts. The danger of sodium sulphate comes from the fact that the existence of two phases with different solubilities stable at room temperature makes supersaturation quite easy to obtain (Chatterji and Jensen 1989).

3. Sodium sulphate

3.1. Mechanism of damage

As stated earlier sodium sulphate is known to be one of the most destructive salts in the standardized accelerated weathering test. It has been used since the 19th century to test the durability of natural building stones (de Thury 1828; Turner 1833). At this time it was used to simulate frost decay in laboratory conditions. For this reason it has been widely studied in the recent literature (Rodriguez-Navarro and Doehne 1999; Rodriguez-Navarro et al. 2000; Flatt 2002; Tsui et al. 2003; Lopez-Arce and Doehne 2006). Its particularity is that it has two different phases stable at room temperature, depending on the relative humidity: an anhydrous phase called thenardite and a decahydrate phase called mirabilite (Fig. ART1-1). Several other metastable phases have been observed under particular conditions, for instance the heptahydrate phase (Sperling and Cooke 1985) or a yet unidentified phase (Geikinger and Putnis 2007).

Stones suffering from sodium sulphate crystallization generally show mostly contour scaling (Rodriguez-Navarro and Doehne 1999; Ioannou et al. 2005; Ruiz-Agudo et al 2007) and sometimes granular disintegration. The occurrence of one or the other damage depends mostly on the experimental conditions (cf. chapter 4 2.2). It has been clearly established that mirabilite is the most damaging phase of sodium sulphate (Tsui et al. 2003). Thus the main difficulty for understanding the mechanism of sodium sulphate decay is to constrain precisely the crystallization sequence of sodium sulphate in the porous network of a stone. This sequence is composed of crystallizations and dissolutions which are exothermic processes: this is the reason why following the thermal evolution of the samples could give crucial information to decipher this sequence.

3.2. Thermal recording during experimental weathering of limestones: the role of imbibition on salt crystallization and rock decay (article1; Journal of crystal growth)

The principle of this work is to perform a thermal monitoring in different locations of the samples in order to record the rapid variations of temperature and the temperature steps. The steps should correspond to changes of state (the energy given by heating is used by the change of state, and thus the increase of the sample temperature stops). The rapid variations correspond to crystallization or dissolution of salts which are either endo- or exothermic: thenardite dissolution is exothermic and mirabilite dissolution is highly endothermic. It is thus possible to evaluate the kinetics of the reactions through thermal monitoring.

“Thermal recording during experimental weathering of limestones: the role of imbibition on salt crystallization and rock decay”

Ronan Hébert¹, Matthieu Angeli¹, Jean-Philippe Bigas² and David Benavente³

¹ Université de Cergy-Pontoise

Département de Sciences de la Terre et Environnement

5 mail Gay-Lussac, Neuville-sur-Oise

95031 Cergy-Pontoise CEDEX

France

² CHRYSO

7 rue de l'Europe

45300 Sermaises

France

³ Universidad de Alicante

Departamento de Ciencias de la Tierra y del Medio Ambiente

Laboratorio de Petrologia Aplicada

Apartado 99

03080 Alicante

España

Submitted to Journal of Crystal Growth on July 27th, 2007

Abstract

Thermocouples have been set up on and within cubic samples in order to record the temperature evolution of limestone during accelerated ageing cycles (EN12370 test) by sodium sulphates under different climatic conditions. Results of this experimental study show that, under certain conditions (temperature and salt concentration), mirabilite starts to crystallize during the imbibition stage because of evaporative cooling allowing the crossing of liquidus of the $\text{Na}_2\text{SO}_4\text{-H}_2\text{O}$ system, and not only during drying. Moreover, these records allow to propose different temperature-composition-time paths within the $\text{Na}_2\text{SO}_4\text{-H}_2\text{O}$ binary system and suggest that the sequence of phases to crystallize may be responsible of different types and mechanisms of damage, as well as different intensities. This study confirms that mirabilite and the reaction between thenardite and mirabilite play a major role on rock decay, whilst thenardite on its own has no or minor effect. In addition, pore-filling salts seem to modify and lower the heat capacity of rock.

Résumé

Des thermocouples ont été fixés sur et à l'intérieur d'un échantillon cubique afin d'enregistrer l'évolution de la température d'un calcaire au cours de tests de dégradation accélérée par cristallisation de sulfate de sodium (EN 12370 1999) sous différentes conditions climatiques. Les résultats de ces expériences montrent que, sous certaines conditions (température et concentration de sels en solution), la mirabilite commence à cristalliser pendant la phase d'imbibition. Le refroidissement dû à l'évaporation permet de franchir la courbe du liquidus du système $\text{Na}_2\text{SO}_4\text{-H}_2\text{O}$, et pas uniquement pendant le séchage. De plus, ces enregistrements proposent différents chemins température-composition-temps pour le système binaire $\text{Na}_2\text{SO}_4\text{-H}_2\text{O}$. Ils suggèrent aussi que la séquence de cristallisation des phases peut être responsable de différents mécanismes d'endommagement, ainsi que de différentes intensités. Cette étude confirme que à la fois la mirabilite et la réaction entre la thénardite et la mirabilite joue un rôle majeur en ce qui concerne l'altération des roches, alors que la thénardite seule n'a que peu d'effets. De plus, les cristaux remplissant les pores semblent diminuer la capacité thermique de la roche.

Introduction

Sodium sulphates are recognized to be among the most destructive salts for porous stones, and other building materials such as concrete or brick (Goudie and Viles 1997). Their study is therefore very important to fully understand their crystallization process in porous networks and, in the future, to find a way to prevent or limit their damage to porous materials.

Sodium sulphates occur under two stable phases (fig. ART1-1; Hougen et al. 1954; Flatt 2002; Kracek 1928): mirabilite (Mir : $\text{Na}_2\text{SO}_4 \cdot 10\text{H}_2\text{O}$) and thenardite (Thnd : Na_2SO_4); a heptahydrated form ($\text{Na}_2\text{SO}_4 \cdot 7\text{H}_2\text{O}$) which is metastable is also known (Partington 1961; Gmelin 1966; Sperling and Cooke 1985; Genkinger and Putnis 2007). According to the $\text{Na}_2\text{SO}_4 - \text{H}_2\text{O}$ binary system (fig. ART1-1a) and the T-Relative Humidity diagram (fig. ART1-1b), Mir and Thnd have very different conditions of stability. At atmospheric pressure, Mir does not exist above 32.4°C (temperature limit of mirabilite stability which will be referred in this paper as TLMS which is actually precisely 32.384°C according to Partington (1961) and Gmelin (1966)). Mir can crystallize either directly below 32.4°C from the cooling of a solution with a Na_2SO_4 content below 30,1 wt.% weight fraction, or as the result of a peritectic reaction (fig. ART1-1a) when cooling a solution with a Na_2SO_4 content above 30,1 wt.% weight fraction. This reaction, improperly called sometimes hydration of thenardite, occurs at 32.4°C and corresponds to a disequilibrium between former precipitated thenardite crystals and residual solution. This disequilibrium leads to the dissolution of thenardite to produce mirabilite, which has been recently observed by Rodriguez-Navarro et al. (2000). This peritectic reaction indicates that mirabilite is just not produced by hydration of thenardite, but results first from a dissolution reaction of thenardite and second from precipitation. Thenardite, on its side, can form directly when cooling a solution with a high Na_2SO_4 content and at high temperature, or by dehydration of Mir ($\text{Mir} \rightarrow \text{Thnd} + \text{H}_2\text{O}$).

Recent studies suggest that the impact effect of weathering is greater for mirabilite than for thenardite and also that the reaction $\text{Mir} \rightarrow \text{Thnd} + \text{H}_2\text{O}$ plays a major role in rock decay (Flatt 2002; Rodriguez-Navarro and Doehe 1999; Scherer 1999; Tsui et al. 2004; Benavente et al. 2004; Steiger 2005). The reaction is very sensitive to relative humidity as shown in figure ART1-1b, but requires high values of relative humidity (above 60%) all the same. In this diagram, mirabilite is the “high relative humidity – low temperature” (HRH-LT) phase, thenardite the “low relative humidity – high temperature” (LRH-HT) phase. According

to Rodriguez-Navarro & Doehe (1999) and Genkinger & Putnis (2007) the reaction $\text{Mir} \rightarrow \text{Thnd} + \text{H}_2\text{O}$ is more efficient in the sense of “hydration” of thenardite which is much faster than the reaction involving dehydration of mirabilite. Despite these numerous recent experimental studies, crystallization of sodium sulphates remains a matter of debate.

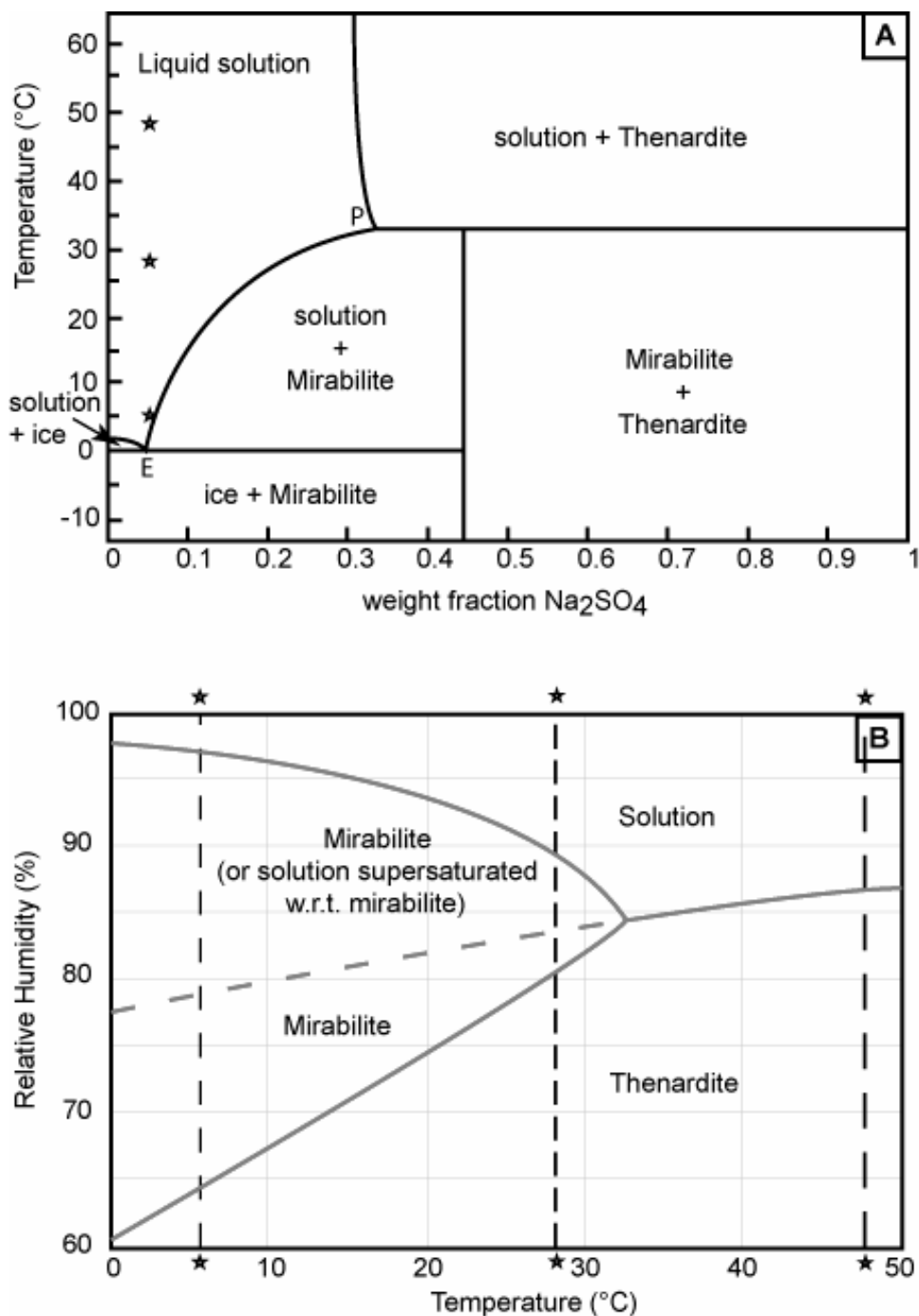


Figure ART1-1. Stability domains of sodium sulphates: (a) into the $\text{H}_2\text{O}-\text{Na}_2\text{SO}_4$ phase diagram (adapted from Hougen et al., 1954); (b) into the T vs RH diagram (after Flatt, 2002; data from Kracek, 1928). Stars represent the three different experimental conditions of this study.

The aim of this experimental study, is to precise the Temperature-Composition-time path (Fig. ART1-1), with the manner of a metamorphic PTt path, of a limestone (well characterized from physical properties point of view; Angeli et al. 2007) during accelerated ageing cycles derived from EN 12370 standard test (1999) in order to better constrain the role of the different sodium sulphates phases on rock decay.

This study confirms that thenardite on its own does not cause any rapid and important damages as mirabilite and the mirabilite-thenardite reaction do (Tsui et al. 2003). Temperature and salt concentration (in particular supersaturation (Correns 1926; Benavente et al. 1999; Scherer 2004; Steiger 2005; Coussy 2006)) play a major role concerning the intensity of these damages. But the most striking result of this study is that crystallization of mirabilite may occur as of the imbibition due to evaporative cooling in addition to the “rehydration” of the system, and not only during drying, and this early crystallization causes intense weathering. This study also suggests different possible Tt paths, i.e. different sequences of phases to crystallize and it is likely that intensity and mechanisms of rock weathering may be different from a sequence to another.

1. Materials and methods

1.1. Materials

Three cubic (~7x7x7 cm) samples of a lutetian aged limestone from the Parisian Basin commercially known as “Roche fine” have been used in this study. This rock has been chosen for several reasons: it is relatively homogenous from a sample to another, it has been widely used for construction in Paris in the past time (buildings and historical monuments), it is one of the rocks imposed for restoration and construction in the protected areas of the “Île de France” region, and it is also the rock that has been used in previous experiments which are at the origin of this study (Angeli et al. 2006, 2007, accepted). It is a fine-grained detritic limestone made of calcite (90%) and quartz (10%) with a high porosity (37.2%) and a very low tensile strength (1.5 MPa) (Angeli et al. 2007). Complete hydromechanic properties are available in table 1. Three thermocouples are set up on and within each sample (fig. ART1-2) in order to record temperature during imbibition-drying cycles. A thermocouple is placed on the upper face of the cube. The two others are placed inside the sample (respectively centre and quarter of the cube; see fig. ART1-2). These two thermocouples are placed inside a drill

“Thermal recording during experimental weathering ...”

75

hole, which is filled up with a similar porous media to the studied rock (a mixing of lime and FL powder resulting from drilling).

Porosity (%)	37.2
Absorption (%)	75.9
Bulk density (g/cm ³)	1.7
Evaporation coefficient (g/m ² /s ^{1/2})	66.9
Capillary coefficient (g/m ² /s ^{1/2})	1106.1
Mean pore radius (μm)	12.004
P wave velocity (m/s)	2898
Tensile strength (MPa)	1.5

Table ART1-1. Hydromechanic properties of the “Roche Fine” (from Angel et al., 2007).

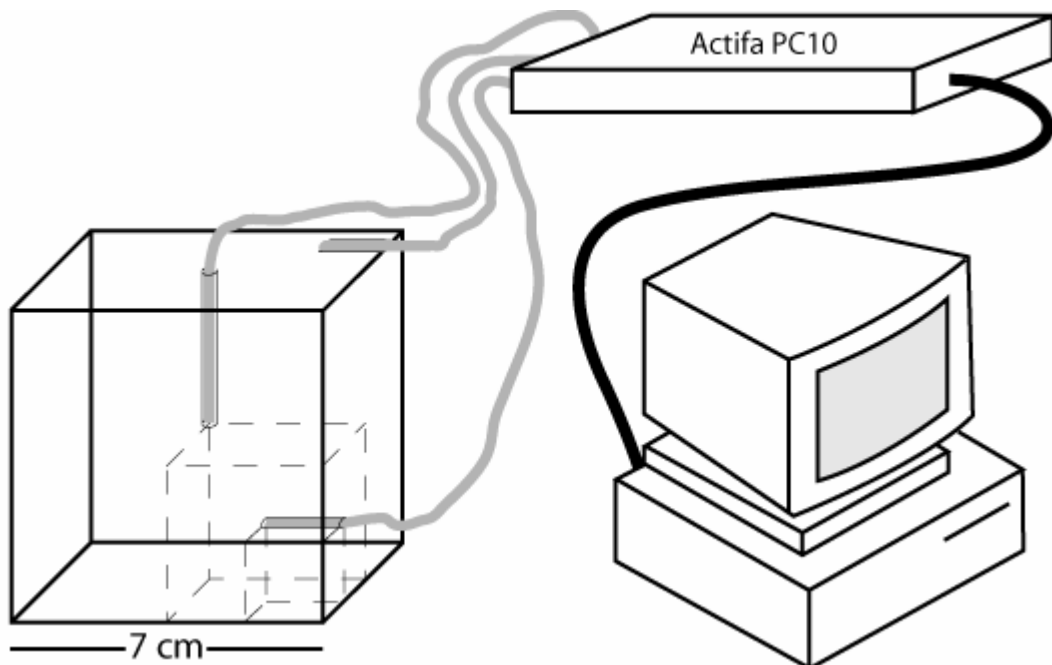


Figure ART1-2. Experimental setup of the thermocouples within the cubic samples used in this study.

Thermocouples (type K) are connected to a thermal acquisition station (Actifa PC10) with 10 to 30 recording channels (fig. ART1-2). The acquisition station is connected to a personal computer using ® actifa LTC-10 software for programming the thermal station and recording data. According to the manufacturer, accuracy of measurement is $\pm 0.5^{\circ}\text{C}$.

1.2. Experimental procedure (fig. ART1-3)

The three samples are placed in three different ambient temperatures (or climatic conditions): 5°C (cooled incubator; relative humidity $\pm 29\%$), room temperature ($\text{RT} = 28\text{-}29^{\circ}\text{C}$ relatively high because tests have been made during dryness period, relative humidity $\pm 40\%$), and 50°C (noted 50°C on sample but actually 47°C ; drying oven; relative humidity $\pm 23\%$). Note that two ambient conditions are below the temperature limit of mirabilite stability (32.4°C), the third one being above which means that no mirabilite will occur for this experimental condition (and relative humidity is below 60%, see figure ART1-1b).

24 hours accelerated ageing cycling performed in this study is made of three different stages: (i) imbibition – (ii) drying – (iii) cooling (return to initial ambient temperature). Timing for each stage is modified from the EN 12370 standard test (1999) about stone resistance to crystallization of salts in pores.

(i) 2 hours imbibition with a solution of 5.5 weight % Na_2SO_4 is realized for the three different ambient temperature conditions. Note that temperatures of imbibition solution are the same as ambient temperatures, i.e. respectively 5°C , RT and 50°C (solutions are stored in the different temperature conditions). Samples soak in 0.6-0.8 mm height of solution. The level of solution is maintained constant during all that stage. Imbibition solution has been prepared with sodium sulphate decahydrate from Roth (Art Nr x892.3; $\geq 98.5\%$ Ph. Eur.) and demineralised water.

(ii) Drying: All the three samples are placed in a drying oven at 105°C for 16 hours.

(iii) Cooling: samples are replaced in their original ambient temperature for 6 hours during which they return from 105°C to respectively 5°C , RT and 50°C .

Five full cycles have been performed during which temperature was regularly recorded (every 5 seconds). A sixth cycle has been started but not completed. Indeed, samples did not undergo the return to ambient temperature but they underwent a longer drying stage instead. The reason for this change will be discuss further (discussion section).

A cooled incubator (® LMS 303NP) is used for the 5°C ambient environment. 50°C ambient temperature is obtained using a ® block fisher drying oven and drying stage takes place in a ® memmert UE600 drying oven. Temperature is set up with a precision of $\pm 0.1^{\circ}\text{C}$ for LMS and memmert instruments.

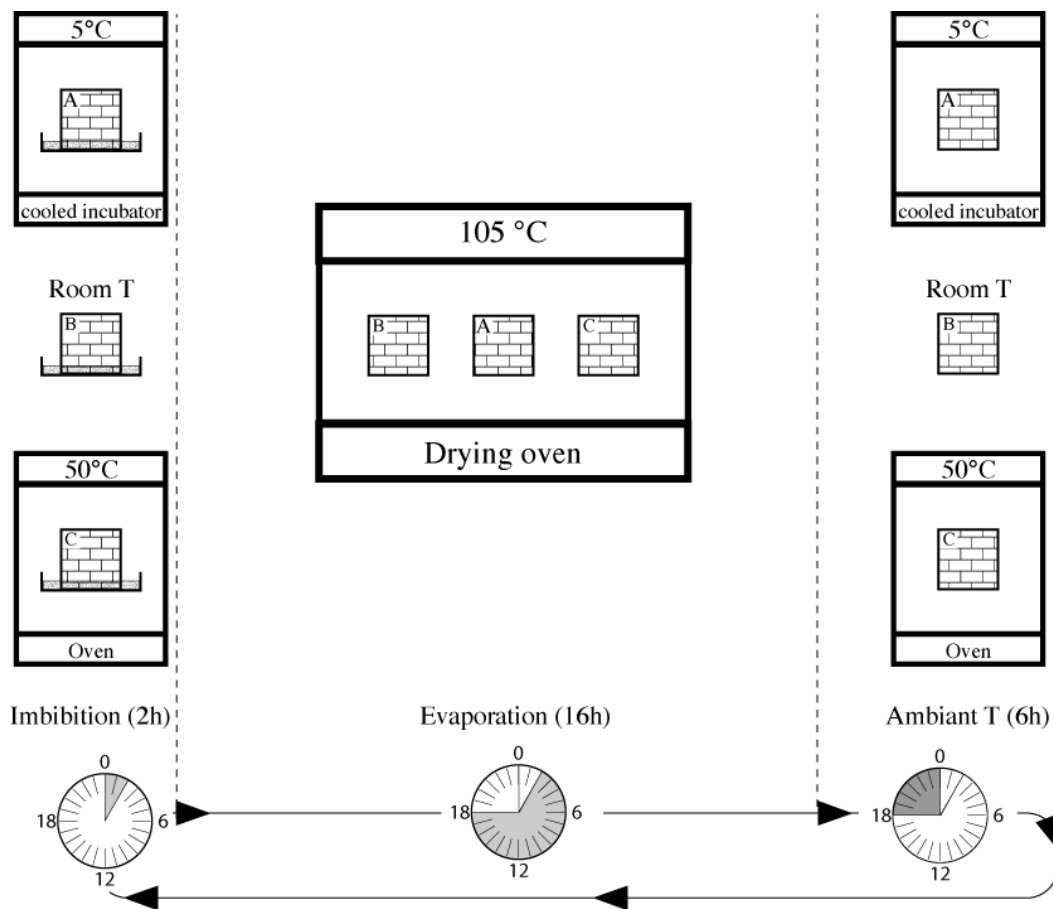


Figure ART1-3. Experimental procedure of accelerated ageing test derived from EN 13270 (1999).

2. Results

In this section we describe on one hand the evolution of rocks decay regarding the weathering cycles (fig. ART1-4), and on the other hand the temperature evolution during 120 hours cycling (fig. ART1-5) for each thermocouple with respect to the stage of the cycle.

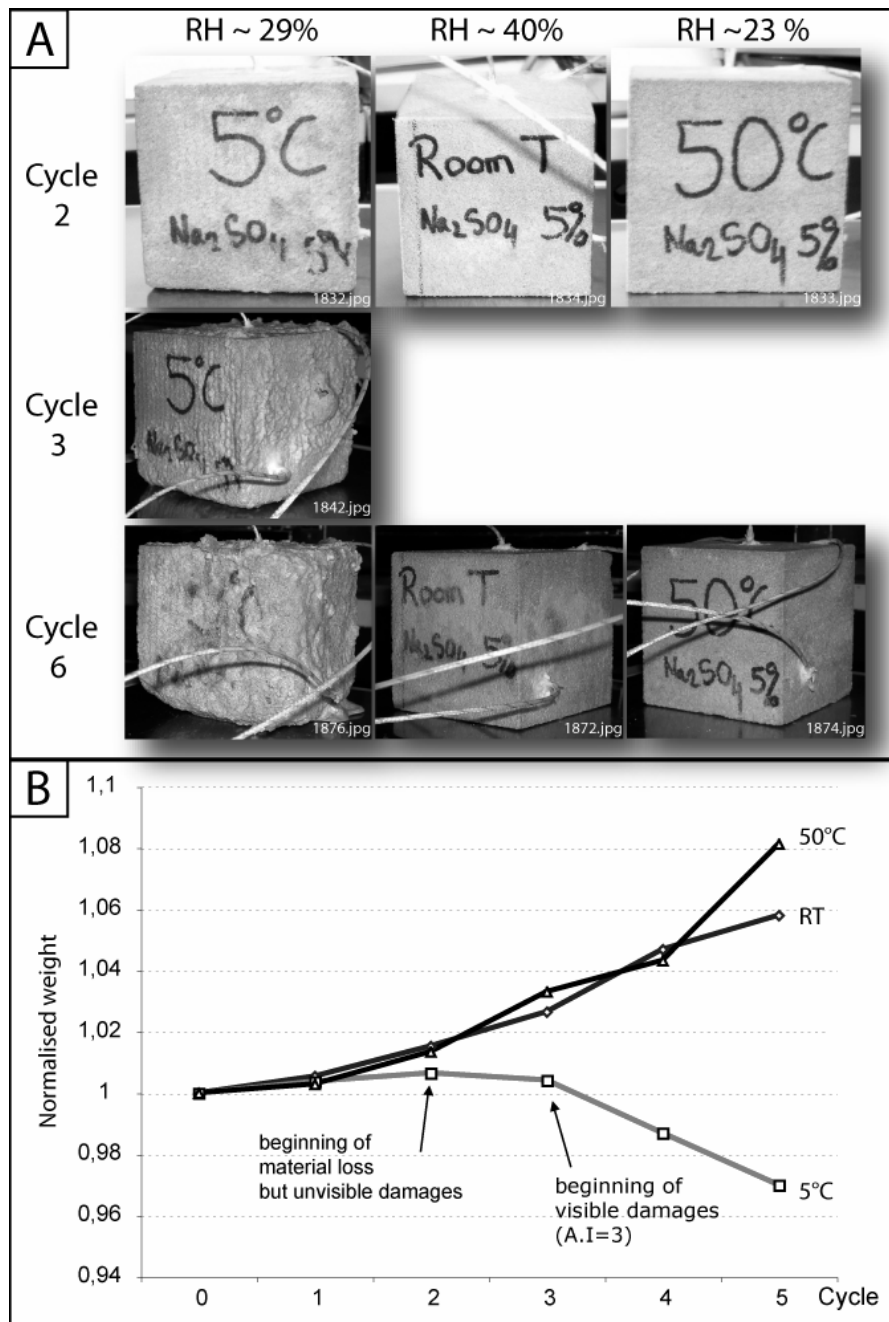


Figure ART1-4. Follow-up of the damages: (a) selected pictures of the samples after 2 and 3 cycles, and at the end of the experiment. Samples RT and 50°C do not show any visual damages. (b) normalized weight evolution during 5 complete cycles for the three different samples.

“Thermal recording during experimental weathering ...”

79

Hébert R, Angeli M, Bigas JP and Benavente D (submitted)

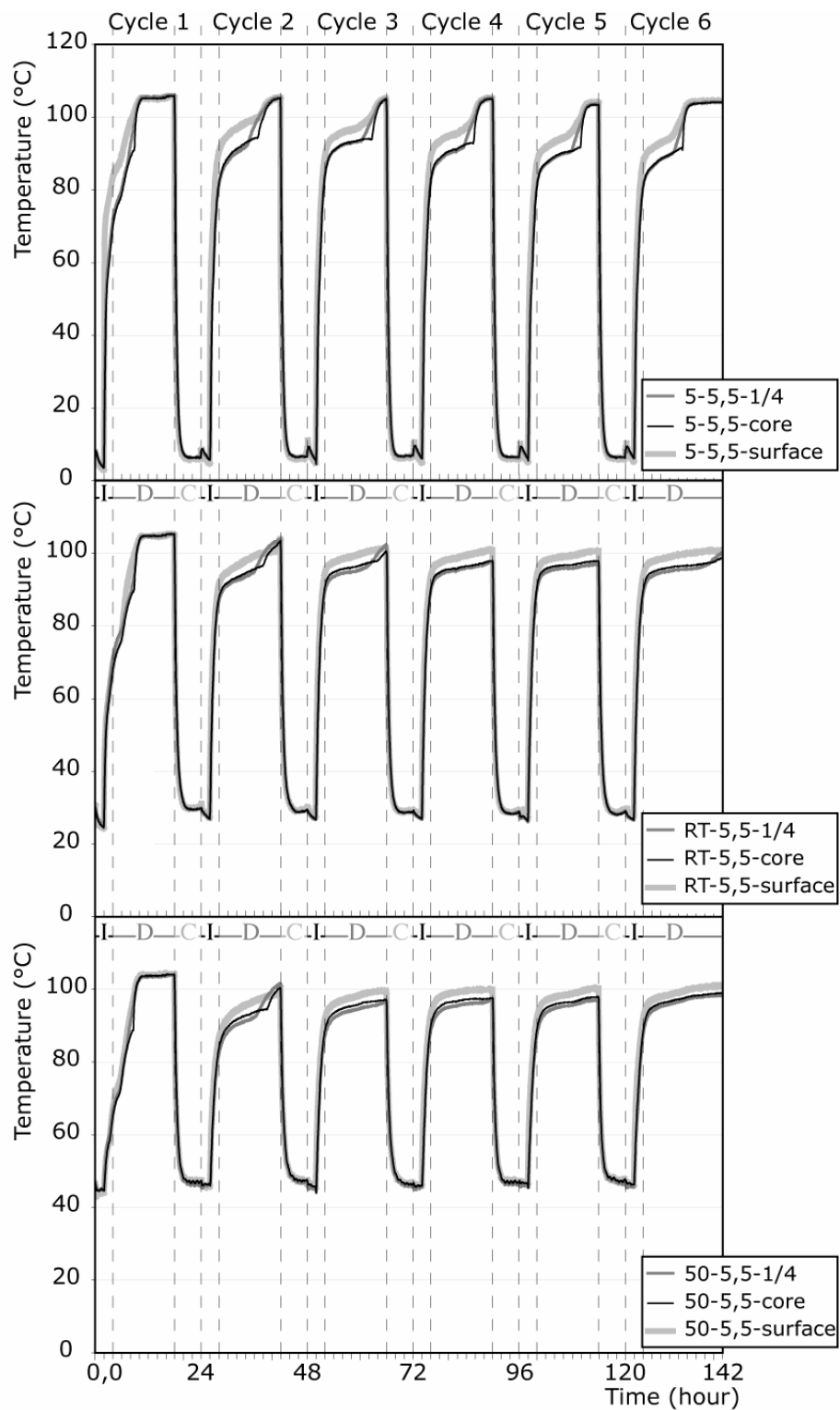


Figure ART1-5. T curves as function of time. T has been continuously recorded all along the 6 cycles. Upper diagram for “5°C ambient condition”, middle diagram for “RT ambient condition”, lower diagram for “50°C ambient condition”. Different stages of cycles are precised (I: imbibition, D: drying, C: cooling).

2.1. Rock decay vs cycle

Figure ART1-4 shows the different samples at different stages of the 6 cycles. Samples RT and 50°C do not present any major damage but just efflorescence that starts to occur just after cycle 1. Note that efflorescence seems to be slightly more developed for sample RT than 50°C. It is important to note also that if the salt content of the imbibition solution is constant and the same for all experimental conditions, the lower the temperature of imbibition, the closer to supersaturation condition (see fig. ART1-1).

On the opposite, sample 5°C shows intense damage starting with efflorescence (from cycle 1), contour scaling (from cycle 3) and crumbling, leading to an important change of shape. The evolution of sample weight during cycles (fig. ART1-4) shows consistent results with the shape evolution described above. All the samples undergo a similar weight increase during first cycle, but the evolution differs from cycle 2. Indeed, samples RT and 50°C show a more or less progressive weight raise, whilst sample 5°C shows a less intense weight increase during the second cycle, before undergoing weight decrease from cycle 3. Note that the weight loss is regular after cycle 3 for this last sample. All these results are consistent with the previous work of Angeli et al. (2006, 2007, in press).

2.2. Differences of temperature evolution within the samples

Besides some exceptions, which will be detailed further, the three thermocouples record generally the same temperature evolution. This is especially true during imbibition and cooling, and also during the first part of the drying stage. The notable differences are a systematic (more or less marked) shift between the curves of the different thermocouples, in particular during the second part of the drying stage. Nevertheless a slight difference of the temperature evolution from core to rim of the sample (i.e from a thermocouple to another) can be observed. Indeed, due to heat diffusion, temperature increases more slowly within the sample than on surface (fig. ART1-5).

It means that a same temperature is reached more rapidly on the surface than in the core of the sample. In addition, the maximum temperature recorded on the surface of the samples RT and 50°C may, according to the cycle, be higher of up to 4 degrees (e.g. fig. ART1-5) than in the core.

2.3. Temperature evolution during imbibition

According to fig. ART1-6, we must distinguish the temperature evolution during the first imbibition from the following ones.

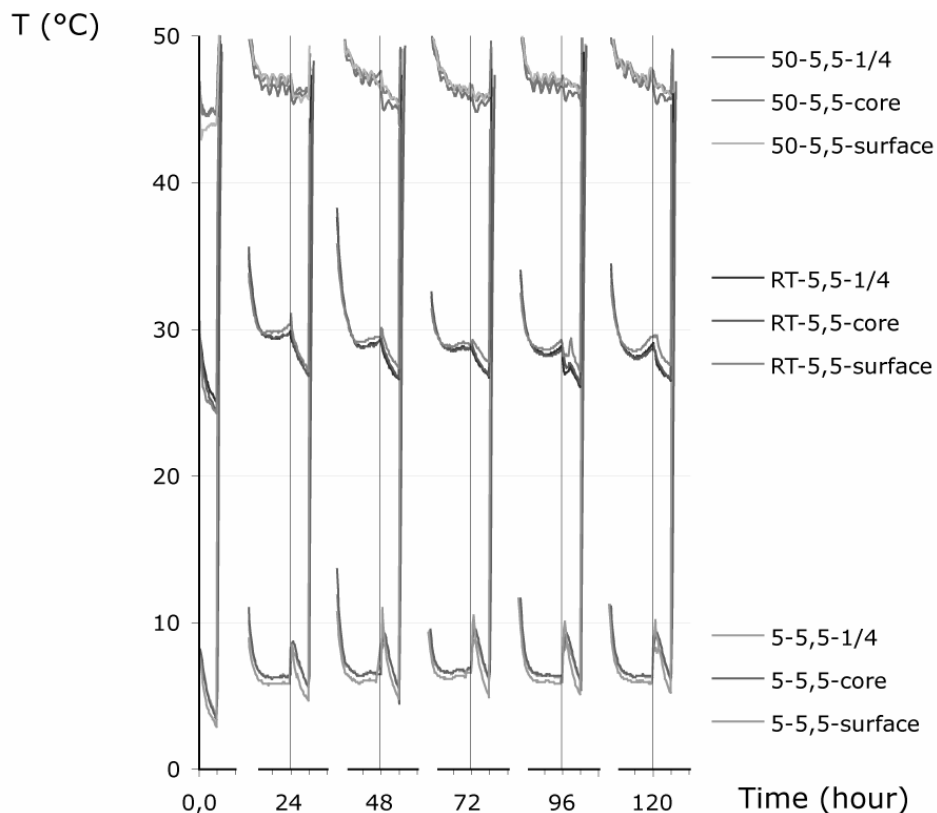


Figure ART1-6. Focus of the temperature evolution during imbibition for the three different experimental conditions.

First imbibition is characterized by a significant temperature decrease of several degrees (up to -3.5°C for sample 5°C, up to -6.0°C for sample RT) that lasts all along this stage. Temperature evolves differently in sample 50°C during the same time. Indeed, we can observe a rapid and linear drop of several degrees (up to -3.5 °C) during the first 30 minutes and then stabilization (or even a slight raise of temperature +1.0°C for thermocouple located on the surface of the sample).

Following imbibitions are characterized by two stages. First a temperature rise ($4\pm1^\circ\text{C}$ for sample 5°C; $2\pm1^\circ\text{C}$ for sample RT) and then a temperature decrease of several degrees (-5 °C for sample 5°C; $-2\pm1^\circ\text{C}$ for sample RT).

$\pm 1^\circ\text{C}$ for sample 5°C ; in the range $-5.5 \pm 1.5^\circ\text{C}$ for sample RT) that lasts until the end of imbibition. Once again, sample 50°C shows a more complicated thermal evolution. For this sample, it is more like frequent alternations of rapid rise and fall of temperature. Nevertheless, these alternations describe a downward trend in temperature.

It is also interesting to note that for all the samples (i) the peak of temperature (maximum T) during imbibition seems to decrease and stabilize after cycle 2, and (ii) minimum of temperature is about constant from cycle 2

2.4. Temperature evolution during drying (fig. ART1-5)

The first and most striking feature is that the temperature evolution during drying of cycle 1 is different from this of the following cycles.

During cycle 1, all the samples present a similar thermal progression which can be decomposed in three parts: first a rapid and linear temperature increase; secondly several slope changes, one at around $\pm 55^\circ\text{C}$, another one at around $\pm 70^\circ\text{C}$ and a last one at around $\pm 90^\circ\text{C}$ (surface thermocouple of sample 5°C show a more complicated trend); and third, a stabilization (plateau) at about 105°C for a period of several hours. This temperature evolution is about the same whatever the sample but nevertheless there are some notable differences which are:

- Maximum temperature recorded differs from a sample to another. 105°C is reached after 10,5h in sample 5°C , at t=16h in sample RT, and never reached in sample 50°C where a maximum T of 104°C is obtained towards the end of the drying stage.

- An inflection point is clearly observed at around 90°C only for the curve of the thermocouple located in the centre of each sample. More precisely, this inflection point occurs at about 90.8°C for sample 5°C , $\sim 89.9^\circ\text{C}$ for sample RT and $\sim 88.5^\circ\text{C}$ for sample 50°C .

During the following cycles, temperature evolution tends to be more repetitive from a cycle to another and even tends to almost perfect reproducibility in particular from cycle 3 for sample 50°C , and from cycle 4 for samples 5°C and RT. Main points are: (i) a rapid and linear temperature increase similar to cycle 1 up to $55\pm2^\circ\text{C}$, then (ii) a slope break (lower temperature increase than for cycle 1) progressively decreasing up to a more or less sharp inflection point (ranging between 90 and 96°C depending of the cycle) which varies in time

depending on the thermocouple, (iii) a new change of the heating rate which increases strongly and then decreases progressively in order to reach maximum temperature where in some cases a plateau can be observed. This three steps evolution is observed in sample 5°C whatever the cycle, in sample RT (cycle 2 and 3) and in sample 50°C (cycle2 only). Indeed samples RT and 50°C show, from respectively cycle 3 and 4, a different temperature evolution that can be reduced to two parts: (i) a rapid and linear increase of temperature similar to previously described and (ii) around 90-95°C depending on the sample, T increases more slowly until the end of the drying stage.

Another striking feature is that the highest or maximum temperatures (peak of T or Tmax) undergone by the samples decrease progressively from cycle 1 to cycle 3 and then stabilize from cycle 4 or 5 regarding samples. Tmax for the three samples, and whatever the location of thermocouples, is close to 105°C for cycle 1. It decreases slightly for sample 5°C (from 105°C to 103°C) and significantly in samples RT and 50°C (up to round 100°C for the surface, and 95-96°C within sample). Curiously, we can also note that Tmax for sample 5°C > Tmax for sample RT > Tmax for sample 50°C. Following this observation, we have extended the drying stage of 6 hours for cycle 6. This extra drying period does not make any difference for sample 5°C for which the maximum temperature was reached before the end of the standard 16 hours of drying. The T vs t curves describe a plateau indicating that T is just hold on during this period. At contrary, the additional drying induces some differences for samples RT and 50°C. For sample RT, surface thermocouple do not show any difference with previous cycles, whilst both internal thermocouples show a reappearance of the inflection points as for cycle 3, indicating that the maximum reachable temperature has not been reached. Concerning sample 50°C, Tmax is about +1.0°C higher than previously after 6 hours of extra drying. Surface temperature is slightly above 100°C, whilst it remains below 100°C within the sample. The reappearance of the inflection point does not take place.

To sum up, the temperature evolution during drying is not continuous and progressive. It shows several slope breaks according to samples: 3 for sample 5°C except for cycle 1; for sample RT we observe 2 or 3 slope breaks for cycle 2, 2 for cycle 3 and just one from cycle4; and for sample 50°C, 2 slope breaks at cycle 2 and just one from cycle 3.

2.5. Temperature evolution during cooling (i.e. return to ambient environment)

Temperature evolution during cooling to ambient environment is more straightforward. It requires about 2 hours for each sample to reach its ambient temperature from the peak of T achieved at the end of the drying stage (fig. ART1-5). This cooling is fast (rate is about -50°C/hour) at the beginning, and slows down when approaching ambient T. We can consider that all the samples have returned to their ambient T after 2 hours and therefore, they do not undergo further temperature variation until the beginning of next cycle (i.e starting of new imbibition).

3. Discussion

3.1. Rock decay vs cycle

Though the samples just underwent 6 cycles of accelerated ageing, the shape (or visual) evolution is consistent with previous studies (Angeli et al. 2006, 2007, in press). The single sample to show intense damages is sample 5°C. According to Angeli et al.(2007), the alteration index for this rock and this environmental condition is 3, i.e. the first observable evidence of alteration occurs during cycle 3. As we used only one type of rock, and one salt concentration for the experiments, this result suggests that the alteration index for a rock depends not only of the type of ageing test as shown by Angeli et al. (2007), but also of the climatic conditions. It means that for a type of rock and for a given salt concentration, the alteration index will be different if the rock is exposed under cold, tempered, or hot (dry?) conditions.

Weight increase, whatever the sample, is interpreted as the result of salt crystallization within pores. Weight decrease is interpreted as material loss. In the case of sample 5°C, it is clear that first evidences of visual damage correspond with important weight loss (fig. ART1-4). More precisely, there must be a competition during this stage between mass supply by salt crystallisation and material loss, this later being more important (Angeli et al. 2007). Because sample 5°C does not show the same weight evolution during cycle 2 compared to the two other samples, it is likely that sample 5°C starts to undergo material loss which is not visibly

perceptible. These results are in good agreement with other studies (Tsui et al. 2005; Angelis et al 2006, 2007, in press).

3.2. T evolution during imbibition

The decrease of temperature observed during first imbibition is due to evaporative cooling, a physical phenomenon in which the evaporation of a liquid, when surrounded by air, cools an object or a liquid in contact to it. T decreases of several degrees during this stage, and as a consequence it enables the crossing of the liquidus in the $\text{Na}_2\text{SO}_4\text{-H}_2\text{O}$ binary system for sample 5°C (fig. ART1-7), and as a result the beginning of crystallization of mirabilite during imbibition. Because mirabilite has a $\Delta H_r = +78.37 \text{ kJ/mol}$ (Price 2000), a small decrease in temperature produces an important precipitation of mirabilite. As soon as mirabilite crystallizes, salt concentration of the equilibrium solution decreases.

This temperature fall of few degrees is not sufficient to make it possible to get into the mirabilite stability field for sample RT during the first imbibitions. But it is just a question of time. Indeed, following imbibitions will raise salt content (by salt supply) up to supersaturation with respect to mirabilite (fig. ART1-7). Once supersaturation condition is achieved, the composition of the imbibition solution will lay along the liquidus curve (it is always the case whatever the T), and then the least drop of temperature of a hundredth of degree leads to get into the $\text{Na}_2\text{SO}_4\text{.10H}_2\text{O}$ stability field, i.e. crystallization of mirabilite. This drop of temperature due to evaporative cooling will allow the crossing of liquidus and then crystallization of mirabilite.

Regarding to T, supersaturation with respect to mirabilite can never be achieved in sample 50°C, and consequently, mirabilite will never crystallize for this experimental condition. Even for supersaturation condition with respect to thenardite, evaporative cooling during imbibition will never lead to salt crystallization, as the drop of T leads to the liquid field (fig. ART1-7).

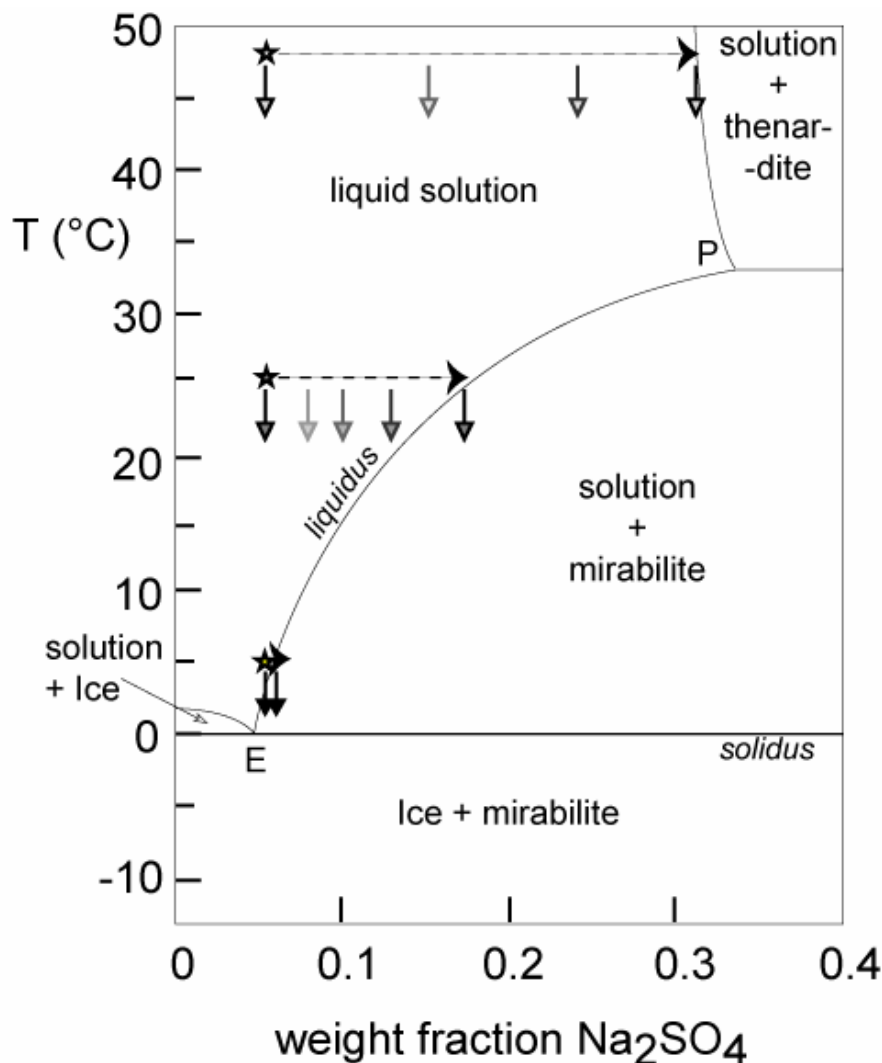


Figure ART1-7. Effect of evaporative cooling during imbibition. Plain arrows show the drop of T which allow under certain circumstances the crossing of liquidus, and consequently crystallization of mirabilite. Dashed arrows describe the displacement of the salinity towards higher values with the salt contributions by the successive imbibitions.

Imbibition stage during the following cycles is first characterised by a temperature raise which is due to dissolution of the salts previously crystallized within pores, in particular the dissolution of thenardite. Indeed, the reaction enthalpy for solubility of thenardite is $\Delta H = -0.217569 \cdot 10^4 \text{ J.mol}^{-1}$ (Price 2002), which means that dissolution of Na_2SO_4 is exothermic and produces heat which is responsible of the observed temperature raise. Dissolution of pore-filling thenardite increases, at least locally within pores, salt concentration of the imbibition solution leading to possible supersaturation with respect to mirabilite.

Because of the observation during first imbibition, we know that evaporation process occurs and lowers the temperature within the sample. Consequently, from second imbibition, there is a competition between three phenomena: dissolution of thenardite and crystallization of mirabilite that raises T up, and evaporation that lowers T. During the first part of imbibition, the production of heat must be higher than the cooling induced by evaporation, and once thenardite has completely dissolved, evaporation is the only occurring phenomena. Then temperature decreases and may, when suitable conditions are reached (crossing of liquidus), enable crystallization of mirabilite.

It is worth noticing that the temperature raise is less important or visible for sample RT, or even more complicated for sample 50°C. It suggests that according to ambient T conditions, evaporation process dominates salt dissolution and therefore temperature increases in a less extent. Comparing the three sample conditions, it is likely that the evaporation rates are different and may play an important role for the thermal evolution. We can also take into account that the sequences of phases occurring during the imbibition stage are different from an experimental condition to another (see further discussion and fig. ART1-8) and therefore different chemical reactions with different heat balances are going to occur.

3.3. T evolution during drying

The first striking feature is that the temperature curves of the first cycle are very different from the following ones. They change form until reaching a perfect reproducibility starting from a variable number of cycles according to the experimental conditions. The second striking feature is the progressive reduction in the maximum temperature at the end of drying in the course of time. This suggests that salt impregnation modifies the thermal behaviour of the rock, decreasing the heat-storage capacity in particular. As T Max remains below 100°C for samples RT and 50°C, it also suggests that water has not been completely removed from the samples, as expected, at the end of the drying stage.

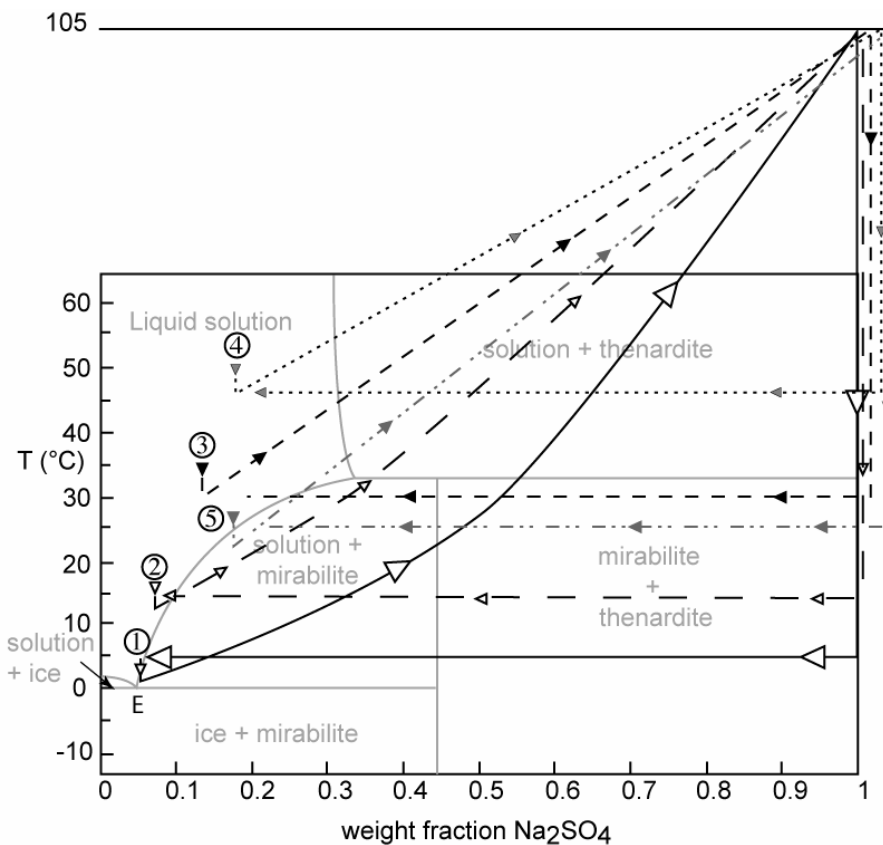


Figure ART1-8. The different possible T-t paths and the associated sequences of phases. Path 4 is the only possible when $T > TLMS$. Paths 1, 2, 3 and 5 are possible when $T < TLMS$. Crossing of liquidus because of evaporative cooling is possible if salt content fulfills supersaturation condition (or very closed to it).

The other outstanding points are the setbacks or slope breaks as well as the inflection points that characterize the curves. They are indicators of thermal conductivity changes that are likely due to either phase crystallizations or chemical reactions (involving also salt crystallization). Unfortunately, it is impossible so far to me more precise and further experiments must be considered.

3.4. *T evolution during cooling*

There is very little to say about the return to ambient temperature except that the heat gradient is roughly the reverse (or the symmetric) of that of the beginning of drying. It is supposed that there is no chemical change during this stage. This is probably not right as suggested by the maximum temperature reached by samples RT and 50°C at the end of drying. Indeed, samples still likely contain water at this stage and therefore they may continue to “dehydrate” during the cooling stage.

3.5. Extended drying of sixth cycle.

The extension of drying during the 6th cycle was carried out to see whether the maximum temperature could increase with respect to the previous cycle and even reach a value similar to cycle 1 (fig. ART1-5). After 6 hours of extra drying at 105°C, the temperature of the samples increased approximately of about 1°C. The increases in temperature described previously (see results section), suggest several comments:

- Pore-filling salts modify the heat capacity of the rock.
- It is very likely that water, in some cases, is not completely removed from the samples. This implies that results of weight monitoring after drying are subject to caution.

This suggests that the accelerated ageing test used in this study (modified from the natural stone test methods EN 12370 (1999) concerning the determination of resistance to salt crystallization) has to be reconsidered. It would require some modifications in order to be sure that free water has been completely released at the end of drying stage. These are either an increase in the duration of drying period, or an increase in the temperature of drying while preserving the duration (i.e. 16 hours).

Conclusion

Experiments performed in this study use one type of rock which is relatively homogenous from a sample to another. Therefore, hydrous and mechanical properties are not parameters for explaining the different evolutions of the samples. Though initial conditions of imbibition use a constant salt content (5.5 Wght % Na₂SO₄; i.e. not supersaturated solution with respect to mirabilite whatever the different ambient temperatures used in this study), it is important to remind that the lower the temperature of imbibition, the closer the condition of supersaturation (see figure 1). Moreover, the accumulation of the ageing cycles leads unrelentingly to salt supersaturation. It is just a question of temperature and time (i.e. number of cycles). Supersaturation condition is rapidly achieved at 5°C. Supersaturation can be achieved for sample RT (because ambient T < TLSM) but it requires more cycles than for sample 5°C. At contrary, sample 50°C will never meet the conditions of crystallization of mirabilite (because T > TLSM). It might possibly achieve supersaturation conditions but with respect to thenardite (but even then, the drop of T due to evaporative cooling does not drive to salt crystallization as liquidus is not crossed). Therefore, if supersaturation is a very major

condition leading to large crystallization pressures (Correns 1926; Benavente et al. 1999; Scherer 2004; Coussy 2006) and then important damages, it must be with respect to mirabilite and not thenardite (Tsui et al. 2003). Consequences of supersaturation, as shown in this study, differ from a phase to another, especially regarding evaporative cooling during imbibition.

The thermal recording allows rebuilding a part of the T-X-t path, considering that this path is made of three different stages (fig. ART1-8):

1- Path during cooling is the simplest. Temperature decreases from Tmax achieved at the end of drying to the ambient temperature. As drying is supposed to have been completely released the water of the system, we assume that this temperature decrease occurs at constant composition (100% Wght fraction of Na₂SO₄ in the Na₂SO₄-H₂O binary system). This is probably not the case regarding Tmax below 100°C at the end of drying.

2- During imbibition, the system is first open to brine at constant T. Therefore, there is a change of composition, shifting the composition towards lower values of weight fraction of Na₂SO₄. Depending on the temperature, different stability field will be crossed during this path, indicating that some chemical and mineralogical reactions are going to take place. Some of these reactions, in particular salt dissolution, is going to produce heat. By the same time, there is also evaporative cooling. Therefore imbibition path, when rocks have undergone at least one complete ageing cycle and for T<T_{lms}, is characterized by a slight temperature increase and then a temperature decrease allowing the crystallization of mirabilite during this stage. Salt supply by the imbibition solution increases progressively the salinity of the system until reaching the conditions of supersaturation. Once supersaturation is achieved, additional salt supply by other imbibition does not make any change: the composition of the liquid will always be located on the liquidus curve. Consequently, any following imbibition will lead to mirabilite crystallization if ambient T is below 32.4°C.

3- Precising the T-t path during drying requires further investigation. Identifying the slope changes of the temperature curves with episodes of crystallisation should allow to constrain the crossing of the different fields within the Na₂SO₄-H₂O diagram, and then to precise the sequence of phases to occur for each experimental condition.

Anyway, there are just four possible complete T-t paths so far (for experimental conditions with a salt concentration above the eutectic composition; i.e. above ~0.5 % Wght fraction of Na₂SO₄) which determine four different sequences of phase to occur during ageing

test (fig. ART1-8). These sequences are, for a complete cycle starting from evaporative cooling at imbibition to next one (in bold the phase(s) of the crossed stability field due to evaporative cooling during imbibition, normal text for drying, italic for imbibition; in this case it is the “rehydration” of the system, i.e. a reaction between thenardite and water which leads to “dissolution” of thenardite to produce mirabilite):

- Sequence 1: **Mir** → Mir + The → **The** → *The + Mir* → Mir
- Sequence 2: **Mir** → The → *The + Mir* → Mir
- Sequence 3: The → *The + Mir* → Mir (possible as far as supersaturation is not reached)
- Sequence 4: The → *The*

Sequences 1, 2 and 3 can take place only for ambient temperatures below TLMS. Sequence 4 is the only possible one for ambient temperature above TLMS. Thenardite is always and only produced during drying. It can crystallize directly from the solution (paths 3 and 4) or from dehydration of mirabilite (peritectic reaction via paths 1 and 2). Thenardite has to be the single phase at the end of drying, assuming the complete loss of water of the system during the drying stage.

A fifth sequence (path 5, fig. ART1-8) can also be considered for certain supersaturation wrtm and T<TLMS conditions. It is a kind of mixing between sequences 2 and 3 that depends of the heating rate during drying. Indeed, if heat transfer is fast, we can expect the following succession of reactions: Crystallization of mirabilite during imbibition (downwards crossing of liquidus due to evaporative cooling), disappearance (= dissolution) of mirabilite (upwards crossing of liquidus), crystallization of thenardite (crossing of Thnd stability field), crystallization of mirabilite and dissolution of thenardite (during new imbibition).

- Sequence 5: **Mir** → Liquid → The → *The + Mir* → Mir

It is very likely that the salt-weathering damages undergone by the rocks may differ from a sequence to another. It is therefore crucial to constrain further the T-t path during drying in order to precise the relationship between damages, sodium sulphates and phase transitions. According to temperature conditions, mirabilite can crystallize during imbibition, directly from liquid due to evaporative cooling and also from “rehydration” of the system, and possibly during drying. Thenardite crystallizes only during drying. This study confirms (once

again) that mirabilite plays a major role in rock decay, and suggests also that imbibition is a major stage of the weathering process. It is worth noticing that, just mirabilite and thenardite are considered in this study, but we cannot exclude a possible role from the metastable phase on rock decay.

Acknowledgements :

We would like to thank Pr. Albert NOUMOWE and Dr Rachid BENNACER, colleagues of the department of civil engineering of the University of Cergy Pontoise, for the loan of the acquisition unit and for scientific discussions.

References

- Angeli M, Bigas JP, Menéndez B, Hébert R, David C (2006) Influence of capillary properties and evaporation on salt weathering of sedimentary rocks – in “Heritage, Weathering and Conservation”, Edité par R. Fort, M. Alvarez de Buergo, M. Gomez-Heras & C. Vazquez-Calvo, Taylor & Francis/Balkema, AK Leiden, The Netherlands, 2006, 253-259
- Angeli M., Bigas JP, Benavente D, Menéndez B, Hébert R. and David C. (2007) Salt crystallization in pores: quantification and estimation of damage. Environmental geology, 52:205-214
- Angeli M, Benavente D, Bigas JP, Menendez B, Hébert R and David C 2007 - Modification of the porous network by salt crystallization of experimentally weathered sedimentary stones. Materials and structures (in press).
- Benavente D., Garcia del Cura M. A., Fort R. and Ordoñez S. 1999 – Thermodynamic modelling of changes induced by salt pressure crystallization in porous media of stone – Journal of Crystal Growth, 204:168-178
- Benavente D, García del Cura MA, García-Guinea J, Sánchez-Moral S, Ordoñez S 2004 - The role of pore structure in salt crystallisation in unsaturated porous stone. Journal of Crystal Growth 260:532-544

Chapter III: Salt crystallization

Correns CW and Steinborn W 1939 – Über die Erklärung der sogennante Kristallisationskraft.
Zeitschrift fur Kristallographie A101:117-135

Coussy O 2006 – Deformation and stress from in-pore drying-induced crystallization of salt.
Journal of the Mechanics and Physics of Solids 54:1517–1547.

EN 12370 1999 - Natural stone test methods – Determination of resistance to salt crystallization.

Flatt RJ 2002 - Salt damage in porous materials: how high supersaturations are generated.
Journal of Crystal Growth 242:435-454

Genkinger S and Putnis A (2007) Crystallization of sodium sulphate: supersaturation and metastable phases. Environmental geology, 52:329-338

Gmelin L 1966 - Handbuch der anorganischen chemie, Aufl. Natrium Erg.Bd. 3, Verlag Chemie Weinheim.

Goudie, A. S. & Viles, H. 1997 - Salt weathering hazard. Chapter 4, p91-122 Chichester: John Wiley & Sons.

Hougen OA, K. W. Watson KW and R. A. Ragatz RA 1954 - Chemical Process Principles.
Part I, 2nd ed., Wiley, New York, 1954

Kracek FC 1928 - Int Critical Tables 3: 371.

Partington JR 1961 - General and Inorganic Chemistry, MacMillan & Co. Ltd., London.

Price 2000 - An Expert Chemical Model for Determining the Environmental Conditions Needed to Prevent Damage in Porous Materials, Archetype Publications Ltd, London.

Chapter III: Salt crystallization

Rodriguez-Navarro, C. & Doehe, E. 1999. Salt weathering: influence of evaporation rate, supersaturation and crystallization pattern. *Earth Surface Processes and Landforms* 24: 191-209.

Rodriguez-Navarro C, Doehe E and Sebastian E 2000 - How does sodium sulphate crystallize? Implications for the decay and testing of building materials. *Cement and Concrete research* 30: 1527-1534.

Scherer G 1999 - Crystallization in pores. *Cement and Concrete Research* 29:1347-1358

Scherer G 2004 - Stress from crystallization of salt. *Cement and Concrete Research* 34:1613-1624.

Sperling CHB and Cooke RU 1985 – Laboratory simulation of rock weathering by salt crystallization and hydration processes in hot, arid environment. *Earth Surface Processes and Landforms* 10, 541-555.

Steiger M 2005 – Crystal growth in porous materials—I: the crystallization pressure of large crystals. *J Cryst Growth* 282:455–469

Tsui N, Flatt RJ and Scherer GW 2003 – Crystallization damage by sodium sulfate, *Journal of Cultural Heritage* 4: 109-115.

Now that the mechanism of damage by sodium sulphate is explained, next chapter will focus on accelerated ageing tests. The modifications of the nine sedimentary stones during salt weathering will be evaluated, first at the scale of the sample and second at the scale of the pore.

SALT DAMAGE

CONTENT

1.	<i>Macroscopic experiments</i>	99
	<i>1.1.Durability estimation</i>	99
	<i>1.2.Crystallization of salts in pores: quantification and estimation of damage (article 2; Environmental geology)</i>	100
	<i>1.3.Effects on mechanical strength</i>	121
2.	<i>Microscale experiment :Modification of the porous network by salt crystallization of experimentally weathered sedimentary stones (article 3; Materials and structures)</i>	122

Chapter IV: Salt damage

All the stones do not suffer the same way from salt damage. This depends on their structure, on their hydraulic properties, on their mechanical strength... The aim of this part is to understand the differences of weathering between the nine chosen stones. The wide variety of stones will help to understand which microstructural features have a crucial influence on salt decay.

1. Macroscopic experiments

1.1. Durability estimation

The problem of durability assessment for a stone has been a topic of interest for a long time. The stone durability has to be known in order to choose adapted stones for building or restoration in particular climatic (temperature, humidity...) or architectural (roof, pavement, columns, decoration...) conditions. The estimation of durability allows choosing an adapted stone with simple tests in a day or two, instead of waiting weeks or even months for accelerated ageing tests or even more in the case of in-situ observations. Generally the durability of stones depends on the fluid flow and the mechanical strength: this comes from the fact that water carries the pollutants (generally soluble salts) in the stone, which causes stresses that can exceed the tensile strength of most stones. The first estimators were based on the porous network properties, since they concern the ability of the stone to contain soluble salts (Hammecker 1995; Ordoñez et al. 1997; Nicholson 2001). They can consider porosity, absorption, pore entry size distribution, mean pore size, specific surface area or a combination of them. For instance Mod'd et al. (1996) have proposed several estimators based on porosity and saturation, and Ordoñez et al. (1997) have proposed an estimator based on the pore entry size distribution. It is quite well known that durability also depends highly on the mechanical strength (Theoulakis and Moropolou 1995). Thus these parameters have also been used to assess the durability of stone, whether they are direct (compressive or flexural strength) or indirect measurements (tensile strength with brazilian test, P-wave velocity) (Theoulakis and Moropolou 1995). Some estimators even take both hydraulic and mechanical parameters into account (Dessandier et al. 2003; Benavente et al. 2004, 2007). Moreover, Benavente et al. (2004) have demonstrated that both parameters have to be taken into account to estimate the durability of a stone.

Nevertheless, those estimators were only created and proved effective in certain particular conditions that depend on the type of damage (frost, salt, thermal...), the experimental conditions (temperature, RH, length of cycles...) and even the way the damages are evaluated (weight loss or crack density at a certain time, in-situ observations...). Moreover, Nicholson (2001) has proved that these estimators were highly dependant on these parameters. One problem in the reliability of estimators between two different tests comes from the fact that these quantifiers are static (observation or measurement after a certain number of cycle), and do not take into account the evolution during the whole accelerated ageing test. The quantifiers should take this evolution into account to be more accurate. This remark is the basis for a study of the long term evolution of stones as a function of their hydromechanic properties.

1.2. Crystallization of salts in pores: quantification and estimation of damage (article 2; Environmental geology)

The starting point of this study was to evaluate the macroscale behaviour of stones regarding salt decay in order to assess their durability. To simplify the study of the general aspect of salt decay, we chose to work with only one salt (sodium sulfate) but many different stones which are described in chapter 2. The aim was to have a wide range of rock types to observe a wide range of decay. The alteration features (starting time, velocity, patterns) have been studied in the following article: "Salt weathering of sedimentary stones: Quantification and Estimation".

The results show a good correlation with the durability expected by the quarry holders or architects. Concerning the three lutetian limestones from the St Maximin quarry, the detritic limestone FL is used for precise ornamental work because of its great softness. On the opposite, RL and especially LL, which are much more durable, are used for basement walls or even outside ground. The Fontainebleau sandstones were clearly named after their durability, the soft one (SF) being much less durable as the hard one (HF). Both Indian sandstones and the Chinese sandstone are used for outside pavement due to their very high durability. Nevertheless, the quarry holder was very surprised (and upset) that this particular set of Chinese sandstone was unexpectedly less durable than the others he receives usually. Finally, the lacustrine limestone SL is also very durable since it has been widely used in the building of monuments like the Sacré-Coeur basilica in Paris or the Sorbonne University.

“Salt crystallization in pores: quantification and estimation of damage”

Matthieu Angeli¹, Jean-Philippe Bigas¹, David Benavente², Beatriz Menéndez¹, Ronan Hébert¹ and Christian David¹

¹ Université de Cergy-Pontoise

Département de Sciences de la Terre et Environnement
5 mail Gay-Lussac, Neuville-sur-Oise
95031 Cergy-Pontoise CEDEX
France

² Universidad de Alicante

Departamento de Ciencias de la Tierra y del Medio Ambiente
Laboratorio de Petrología Aplicada
Apartado 99
03080 Alicante
España

Published in a special issue on salt decay for Environmental Geology: Angeli M., Bigas JP, Benavente D, Menéndez B, Hébert R. and David C. 2007 – Salt crystallization in pores: quantification and estimation of damage – Environmental geology, 52:205-214

Abstract

The objective of this study is to understand and predict the alteration of any rock by crystallization of salts. Samples of different rocks have been tested thanks to the EN 12370 standard test. Two parameters are proposed to evaluate the alteration of a rock during these tests. The alteration index AI represents the cycles in which the first damages occur. The alteration velocity AV is the alteration rate at the end of the experiment, when the decay has become regular. These parameters can be estimated with the help of a microstructural study of the rocks. The intrinsic parameters of the stones that are the most relevant for this estimation are capillary coefficient, evaporation coefficient, tensile strength and P-waves velocity. An evaluation of the alteration pattern is also proposed depending on the eventual heterogeneities and anisotropies of the rocks. The influence of the dimension and shape of the samples is also discussed.

Résumé

L'objectif de cette étude est de comprendre et prévoir l'altération d'une roche par la cristallisation de sels. Des échantillons de différentes roches ont été testées selon la norme européenne EN 12370. Deux paramètres sont proposés pour évaluer l'altération des échantillons pendant ces tests. L'indice d'altération AI représente le numéro du cycle où les premiers dégâts apparaissent. La vitesse d'altération AV est le taux d'altération à la fin de l'expérience, quand celle-ci est devenue régulière. Ces paramètres peuvent être estimés avec l'aide d'une étude microstructurelle des roches. Les paramètres intrinsèques qui sont les plus pertinents pour cette estimation sont le coefficient capillaire, le coefficient d'évaporation, la résistance en traction et la vitesse des ondes P. Une évaluation de la forme générale des altérations est aussi proposée en fonction des éventuelles anisotropies et hétérogénéités. L'influence des formes et dimensions des échantillons sur l'altération est aussi discutée.

Introduction

Salts, and particularly sodium sulphate, are known to be among the most destructive agents in porous stones, concrete or brick weathering. Their study is thus very important to fully understand their crystallization process in porous networks and, in the future, to find a way to prevent or limit their damage to porous materials. Recent studies attribute the decay to the salt crystallization pressure of mirabilite ($\text{Na}_2\text{SO}_4 \cdot 10\text{H}_2\text{O}$), rather than thenardite (Na_2SO_4) (Rodriguez-Navarro & Doehe 1999, Scherer 1999, Flatt 2002, Benavente et al. 2004a, Steiger 2005). This damage depends on the quantity of salt in the stone as well as the characteristics of the porous network (a review can be found in Steiger, 2005).

This study aims to evaluate building stone behaviour during accelerated ageing, and to understand how the porous network is affected. Then weathering will be quantified by few intrinsic parameters and evaluated thanks to a microstructural study. A review about estimation of damage can be found in Benavente et al. (2004b). Most of existing estimators evaluate weathering with only one parameter. This study proposes two parameters, the alteration index (AI) and the alteration velocity (AV), to quantify weathering, and a method to preview how these damages will be organised in the stone. The influence of the shape and dimensions of the samples is also discussed.

1. Materials and Methods

1.1. Materials

Nine stones from different lithologies have been used in this study: four limestones and five sandstones. The four limestones come from the Parisian Basin. Three of them are of lutetian age: the “roche fine” (FL), the “roche franche” (RL) and the “liais” (LL). These three limestones have high porosity compared to the other stones in this study (respectively 37.2, 18.5 and 14.4%). FL is a detritic limestone made of calcite (90%) and quartz (10%). Its tensile strength is very low (1.5 MPa). RL and LL are two boundstones composed by more than 90% of calcite, with traces of iron oxides. They also contain some macrofossils (bivalves, gasteropods) responsible of an heterogeneous aspect. The other limestone is of bartonian age: the “Pierre de Souppes” (SL), a variety of the “Calcaire de Chateau-Landon”. It is just made of calcite. Its porosity is low (4.2%) and its tensile strength high (5.2 MPa).

Two sandstones are Fontainebleau sandstones (Oligocene). These two varieties are called hard (HF) and soft (SF). They are composed of more than 99% of quartz. Their porosity are low (respectively 4.1 and 5.5%). The main difference between the two is their tensile strength: very high for HF (5.2 MPa) and very low for SF (1.5 MPa). The three others sandstones are three layered sandstones: one from China: the white sandstone (CS); and two from India: the green sandstone (VS) and the brown sandstone (MS). The white sandstone is composed of more than 99% of quartz. The two others are also composed mostly of quartz, but contain some clay which give the general colour of the rock. All three sandstones present a very high tensile strength (6.1, 15.0 and 16.0 MPa) and low porosity (2.6, 4.5 and 4.7%). Complete hydromechanic properties of these nine sedimentary rocks are given in table ART2-1.

The capillary coefficient C is the sorptivity expressed in $\text{g}/(\text{m}^2 \cdot \text{s}^{1/2})$. The evaporation coefficient E is also expressed in $\text{g}/(\text{m}^2 \cdot \text{s}^{1/2})$, and corresponds to the slope of the curve representing the weight loss as a function of the square root of time. This parameter is related to the diffusive part of evaporation (second stage), during which the external conditions (temperature, relative humidity or wind) have no influence (Hammecker 1993).

1.2. Methods

Two experiments have been performed, according to the EN 12370 standard about stone resistance to crystallization of salts in pores. They differ in the size and shape of the samples and in the number of cycles. They are composed of cycles which last 24h:

- 2 hours of immersion in a saturated solution with respect to sodium sulfate (14 wt. %);
- 15 hours of drying at 105°C in order to prevent mirabilite crystallization during drying of the samples (Fig. ART2-1);
- 7 hours of cooling at room temperature (20-25°C, 30-40% relative humidity RH). The samples were weighed after 2 hours during this stage.

The first test concerns 4x4x4 cm³ cubes with two samples per type of stone (18 cubes in total). The test has been run for 30 cycles. In the second test, cylinders of 2.5 cm diameter and 4.5 cm height were used. Two samples of each stone were used for all stones except FL (5 samples), SF (4 samples) and WS (1 sample), that is 22 cylinders. Most of the samples suffered 15 cycles except one sample of FL and one of RL (11 cycles).

	porosity %	absorption %	bulk density g/cm ³	evaporation coef. g/m ² /s ^{1/2}	capillary coef. g/m ² /s ^{1/2}	mean pore radius μm	P wave velocity m/s	tensile strength MPa
liais (St Maximin) LL	14,4	58,2	2,3	26,7	32,25	0,444	4879	4,2
roche franche (St Maximin) RL	18,5	59,7	2,2	40,7	37,55	4,710	4645	3,0
roche fine (St Maximin) FL	37,2	75,9	1,7	66,9	1106,1	12,004	2898	1,5
pierre de Souppes SL	4,2	55,0	2,57	8,0	1,47	0,082	6249	5,2
hard Fontainebleau HF	4,1	29,0	2,54	15,4	6,39	2,866	3903	5,2
soft Fontainebleau SF	5,5	48,2	2,5	12,6	40,12	3,761	1514	1,5
white CS	2,6	94,2	2,6	6,4	5,45	0,310	3329	6,1
green VS	4,5	88,3	2,54	12,3	5,81	0,047	4598	15,0
brown MS	4,7	81,5	2,53	10,5	3,86	0,034	5115	16,0

Table ART2-1. Hydromechanic properties of the studied stones

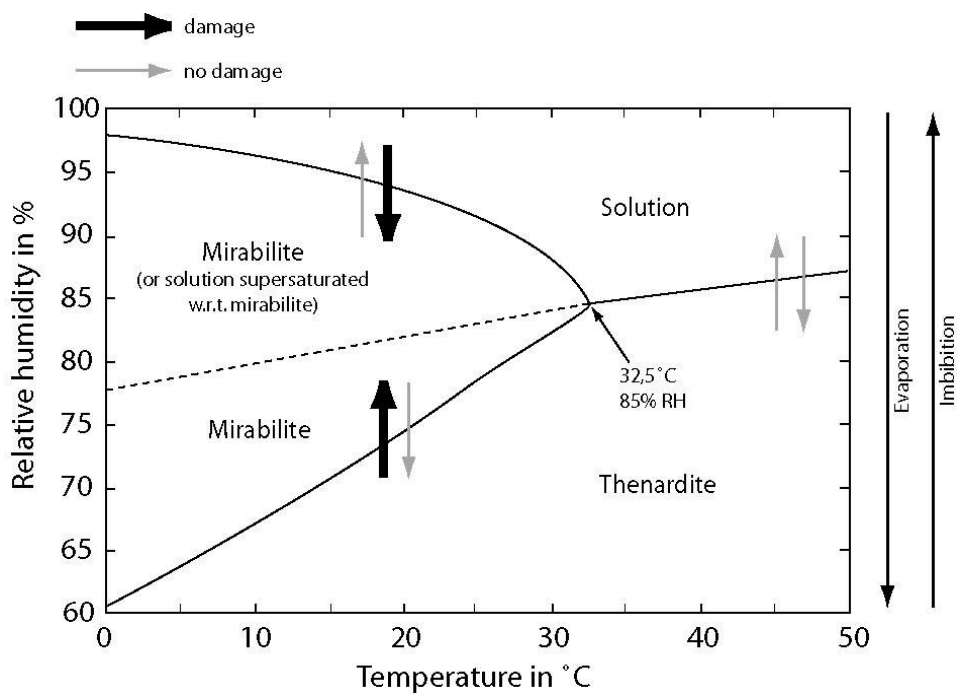


Figure ART2-1. Phase diagram of mirabilite (after Flatt 2002, data from Kracek 1928)

2. Results

2.1. Quantification of alteration

2.1.1. Representation of results

For each sample, results are plotted in diagrams showing normalised weight vs number of cycles. Three representative examples of those graphs are presented on figures ART2-2a, ART2-2b and ART2-2c. All the samples show the same evolution as a function of time. It can be described in two or three stages that are:

- stage I: weight increase due to salt supply;
- stage II (sometimes nonexistent, starts after the first visual damage): weight variation depending on a competition between salt supply and stone damage. It can be either a weight increase or decrease;
- stage III: weight decrease because salt uptake becomes negligible compared to stone damage.

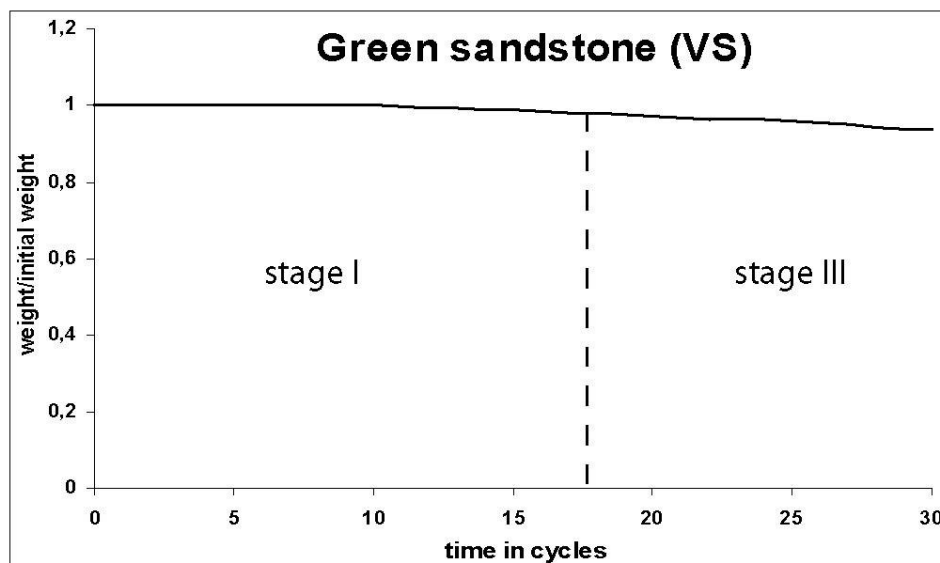


Figure ART2-2a. Normalized weight evolution during the 30 cycles (first test) of a VS sample.

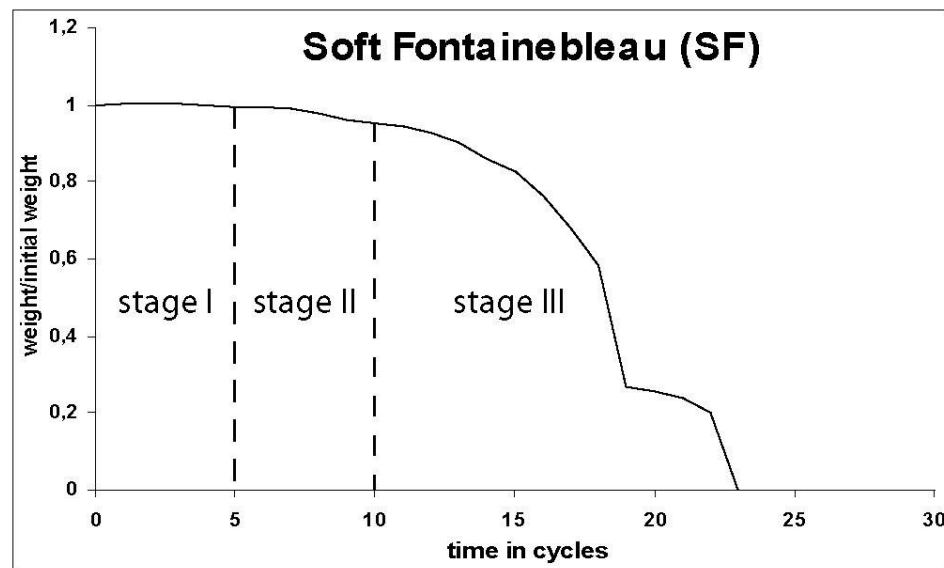


Figure ART2-2b. Normalized weight evolution during the 30 cycles (first test) of a SF sample.

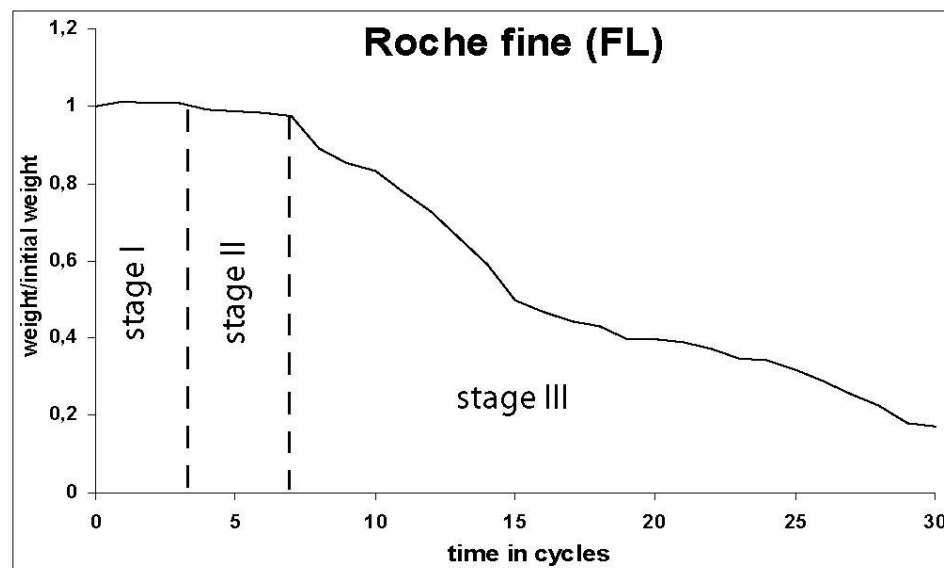


Figure ART2-2c. Normalized weight evolution during the 30 cycles (first test) of a FL sample.

2.1.2. The Alteration Index

The alteration index (AI; Angeli et al. 2006) is defined as the number of the cycle during which the first visible damage occurs (Table ART2-2). This damage, which is firstly esthetical, may imply a change of physical properties, and happens the first time the crystallization pressure is high enough to alter the stone. AI depends only on water circulation possibility, and on mechanical strength (the tensile strength, which evaluates the cohesion

between the grains). According to AI, it is possible to classify the nine studied rocks into three categories:

- high AI (19 and more in experiment 1, 10 and more in experiment 2): SL, HF, MS;
- medium AI (10 to 18 in experiment 1, 5 to 9 in experiment 2): LL, RL, CS, VS;
- low AI (up to 8 in experiment 1, up to 5 in experiment 2): FL, SF.

AI does not represent exactly the stone resistance to salt crystallization, since some stone can present visual damage rapidly and alter slowly afterwards (e. g. VS with relatively low AI compared to its actual durability). On the opposite, some stones can seem rather resistant at first, have no visual damage during few cycles, and then totally break down in 3 or 4 cycles (e. g. CS with relatively high AI compared to its durability). This observation leads to the introduction of the concept of alteration velocity (AV).

Experience 1 (cubes)			Experience 2 (cylinders)			
		Alteration Index	Alteration Velocity	Alteration Index	Alteration Velocity	
liais LL	L7	19	1,33	L3	8	0,19
	L8	13	1,93	L4	9	0,25
roche franche RL	R7	17	3,78	R3	7	4,32
	R8	11	3,62	R4	7	2,80
roche fine FL	F7	3	1,81	F1	3	8,25
	F8	3	2,40	F3	3	9,52
				F4	3	8,58
				F5	4	8,14
				F6	3	9,18
pierre de Souppes	S1	19	0,07	S2	13	0,10
	S2	20	0,13	S3	12	0,05
grès dur HF	D1	19	0,06	D2	12	0,46
	D2	19	0,10	D3	10	0,12
grès tendre SF	T1	6	4,02	T1	2	43,90
	T2	5	10,93	T4	2	29,71
				T5	2	32,77
				T6	3	31,63
white sandstone CS	C1	15	5,94	C3	9	5,81
	C2	13	8,10			
green sandstone VS	V1	16	0,30	V2	9	0,68
	V2	17	0,34	V3	9	0,59
brown sandstone	M1	23	0,16	M1	12	0,17
	M2	23	0,16	M3	11	0,30

Table ART2-2. Alteration index and alteration velocity for the tested samples

2.1.3. The Alteration Velocity

The alteration velocity (AV) is introduced to evaluate the process of weathering in longer term than AI. Mostly, in usual characterization of weathering, only the dry weight loss of samples at a certain stage is used (EN 12370). But the results can be very different if the experiment is stopped after 10 or 20 cycles. AV is used to evaluate the long term behaviour of the stone independently of the number of cycles. It is the final value of the derivative of the function representing the normalised weight as a function of the number of cycles (Table ART2-2). The nine stones can also be classified by their AV:

- low AV (up to 1 %weight/cycle for both experiments): SL, HF, VS, MS;
- medium AV (1 to 5 in experiment 1, 1 to 10 in experiment 2): LL, RL, FL;
- high AV (5 and more in experiment 1, 10 and more in experiment 2): SF, CS.

It is important to notice that the classification is different for AI and AV indicating that these two parameters are independent from each other. It suggests that these two parameters must be used together in order to evaluate more accurately the ageing of the stone.

2.2. Alteration pattern

A careful observation of samples through weathering cycles allow to distinguish two different categories of alteration patterns. Figure ART2-3 shows three examples of these alteration patterns. The size of the pictures is 4.5cmx4.5cm, the original size of the samples being 4cmx4cm.

2.2.1. Homo/Heterogeneity

It is possible to evaluate the regularity of the weathering of a set of samples from the same type of stone. Some stones present a regular weathering, starting with the progressive smoothing of corners and edges. This type of weathering is regarded as homogeneous, which means it is regular for one sample and approximately the same from a sample to another. Figure ART2-3a gives a good example of this alteration for the FL. The stones which present a homogeneous behaviour are FL, SL and HF.

On the other hand, some stones present various alteration behaviours from one sample to another from the same type of rock, even from one zone to another in a single sample. This

is due to pre-existent heterogeneities in the rock. These heterogeneities act as local weaknesses, and thus differential weathering can occur. These weaknesses can be obvious (e.g. fossils in RL or LL) or hidden (e. g. very competent zone in SF, Fig. ART2-3b). They can either consolidate or weaken the sample. For instance, a fossil creates a weak zone and when this zone breaks, the entire fossil can fall at once, even if the fossil itself is not altered. The stone with a heterogeneous decay are LL, RL and SF.

2.2.2. Anisotropy

The second type of alteration pattern concerns anisotropy. It means that alteration has a favourite direction for a stone (Fig. ART2-3c). Anisotropy is an intrinsic property of the material and if it exists, it controls the anisotropy of decay. Four different origins can be identified: the grains (mineral composition due to sedimentation, shapes and orientation), the pores (shape, orientation), the joints and the fractures. This predisposition will influence the decay in several ways: for example, layers that contain hygroscopic clays can cause damage during imbibition, less competent layers can be damaged easier by salt crystallization pressure, cracks can act as a localisation of crystallization and thus of damage... The stones from this study which present anisotropy in the decay are CS, VS and MS.



Figure ART2- 3a. Sample of FL after 15 cycles:
homogeneous behaviour.



Figure ART2-3b. Sample of SF after 15 cycles:
heterogeneous behaviour.

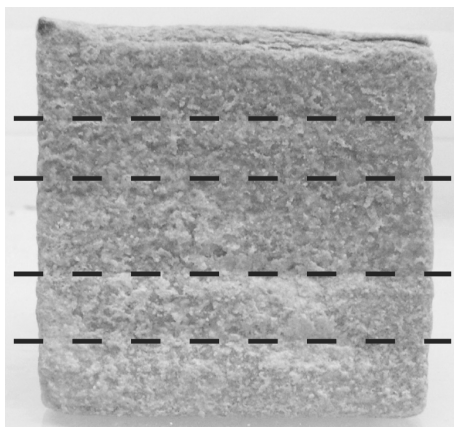


Figure ART2-3c. Sample of VS after 15 cycles: anisotropic behaviour.

3. Discussion

3.1. The stages of accelerated ageing

The duration and importance of the three stages of accelerated ageing (I, II, III) depend on the microstructure of the stone. During stage I, weight increase depends mainly on the characteristics of the porous network (porosity, pore size distribution...). The process of crystallization in pores starts during the evaporation. At first, all the pores that can be reached by capillary rise are filled with the brine. During the first stage of evaporation, the capillary phase, the solution and the ions it contains are driven out of the porous network. This means that all the salt here only crystallizes as efflorescences on the surface of the samples. The most important stage of evaporation starts at this moment: when the continuity of water is broken in the sample, the diffusion stage of evaporation starts (Fig. ART2-4). The water starts to circulate as vapour in the porous network, thus allowing salts to crystallize in pores. Stage I stops as soon as enough salt has crystallized in pores to allow further supersaturation and cause damage to the sample (Flatt 2002).

Then there are two possibilities: the first visual damage is either before the loss of weight or after. When the first visual damage occurs before the loss of weight, there is still room in the sample for salt to crystallize, and the loss of material is inferior to its salt uptake. The weight variation is then a competition of these two processes, and there is a stage II. When the loss of weight occurs first, it means that most of the room where salt can crystallize has been filled up. The damage starts when the stresses created by the crystallization pressure

and transmitted through the supersaturated solution is higher than the stone's tensile strength, and in this case there is no stage II.

Phase III starts when the relationship between normalized weight and the number of cycles starts to become approximately linear (Figs. ART2-2a, ART2-2c), i. e. when the salt uptake starts to be negligible compared to material loss. More precisely, it is linear for homogeneous stones. For the heterogeneous stones, the curve shows several steps, which are each approximately linear, but separated by sudden drops (Fig. ART2-2b). For instance, for RL or LL, these drops can be caused by the loss of an entire fossil.

3.2. Estimators

3.2.1. Alteration Index

In order to estimate the alteration index, a decomposition of the process of accelerated salt weathering has been proposed. This decomposition is based on the existing works about the phase diagram of sodium sulphate (Flatt 2002) and on the drying kinetics presented in figure ART2-8:

- imbibition of saline solution: pores are invaded by the brine;
- as relative humidity (RH) grows, thenardite hydrates into mirabilite by dissolution and reprecipitation (Rodriguez-Navarro et al. 2000) if temperature is below 32.5°C;
- with even higher RH, mirabilite is dissolved in the brine. Here stops the imbibition phase.
- evaporation starts with capillary evaporation and development of efflorescences;
- diffusive evaporation and crystallization of thenardite in the pores.

The crucial phase of this scheme is the crystallization of mirabilite in the pores after the dissolution of thenardite, when the temperature is below 32.5°C (Rodriguez-Navarro and Doehe 1999): this is the part of the cycle when the damages occur. The first damage will anyway appear on the weakest part of the sample. The only characteristics that matter are the hydric properties (capillary C and evaporation E coefficients both in $\text{g}/(\text{m}^2 \cdot \text{s}^{1/2})$) and the mechanical strength of the weakest part of the rock (tensile strength σ_T in MPa). This corresponds also to the parameters used in the estimation of the crystallization pressure for most models (Benavente et al. 2004b, Scherer 2004).

It is also important to recall that this study is only about sodium sulphate, and thus the estimator is only valid for damages induced by sodium sulphate crystallization. Figure ART2-5a and ART2-5b represent the estimator of AI (1) as a function of AI for the two experiments.

$$AI_{estim} = \ln\left(\frac{100.C}{E \cdot \sqrt{\sigma_T}}\right) \quad (1)$$

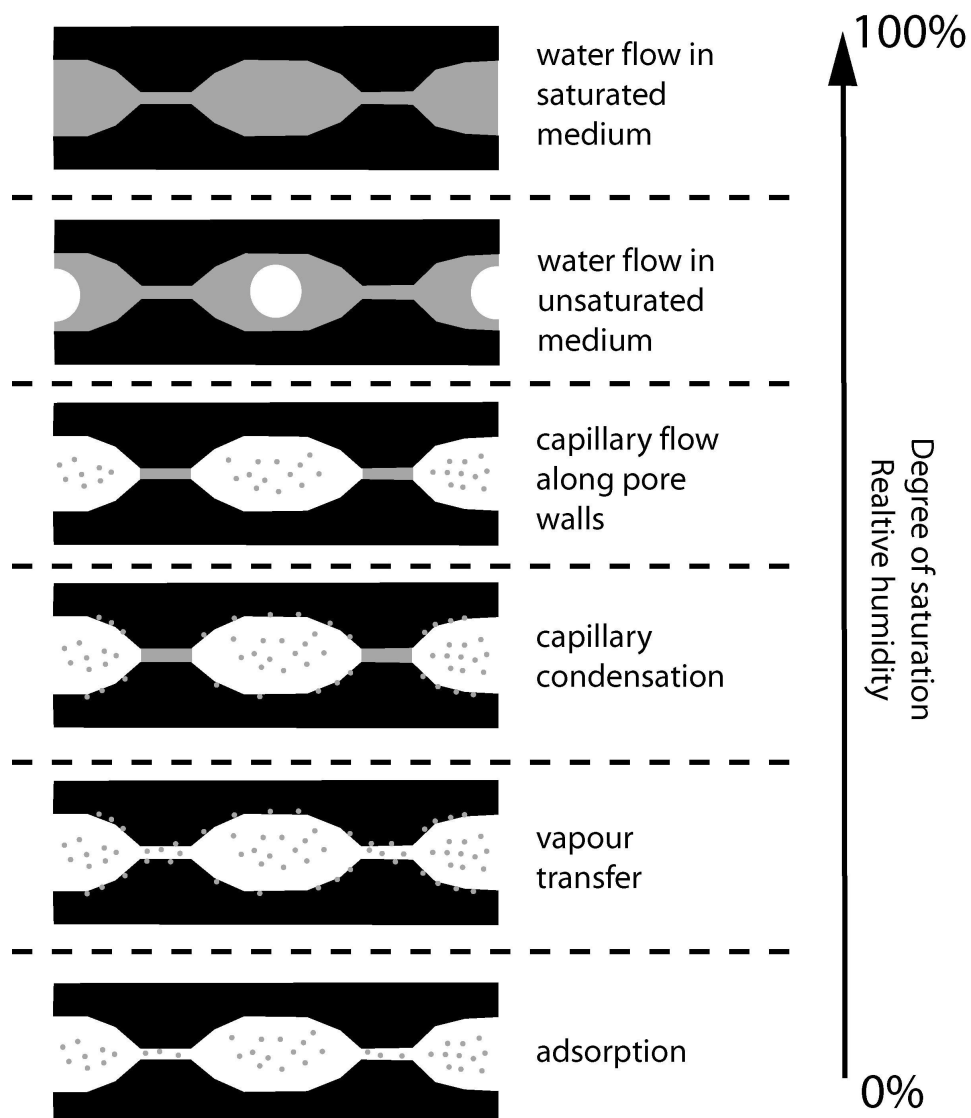


Figure ART2-4. Stages in the wetting of a porous system

(Beck et al. 2003, after Rose 1963).

3.2.2. Alteration Velocity

During stage III, the pores are considered to be always filled with salt and the supersaturation with respect to mirabilite reached at every cycle. The salts will crystallize and cause damages in the cracks and pores. Thus the more pre-existing cracks and pores in the rock, the more damage. And also the more cracks and pores in a rock, the lower the P-waves velocity (V_p).

On the other hand, these damages will be more important if the joints between the grains are weak, since in this case the cohesion of the stone is lower. When the grains are weakly bonded, the loss of energy at the interfaces is higher and thus V_p decreases.

These two features have the same influence on V_p . This means that V_p can estimate the long term behaviour of a rock. Since this long term behaviour is given by AV, V_p can be considered as a good trend for AV. However, the low values of the coefficient of determination of the linear regression (R^2) given on figures ART2-6a and ART2-6b show that it can not still be considered as a good estimator.

A part of this error comes from the fact that the velocity of the P-waves is slightly different in quartz (6050m/s) and in calcite (6600m/s). Another part comes also from the fact that one of the two cubes of SF turned out to be much more competent than the others, as competent as HF. If this value is withdrawn from the experimental values, R^2 rises up to 0.61 (instead of 0.45). The presence of clays can also be very damaging to a stone while not having a strong influence on the estimator, and by this could make this estimation incorrect.

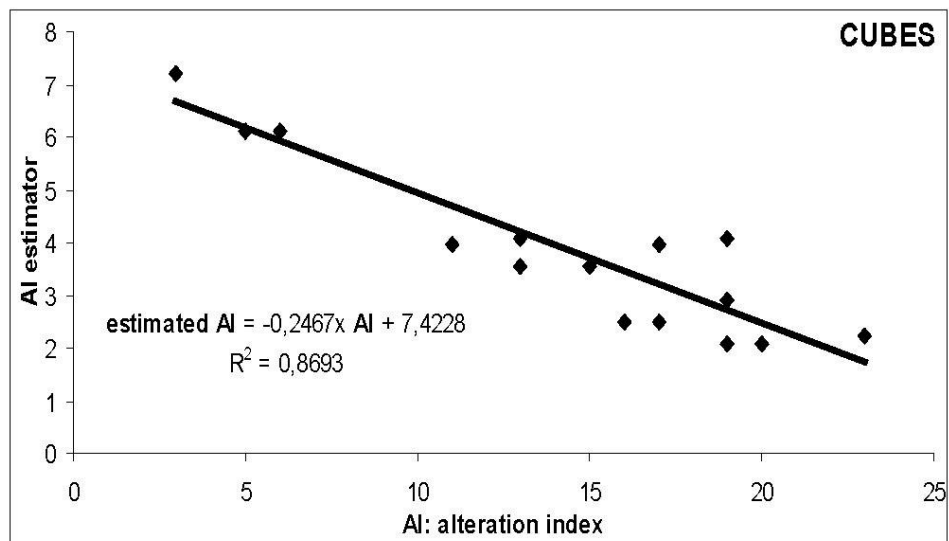


Figure ART2-5a. Estimation of the AI for the first experiment.

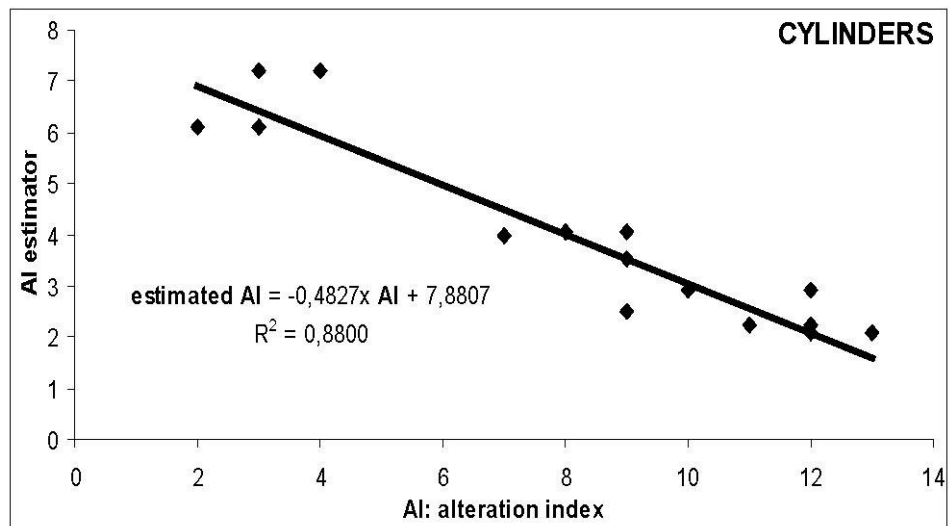


Figure ART2-5b. Estimation of the AI for the second experiment.

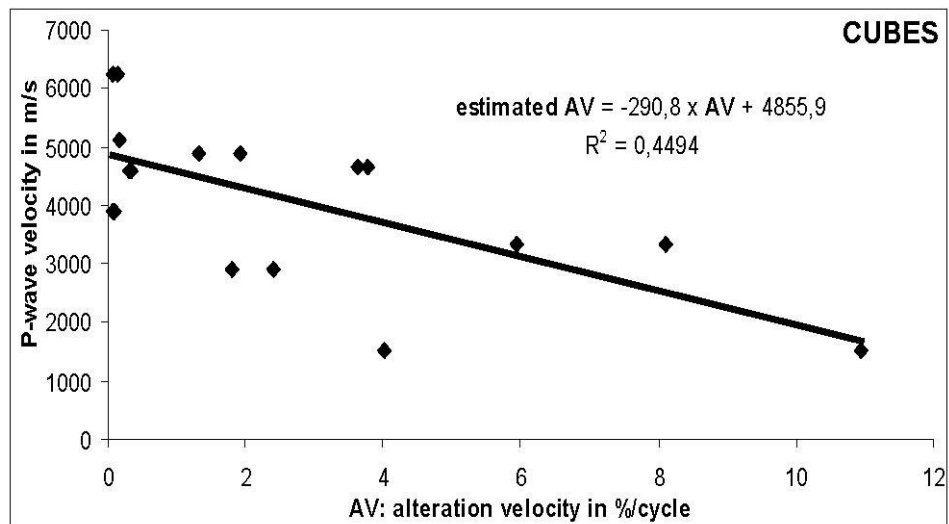


Figure ART2-6a. Estimation of the AV for the first experiment.

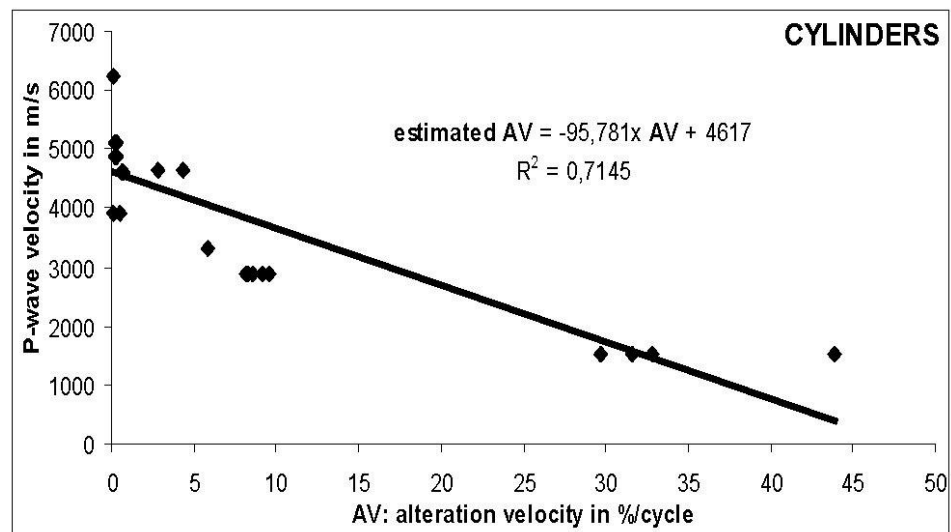


Figure ART2-6b. Estimation of the AV for the second experiment.

Nevertheless, this estimation can be useful because the P-wave velocity is non-destructive and easy to measure on-field, and a mineral analysis can help us to determine if this estimation is relevant or not.

3.3. Dimension effect

The resistance of a sample to salt decay has been estimated for both experiments. Now the importance of the dimension of the sample will be discussed.

3.3.1. Alteration Index

As shown in 4.2.1., evaporation is a very important phenomenon when it comes to salt crystallization in porous networks (Rodriguez-Navarro and Doehe 1999). When evaporation is impossible through a face of a sample, this face is not altered and the weathering of the whole sample is slowed down (Angeli et al. 2006). The easier the sample can be dried, the easier sodium sulphate can crystallize in the porous network.

For the same volume, the core of a sample will be dried faster if there is a dimension which is significantly smaller than the others. Figure ART2-7 explains this fact in a very simple way. Hence, the smallest dimension of a sample will affect its resistance to salt weathering. It can be considered in multiplying the slope of the linear regression by the smallest dimension of a sample (4cm for the first experiment, 2.5cm for the second) for each

experiment. It gives two values of 0.99 and 1.20 cm, which differ from 18% (the difference between the two slopes is 50%).

It is important to notice that this estimation is only relevant for the middle term behaviour. For the very short term, other parameters are to be taken in account: for instance, the cubes will alter faster than cylinders since there are more edges and corners.

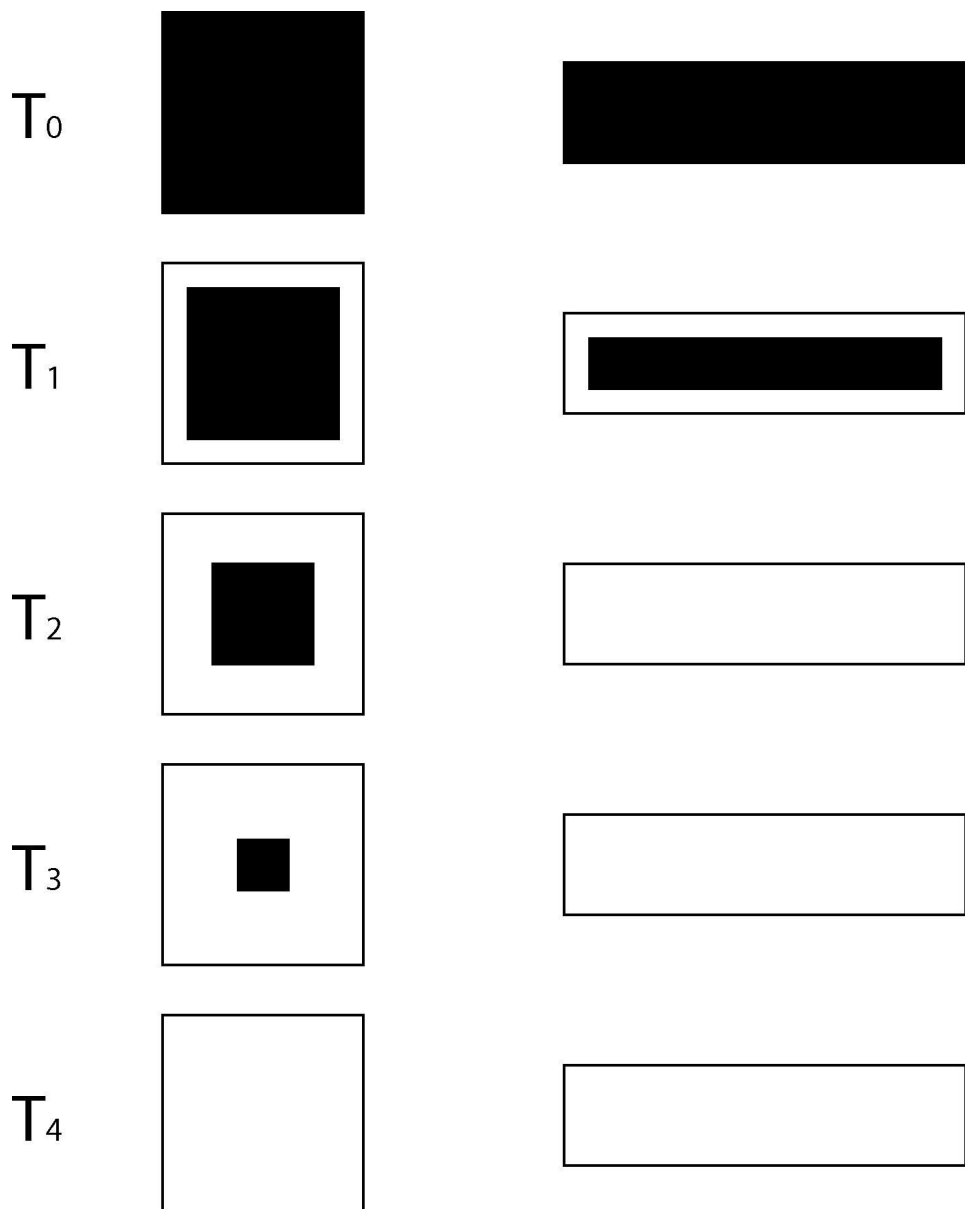


Figure ART2-7. Simplified evaporation kinetics of two samples of the same volume but different dimensions. The same thickness of water evaporates in the two samples between two instants. The part of the sample which is wet is in *black*, the dry part is in *white*.

3.3.2. Alteration Velocity

For a given sample, AV will depend on the total surface exposed to evaporation. The samples seem to lose a small thickness of grain on every side that was exposed to evaporation. During stage III, the samples seem to lose a small thickness of material during each cycle. By using the same approximation technique as in last paragraph, this fact can be estimated by dividing (not multiplying because a resistant stone has a low AV) the slope of the linear regression by the total surface of the sample (the samples are immersed in our experiments). It gives two values of 4.33 and 4.54 cm⁻², which differ from 4.5% (the difference between the two slopes was 66%).

Nevertheless, those two evaluations need more data to be confirmed, with more shapes tested. In addition to that, the linear regressions in both cases are very approximate. Anyway it is clear that the shape and size of a sample has an influence on its alteration. For a given volume, the most resistant shape is the one that minimizes the exposed surface and maximizes the smallest dimension: the sphere.

Conclusion

A new way for evaluating accelerated ageing through crystallization of salt is proposed. It is composed of two parameters: alteration index (AI) and alteration velocity (AV). It is then possible to classify the different stones according to these two indicators: the results show that the stones that are the most resistant at first (high AI) are not necessarily the most resistant at the end (low AV). It allows characterizing the alteration during the whole test and not just at the end of it.

Another classification of alteration is also proposed. It takes into account the alteration patterns: homogeneous, heterogeneous or anisotropic. This can be estimated by a microstructural study of the stone.

The accelerated ageing can be decomposed into 3 stages. Stage I corresponds to the weight gain due to salt crystallization in the pores. Stage II, when it exists, is an intermediate stage during which there is a competition between salt supply and material loss. Stage III corresponds to the long term alteration, when the weight loss is approximately linear.

Two estimators have been given for respectively AI and AV. Those estimators underline the fact that it is crucial to perform a microstructural study of the stone to predict its weathering. The main result is that the P-wave velocity in the stone gives a good idea of the long term behaviour of the stone: the higher the P-wave velocity, the more resistant the stone.

The shape of a sample has also an important influence on its weathering through crystallization of salts, because it directs the evaporation kinetics. A sample that has a significantly smaller dimension with respect to the two others will alter faster as a more regular, the most resistant shape being the sphere.

Acknowledgements

The authors would like to thank M. Pallix from ROCAMAT (Saint-Maximin-sur-Oise) for providing LL, RL and FL, and M. Oliveira (Moigny-sur-Ecole) for the other samples.

References

Angeli M, Bigas JP, Menéndez B, Hébert R, David C (2006) Influence of capillary properties and evaporation on salt weathering of sedimentary rocks. Paper presented at the Heritage Weathering and Conservation conference in Madrid, 21-24 june, 2006

Beck K, Al-Mukhtar M, Rozenbaum O, Rautureau M (2003) Characterization, water transfer properties and deterioration in tuffeau: building material in the Loire valley - France. Building and Environment 38:1151-1162

Benavente D, García del Cura MA, García-Guinea J, Sánchez-Moral S, Ordoñez S (2004a) The role of pore structure in salt crystallisation in unsaturated porous stone. Journal of Crystal Growth 260:532-544

Benavente D, Garcia del Cura MA, Fort R, Ordoñez S (2004b) Durability of porous building stones from pore structure and strength. Engineering Geology 74:113-127

EN 12370 (1999) Natural stone test methods – Determination of resistance to salt crystallization. 1999-03

Chapter IV : Salt damage

Flatt RJ (2002) Salt damage in porous materials: how high supersaturations are generated. Journal of Crystal Growth 242:435-454

Hammecker (1993) Importance des transferts d'eau dans la dégradation des pierres en œuvre. Ph-D Thesis University of Strasbourg, France

Kracek FC (1928) Int. Critical Tables 3 (p. 371)

Rodriguez-Navarro C, Doehne E (1999) Salt weathering: influence of evaporation rate, supersaturation and crystallization pattern. Earth Surface Processes and Landforms 24:191-209

Rodriguez-Navarro C, Doehne E, Sebastian E (2000) How does sodium sulphate crystallize? Implications for the decay and testing of building material. Cement and Concrete Research 30:1527-1534

Rose DA (1963) Water movement in porous materials – II: the separation of the components of water movement. British Journal of Applied Physics 14 :491-496

Scherer G (1999) Crystallization in pores. Cement and Concrete Research 29:1347-1358

Scherer G (2004) Stress from crystallization of salt. Cement and Concrete Research 34 :1613-1624

Steiger M (2005) Crystal growth in porous materials – I: the crystallization pressure of large crystals. Journal of Crystal Growth 282:455-469

Comment on this article

It has been assessed in the second chapter that the red Agra sandstone has a very high SSA, $3.29 \text{ m}^2/\text{g}$, due to the presence of clays. This study proves that this sandstone is one of the most durables stones among those which have been tested. This is quite unexpected because clays are generally known to enhance damage due to salt crystallization (McGreevy and Smith 1984). This study brings thus new information to properly evaluate the influence of clay minerals in the salt weathering of sedimentary stones. Nevertheless a more precise study of the clay minerals contained in this stone (and specially their expandability) and of their quantity should bring decisive information to understand their effect in this kind of weathering.

1.3. Effects on mechanical strength

The aim of this study is to try to evaluate the evolution of the mechanical strength of two limestones (the biotitic limestone LL and the detritic limestone FL) during the tests of accelerated ageing. It is clear from previous experiments that only the parts of the stone that are exposed to evaporation are subjected to salt weathering (cf. Chapter V 1.1.). Thus it should imply that the mechanical strength of the stones is only altered on the surface. Nevertheless no study has described the evolution of the stone mechanical strength during weathering cycles to the author knowledge.

In order to monitor this evolution of mechanical strength, cubic samples of 7cm side of LL and FL have suffered 15 cycles of salt weathering by sodium sulphate. The testing method was exactly the same as the one exposed in this chapter (1.2.; Angeli et al. 2007). Two samples of each stones have been taken at cycles 2, 4, 6, 9, 12 and 15. In the heart of one sample three cylinders of 2.5cm diameter and 5cm height have been cut in order to perform four uniaxial compressive tests. In the heart of the other sample, three cylinders of 4cm diameter and 2cm height have been cut, this time to perform three Brazilian tests as indirect measurements of the tensile strength. Note that the samples are cut from the heart of the sample, which appears still sane. Those mechanical tests were performed according to the method exposed in chapter II 3.2. These tests are considered since the weight and picture monitoring of the samples is similar to all the other tests performed on both stones (Angeli et al. 2006, 2007, accepted; Hébert et al. submitted). The average values and standard deviation are presented in figure IV-1.

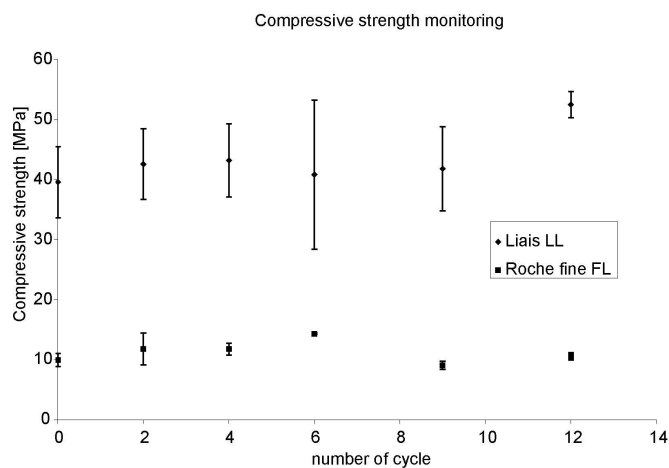


Figure IV-1a. Compressive strength monitoring of “roche fine” FL and “liais” LL during accelerated salt decay cycles.

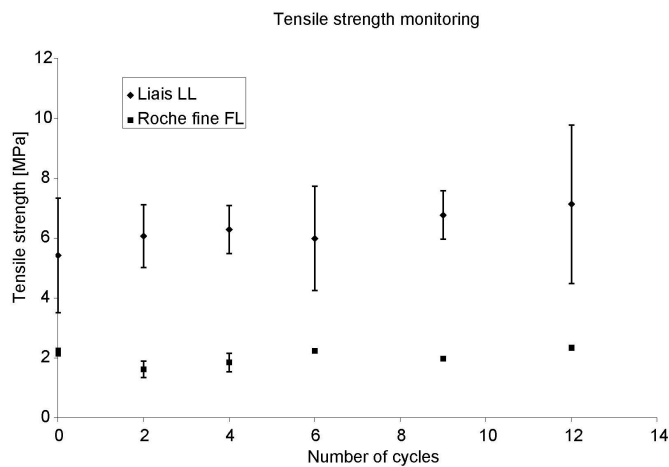


Figure IV-1b. Tensile strength monitoring of “roche fine” FL and “liais” LL during accelerated salt decay cycles.

The first thing to notice is that the measures are more homogeneous for FL than for LL. This can be correlated to the macroscopic structure of the stones, LL being much more heterogeneous than FL. These values are even more different since macrofossils can act as local weaknesses during the tests, and the standard deviation can reach up to one third of the average value. The most important thing to notice is that, although the samples of FL are starting to be weathered on the surface since cycle 3 or 4 (depending on the sample), both compressive and tensile strength in the heart of the sample stay constant, suggesting that weathering had not accessed the inner part of the sample. This corroborates the general knowledge of sodium sulphate which is known to crystallize close to the surface (Ruiz-Agudo et al. 2007).

2. Microscale experiment

2.1. Modification of the porous network by salt crystallization of experimentally weathered sedimentary stones (article 3; Materials and structures)

This study aims at understanding how the damage is initiated and occur inside the porous network. Once a good knowledge of the macroscopic processes has been reached, it is important to try to understand the microscopic origin of the macroscopic features. The main technique used for this will be MIP supported by image analysis. For a single stone, three samples from a fresh sample have been tested: one fresh, another weathered, and the last one weathered but cleaned from the salt. The experiments have been led on the nine stones but only analyzed for the five stones with a unimodal distribution of pores, the others having a too high natural variability. The differences between the MIP spectra give information about the size of cracks and the location of salt crystals. Those results are completed by thin sections observations.

“Modification of the porous network by salt crystallization in experimentally weathered sedimentary stones”

Matthieu Angeli¹, David Benavente², Jean-Philippe Bigas^{1,3}, Béatrice Menéndez¹, Ronan Hébert¹ and Christian David¹

¹ Université de Cergy-Pontoise

Département de Sciences de la Terre et Environnement
5 mail Gay-Lussac, Neuville-sur-Oise
95031 Cergy-Pontoise CEDEX
France

² Universidad de Alicante

Departamento de Ciencias de la Tierra y del Medio Ambiente
Laboratorio de Petrologia Aplicada
Apartado 99
03080 Alicante
España

³ CHRYSO

7 rue de l'Europe
45300 Sermaises
France

Accepted by Materials and structures on September 10th, 2007

Abstract

The aim of this study is to understand how the porous network of a stone is modified by the crystallization of sodium sulphate. Samples of five different stones have been experimentally weathered and evaluated thanks to mercury porosimetry in three different states: fresh, weathered by salt, and weathered cleaned from the salts. Optical and electronic microscopy observations have also been led to complete these measurements. The results show that porosity and the general aspect of the porous network remain quite similar after weathering. Nevertheless, crystals tend to grow on all the grains regardless of the size of the related voids (pores or cracks), and these crystallizations seem to be harmful for the stone: a lot of voids of different entry sizes (from 10 nm to 20 μm) have been affected by the accelerated ageing tests. This study confirms that generally stones with a high amount of small pores (up to several μm) are the most susceptible to suffer from salt damage. Nevertheless, the influence of a few other features (high porosity, pore shape, pre-existent intragranular cracks) on the long-term behaviour of the stones suffering from salt decay is discussed.

Résumé

L'objectif de cette étude est de comprendre comment les réseaux poreux sont modifiés par la cristallisation de sulfate de sodium. Des échantillons de cinq roches différentes ont été vieillis expérimentalement, et leurs distributions porales ont été obtenues dans trois états différents : frais, altérés et altérés avec nettoyage complet des sels. Des observations en microscopie optique et électronique ont confirmé ces mesures. Les résultats montrent que la porosité et l'aspect général du réseau poreux reste assez similaires après l'altération. Cependant, les cristaux ont tendance à croître sur tous les grains quelque soit la taille des vides associés. Ces cristallisations semblent d'endommager la roche : beaucoup de vides de tailles variées (entre 10nm et 20 μm) ont été affectés par les tests de vieillissement accéléré. Cette étude confirme qu'en général les roches avec une grande proportion de petit pores (jusqu'à quelques μm) sont les plus sensibles à l'altération par les sels. De plus, l'influence de quelques autres paramètres (porosité élevée, forme des pores, fractures intragranulaires préexistantes) sur le comportement à long terme des roches sous l'effet de la cristallisation de sels est discuté.

Introduction

Salts, and particularly sodium sulphate, are known to be among the most destructive agents in porous stones, concrete or brick weathering. Their study is thus very important to fully understand their crystallization process in porous networks and, in the future, to find a way to prevent or limit their damage to porous materials. Recent studies attribute the decay to the salt crystallization pressure of mirabilite ($\text{Na}_2\text{SO}_4 \cdot 10\text{H}_2\text{O}$), rather than thenardite (Na_2SO_4) (Rodriguez-Navarro & Doehe 1999, Scherer 1999, Flatt 2002, Benavente et al. 2004a, Steiger 2005a,b). This damage depends on numerous factors: the type and quantity of salt in the stone, the characteristics of the porous network, the environmental conditions (a complete review can be found in Ruiz-Agudo, 2007). The aim of this study is to understand how the porous network of the stone can be modified by crystallization of salts in pores. Mercury porosimetry will help to find in which range of pore entry size sodium sulphate crystallizes, what is the size of the new cracks due to crystallization pressure, and if these characteristics differ from one stone to another, that is to say to what extend salt damage depends on the porous network of the stones. This will help to have an experimental illustration of the thermodynamical theories about crystallization of salts in pores (Scherer 2004; Steiger 2005a,b; Coussy 2006) in order to enhance the general comprehension of the process, and in the longer term find a way to reduce their damage.

Several studies have already been led to understand the influence of the stone microstructures on its durability to salt weathering. Russell (1927) was the first to introduce the idea that the stones with the most micropores are the most susceptible to salt decay. This idea has been confirmed later by other studies (Schaffer 1932; Honeyborne and Harris 1958; Fitzner and Snethlage 1982).

Fitzner (1988) compared the porous network from different samples of Schilfsandstein, a german sandstone. One sample was fresh from the quarry; one was taken from a building, and the last one came from the flaking of the stone. He concludes that pores with entries under 100 nm are unchanged, and that the mean size of the pores rises. Fitzner (1988) concluded that pores with entries under 100 nm are not reached by the fluids, and that the pore size raise is due to the progressive destruction of grains.

Benavente et al. (1999) has worked on 3 different types of Bateig stone with porosity around 15% (white, blue and layered) and a quartzarenite with 6.4% total porosity. The authors compared the size of the pore entry for fresh samples and experimentally weathered samples cleaned from salt (sodium sulphate). They have observed that the porosity and pore size raises more for stones with a high proportion of pores from 0.1 to 2500 µm. In this range of pore size, as the flow is governed by capillarity, the brine flows easily and thus cycles of imbibition followed by drying occur more easily, which increases significantly the possibility for the salt to crystallize. They also concluded, as did Fitzner (1988), that damage associated with the smallest pores (under 0.1 µm) is difficult to observe. A solution to this problem would be to use helium pyknometry and compare it to mercury porosimetry to see how these smallest pores are affected by salt weathering.

Such a comparison has been undertaken by Dei et al (1999) on four different building stones with relatively low porosity: two stones of clastic origin (Pietraforte and Firenzuola stone) with total porosity around 8% and two carbonate stones with very low porosity: Travertine and Carrara marble (resp. 4.4 and 2.7%). The accelerated salt weathering experiments have been performed with KNO_3 , and the weathered samples have not been cleaned from salt before mercury porosimetry and helium pyknometry testing. The mean pore size rose for the 4 stones used. According to the authors, the crystals of KNO_3 grow not only beneath the external surface of the sample but also deeper within the porous structure. These crystals tend to grow in large pores and close the entrance of small pores, which become undetectable to mercury porosimetry.

Rodriguez-Navarro and Doehne (1999) have worked on an oolithic limestone widely used as a building stone in the United Kingdom: the Monks Park stone. They used both sodium sulphate and chloride for their accelerated weathering tests. This stone has a porosity of 20.0% and a mean pore radius between 0.20 and 0.30 µm. After the tests, the samples tested with sodium chloride were slightly destroyed compared to the samples tested with sodium sulphate which presented contour scaling and lost up to 20% of their initial weight. The mercury porosimetry tests performed with the salts still in the porous network showed that the porosity has not really changed with sodium sulphate. The peak of pore entry around 1 µm has slightly shrunk and shifted to smaller values indicating that a large part of the pore entries has been slightly obstructed by the crystals of sodium sulphate. Nevertheless, the

sodium chloride has filled all the smaller pores of the stones (entry under $0.2\mu\text{m}$), and thus reduced the porosity to its half. The reason why it damages less Monks Park limestone is because sodium chloride reaches lower supersaturation ratios, and thus lower crystallization pressure (Correns 1949). The authors indicate that supersaturation during drying takes place in the smaller pores where higher crystallization ratios can be achieved, the larger ones acting like reservoir to supply the solution. According to them, this explains why stones with a large proportion of micropores connected to large pores are very sensitive to weathering (Everett, 1961). These conclusions are a bit different from Dei et al. (1999) who suggest that there are more damages when crystals grow in large pores, close to the entrance of small ones.

1. Materials and Methods

1.1. Materials

Five stones from different lithologies have been used in this study: two limestones and three sandstones. The analysis of the damage has also been performed on two other sandstones. The two limestones are of lutetian age: the “roche fine” (FL) and the “liais” (LL). These limestones come from the Parisian basin. They have high porosity compared to the other stones in this study (respectively 36.1 and 17.0 %). FL is a detritic limestone made of calcite grains (90 %) and quartz (10 %). It contains lots of microfossils (mainly nummulites). Its tensile strength is very low (1.5 MPa). LL is a biodetritic limestone composed of more than 90 % of calcite, with traces of iron oxides. It also contains some microfossils like nummulites, but also numerous macrofossils (bivalves, gasteropods) giving to the stones a heterogeneous aspect. During diagenesis, which was very similar for both stones since they come from the same quarry, secondary micrite crystals have precipitated and entailed a secondary porosity.

One of the sandstones is Fontainebleau sandstone (HF). It is composed of more than 99% of quartz. Its porosity is low (4.6%). The two other sandstones are two layered sandstones from India: the brown sandstone (MS) and the green sandstone (VS), two commercial varieties of the Agra sandstone. They are composed mostly of quartz, but contain some clay which gives the general colour of the rock and the layering. These sandstones have a very high tensile strength (16.0 and 15.0 MPa) and low porosity (5.2 and 4.6%).

Complete hydromechanic properties of our seven sedimentary rocks are given in Table ART3-1. The Alteration Indices (AI) and Velocities (AV) introduced by Angeli et al. (2007) are also reported in order to evaluate the durability of these stones. For recall, AI corresponds to the number of cycles experienced by the stone sample when the first visual damage appears. This means that the most durable stones have a high AI and a low AV.

The three sandstones and the FL limestone have a detritic origin, and thus a quite simple porous network with only one main family of pores. This study will mostly focus on these four stones, and then we will compare the results obtained to a much more complicated stone: the biodetritic lutetian limestone LL. These five stones were chosen among the ones used in the experiments presented in Angeli et al. (2007) because they show a regular decay and their porous network can be easily studied. The mercury porosimetry tests have also been performed on two other sandstones presented in Angeli et al. (2007): a soft variety of the Fontainebleau sandstone (SF) and a Chinese sandstone (CS). Due to the very low durability of these stones, it was not possible to include these data in our analysis. Nevertheless, a thin section study of these stones has been performed to try to explain their low durability.

Total open porosity P(He) and grain density were characterised using mercury intrusion porosimetry (MIP) technique and helium pyknometer. An underestimated open porosity P(Hg), bulk density, pore size distribution and mean pore radius were obtained in an Autopore IV 9500 Micromeritics mercury porosimeter. Pore size interval characterisation by MIP ranges from 0.006 to 200 μm , which corresponds to the highest and the lowest head pressures, respectively. Note that during this study, pore size will refer to the pore radius. In order to quantify porosity fraction below 0.006 μm , which can not be measured by MIP, total open porosity was calculated. Total open porosity (P(He)) is the volume of pores accessible to Helium, as opposed to what is called here “underestimated open porosity” which the volume of pores accessible to mercury. Consequently, “underestimated open porosity” is a fraction of the total open porosity.

Porosity (He) %	Porosity (Hg) %	submicro-porosity (Hg poro) % of total porosity	bulk dens. g/cm ³	Evap. coef.	Capillary coef.	mean pore radius μm	Specific Surface area m ² /g	P wave velocity m/s	Tensile strength MPa from Angelis et al. 2007	Alteration Index	Alteration Velocity
Hard Fontainebleau HF	4.6	4.60	0.0	2.54	15.4	6.39	2.866	0.15	3903	5.2	11
Brown Agra MS	5.2	4.64	12.3	2.53	10.5	3.86	0.034	3.59	5114	16.0	11.5
Green Agra VS	4.6	3.99	10.4	2.54	12.3	5.81	0.047	1.25	4597	15.0	9
Fine (St Maximin) FL	36.1	34.44	4.5	1.70	66.9	1106.10	12.004	1.48	2897	1.5	3
Liais (St Maximin) LL	17.0	14.23	16.3	2.30	26.7	32.25	0.444	0.92	4879	4.2	8.5
Chinese sandstone CS	2.7	2.1	22.2	2.58	6.4	5.45	0.31	0.73	3329	6.1	9
Soft Fontainebleau SF	7.4	7.1	4.05	2.44	12.6	40.12	3.761	0.4	1514	1.5	2.25
											34.50

Table ART3-1: Hydromechanical and durability properties of the studied stones.

Pore size (μm)	Hard Fontainebleau HF	Brown sandstone MS	Green sandstone VS	"Roche Fine" FL	Liais LL							
	fresh	altered	cleaned	fresh	altered	cleaned	fresh	altered	cleaned	fresh	altered	cleaned
< 0.01	0.00	0.00	0.00	0.15	0.05	0.04	0.07	0.06	0.11	0.00	0.00	0.00
0.01 -> 0.1	0.03	0.01	0.00	3.90	3.40	3.59	3.41	3.39	3.46	0.19	2.19	2.09
0.1 -> 1	0.46	0.80	0.86	0.00	0.13	0.27	0.09	0.09	0.27	3.04	4.04	3.93
1 -> 10	3.45	3.84	4.04	0.22	0.32	0.19	0.06	0.30	0.25	11.24	13.06	12.08
10 -> 100	0.49	0.54	0.53	0.21	0.26	0.37	0.22	0.44	0.30	19.45	14.46	18.43
> 100	0.18	0.25	0.20	0.16	0.17	0.23	0.14	0.19	0.18	0.51	0.75	1.03
Porosity (Hg)	4.60	5.45	5.64	4.64	4.34	4.69	3.99	4.47	4.57	34.44	34.50	37.56
												14.23
												13.07
												13.99

Table ART3-2: Evolution of the porosity corresponding to ranges of pore entry sizes before and after accelerated weathering

The volume of the smallest pores (fewer than 6nm) has thus been estimated thanks to Helium pyknometry. As Helium is a gas, it has access to more pores than mercury which has a higher surface tension. The difference between the two values of porosity obtained gives the submicroporosity (Dei et al. 1999). For each stone, the bulk and grain densities from mercury porosimetry have been used, as well as the grain density obtained by an AccuPyc 1330 Helium pyknometer. Equation (ART3-1) gives the value of the connected porosity from mercury porosimetry $P(Hg)$, and equation (ART3-2) gives the value of the total open porosity. The submicroporosity is expressed as a percentage of $P(He)$ after equation (ART3-3).

$$P(Hg) = 100 \left(1 - \frac{d(\text{grain}, Hg)}{d(\text{bulk}, Hg)} \right) \quad (\text{ART3-1})$$

$$P(He) = 100 \left(1 - \frac{d(\text{grain}, He)}{d(\text{bulk}, Hg)} \right) \quad (\text{ART3-2})$$

$$\text{submicroporosity} = 1 - \frac{P(Hg)}{P(He)} \quad (\text{ART3-3})$$

Obviously this value cannot be precisely defined since the mercury porosimetry measurements are not as accurate as the helium pyknometry measurements. Nevertheless, the given values can be interpreted as reliable trends, since the bulk and grain densities have been measured on at least five different fresh samples for each stone. We can see in Table ART3-1 that submicroporosity is low for the two stones with large grains (0.0% for HF and 4.5% for FL), and higher for the three other stones (12.3% for MS, 10.4% for VS and 16.3% for LL). This means that the proportion of very small pores (under 6nm) is higher in the latter stones. As will be seen later, this is confirmed by the fact that the MIP spectra for these three stones are open on the left side of the spectrum, suggesting pores with entry smaller than 6 nm, in agreement with the fact that the two Agra sandstones are highly compacted with very small pores. For the liais LL, the high submicroporosity could result from the secondary micrite reducing the mean pore entry size of this stone, but could also be exaggerated due to the heterogeneities from one sample to the other.

Figure ART3-1 presents the MIP spectra obtained for three samples for each stone. Four of these stones have a relatively simple mercury porosimetry spectrum with most of the pore entry size around a mean value: 0.03µm for MS, 0.06µm for VS, 3µm for HF and 10µm

for FL. The last stone, LL, shows several pore entry sizes from 0.01 to 20 μm , with a main peak at around 0.1 and secondary random peaks from 1 to 100 μm approximately. It should be noted that the porosity due to diagenesis for the two limestones (LL and FL) is present in both mercury porosimetry spectra as a peak at around 0.150 μm with a height of approximately 0.40 ml/g. For the five different stones, there is a final peak in the spectra at around 100-200 μm . The height of this peak varies from 0.005 to 0.02 ml/g. This is due to the fact that the rocks are composed of grains (or fossils for LL), and the interstices between grains fall into a range of about 100 μm . Nevertheless, according to all the theories about salt crystallization (Scherer 2004; Steiger 2005a,b; Coussy 2006), no damage should occur in such big pores.

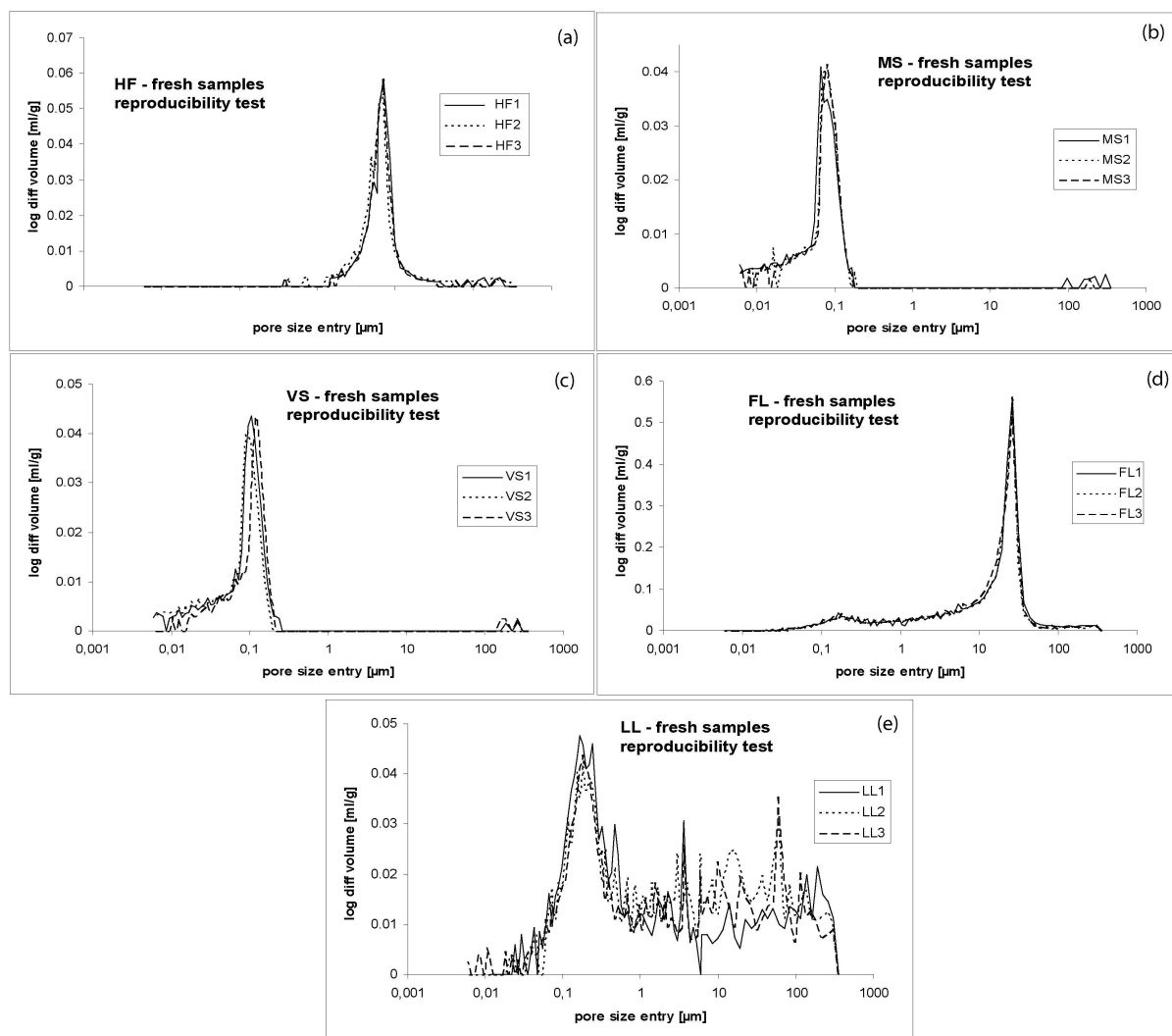


Figure ART3-1. Mercury porosimetry spectra of three adjacent fresh samples ($\sim 3\text{cm}^3$) of (a) Fontainebleau sandstone (HF); (b) brown Agra sandstone (MS); (c) green Agra sandstone (VS); (d) detritic limestone called “roche fine” (FL); (e) bidetritic limestone called “liais” (LL).

The capillary coefficient has been obtained by using the EN 1925 European standard test. The tensile strength has been evaluated with Brazilian tests. The evaporation coefficient has been obtained similarly to the capillary coefficient: it is expressed as the slope of the graph presenting the weight variation divided by the evaporation surface as a function of the square root of time. In this kind of plot, phase 2, which depends mainly on the characteristics of the stones and less on the environmental conditions, is linear (Hammecker 1993). The reason why this evaporation coefficient is used instead of the usual coefficient (linear coefficient of weight loss as a function of time during phase 1) is because this coefficient is independent of the environmental conditions, which is not the case for the usual coefficient.

The salt used in this study is sodium sulphate for practical reasons. This salt is known as the most destructing salt regarding accelerated ageing tests; hence noticeable results are obtained easily. This is the reason why it has been widely studied before, and the damage mechanisms are rather well known (e.g. Rodriguez-Navarro and Doehne 1999, Rodriguez-Navarro et al 2000, Lopez-Arce and Doehne 2006, Ruiz-Agudo et al 2007).

1.2. Methods

1.2.1. Experimental weathering test

The durability of the rocks has been tested according to the EN 12370 standard (1999) about stone resistance to crystallization of salts in pores. The samples are cylinders of 2.5cm diameter and 4.5cm height, and two samples have been used for each stone. The test is composed of cycles which last 24h:

- 2 hours of immersion in a saturated solution with respect to sodium sulfate;
- 15 hours of drying at 105°C in order to prevent mirabilite crystallization during drying of the samples;
- 7 hours of cooling at room temperature (20-25°C, 30-40% relative humidity RH). The samples were weighed after 2 hours during this stage.

Since the experimental conditions are similar for all the samples (type and quantity of salt, environmental conditions), the only difference of weathering between the samples can be associated with differences in the microstructures.

1.2.2.Characterization of the samples

First, a slice of approximately 1cm thickness has been taken from the fresh samples, and the pore size entry distribution has been obtained. Then, fifteen cycles have been performed on the remaining part of the samples. Sample weight has been monitored during the experiment in order to have an idea of the evolution of the decay. After 15 cycles, a slice of the more damaged sample of each stone type has been removed and cut into halves. This slice has been cut on the side where the first fresh slice has been taken before the beginning of the tests, in order to limit the impact of the natural variability of the stones. The distribution of the porous network of one half was measured directly with mercury porosimetry. For the other half, the salt has been removed before the mercury porosimetry test was performed.

To remove the salts from the samples, they have been immersed in distilled water at 50°C to prevent damage during cleaning, and the water was changed every day. Electrical conductivity of the water used to wash the samples was monitored to follow its degree of saturation, since the concentration of sodium sulphate in the solution has a significant influence on it. After the first days of cleaning, it was reaching values up to several hundreds of mS/m. The samples were considered clean when the electrical conductivity was stable around 0.3mS/m while deionised water had a conductivity of 0.1mS/m. The spectrum values for the fresh, weathered and clean samples of the five stones are presented in Table ART3-2.

For all the mercury intrusion porosimetry measurements, the contact angle for the mercury-solid interface has been set to 130° which is typical for most solids (Good and Mikhail 1981). The effect of the presence of salt in the weathered samples has been neglected, although the mercury-salt and mercury-stone contact angles are certainly different (Ruiz-Agudo et al 2007).

Thin sections of the fresh stones have been observed to complete the mercury porosimetry measurements, as well as SEM observations of clean and weathered samples.

1.2.3. Influence of salt crystallization on mercury porosimetry data

First and foremost, it is important to work with mercury porosimetry data using volume data and not percentage data. Results show that the global porosity of the samples changes during the tests. The porosity decreases with the presence of crystallized salts, and rises with the creation of cracks with propagation of existing cracks and with enlargement of pores. Therefore the only good comparison of the porous spaces is with volume of mercury intrusion.

We will first assume that the porous network is not modified during the final dissolution of the salts, which aims to clean the samples. We can think that while we add pure water in the samples at a temperature higher than 32.4°C (temperature limit of mirabilite stability), mirabilite precipitation is prevented and thus no damage is done to the porous network during the progressive desaturation of the samples. So all the modification observed on the porous network occurred before the final dissolution of the salts. Stresses are released when a crystal is dissolved and the void (pore or microcrack) in which it lies can close down after the dissolution. But it will not change anything on the mercury porosimetry data, since in both cases we will see this void neither with the crystals (void filled) nor without the crystals (void closed). Let us now consider different mechanisms which might affect the MIP spectra.

Case 1: If the pore entry is obstructed (fig. ART3-2a), the entire pore volume is seen by the device with a lower diameter, hence the peak will shift to lower values and the global porosity value will remain almost unchanged. (fig. ART3-2b)

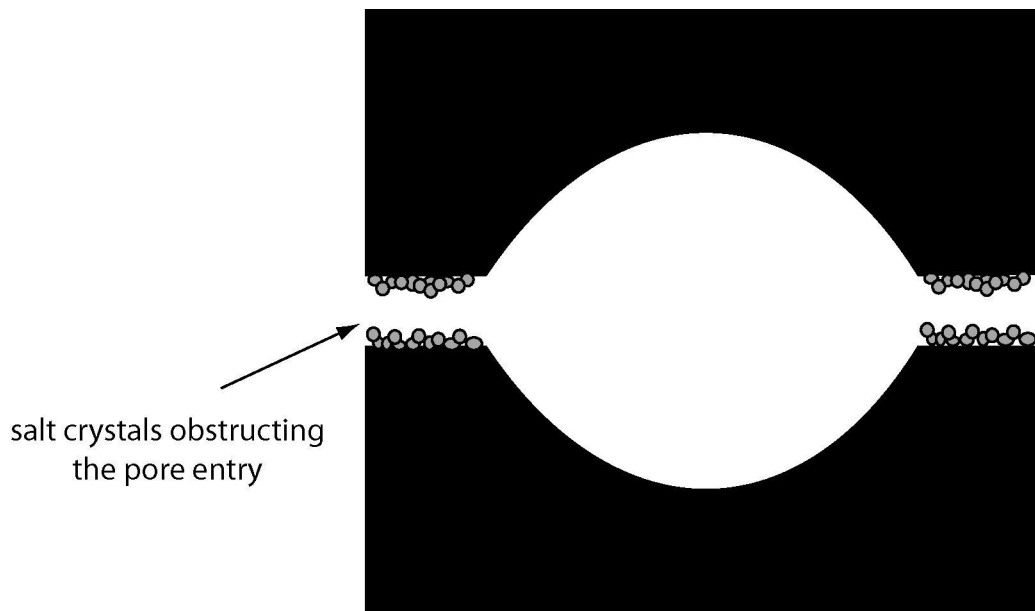


Figure ART3-2a. Salt crystals obstructing a pore entry (Case 1).

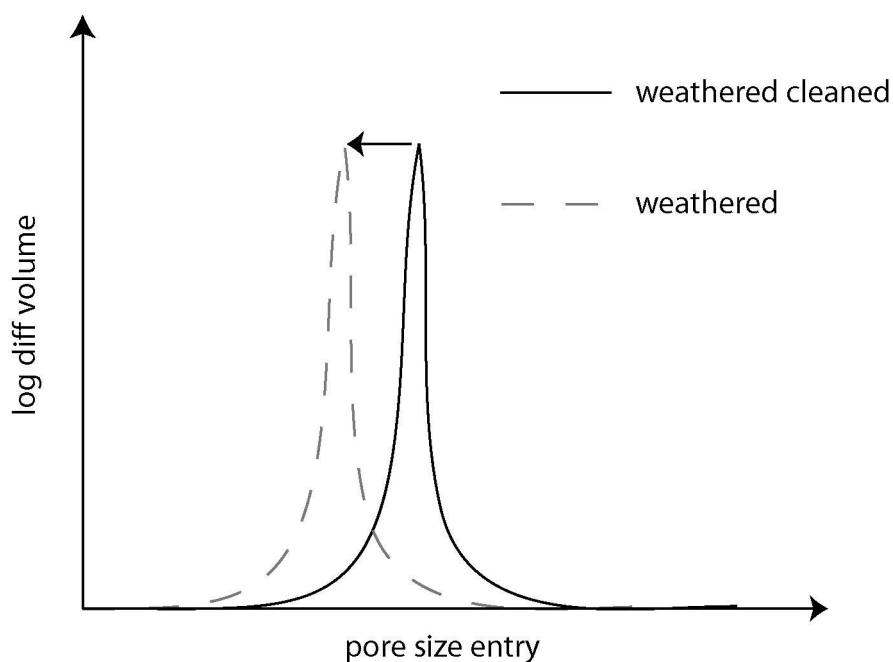


Figure ART3-2b. Interpretation on mercury porosimetry data of salt crystals obstructing a pore entry (Case 1).

Case 2: If crystals grow inside the pore (fig. ART3-3a), the pore entry size is not modified, but the global volume will appear smaller. The volume attributed to this size of pore entry will be lower. In both cases, since we assume there were no cracks induced by the crystal growth, the pore volume should rise back to its original value after the final dissolution (fig. ART3-3b).

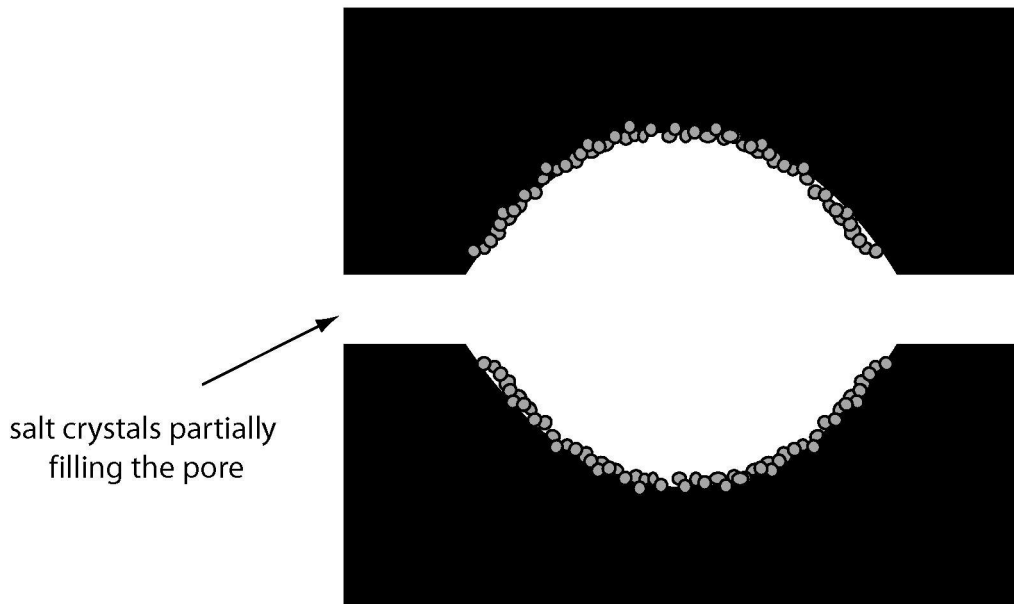


Figure ART3-3a. Salt crystals partially filling a pore (Case 2).

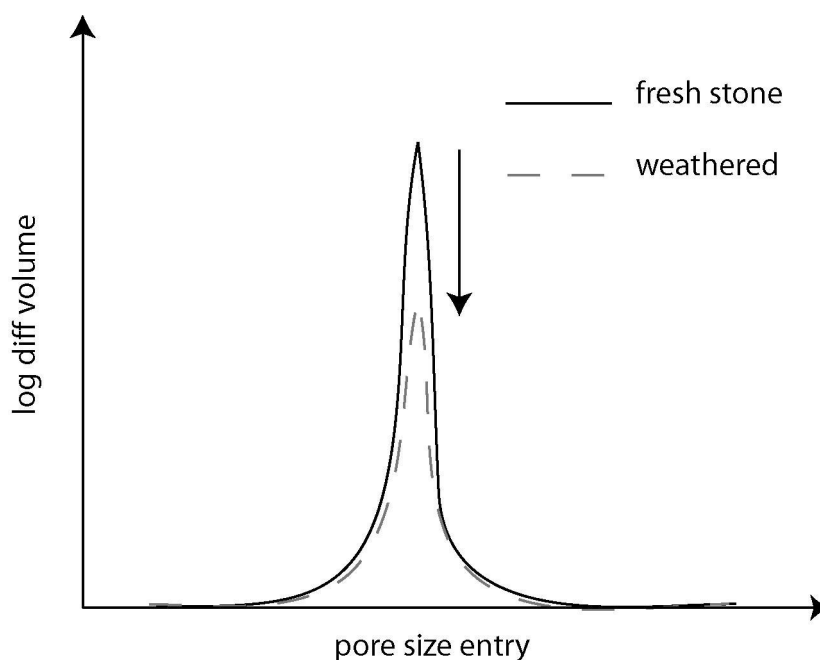


Figure ART3-3b. Interpretation on mercury porosimetry data of salt crystals partially filling a pore (Case 2).

Case 3: Most of the time the last two features are observed at the same time, that is to say the crystals both obstruct the entrance and diminishes the volume inside the pores (fig. ART3-4a, b). It should be noted that, if some of the pores are completely blocked, Case 3 cannot be distinguished from Case 1. That is to say there could be precipitation exclusively in small pore entries, but the pore volume would drop because some large pores are sealed off by complete blocking of their entries.

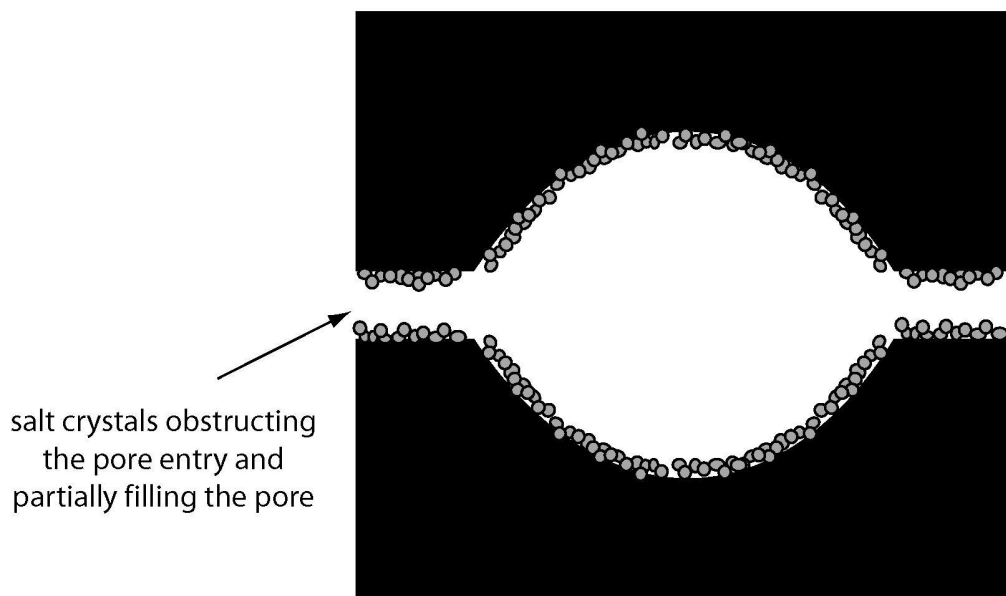


Figure ART3-4a. Salt crystals obstructing a pore entry and partially filling it (Case 3).

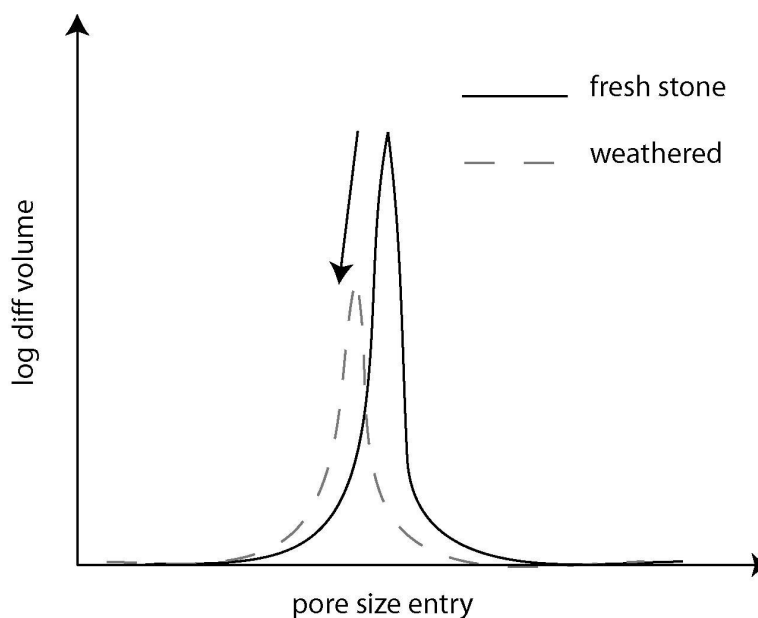


Figure ART3-4b. Interpretation on mercury porosimetry data of salt crystals obstructing a pore entry and partially filling it (Case 3).

Case 4: If crystals grow in the porous network, create cracks and fill them entirely (or at least their entry), these cracks will not be seen in the altered stone spectrum. Hence, once the samples are clean from their salt, these new cracks will appear in the spectrum (Fig. ART3-5). These microcracks have been of course only discovered after the dissolution, and not induced by this dissolution. Nevertheless, there can be other interpretations for figure ART3-5. This situation can also happen if the lower pore entry sizes correspond to micropores and not microcracks. In this case, this situation could be interpreted as an exaggeration of the ink bottle phenomenon: the weathering would have caused an increase of the pore chamber without changing the pore entry size (fig. ART3-6). This can be due for instance to salt-induced dissolution. This new porosity could also result from the formation of porous aggregate of thenardite from dehydration of mirabilite after the oven drying of the samples (Ruiz-Agudo et al. 2007). This type of porosity would be observed only when salt is in the sample, for the weathered sample, but not on the fresh and clean samples.

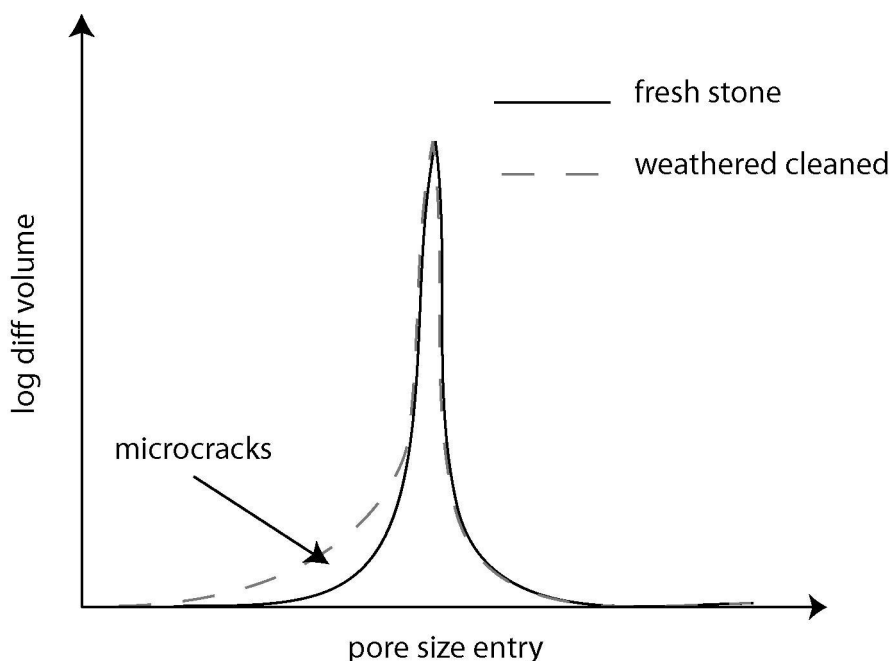


Figure ART3-5. Interpretation on mercury porosimetry data of the creation of microcracks or extension of microcracks without changing the pore entry (Case 4).

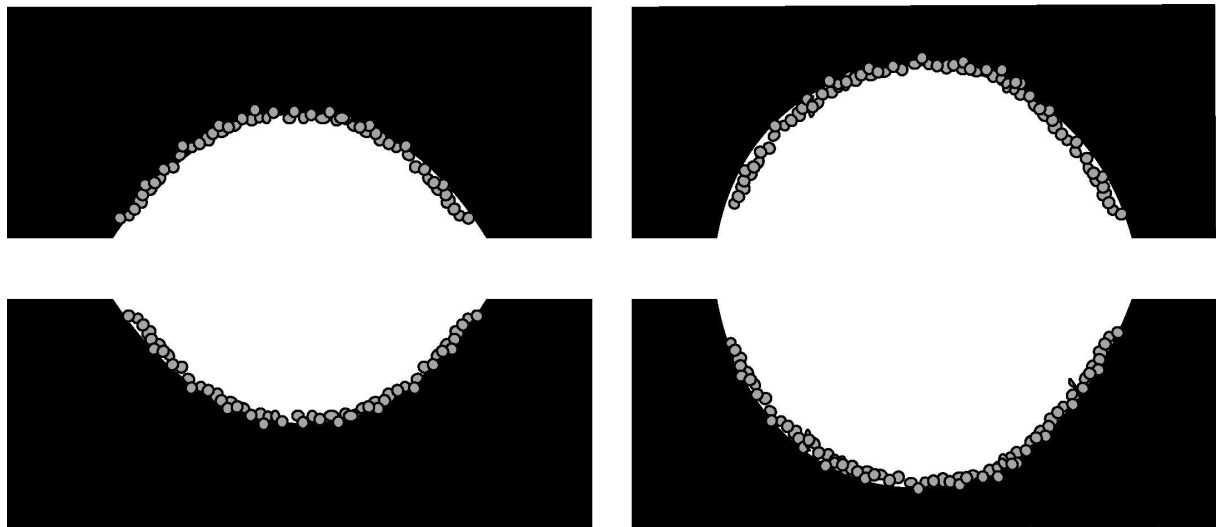


Figure ART3-6. Model explaining the increase in volume of a pore without increasing its pore entry (Case 4).

Case 5: If crystals grow in a pore and widen its entry, by nucleating a crack on the strength-limiting flaw that is its entry for instance, there will be no noticeable variation of pore entry size between fresh and weathered (fig. ART3-7a). But once the salts are dissolved, the entrance will appear bigger, and this will be represented on the spectrum like on figure ART3-7b.

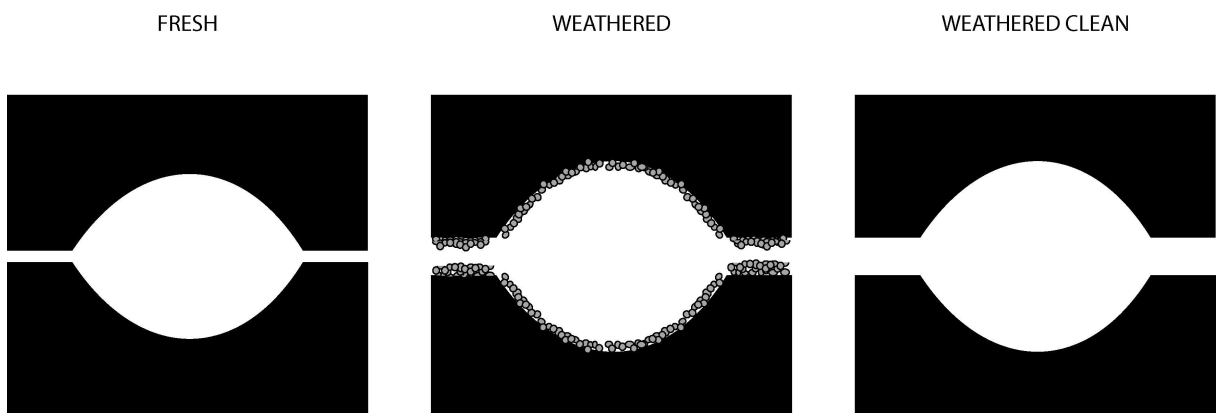


Figure ART3-7a. Theoretical model of the widening of pore entry and filling of a pore (Case 5).

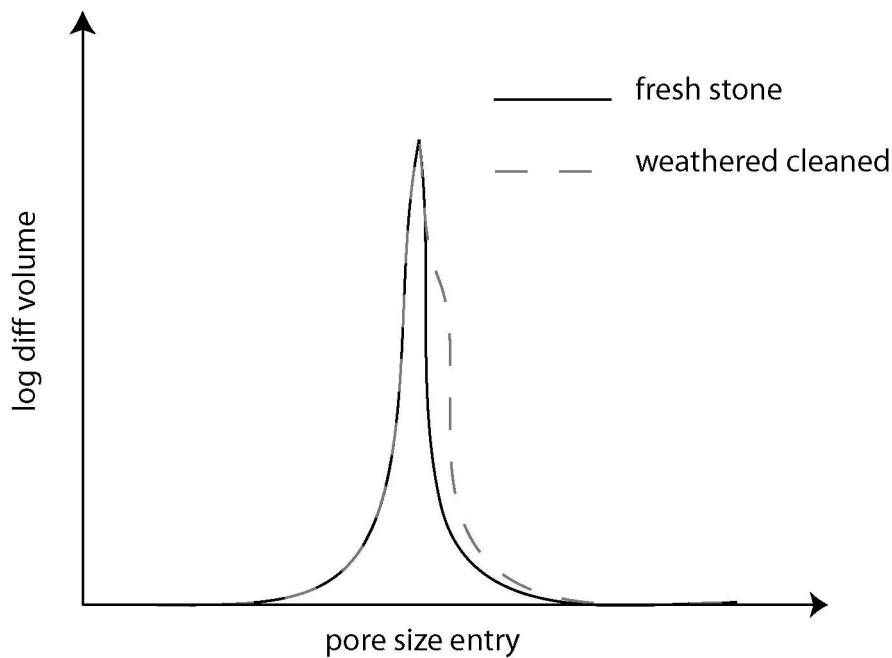


Figure ART3-7b. Interpretation on mercury porosimetry data of the widening of pore entry and filling of a pore (Case 5).

It is easier to work on rocks with a unimodal distribution of pore size entry (HF, MS, VS, FL), and thus these stones will be studied first in order to find the main common characteristics. Afterwards, these results will be compared to a much more complicated stone (biotitic limestone LL) in order to find common features.

1.2.4. Relevance of the method

A preliminary study has been performed to test the reproducibility of the mercury injection tests and therefore the relevance of the proposed method. Three fresh samples of each stone have been taken in the exact same conditions than described previously, corresponding to adjacent slices of a single cylinder. The samples obtained contain absolutely no salt, and have a volume of approximately 3 cm^3 . Figure ART3-1 shows the spectra of the three samples for each stone. The spectra for the Fontainebleau sandstone (fig ART3-1a), the two Agra sandstones (fig. ART3-1b,c) and the detritic limestone (fig. ART3-1d) clearly demonstrate that, for these four stones, natural variability is negligible. For the biotitic limestone (fig. ART3-1e), the situation is a bit different. The peak at around $0.150\mu\text{m}$ is present on the three spectra, although a bit fuzzier than for the other stones. Thus major modifications concerning this peak can be interpreted as effect of salt crystallization. Nevertheless, the pores with entries bigger than $1\mu\text{m}$ are quite different in the three spectra.

Even though the values are quite similar, their distribution has a too big natural variability to be studied. Finally, these results show that the spectra are similar enough to make sure the differences observed between weathered, clean and fresh samples are meaningful (except for the pores with entry bigger than 1 μm for LL).

2. Results

2.1. Porosity changes

The first thing to notice is that the evolution of the total open porosity before and after the tests is reliable: for all the samples, the porosity is higher for the weathered and cleaned samples than for the fresh samples. This confirms the fact that some cracks or pores in the samples have been created or enlarged by the crystallization pressure of sodium sulphate. Secondly, the porosity is higher for the weathered and cleaned sample than for the weathered samples with salt. Obviously the presence of salt in the pore space reduces the porosity of the samples. The only type of rock that does not exactly respect these two rules is the biodetritic limestone LL. This is due to the global heterogeneity of the samples coming from its high amount of macrofossils.

Table ART3-3 presents the changes of porosity due to the crystallization of salts in the porous networks. The first values correspond to the space occupied by thenardite during the measurements of mercury porosimetry, that is to say under vacuum. The second value is an approximation of the equivalent volume occupied by mirabilite during the imbibition phase, taking into account the 314% of volume raise. The third value corresponds to the porosity evolution before and after the test, that is to say the increase of porosity due to salt decay.

	Porosity (Hg)			porosity occupied by thenardite (cleaned-altered)		evaluation of porosity occupied by mirabilite		modification of the porous network (clean-fresh)	
	fresh	altered	cleaned	absolute	%	absolute	%	absolute	%
Hard Fontainebleau HF	4.60	5.45	5.64	0.19	3.36	0.57	10.11	1.04	0.18
Brown Agra MS	4.64	4.34	4.69	0.35	7.46	1.05	22.39	0.05	0.01
Green Agra VS	3.99	4.47	4.57	0.10	2.19	0.30	6.56	0.58	0.13
Liais (St Maximin) LL	14.23	13.07	13.99	0.92	6.58	2.76	19.73	-0.24	-0.02
Roche Fine (St Maximin) FL	34.44	34.50	37.56	3.06	8.15	9.18	24.44	3.12	0.08

Table ART3-3. Evolution of porosity during the tests.

2.2. Size of the microcracks

In order to find the approximate size of the cracks induced by salt crystallization, mercury porosimetry spectra obtained from the fresh samples and from the altered samples after salt cleaning will be compared (Fig. ART3-8). As we assume there is no more salt in the sample after cleaning, the difference between the two spectra comes from the formation of cracks.

The method consists in pointing the areas where the spectrum of the fresh sample lies under the spectrum of the altered sample: this represents the pore size entry for which the volume has risen during the accelerated ageing test. This method is directly drawn from the mercury porosimetry analysis presented in the last part. Since the porosity of the five types of stones is quite different, the vertical scale of the graphs is different from one stone to another to make the figure easier to read.

First, for the porous network of HF (fig. ART3-8a), the family of pores whose entries seem to have widened during the test ranges from $3\mu\text{m}$ to $15\mu\text{m}$ (case 5). It is important to recall that the size of the main family of pore entry is still around $3\mu\text{m}$ after the test. Nevertheless, this variation appears like a step, and then the spectrum continues with the same slope as before the step: this could also be due to a too small equilibrating time during the mercury porosimetry test. The secondary peak around $0.35\mu\text{m}$ corresponds to the nucleation or widening of cracks (case 4). It should be also noted that the spectra presented here are slightly different from those presented on figure ART3-7a: there is an unexpected low value of volume for entry around $2\mu\text{m}$. But since this low value is present on the three spectra, it is considered as a local variability of the natural stone, and not as an effect of salt

The second stone, MS (fig. ART3-8b), shows a main family of pore entry at around $0.05\mu\text{m}$ for the fresh facies. The volume corresponding to the main pore entry size of this family diminishes a bit and the lower pores of this family have risen in volume: salts have crystallized in these pores (case 2). The secondary new peak at around $0.02\mu\text{m}$ corresponds to the creation of cracks (case 4).

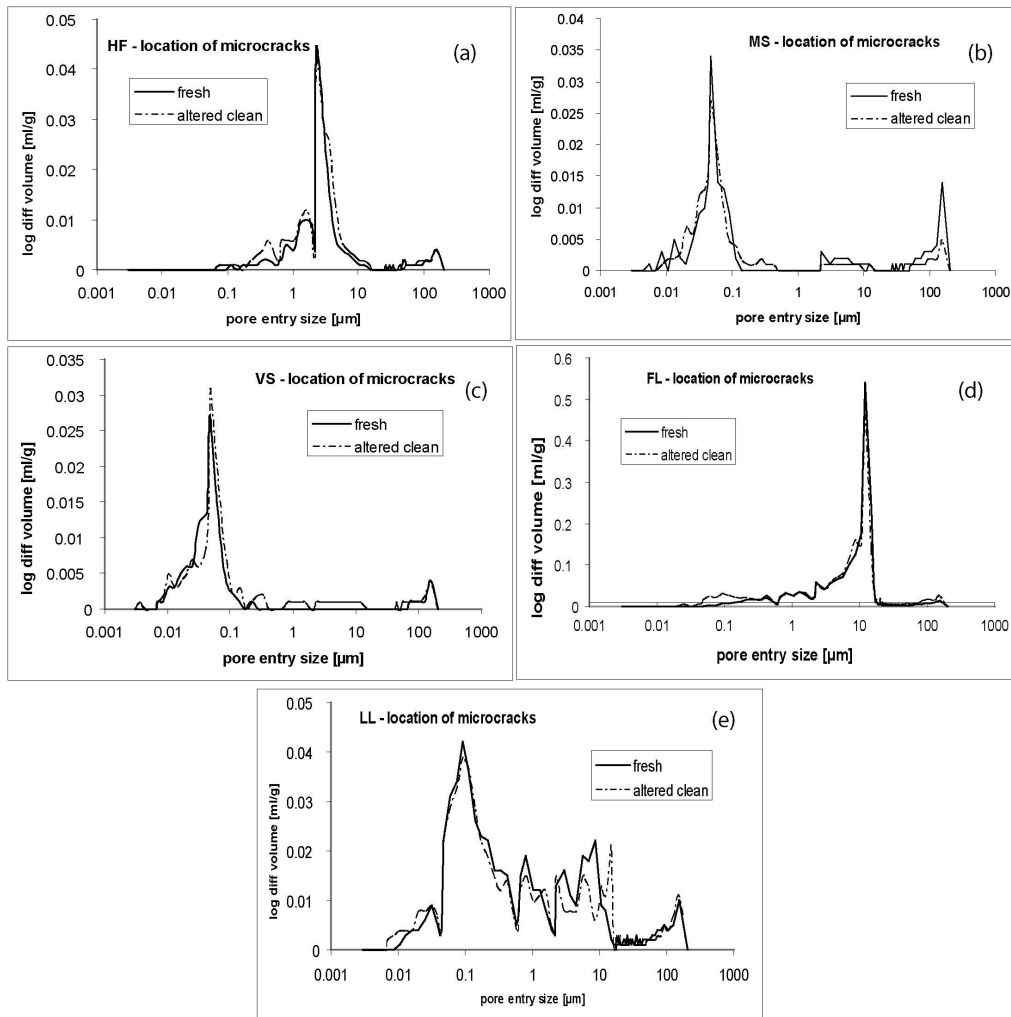


Figure ART3-8. Size of microcracks of (a) Fontainebleau sandstone (HF); (b) brown Agra sandstone (MS); (c) green Agra sandstone (VS); (d) detritic limestone called “roche fine” (FL); (e) biodetritic limestone called “liais” (LL).

In the third stone, VS (fig. ART3-8c), the main family of pores in the fresh stone is around $0.06\mu\text{m}$. The smallest new microcracks have a size around $0.01\mu\text{m}$, (case 4). On the other hand, some pores from 0.06 to $0.1\mu\text{m}$ have been extended (case 5). A new family of microcracks seem to have appeared in the range 0.2 - $10\mu\text{m}$ (case 4).

For FL limestone (fig. ART3-8d), the main pore entry size is much larger than for the three sandstones: $10\mu\text{m}$. A new family of cracks from 0.03 to $0.3\mu\text{m}$ has appeared or existent cracks of this size have widened (case 4).

For LL limestone (fig. ART3-8e), the range of pore entry of the fresh stone is particularly wide, from $0.01\mu\text{m}$ to $20\mu\text{m}$. The only major difference between the samples before and after

“Modification of the porous network by salt crystallization ...”

145

the test concerns the pores with entries from 0.006 to 0.03 μm which seem to have doubled in volume (case 4). Nevertheless, considering the results of the relevance test (fig. ART3-7e) could lead to match these variations to the natural heterogeneity of this stone. A few other cracks seem to have appeared here and there in the whole range of pore size entries but the natural heterogeneity due to macrofossils of the stone prevents us from drawing any conclusion.

2.3. Location of sodium sulphate crystals

In order to find the places of sodium sulphate crystallization, the results of mercury porosimetry for the samples that have been altered, before and after removing the salt by dissolution, will be compared (fig. ART3-9). The difference between the two samples is related to the salts that have been dissolved. In addition, the difference between the two distributions of pores for a same stone will help to understand where sodium sulphate does crystallize in the porous network.

The method consists in finding where the spectrum of the cleaned stone is over the other. This gives the entry sizes of pores in which the crystals lie. Then correlating this finding with the zones where the spectrum of the cleaned stone is below the other allows us to find if the crystals have filled the pores, obstructed and/or widen their entries.

For all these stones, the porosity is reduced from 2.2 (VS) to 8.15% (FL) by the presence of thenardite. Although sodium sulphate is a very destructive salt, this confirms that it does not occupy much room, when under the thenardite form, in the porosity of the stone compared to other salts: around 55% for sodium chloride (Rodriguez-Navarro and Doehe 1999) or around 25% for magnesium sulfate (Ruiz-Agudo et al 2007). Nevertheless, this observation is done on the final state of the samples. This is not an image of the microstructures and salts during the wetting stage during which the damage. First, it must be kept in mind that the salt present in the pores during the mercury porosimetry measurements is thenardite, but the damaging phase of sodium sulphate is known to be mirabilite (Tsui et al 2003). Thus the volume of salt during the damaging phase is approximately three times higher than the volume of salt observed with this technique, that is to say 6.5 to 24.5% of equivalent mirabilite occupy the pore space of the stones during imbibition (Table ART3-3). Second, during the capillary part of evaporation, the water flowing in the pores towards the surface

changes the distribution of the salt crystals in the porous network by remobilizing them (Angeli et al. 2006).

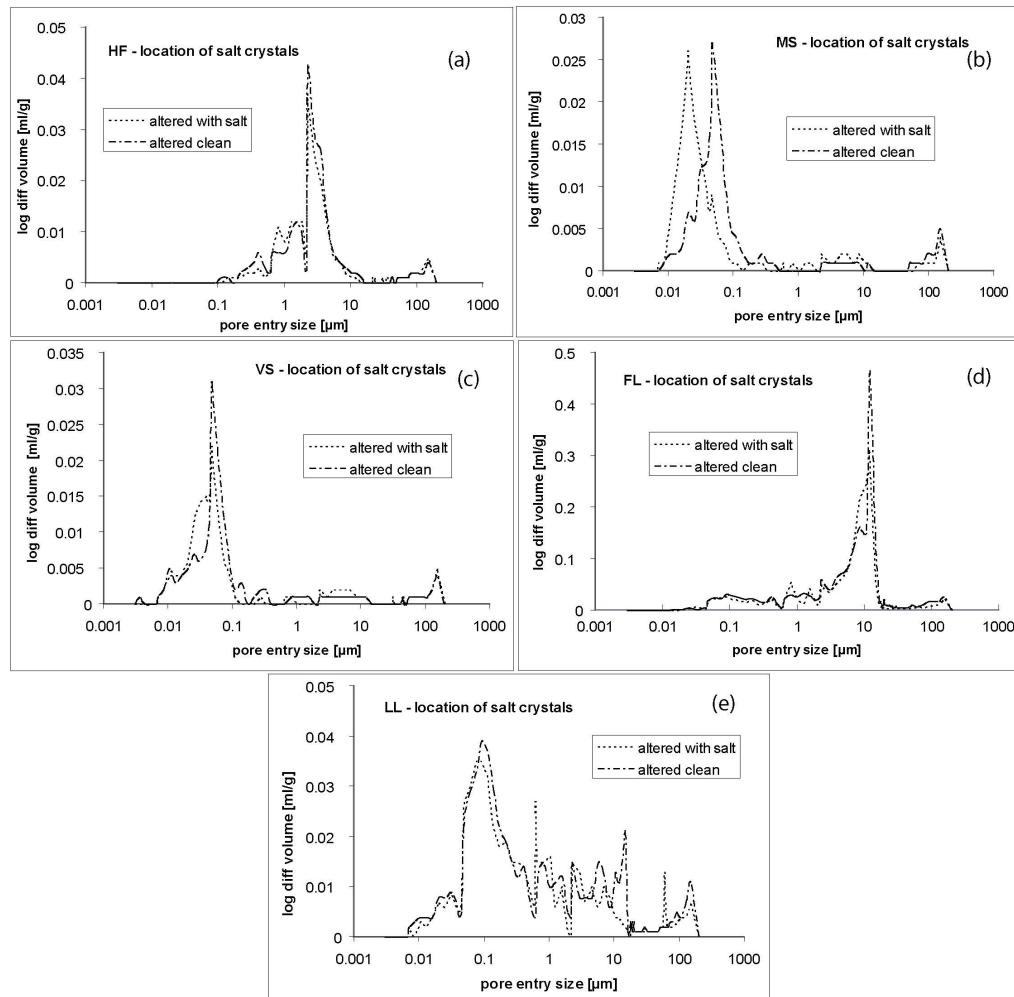


Figure ART3-9. : Location of sodium sulphate crystals in (a) Fontainebleau sandstone (HF); (b) brown Agra sandstone (MS); (c) green Agra sandstone (VS); (d) detritic limestone called “roche fine” (FL); (e) biodetritic limestone called “liais” (LL).

In the porous network of HF (fig. ART3-9a), there are three main sizes of pores which the crystals seem to have filled: 0.2-0.6 μm , 3-5 μm and 10-15 μm . These sizes correspond exactly to the pore entries which seem to have been widen during the experiments. They also do not have a corresponding lower peak of uncleaned stone, which means that these crystals have obstructed the pores they lie in, as well as their entry (case 1).

For MS (fig. ART3-9b), the peak has shifted from 0.06 to 0.03 μm , with a very small diminution of the global volume. This means that the salt have crystallized in the main family

of pores, and obstructing their pore entry (case 2). Nevertheless, since the height of the peak is almost the same, we can assume that the volume occupied by the salt in these pores is very small compared to the global porosity.

For VS (fig. ART3-9c), we can notice a volume diminution of the main peak, and a blister towards the smaller pore entry sizes. This means that a large amount of pore entries of this size have been reduced from 0.06 to 0.03 μm , thus obstructed by salts (case 3). Once again, the volume is almost the same for the two spectra, meaning that the volume of salt in the pores is very small even though it reduces significantly the size of the pore entries.

Mercury porosimetry spectra of FL (fig. ART3-9d) show the same pattern as for VS, i.e. a decrease of the main peak and a blistering to the smaller values. This corresponds to the partial obstruction of the pore entries by salt crystals (case 3), reducing these entries from 10 μm down to 6 μm . SEM observations from the porous network on an altered sample of FL (fig. ART3-12) show that walls of calcite grains are coated with salt crystals. According to its size, salt coating could be responsible for this reduction of the void size approximately from 12 μm to 6 μm . There are also few pores around 0.2 μm whose entry seems to be obstructed by crystals.

Finally, for LL (fig. ART3-9e), if we consider the hypothetical new microcracks from 0.005 μm to 0.03 μm that were created during the test, it appears that they are filled with salt crystals (case 1). Some crystals also fill up few pores from the main family, around 0.1 μm , and slightly obstruct the entrance (from 0.1 μm to 0.08 μm). Nevertheless, the high natural heterogeneity of this stone should be kept in mind when interpreting these results. In the whole range of remaining pores, from 0.5 μm to 20 μm , here and there crystals are filling pores but the heterogeneity of the stone prevents us from drawing any reliable conclusion.

3. Discussion

First it is important to recall two important points of this study: first, it deals only with damage related to sodium sulphate; second, what is observed on mercury porosimetry and SEM is only the dry state of the porous network, and the damage with sodium sulphate

appears during the imbibition of the stones, while the dissolution of thenardite entails a supersaturation of the brine with respect to mirabilite (Flatt 2002, Tsui et al 2003).

In the experiments discussed in this paper where damage is due to imbibition and drying cycles, the crystallization occurs during wetting, when the invading water dissolves thenardite and causes mirabilite precipitation (Flatt 2002). Therefore, the crystals probably form in pores of all sizes and grow so quickly that equilibrium cannot be preserved. The damage then occurs under nonequilibrium conditions analogous to those created during cooling of a saturated solution (Scherer 2004; Steiger 2005a,b). Since supersaturation of the brine is rapidly similar in pores of all sizes due to diffusion, the higher crystallization pressures should occur in the smallest pores of a stone. This result corroborates the fact that according to numerous studies (e. g. Russell 1927; Schaffer 1932; Rodriguez-Navarro and Doehe 1999; Scherer 1999), the stones that are the most susceptible to salt decay are, all other factors equal, the one with the highest proportion of small pores.

3.1. Durability

Let us have a look now on the durability of the tested stones. The most damaged stone is by far FL (Tab. ART3-1). It has the lowest AI and an AV up to 10 times higher than the second less durable stone. Then the second most damaged is VS, then LL and finally the two others with a very similar durability (MS and HF). Figure ART3-10 presents the final state of samples after 30 cycles. Note that the samples presented here are cubes and not cylinders: these samples have been experimentally weathered in the same time than the cylinders, as explained in Angeli et al (2007). They are presented here just because the state of weathering is more obvious on these samples. It is also important to recall that the samples were not in the same state of decay when they have been measured, but they have all experienced the same number of cycles (15) when the mercury porosimetry tests have been performed.

Let us consider now the quantity of pores with entries under 100nm. The stones with the most pores of this size are MS and LL (resp. 0.0128 and 0.0126ml/g), then VS (0.0082ml/g) and finally FL and HF which almost contain no pore with entry less than 100 nm (resp. 0.0005 and 0.0001ml/g). If we consider the quantity of pores with entries under 1μm, the stone with the most pores of this size is LL (0.0356ml/g), then FL and MS (resp. 0.0156 and 0.0140ml/g), VS (0.0102ml/g) and HF which again contains very few pores with

entry under $1\mu\text{m}$ (0.0015ml/g). This would lead us to think that the most weathered stone would be LL, then MS, VS and FL almost with the same proportion of small pores, and finally HF should be the least altered stone. These expectations seem a bit different than the actual durability obtained by the experimental ageing. Obviously the durability of HF and VS, which have the same porosity (4.6%), fit very well with this interpretation since VS has much more micropores than HF. It is not so clear for the three other stones, but other factors have to be taken into account.

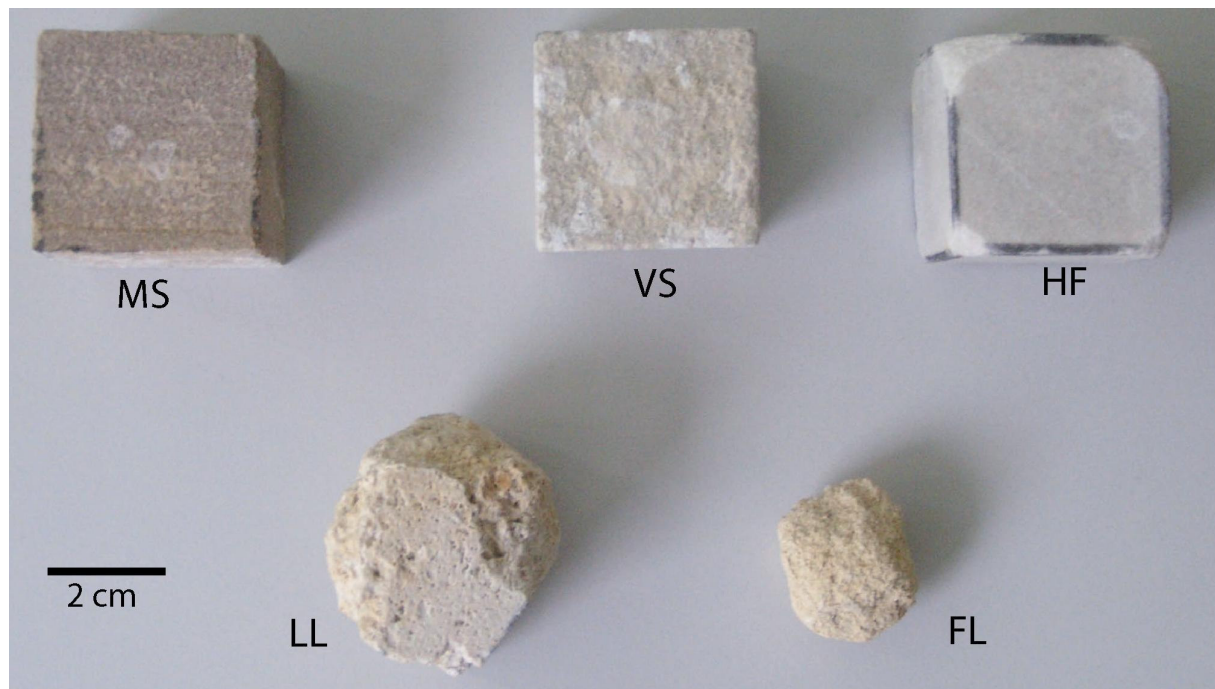


Figure ART3-10. Weathering advancement of the five types of stones after 30 cycles.

First, these figures have to be counterbalanced by the fact that FL is much more porous than the other stones, and has a much faster capillary flow in its porous network (Tab. ART3-1). Thus salt uptake is faster for this stone, implying a faster supersaturation of the brine with respect to mirabilite by dissolution of thenardite. This seems to be a reliable explanation for the very low durability of FL. LL, which has a high porosity of 17.0% and the most micropores of all five stones, has a porous network which is very different from those of the four other stones. Its biotitic nature gives not only a very heterogeneous aspect, but also a very chaotic porous network. The components of this stone are fossils of very different sizes and shapes, hence the pores have also a high natural variability. Diagenesis-induced calcite reprecipitations should also have a significant influence. All these reasons should

certainly imply a porous network with high tortuosity and low connectivity, leading to low hydraulic properties. This might explain the high durability of the LL stone.

3.2. Crystals and microcracks

Figure ART3-11 presents a summary of the data collected about the microcracks which seem to have appeared during the accelerated ageing test, and about the supposed location of sodium sulphate crystals.

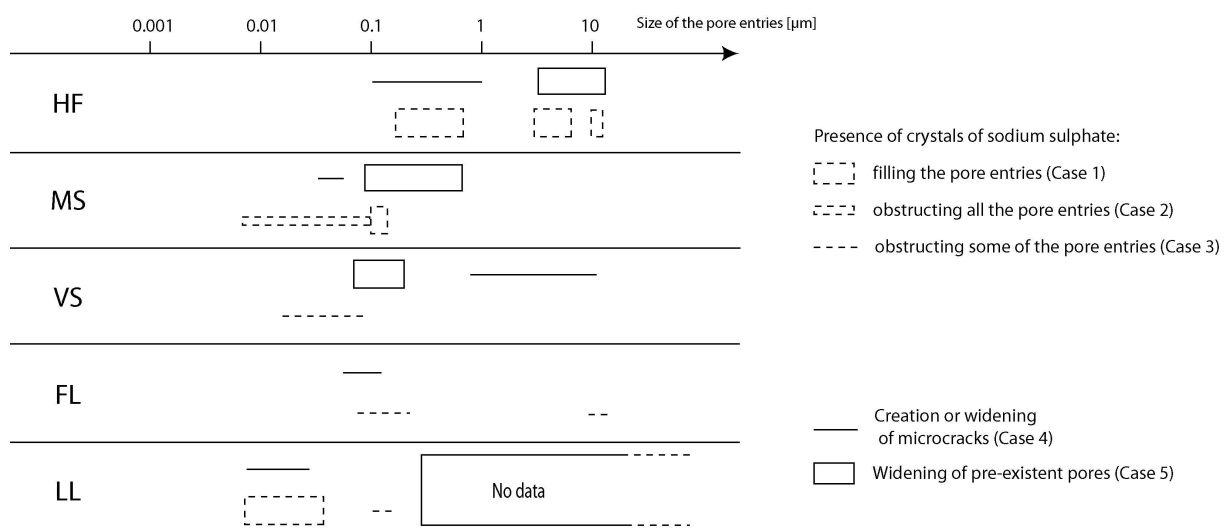


Figure ART3-11. Summary of the location of sodium sulphate crystals in the porous networks of the five studied stones.

For FL, HF and VS, the mercury porosimetry data indicate that crystals have grown in the pore entries and chambers of the three respective main families of pores. This MIP pattern (case 3, fig. ART3-3b) is very similar to what can be observed on the spectra from Rodriguez-Navarro and Doehe (1999) and from Ruiz-Agudo et al (2007). It is very clear for FL and VS.

For HF, the shape of the spectra are different (case 1) but, as explained above, case 1 and 3 are very similar and cannot be always distinguished. SEM observations of the inner part of the porous network of the FL weathered sample (fig. ART3-12) tend to confirm that crystals grow in pores of all size: crystals can be seen on all the grain surfaces regardless of the pore size. These crystals seem to result from the crystallization of thenardite on all pore walls during drying.

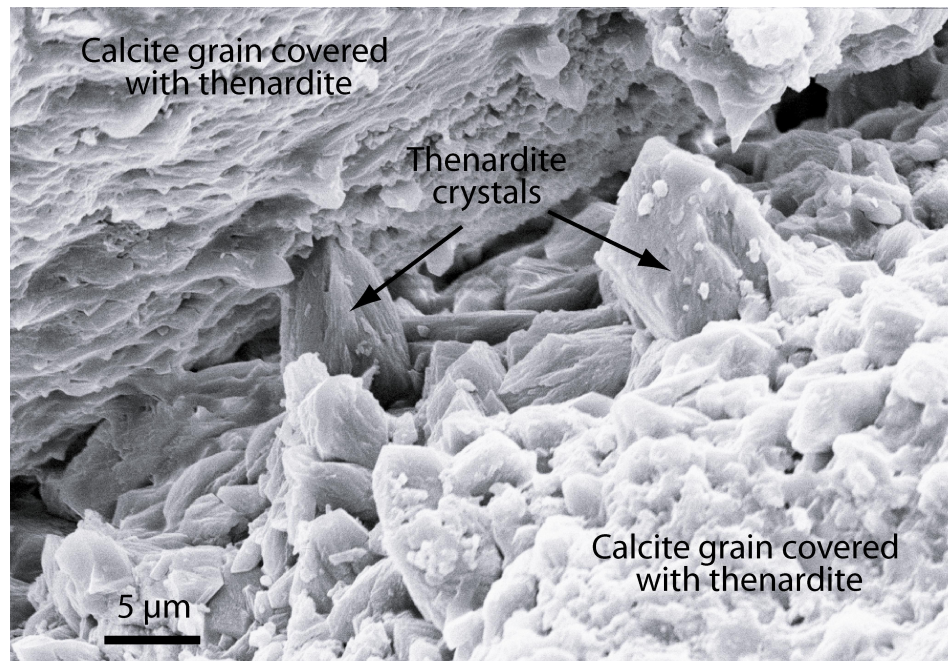


Figure ART3-12. SEM picture of sodium sulphate crystals in a pore of FL.

It seems to be a little different for MS. There seem to be apparently only salt crystals in the pore entries, but not in the pore chamber. A probable explanation would be that the “ink bottle” effect is less important in its porous network than in the three other stones. This means that its pores are closer than usual to the classical cylindrical pore model. This could be related to the unexpected high specific surface area of MS ($3.59\text{m}^2/\text{g}$) as a comparison to VS ($1.25\text{m}^2/\text{g}$) which has very similar porosity and pore size entry distribution. This could explain also the higher durability of MS: these cylindrical pores limit the number of sites where micropores are connected to macropores, sites where the highest crystallization pressure are expected (Scherer 2004).

Finally, for LL, it is very difficult to draw any conclusion on the location of the sodium sulphate crystals, given its very high natural variability. The only thing that can be noticed is that the peak at approximately $150\mu\text{m}$ does not seem much affected. Thus it appears that, due to the very bad fluid flow in its porous network, crystallization of salts is quite difficult in this range of pore size. This could explain the high durability since the highest crystallization pressures occur in the small pores (Correns 1949; Benavente et al. 1999; Scherer 2004; Steiger 2005a,b; Coussy 2006). But this result has to me considered as a hypothesis since more precise studies are necessary for this complicated stone.

Thus, it seems that sodium sulphate crystallizes in almost any size of pore entries from 0.01 to 20 μm . All the pore sizes in a given stone seem to be affected by the crystallization of sodium sulphate, as confirmed by SEM observations (fig. ART3-12). Indeed grains appear entirely coated with sodium sulphate crystals. The presence of crystals in all the possible pore sizes makes both mechanisms of decay possible (equilibrium and non-equilibrium).

These observations are confirmed by the fact that, in the five studied stones, pre-existent pores and cracks have been affected. This means that the pores of all entry sizes are damaged. This is consistent with Steiger (2005) who concluded that crystals can grow not only in the smaller pores (0.01-0.05 μm and lower) and damage them permanently in a thermodynamically equilibrated situation (Scherer 2004), but also in the larger pores (up to several μm) and damage them during their growth, in a non-equilibrated situation.

3.3. Pre-existent cracks

Thus, the more available surface in the porous network, the better opportunity for salt to crystallize and damage the rock. In particular, the presence of numerous cracks in the stone could explain the unexpected vulnerability of a rock to salt decay (Nicholson 2001). In a previous work (Angeli et al. 2007), the behaviour of nine sedimentary stones towards salt weathering has been evaluated. For only two stones, CS and SF, the durability was wrongly estimated: the authors expected a very high durability and found out that the stones were severely decayed by salt damage. These stones have also been tested in this study, but the samples were so severely damaged that they crumbled in the mercury porosimetry chamber. After an analysis of thin sections of each fresh stone they appeared to be the only two stones with extensive intragranular cracking. The crack density estimated was relatively high (63.2 cracks/ mm^2 for SF and 82.6 cracks/ mm^2 for CS), while it was close to zero for the other stones tested in this study. The high density of cracks can explain why the two varieties of Fontainebleau sandstones, HF and SF, have such a different durability despite of their similar hydromechanical behaviour (Fig. ART3-13).

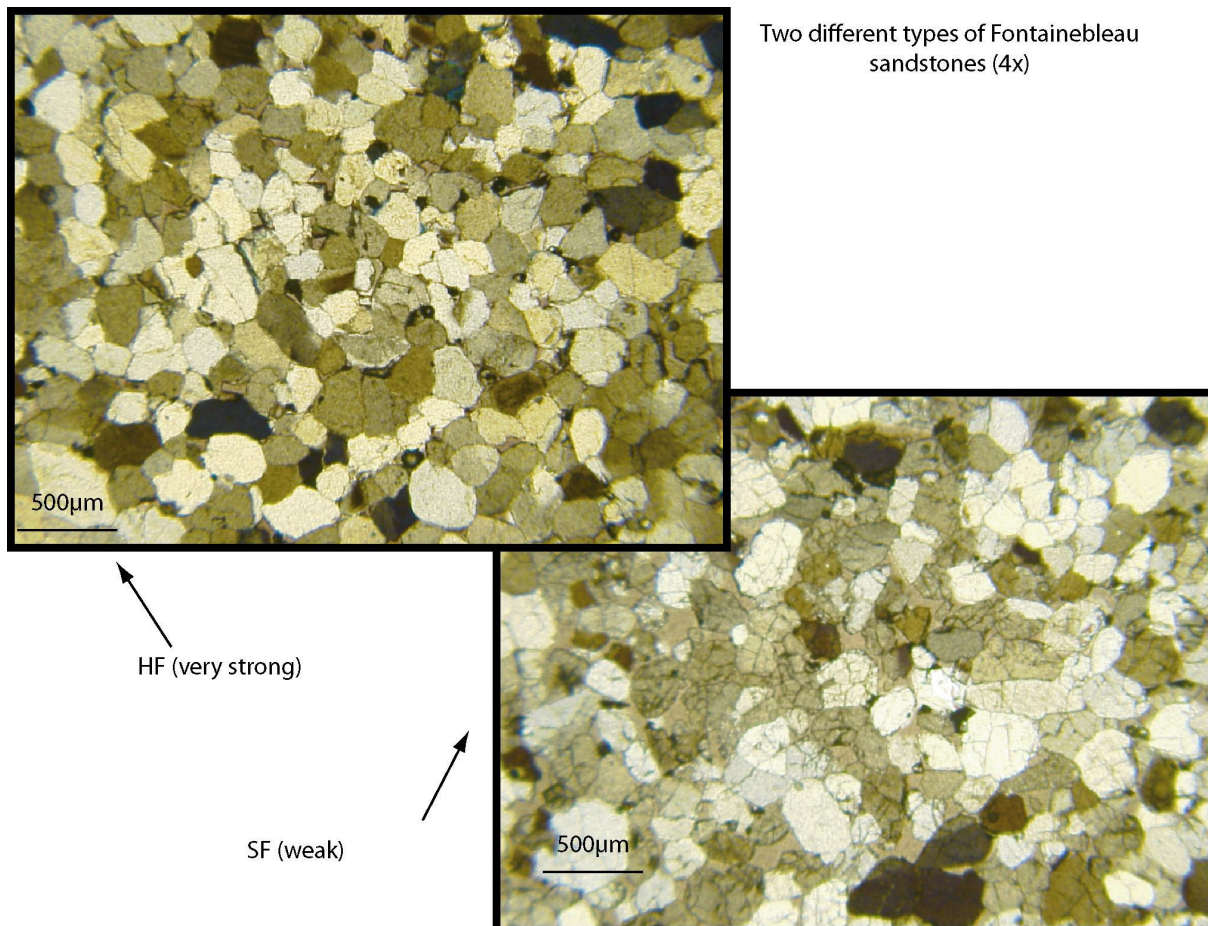


Figure ART3-13. Thin sections of two varieties of Fontainebleau sandstones with a similar hydromechanic behaviour and completely different durability: the weak stone on the right shows many intragranular cracks as opposed to the durable stone on the left.

This could be a reason to think that case 4, the volume raise for the lowest pores available in a stone, would correspond to an increase of the length of the pre-existent cracks rather than a creation of new microcracks. The nucleation of cracks does certainly happen, but the increase of the length of the pre-existent cracks seems to be an important factor that entails the unexpected weathering rate of SF and CS. It would confirm the fact that crystallization of salts would be thermodynamically easier and more destructive when occurring at the tip of a pre-existent crack or strength limiting flaw (Scherer 1999, Flatt 2002). This is in agreement with the fact that heterogeneities, and particularly cracks, act as local weaknesses and localizers of damage in rock mechanics. This allows us to complete the evaluation of durability proposed in Angeli et al. (2007): an important parameter influencing AV is thus the crack density. A precise study of the crack density on thin sections should give a more precise value for the estimator of AV, that is to say the estimator of the long term behaviour of the stone regarding salt decay.

Conclusion

The first important conclusion is that there is no significant change in the porosity during the weathering process: the global porosity of the samples as well as the distribution of their pore size entry has not drastically changed between the fresh sample and the clean samples. As described in Rodriguez-Navarro and Doehe (1999), the sodium sulphate crystals in anhydrous phase do not seem to fill much of the pores (up to 8% of total open porosity) at the end of the experiment. Nevertheless, this volume rises to 24% of total open porosity approximately if we consider the volume of mirabilite during the damaging imbibition phase, which is almost the amount of volume occupied by magnesium sulphate in the calcarenite at the end of the experiment described by Ruiz-Agudo et al (2007).

Second, most of the pores seem to be affected by the crystallization of salts, since in all the studied stones pores from 10nm up to 20 μm of entry have been affected during the accelerated ageing tests. SEM observations as well as mercury porosimetry spectra analysis suggest also that sodium sulphate tends to crystallize on all the grain surfaces regardless of the size of the related pore. Thus, this study confirms the work of Scherer (2004) and Steiger (2005) about the fact that a crystal growing (thus not in equilibrium) in a pore of size up to several μm can exert a crystallization pressure high enough to nucleate or propagate cracks in a porous network.

As a consequence this study confirms the fact that the stones with a high amount of small pores (up to several μm) are more susceptible to decay, but still introduces some issues: for instance a very high porosity (case of FL) or an uncommon porous network (high tortuosity and low connectivity for LL, or cylindrical pores for MS) can also have an influence on the durability of stones.

It has been established numerous times that the hydric properties of stones as well as their tensile strength are the critical parameters governing the durability of stones to salt decay, and these parameters are widely used to estimate this durability (Punuru et al. 1990; Benavente et al. 2004b; Angeli et al 2007). This study suggests the importance of pre-existent cracks on the durability of stone regarding salt decay. The presence of cracks is absolutely not necessary for the damage through salt decay, but it seems to greatly accelerate the process in the long term. This would confirm experimentally the theory saying that crystallization of

salts would be thermodynamically easier and more destructive when occurring at the tip of a pre-existent crack or heterogeneity (Scherer 1999). This justifies the proper use of the P-wave velocity as a good estimator of the long term durability of a stone regarding salt decay: this velocity depends of course on the mineral composition of the stone, on its cohesion or mechanical strength, on its porosity, but the crack density also has a strong influence on it (Jeffreys 1931, Hudson 1981). Thus measuring the intragranular crack density of a fresh stone on thin sections, in addition to the other usual petrophysical tests (porosity, capillarity, tensile strength, pore size entry...), allows having a better estimation of its durability.

Acknowledgements

The authors would like to thank M. Pallix from ROCAMAT (Saint-Maximin-sur-Oise) for providing LL and FL, M. Oliveira (Moigny-sur-Ecole) for the other samples, Manuel Palomo (Alicante) for preparing the sample, Irene Martin (Alicante) and Fabien Piguet (Cergy) for performing most of the mercury porosimetry measurements, and the two anonymous reviewers for their comments which greatly helped to improve this paper.

References

Angeli M, Bigas JP, Menéndez B, Hébert R, David C (2006) Influence of capillary properties and evaporation on salt weathering of sedimentary rocks – in “Heritage, Weathering and Conservation”, Edité par R. Fort, M. Alvarez de Buergo, M. Gomez-Heras & C. Vazquez-Calvo, Taylor & Francis/Balkema, AK Leiden, The Netherlands, 2006, 253-259

Angeli M., Bigas JP, Benavente D, Menéndez B, Hébert R. and David C. (2007) Salt crystallization in pores: quantification and estimation of damage – Environmental geology, 52:205-214

Benavente D., Garcia del Cura M. A., Fort R. and Ordoñez S. (1999) Thermodynamic modelling of changes induced by salt pressure crystallization in porous media of stone – Journal of Crystal Growth, 204:168-178

Chapter IV : Salt damage

Benavente D, García del Cura MA, García-Guinea J, Sánchez-Moral S, Ordoñez S (2004a) The role of pore structure in salt crystallisation in unsaturated porous stone. *Journal of Crystal Growth* 260:532-544

Benavente D, Garcia del Cura MA, Fort R, Ordoñez S (2004b) Durability of porous building stones from pore structure and strength. *Engineering Geology* 74:113-127

Correns C. W. (1949) Growth and dissolution of crystals under linear pressure, *Discuss. Faraday Soc.*, 5:267-271

Coussy O. (2006) – Deformation and stress from in-pore drying-induced crystallization of salt. *Journal of the Mechanics and Physics of Solids* 54:1517–1547

Dei L., Mauro M., Baglioni P., Manganelli Del Fà C. and Fratini F. (1999) Growth of Crystal Phases in Porous Media, *Langmuir*, 15:8915-8922

EN 12370 (1999) Natural stone test methods – Determination of resistance to salt crystallization. 1999-03

Everett D. M. (1961) The thermodynamics of frost damage to porous solids – *Transactions of the Faraday Society*, 57:2205-2211

Fitzner B. and Snethlage R. (1982) Über Zusammen Hange Zwischen Saltzkristallisationsdruck und porenradienverteilung, *GP Newsletter*, 3:13-24

Fitzner B (1988) Porosity properties of naturally or artificially weathered sandstones – Proc VIth international Congr on Deterioration and Conservation of Stonee, Torun, 12-14 Sept 1988, 236-245

Flatt RJ (2002) Salt damage in porous materials: how high supersaturations are generated. *Journal of Crystal Growth* 242:435-454

Good RJ, Mikhail RS (1981) The contact angle in mercury intrusion porosimetry. Powder Technol 29:53–62

Hammecker C (1993) Importance des transferts d'eau dans la dégradation des pierres en œuvre, Ph.D. Thesis, University Louis Pasteur of Strasbourg, France

Honeyborne D. B. and Harris P. B. (1958) The structure of porous building stones and its relation to weathering behaviour – in Everett D. H. and Stone F. S. (Eds), Proceedings 10th Symposium of the Colston Research Society, Butterworths Scientific Publications, London, 343-365

Hudson J. A. (1981) Wave speeds and attenuation of elastic waves in material containing cracks – Geophys. J. R. astr. Soc. – 64:133-150

Jeffreys H. (1931) Damping in bodily seismic waves – Mon. Not. R. astr. Soc. Geophys. Suppl. – 3:318-323

Lopez Arce P. and Doehne E. (2006) Kinetics of sodium sulphate efflorescence as observed by humidity cycling with SEM – in “Heritage, Weathering and Conservation”, Edité par R. Fort, M. Alvarez de Buergo, M. Gomez-Heras & C. Vazquez-Calvo, Taylor & Francis/Balkema, AK Leiden, The Netherlands, 2006, 285-291

Nicholson D. T. (2001) Pore properties as indicators of breakdown mechanisms in experimentally weathered limestones - Earth Surface Processes and Landforms, 26:819–838

Punuru A. R., Chowdhury A. N., Kulshreshtha N. P. and Gauri K.L. (1990) Control of porosity on durability of limestones at the Great Sphinx, Egypt – Environmental Geology and Water Sciences, 15:225-232

Rodriguez-Navarro C, Doehne E (1999) Salt weathering: influence of evaporation rate, supersaturation and crystallization pattern. Earth Surface Processes and Landforms 24:191-209

Chapter IV : Salt damage

Rodriguez-Navarro C, Doehne E, Sebastian E (2000) How does sodium sulphate crystallize? Implications for the decay and testing of building material. *Cement and Concrete Research* 30:1527-1534

Ruiz-Agudo E, Mees F, Jacobs P and Rodriguez-Navarro C (2007) The role of saline solution properties on porous limestone salt weathering by magnesium and sodium sulfates. *Environmental geology* 52:269–281

Russell, S.A. (1927) Stone preservation committee report. Appendix 1. H.M. Stationery Office, London

Schaffer R. J. (1932) The weathering of natural building stones, DSIR, Building Research Special Report 18, Stationery Office, London, 34 pp.

Scherer G (1999) Crystallization in pores. *Cement and Concrete Research* 29:1347-1358

Scherer G (2004) Stress from crystallization of salt. *Cement and Concrete Research* 34:1613-1624

Steiger M (2005a) Crystal growth in porous materials—I: the crystallization pressure of large crystals. *J Cryst Growth* 282:455–469

Steiger, M. (2005b) Crystal growth in porous materials – II: Influence of crystal size on the crystallization pressure. *Journal of Crystal Growth* 282: 470-481

Winkler E. M. (1997) Stone in Architecture – Springer Verlag, Berlin, 313 pp.

The variation of alteration as a function of the microstructures has been studied in this part. But the stone properties are not the only parameters influencing salt decay: it is also highly dependent of the environmental conditions. The influence of some of these conditions (evaporation, temperature and concentration of the brine) is evaluated in the following chapter.

INFLUENCE OF ENVIRONMENTAL PARAMETERS

CONTENT

<i>1.Influence of capillary properties and evaporation on salt weathering of sedimentary rocks</i> <i>(HWC 2006)</i>	<hr/> <i>163</i>
<i>2.Influence of temperature and salt content on the salt weathering of sedimentary rocks</i> <i>(GSL special publication)</i>	<hr/> <i>185</i>

Chapter V: Influence of environmental parameters

The principle of these experiments is to work only on one stone to study the influence of the external parameters on weathering. We chose to work with the detritic limestone: the “roche fine”. This stone has numerous advantages. First, it is very homogeneous from one sample to the other which allows a good reproducibility of the measurements. Its porous network is quite simple, with a unimodal distribution of pores with sizes around $12\mu\text{m}$. The size of the pores is around $100\text{-}150\mu\text{m}$ and the size of grains around $400\text{-}500\mu\text{m}$. Then, it is very sensitive to salt decay which allows having significant damage in a short notice (generally around 10 to 15 cycles). This is due to its very low tensile strength as well as the ease for water to flow in and out of the porous network (high permeability). Third, this stone has a cultural value since it has been chosen for the restoration of cultural heritage in the Paris area.

During these experiments, cycles are performed on samples with varying external parameters. The easiest possibility is to constraint evaporation (possibility of salt crystallization in the porous network) and temperature (governing the crystallization sequences of sodium sulphate).

1. Influence of capillary properties and evaporation on salt weathering of sedimentary rocks (HWC 2006)

Usually in weathering tests, all the faces of the tested samples are left exposed. This is not exactly the case in buildings and monuments, since the stones only have one face exposed to the outside (two in the case of corner stones). This work evaluates the influence of this particular configuration that limits evaporation to only one face of the sample. The influence of the salt supply mode is also discussed (capillary imbibition, immersion, salt coming from the inside sample).

“Influence of capillary properties and evaporation on salt weathering of sedimentary rocks”

Matthieu Angeli, Jean-Philippe Bigas, Beatriz Menéndez, Ronan Hébert and Christian David

Université de Cergy-Pontoise
Département de Sciences de la Terre et Environnement
5 mail Gay-Lussac, Neuville-sur-Oise
95031 Cergy-Pontoise CEDEX
France

Published as the proceedings of the 2006 “Heritage, Weathering and Conservation” conference (held in Madrid on 21st – 24th of June) in “Heritage, Weathering and Conservation”, edited by R. Fort, M. Alvarez de Buergo, M. Gomez-Heras & C. Vazquez-Calvo, Taylor & Francis/Balkema, AK Leiden, The Netherlands, 2006, 253-259

Abstract

The importance of capillary imbibition and evaporation processes in the decay of stone through salt crystallization is estimated by different experiments adapted from the European standard EN 12370. The various tests consist in slightly modifying the salt (sodium sulphate) supply in the porous network of stones as well as the amount of evaporation and in checking the weathering evolution of the stone. The results show that ionic diffusion and dissolution of pre-existent salts are not efficient enough to imply supersaturation, hence to visually alter the stone. An exterior supply of salt is required. The influence of evaporation is clearly shown when evaporation process could not occur through a side of the sample. In this case, isolated sides are never subjected to weathering, even to simple salt efflorescences.

Résumé

L'importance de l'imbibition capillaire et des processus d'évaporation dans l'altération des pierres par la cristallisation de sels est estimée par différentes expériences adaptées des normes européennes EN 12370. Les différents tests consistent en modifiant légèrement l'apport de sel (sulfate de sodium) dans le réseau poreux ainsi que les possibilités d'évaporation, puis de suivre l'évolution de l'altération de la roche. Les résultats montrent que la diffusion ionique et la dissolution des sels préexistants ne sont pas suffisants pour entraîner la sursaturation de la saumure, et donc de causer des dégâts visibles. Un apport de sel extérieur est nécessaire. L'influence de l'évaporation est clairement démontrée lors de l'expérience où l'évaporation est limitée par l'isolement de toutes les faces sauf une. Dans ce cas, les faces isolées ne sont pas altérées et ne présentent même pas d'efflorescences.

Introduction

Salts are one of the main destructive agents governing the decay of natural building stones and historic masonry. Salt crystallization is identified in many cases of building stones weathering, from simple harmless efflorescence to alveolar erosion and sometimes contour scaling. Salts and sources of salts from the atmosphere (halite from the seashore; carbonates, nitrates and sulphates from urban pollution), external agents (de-icing salts) or cement repointing mortars may be carried by water, penetrate by capillary imbibition or ionic diffusion into the stone porous network. It is well known that the pore network characteristics, as tortuosity, constrictivity or mean pore radius, can interact in the process of decay of porous media by crystallization of salt as well as the salt chemical nature.

Recent researches on salt crystallization in porous networks, using thermodynamic approach based on Correns (1949) or Pitzer (1991) equations have shown that stone decay due to crystal growth is related to the mechanical stress induced by salt crystallization pressure. This stress is transmitted to the stone by a thin film (2 or 3 nm thick) of supersaturated solution which lays between the growing crystal and the pore walls. This stress is inversely proportional to the mean pore radius, which means that stress is higher in smaller pores (La Iglesia et al. 1997, Scherer 1999, 2004, Nicholson 2001, Flatt, 2002, Benavente et al. 2004, Steiger 2005a,b).

In our study, capillary imbibition is considered as the source of salt penetration into the porous network of sedimentary rocks. We evaluate the influence of evaporation in the crystallization process by running various tests with various evaporation configurations, by isolating 0, 3 or 4 faces of the samples. Five natural building stones were studied regarding to the penetration of mirabilite saturated solution (14 wt. %).

1. Materials and methods

1.1. Materials

Five different stones were used, three Lutetian limestones and two Fontainebleau sandstones from the Parisian basin (Tab. ART4-1). The Lutetian limestone has been widely used in the construction of the oldest monuments in Paris and its surroundings (e. g. Notre-Dame cathedral). In the following sections, we will focus on the influence of capillary properties and evaporation on salt weathering of sedimentary rocks (Steiger et al., 2005a,b).

Dame-de-Paris). The Fontainebleau sandstone is the main stone used in the Parisian basin for the paved streets, but also for some monuments around Fontainebleau (castle of Fontainebleau, tower of Montlhéry...).

The three lutetian limestones come from Saint-Maximin-sur-Oise (France). The “roche fine” (FL) is a detritic micritic limestone with more than 90% calcite, few grains of quartz and oxides. Its porosity is interparticle and around 36%. It has a very low tensile strength around 1.5 MPa. The “roche franche” (RL) is a lime-stone with many microfossils (mainly milioles), a few macrofossils (bivalves) and traces of oxides. Its porosity is mainly interparticle but also intraparticle (macrofossils) and ranges from 19 to 21%. Its tensile strength is 3.0 MPa. The “liais” (LL) is very similar to RL. The fossils are the same, but the intraparticle porosity has been partly filled with calcite precipitation. The porosity is between 13 and 15%. Its tensile strength reaches 4.2 MPa.

The two sandstones come from Moigny-sur-Ecole near Fontainebleau (France) and are called the “grès dur” (HF) and the “grès tendre” (SF). They are both very pure sandstones with porosity around 6% for HF, while it varies for SF from 7 to 13%. The other striking feature is their contrast in tensile strength: 5.2 MPa for HF and 2.5 MPa for SF.

	FL	RL	LL	SF	HF
Porosity [%]	36.1	20.3	14.0	10.7	5.9
Absorption [%]	28.2	10.4	8.4	1.9	0.8
Apparent density [g.cm ⁻³]	1.72	2.13	2.30	2.36	2.49
Bulk density [g.cm ⁻³]	2.69	2.67	2.67	2.64	2.64
Capillary coef. [g.m ⁻² .s ^{-1/2}]	1250	101	34	95	3
Tensile strength [Mpa]	1.5	3.0	4.2	2.5	5.2

Table ART4-1. Physical parameters of the stones used in the experiments.

1.2. Methods

The EN 12370 standard test concerning salt crystallization of stone has been widely used and provides us with a large amount of data on the resistance of stone to salt weathering, data which are reviewed by Goudie & Viles (1997). In order to take into account the effect of capillary imbibition and evaporation on salt crystallization process, four different tests adapted from EN 12370 standard were performed on our samples. Using 7x7x7 cm³ samples, four experimental configurations for salt supply and evaporation are chosen for 24 hours crystallization cycles. The different conditions of salt supply are respectively immersion as in standard test, capillary imbibition, remobilisation, and for the last test, both capillary imbibition and remobilisation of the salts in the sample (explained below). For each experimental configuration, the cycle consists in two hours of salt supply, sixteen hours of drying at 105±5°C, and six hours of drying in laboratory conditions (20-25°C, 40-55% RH). All the samples are weighed after each cycle with a precision balance ($\pm 0.01\text{g}$).

In the immersion test (IMM) the stone samples are immersed in a 14 wt. % saturated mirabilite solution as indicated in the EN 12370 standard. For capillary imbibition test (CAPI), the samples are partially immersed (8±3mm) in a mirabilite saturated solution. In the remobilisation test (REMOB), the samples are immersed before the test during two days in a mirabilite saturated solution, dried until constant weight, and partially immersed (8±3 mm) in demineralised water, i.e. there is no additional salt supply. Finally, the capillary imbibition and remobilisation test (CAPI&REMOB) is a combination of the last two: the samples are immersed two days in a mirabilite saturated solution before the test, dried until constant weight, and partially immersed (8±3 mm) in a mirabilite saturated solution.

In order to be as close as possible to stone conditions in buildings and monuments (i.e. taking into account the fact that evaporation is not possible through every side of the stone), the same experiments were per-formed with only one side exposed (or two in case of corner stones) to evaporation, and the others isolated by an aluminium film.

After 7 cycles, one sample in each experiment has been dried at 105±5°C until constant weight. Then new salt supply cycles were performed on these samples. The interest

of this experiment is to evaluate the fraction of water in the isolated samples weight evolution. Once the water has entirely evaporated, the only weight variation is due to presence of salt alteration.

2. Results and discussion

2.1. Quantification of alteration

Decay of stone is evaluated by the number of the cycle during which the first observable feature of alteration appears. AI as alteration index is used, after each experiment (Tab. ART4-2), for the quantification of the samples alteration. AI index was defined on three samples for each experiment after 10 cycles for the immersion test and 15 cycles for the other tests. If the sample does not show alteration at the end of an experiment, the value of AI is 10 for the immersion test, and 15 for the other tests.

2.2. Brief overview of the stones resistance by the immersion test (IMM)

This test was performed to evaluate the general behaviour of our stones with salt crystallization. HF is the least altered stone by mirabilite crystallization (AI=10). Its weak capillary coefficient as well as its low porosity is certainly responsible for its resistance to salt decay. LL (AI=6) and RL (AI=4) suffer from slight decay, but after several cycles of salt uptake without apparent alteration. In contrast, SF (AI=3) and FL (AI=2) are strongly altered with a high weight loss, mainly due to high capillary coefficient (hence high and rapid salt uptake) as well as low tensile strength.

2.3. Capillary imbibition (CAPI)

The first step to evaluate stone resistance is to consider the importance of salt supply in the samples. Figures ART4-1a, b, c show the relationships between alteration index and three water-supply related properties (porosity, absorption and capillary coefficient) for each

stone and three tests (immersion, capillary imbibition and capillary imbibition & remobilisation).

	IMM	CAPI	REMOB	CAPI& REMOB
Non-isolated				
LL	6	10	15	8
RL	4	8	15	5
FL	2	3	15	2
SF	3	5	15	3
HF	10	15	15	15
4 faces isolated				
LL	10	15	15	15
RL	6	10	15	8
FL	2	3	15	2
SF	4	6	15	4
HF	10	15	15	15
3 faces isolated (corner stone)				
FL	No data	2	No data	1
SF	No data	5	No data	3

Table ART4-2. Values of alteration index (AI) for each test: immersion (IMM), capillary imbibition (CAPI), remobilisation (REMOB) and capillary imbibition & remobilisation (CAPI&REMOB).

The correlation is better with the log of the capillary coefficient, which confirms that this parameter, and thus this process, is more representative of the salt supply governing salt decay (Benavente et al. 2001, Scherer 2004). During this test, the zones which undergo the

more damage from salt are those which are immersed during the salt supply, specially the four lower corners of the samples (Fig. ART4-2).

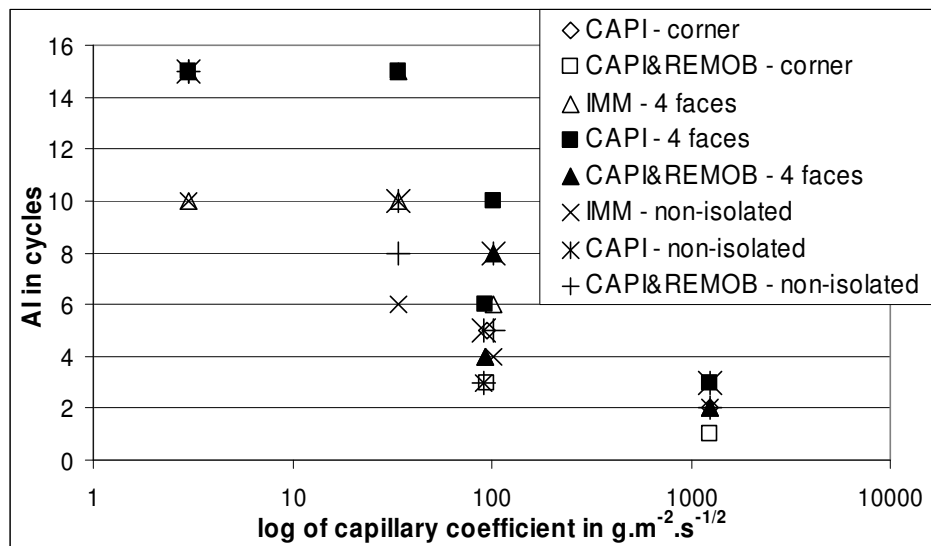


Figure ART4-1a. Correlation between alteration indicator and the log of the capillary coefficient.

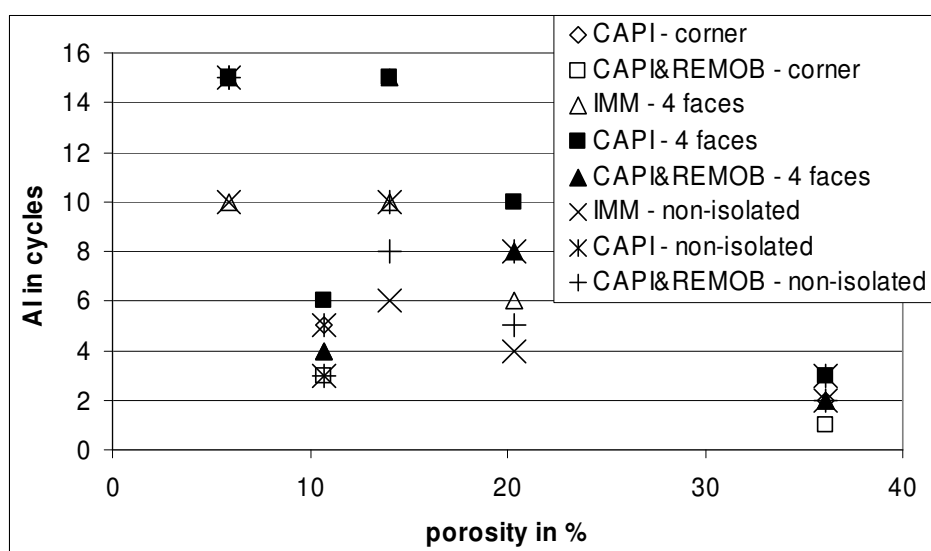


Figure ART4-1b. Correlation between alteration indicator and porosity.

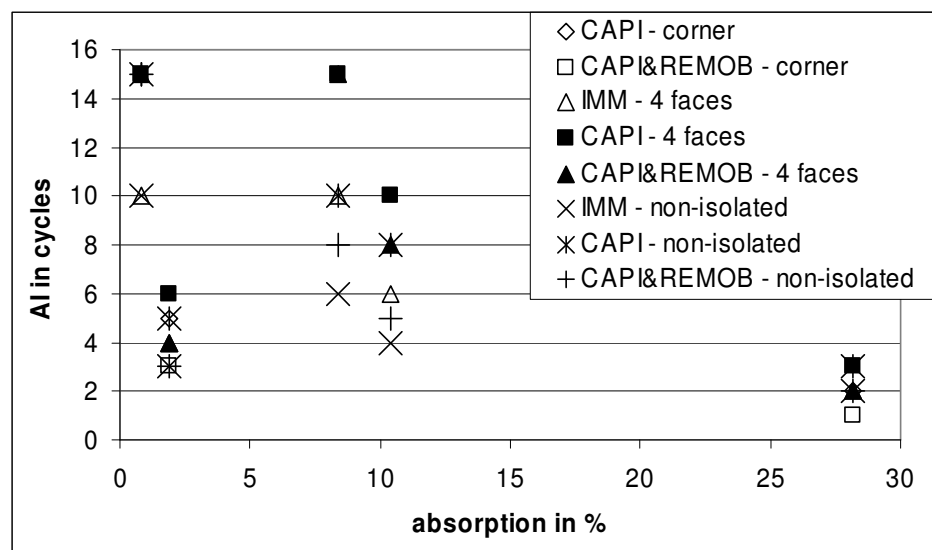


Figure ART4-1c. Correlation between alteration indicator and absorption at atmospheric pressure.



Figure ART4-2. 7x7x7 cm³ sample with the four lower corners damaged (SF, capillary imbibition & remobilisation after 7 cycles).

2.4. Capillary imbibition and remobilisation (CAPI&REMOB)

The aim of this experiment is to illustrate the fact that supersaturation is a major process in the stress from crystallization of salt. The damages occur faster in this case than with only capillary imbibition (Figs. ART4-3, ART4-4a, b), which means that higher stresses are induced earlier.

Comparing both tests, we can notice that the first signs of decay appear approximately for the same proportional weight increase, i.e. with the same proportion of salt in the sample (Figs. ART4-5a, b). This suggests, for a given stone, that the amount of salt supplied by capillary imbibition necessary to imply decay is roughly constant in the conditions of our experiments.

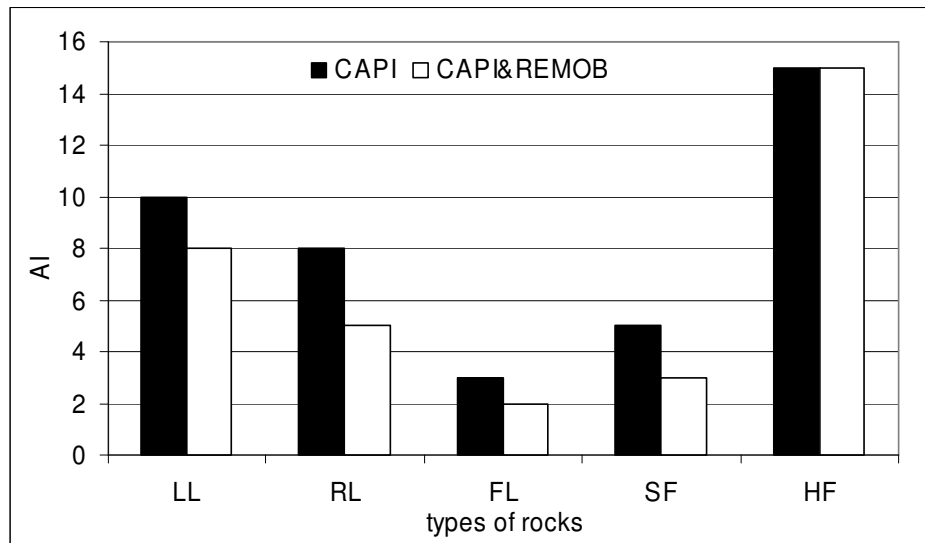


Figure ART4-3. Capillary imbibition experiment vs capillary imbibition and remobilisation for the five stones.



Figure ART4-4a. Picture of a $7 \times 7 \times 7$ cm 3 sample of FL after 6 cycles of capillary imbibition.



Figure ART4-4b. Picture of a $7 \times 7 \times 7$ cm 3 sample of FL after 6 cycles of capillary imbibition & remobilisation.

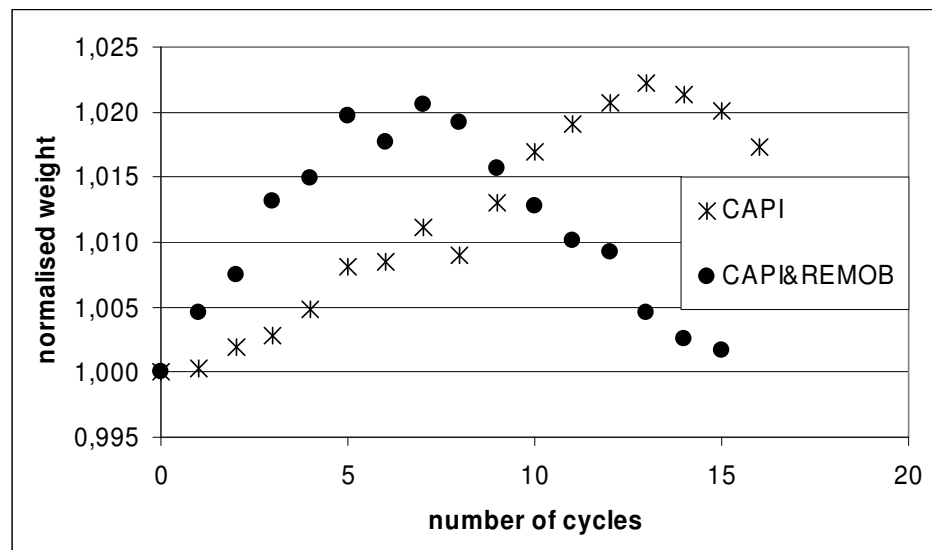


Figure ART4-5a. Evolution of samples weight during capillary imbibition and capillary imbibition & remobilisation for RL (non-isolated samples).

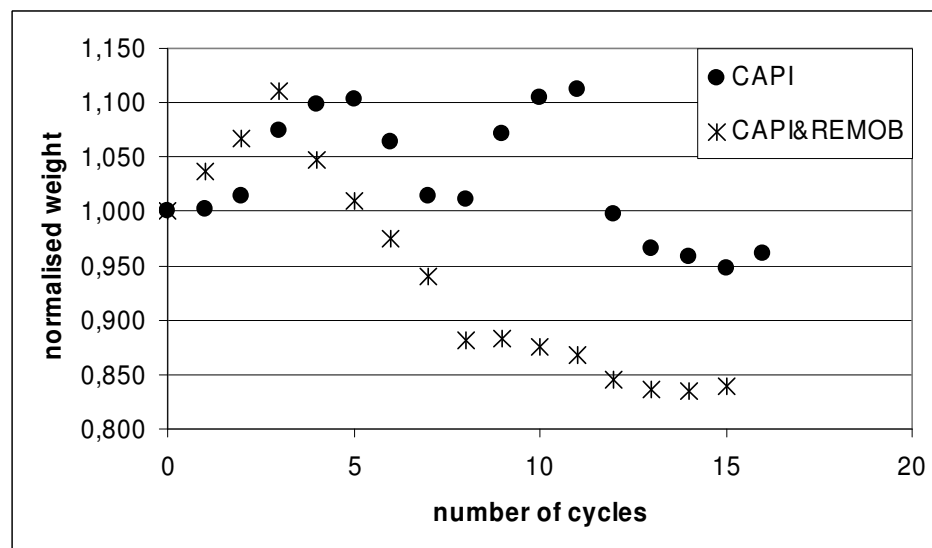


Figure ART4-5b. Evolution of samples weight during capillary imbibition and capillary imbibition & remobilisation for FL (non-isolated samples).

2.5. Consistency of the remobilisation test (REMOB)

In the remobilisation experiment with non-isolated samples, the weight is roughly constant and no damage is visible during the entire experiment (Fig. ART4-6). The weight only decreases for stones with massive efflorescences: this decrease is due to sample manipulations during the cycles. Assuming that the salt quantity is constant in the samples during the cycles, and that the samples are totally dried before weighing, this constant weight means that there is no loss of material during this test.

This means that the water has remobilized the salt in the porous network without involving high enough stresses to damage the sample. It suggests that no damage has been induced by the only presence of salts at the beginning. This is the illustration of the fact that the simple dissolution of thenardite in the solution cannot imply supersaturation with respect to mirabilite, according to the commonly admitted models (Benavente et al. 1999, Rodriguez-Navarro et al. 2000, Flatt 2002).

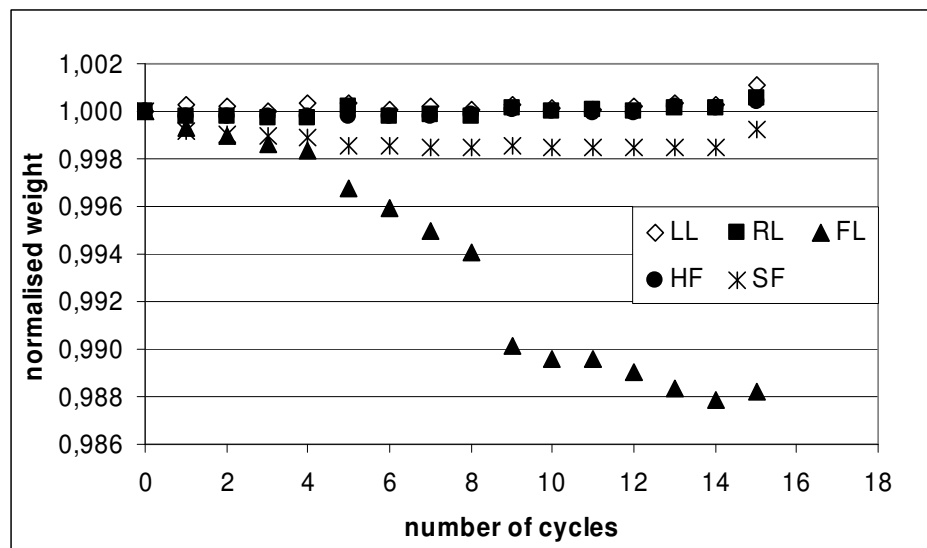


Figure ART4-6. Percentage of initial weight vs number of cycles of remobilisation test on isolated samples for the five stones.

2.6. Consistency of evaporation tests: the drying after seven cycles

Let us focus on the remobilisation test with 4 faces isolated. With the new results from the experiment above, we can assume that the weight increase is only due to the water trapped in the porous network which cannot evaporate. This raise stops as soon as the zones of the porous network where water cannot evaporate (in the conditions of the experiment) are totally filled. Drying the samples after seven cycles tends to prove it: when the sample is totally dry, its weight becomes approximately the same as at the start of the experiment (Fig. ART4-7).

The same behaviour is observed when the sample is totally dried until constant weight in the case of the capillary imbibition test (Figs. ART4-8a, b). Just after the drying, at the 8th cycle, the isolated and non-isolated samples show the same relative weight increase. This means that the difference between the two weight curves comes from the water which cannot evaporate inside the isolated samples during the 16 hours at $105\pm 5^\circ\text{C}$, and that this difference of evaporation has no influence on the samples salt uptake. Hence, the variation in the decay comes from the difference in evaporation pathways of the solution trapped in the pores, since salt supply and mechanical strength are the same for both samples.

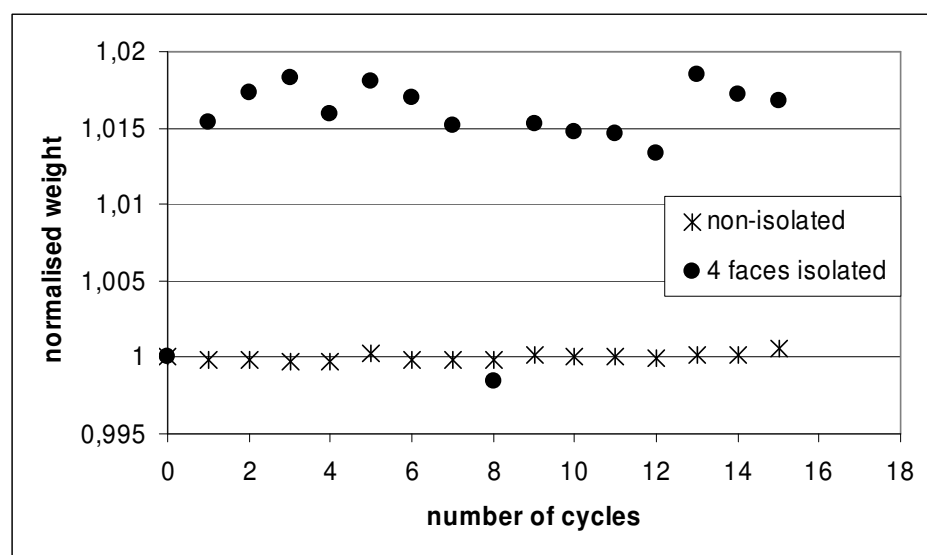


Figure ART4-7. Percentage of weight variation vs number of cycle - remobilisation experiment for RL.

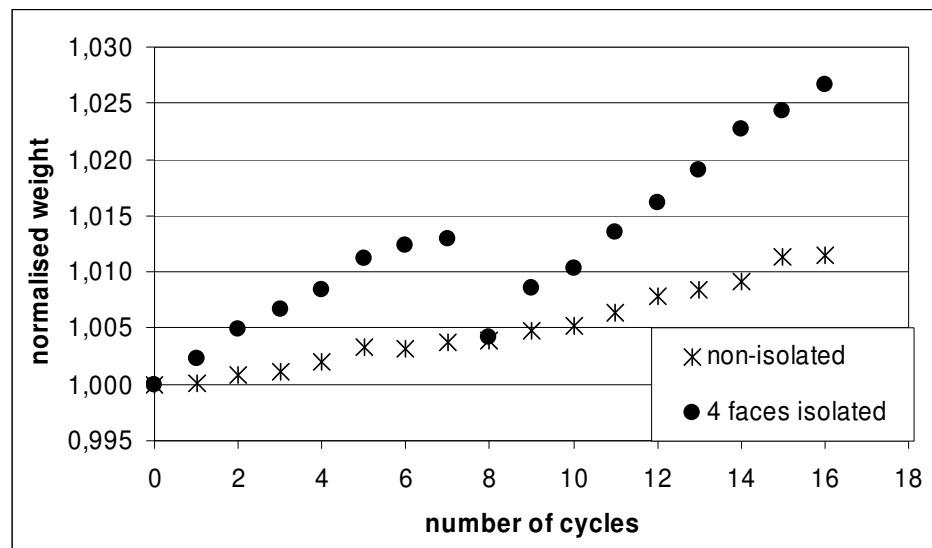


Figure ART4-8a. Capillary imbibition with non-isolated and 4 faces isolated samples for LL.

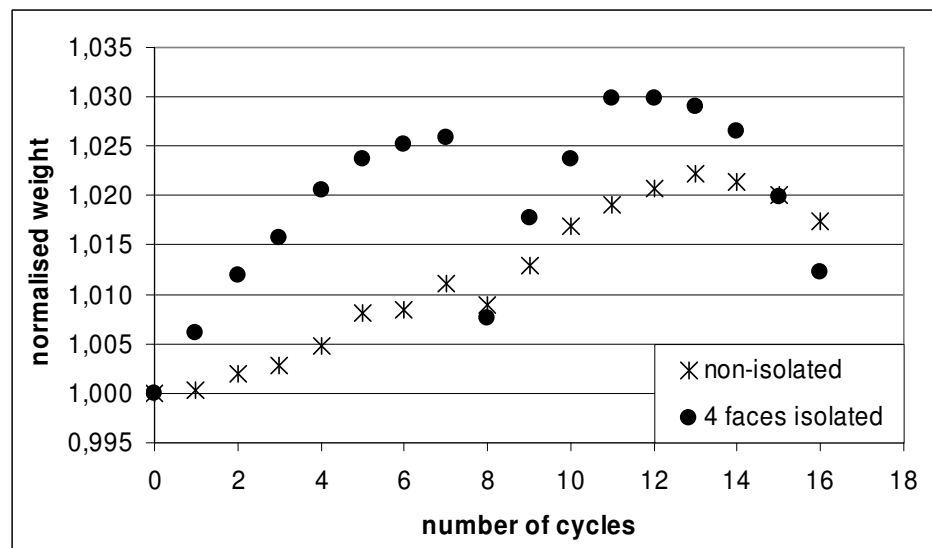


Figure ART4-8b. Capillary imbibition with non-isolated and 4 faces isolated samples for RL.

2.7. *Influence of the isolation of some faces on the weight loss*

In order to quantify the importance of the evaporation process as suggested above, tests were performed using samples with three or four of their faces isolated by an aluminium film. We notice that for each test, the more faces are subjected to evaporation, the greater the decay of the sample (Table ART4-2, Figs. ART4-9a, b, c). But there is a contradiction with our observations in the capillary tests. We noticed that the samples were more damaged in the zones that were immersed during the capillary imbibition. If we consider that this statement is true in every situation, the zones of the samples which are always filled with mirabilite-saturated solution due to lack of evaporation should be also damaged. But on the opposite, these zones, which are located close to the isolated faces, are totally intact. It shows that total immersion is not always destructive, only in the cases where evaporation is possible.

This confirms that in addition to capillary imbibition, evaporation is another important process governing salt decay as suggested in the literature (Goudie & Viles 1997, Rodriguez-Navarro & Doehne 1999, Rodriguez-Navarro et al. 2000).



Figure ART4-9a. Picture of a $7 \times 7 \times 7$ cm 3 non-isolated sample of FL after cycle 12.



Figure ART4-9b. Picture of a $7 \times 7 \times 7$ cm 3 sample of FL with 3 faces isolated after cycle 12.



Figure ART4-9c. Picture of a $7 \times 7 \times 7$ cm 3 sample of FL with 4 faces isolated after cycle 12.

Conclusion

The capillary coefficient as measured in the EN 1925 is the experimental parameter which is the most relevant to estimate stone decay by crystallization of salts regarding the characteristics of the porous network. It quantifies the possibility of the water to flow into the stone and to enable the mechanism of crystallization-dissolution which is harmful for the porous stones.

The remobilisation test suggests that no stress related to salt crystallization can be transmitted to the samples if no salt is provided by the solution, even if the sample is already loaded with salt.

All the tests concerning the possibility of evaporation show that the easier the evaporation, the faster and the larger the decay. They also show a contradiction with phenomenon occurring on old masonries in the fact that the main damages happen in the immersed zones of the sample.

Even if the experiments presented in this study try to be as close as possible to the situation in buildings, their results are still representative of what happens in a laboratory. We can only assume that the difference in duration, temperature, RH and evaporation mechanisms does not imply drastic changes in the processes.

This study, which characterizes the important fluid properties which participate to the mechanism of salt decay, can be continued in several natural directions. One would be to quantify more precisely salt decay by using the dry weight loss indicator instead of AI. It would be also interesting to take into account the stone strength in order to fully understand what makes a stone sensitive to salt alteration, and eventually use these processes as a basis for a simple numerical model of experimental ageing of natural stone through crystallization of salt.

References

Benavente D, García del Cura MA, Bernabéu A and Ordóñez S (2001) Quantification of salt weathering in porous stones using an experimental continuous partial immersion method. *Engineering Geology* 59: 313-325.

Benavente D, García del Cura MA, Fort R and Ordóñez S (1999) Thermodynamic modelling of changes induced by salt pressure crystallisation in porous media of stone. *Journal of Crystal Growth* 204: 168-178.

Benavente D, García del Cura MA, García-Guinea J, Sánchez-Moral S and Ordóñez S (2004). Role of pore structure in salt crystallisation in unsaturated porous stone. *Journal of Crystal Growth* 260: 532-544.

Correns CW (1949) Growth and dissolution of crystals under linear pressure. *Discussions of the Faraday society* 5: 267-271.

EN 12370 (1999) Natural stone test methods – Determination of resistance to salt crystallisation. 1999-03.

EN 1925 (1999) Natural stone test methods – Determination of water absorption coefficient by capillarity. 1999-03.

Flatt RJ (2002) Salt damage in porous materials: how high supersaturations are generated. *Journal of Crystal Growth* 242: 435-454.

Goudie AS and Viles H (1997) Salt weathering hazard. Chapter 4, p91-122 Chichester: John Wiley & Sons.

La Iglesia A, González V, López-Acevedo V and Viedma C (1997) Salt crystallization in porous construction materials I Estimation of crystallization pressure. *Journal of Crystal Growth* 177: 111-118.

“Influence of capillary properties and evaporation on salt weathering of sedimentary rocks” 183

Angeli M, Bigas JP, Menéndez B, Hébert R and David C (2006)

Nicholson DT (2001) Pore properties as indicators of breakdown mechanisms in experimentally weathered limestones. *Earth surface processes and landforms* 26: 819-838.

Pitzer KS (1991) Ion-interaction approach: theory and data correlation. In K. S. Pitzer (ed.) *Activity coefficients in electrolyte solutions*. Boca Raton: CRC Press: chapter 3.

Rodriguez-Navarro C and Doehe E (1999) Salt weathering: influence of evaporation rate, supersaturation and crystallization pattern. *Earth Surface Processes and Landforms* 24: 191-209.

Rodriguez-Navarro C, Doehe E and Sebastian E (2000) How does sodium sulphate crystallize? Implications for the decay and testing of building materials. *Cement and Concrete research* 30: 1527-1534.

Scherer GW (1999) Crystallization in pores. *Cement and concrete Research* 29: 1347-1358.

Scherer GW (2004) Stress from crystallization of salt. *Cement and Concrete Research* 34: 1613-1624.

Steiger M (2005a) Crystal growth in porous materials – I: The crystallization pressure of large crystals. *Journal of Crystal Growth* 282: 455-469.

Steiger M (2005b) Crystal growth in porous materials – II: Influence of crystal size on the crystallization pressure. *Journal of Crystal Growth* 282: 470-481.

Vergès-Belmin V (2001) Altération des pierres mises en œuvre. In B. Schrefler & P. Delage (eds) *Géomécanique environnementale, risques naturels et patrimoine*. Paris: HERMES Science

2. Influence of temperature and salt content on the salt weathering of sedimentary rocks (GSL special publication)

Sodium sulphate is known to be a very damaging salt for masonries. Its particularity is to have two phases that are stable at room temperature. Both phases do not have the same impact on the stones: the dehydrate phase, thenardite, is almost harmless whilst the decahydrate phase, mirabilite, is very damaging (Tsui et al. 2003; Hébert et al. submitted). Temperature, which influences the presence of these two phases and their solubility, has thus a crucial influence on this type of weathering. In parallel of this study, the influence of the quantity of salt in the sample is also evaluated.

“Influence of temperature and salt content on the salt weathering of sedimentary rocks”

Matthieu Angeli¹, Ronan Hébert¹, Beatriz Menéndez¹, Christian David¹ and Jean-Philippe Bigas²

¹ Université de Cergy-Pontoise

Département de Sciences de la Terre et Environnement

5 mail Gay-Lussac, Neuville-sur-Oise

95031 Cergy-Pontoise CEDEX

France

² CHRYSO

7 rue de l'Europe

45300 Sermaises

France

Submitted to a special publication of the Geological Society of London on September 26th, 2007

Abstract

The aim of this study is to evaluate how the ambient temperature and the salt concentration affect the salt decay of sedimentary stones. Samples of a detritic limestone have suffered cycles of accelerated ageing at 5, 25 and 50°C at different brine concentration. The weight of the samples and of the pieces fallen off during the cycles has been monitored. The results show that the damage is more important at 5°C than at 25°C. The samples at 50°C were intact at the end of the experiment. Second, the size of the pieces fallen off the samples is significantly smaller for low temperatures: at 5°C, the decay produces a fine powder; at 25°C, the pieces fallen off are millimetric to centimetric: the mechanisms at stake are thus different at these two temperatures. The salt uptake seems quite similar for a given concentration whatever the temperature. The decay seems also to be of a different kind for each concentration. Crystallization seems to take place deeper inside the porous network of the stone when the concentration of salts in the brine is higher, that is to say when the brine viscosity is higher.

Résumé

Le but de cette étude est d'évaluer l'influence de la température et de la concentration en sels sur l'altération par le sel de roches sédimentaires. Des échantillons de calcaire détritique ont subi des cycles de dégradation accéléré par le sel à 5, 25 et 50°C à différentes concentrations de saumure. Le poids des échantillons ainsi que celui des pertes de matériel a été suivi au cours des cycles. Les résultats montrent que les dégâts sont plus importants à 5 qu'à 25°C. Les échantillons à 50°C étaient intacts à la fin de l'expérience. Ensuite, la taille des pertes de matériel est nettement inférieur pour les basses températures: à 5°C, les pertes consistent en une fine poudre; à 25°C, les morceaux sont millimétriques à centimétriques. La prise en sel apparaît similaire pour une concentration donnée, quelque soit la température. Les dégâts semblent aussi d'aspect différent pour chaque concentration. La cristallisation semble avoir lieu plus profondément dans le réseau poreux de la roche quand la concentration de la saumure augmente, donc quand la viscosité est plus élevée.

Introduction

Salts, and particularly sodium sulphate, are known to be among the most destructive agents in porous stones, concrete or brick weathering. The study of its crystallization mechanism is thus very important to fully understand its damaging effect on porous networks and, in the future, to find a way to prevent or limit it. Recent studies attribute the importance of sodium sulphate decay to the salt crystallization pressure of its decahydrate phase (mirabilite $\text{Na}_2\text{SO}_4 \cdot 10\text{H}_2\text{O}$), rather than of its anhydrous phase (thenardite Na_2SO_4) (Rodriguez-Navarro and Doehe 1999, Tsui et al 2003, Hébert et al submitted). Thermodynamical studies (Benavente et al. 1999; Flatt 2002; Scherer 2004; Steiger 2005a,b; Coussy 2006) as well as experimental studies (Goudie 1986, 1993; Rodriguez-Navarro and Doehe 1999; Angeli et al. 2007) show that damage depends on the quantity of salt in the stone as well as the characteristics of the porous network.

This study aims to understand what role the temperature and the salt content in the sample play in the decay of sedimentary stones, regarding the type and intensity of damage. For this, accelerated ageing tests are performed on only one type of stone, a detritic limestone, and with only one salt, sodium sulphate, but in different thermodynamic conditions (temperature and salt concentration of the brine).

1. Materials and methods

1.1. Materials

Twelve cubic ($\sim 7 \times 7 \times 7 \text{ cm}^3$) samples of a lutetian limestone from the Parisian Basin commercially known as “Roche fine” have been used in this study. This rock has been chosen for several reasons: its detritic structure with unimodal porosity is much simpler to study than other bioconstructed or crystallized limestones; it has been demonstrated in previous tests (Angeli et al. 2006, 2007) that it is not very resistant to salt decay hence the tests are quite fast; it is homogeneous and very regular from one sample to the other, which allows a very good reproducibility of the tests; it has been widely used for construction in Paris in the past time (buildings and historical monuments); and it is one of the rocks imposed for restoration and construction in the protected areas of the “Île de France” region. It is a fine-grained

detrinitic limestone made of calcite (90%) and quartz (10%) with a high porosity (37.2%) and a very low tensile strength (1.5 MPa). Its pore distribution is unimodal which makes the study of its modification easier. Complete hydromechanic properties are given in table ART5-1.

Porosity (%)	37.2
Absorption (%)	75.9
Bulk density (g/cm ³)	1.7
Evaporation coefficient (g/m ² /s ^{1/2})	66.9
Capillary coefficient (g/m ² /s ^{1/2})	1106.1
Mean pore radius (μm)	12.004
P wave velocity (m/s)	2898
Tensile strength (MPa)	1.5

Table ART5-1. Hydromechanic properties of the “Roche Fine” (from Angel et al., 2007).

1.2. Methods

The twelve samples suffered accelerated ageing tests adapted from the European standard EN 12370. Those tests were run under three different ambient temperatures: 5°C, room temperature (RT ~ 25°C), and 50°C. It is important to notice that two ambient conditions are below the temperature limit of mirabilite stability (32.4°C), the last one being above which means that no mirabilite crystallization will occur for this experimental condition.

Three different concentrations of salt in solution have been used in this study: 5, 12 and 25% in weight. Until the end of the paper the concentration in % will be considered as concentration in % in weight. The tests have only been performed under six thermodynamics conditions: indeed the three following conditions (5°C/12%, 5°C/25% and 25°C/25%) are supersaturated with respect to mirabilite, i.e. that under these conditions a liquid solution does not exist. The six thermodynamic conditions tested here are represented as stars on the phase diagram (fig. ART5-1): 5%/5°C; 5%/RT; 5%/50°C; 12%/RT; 12%/50°C; 25%/50°C.

190 “*Influence of temperature and salt content on the salt weathering ...*”

Angel M, Hébert R, Menéndez B, David C and Bigas JP(submitted)

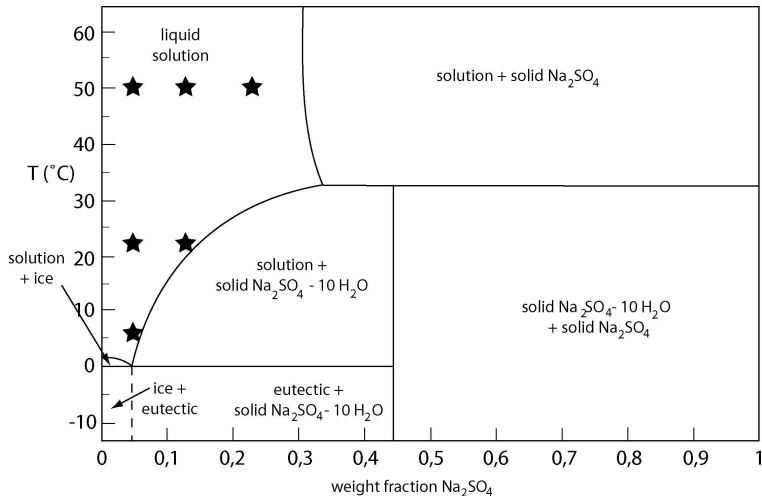


Figure ART5-1. Sodium sulphate phase diagram (Hougen et al. 1954). The black stars represent the six thermodynamic conditions studied.

These tests are composed of cycles which have a duration of 24 hours. The cycles are made of three different stages: imbibition at ambient temperature; drying; return to initial ambient temperature. Timing for each stage is modified from the EN 12370 (1999) standard about stone resistance to crystallization of salts in pores.

Let us describe in more details the three steps:

(i) 2 hours imbibition with a brine (concentration of Na_2SO_4 is fixed by the 6 thermodynamic conditions) is realized for the three different ambient temperature conditions. Note that temperatures of imbibition solution are the same as ambient temperatures, i.e. respectively 5°C, RT and 50°C. Samples soak in a container with 1 cm height of solution. The level of solution is maintained constant during all that stage. Imbibition solution has been prepared with sodium sulphate decahydrate and demineralised water. The cycles start at 16h in the afternoon, the weighing at the beginning of this step will be called 16h weighing..

(ii) Drying: All the samples are placed in a drying oven at 105°C for 16 hours. The weighing performed at the beginning of this step will be called the 18h weighing. This step ends at 10h in the morning

(iii) Return to initial ambient temperature, i.e. 6 hours of cooling from 105°C to respectively 5°C, RT and 50°C. The weighing performed at the beginning of this step is the 10h weighing.

Sixteen full cycles have been performed during which all the samples have been weighed three times per cycle (before imbibition, after imbibition, after drying). The wastes with size from approximately 0.5mm were collected and weighed every cycle after drying. The only wastes which were not collected consist in powder resulting from crumbling.

A cooled incubator is used for the 5°C ambient environment. 50°C ambient temperature is obtained using a drying oven and drying stage takes place in a drying oven. Temperature is set up with a precision of $\pm 0.1^\circ\text{C}$.

2. Results

2.1. General observations

The first thing to notice is that all the samples present a different decay from one thermodynamic condition to the other. Some pictures of each sample that are characteristic of the decay are presented in figure ART5-2. Future references to this figure will refer precisely to the experimental condition and the number of the cycle.

At 50°C, no damage has been noticed on none of the 6 samples, only harmless efflorescences on the sides of the samples (Fig. ART5-2; 50°C, cycle 15). At 5°C, the damage starts directly as soon as the samples contain salt, i.e. during the second cycle. After this cycle, few signs of very thin contour scaling appear (a few tenths of millimeters). During the third cycle, the thin contour scaling almost ends and is followed by crumbling. This crumbling is very regular throughout the cycles until the end of the test, and the particles lost form a very fine powder.

At RT, the decay processes are a little different. During the 5-6 first cycles, the samples are slowly damaged. Efflorescences are observed as well as a decay of the lower parts of the samples, those who are immersed during the tests. The efflorescences are unexpectedly more important on the sample saturated with the 5% brine, that is to say with the lowest salt concentration. But at this point no major difference is observed between the two concentrations of salts (5 and 12%). From approximately the 6th cycle, contour scaling

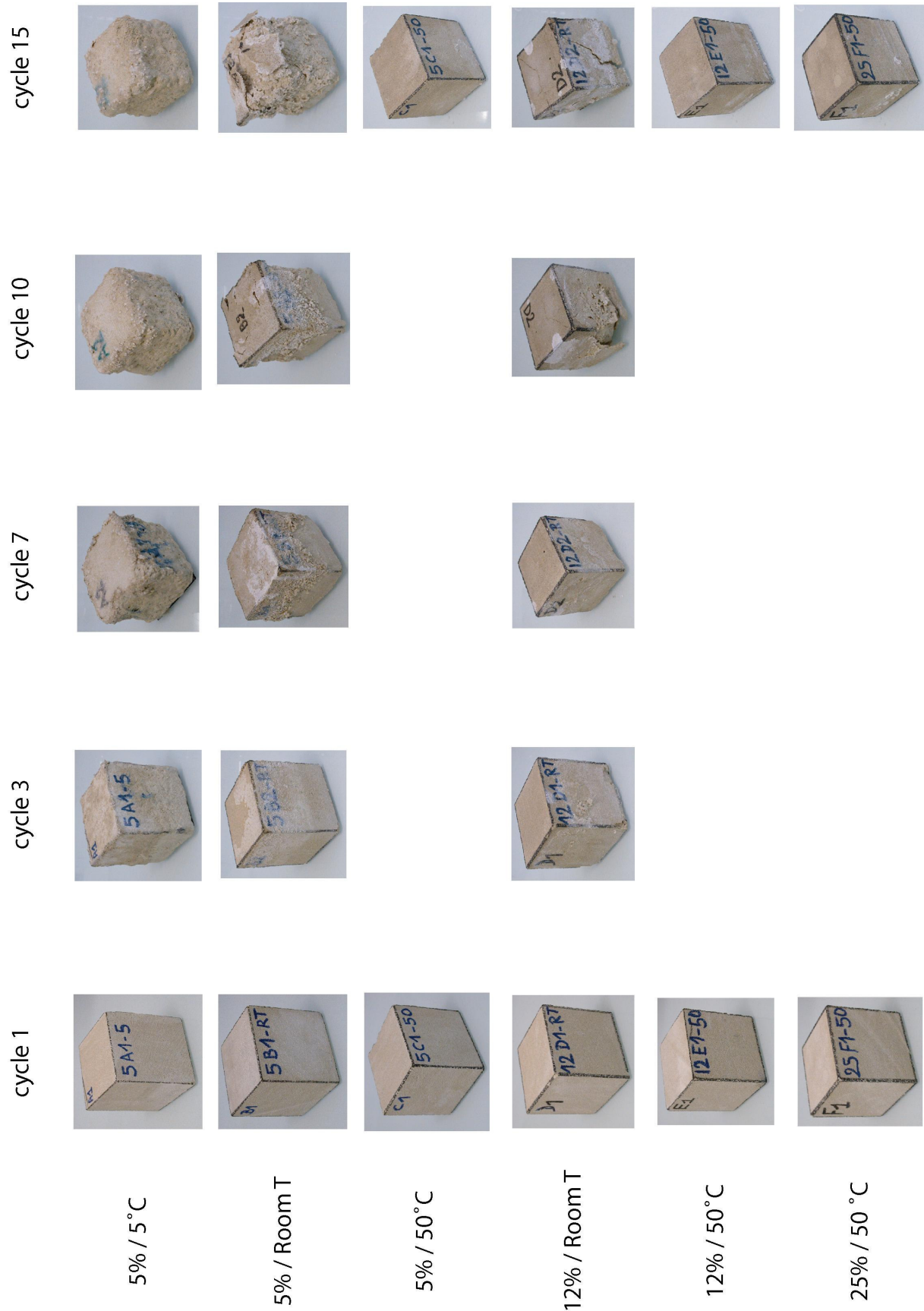


Figure ART5-2. Evolution of the samples in the six thermodynamic conditions during the 25 weathering cycles. The picture of the most characteristic sample is shown to illustrate decay.

“Influence of temperature and salt content on the salt weathering ...”

Angeli M, Hébert R, Menéndez B, David C and Bigas JP(submitted)

starts to appear on all samples, with the detached part thicker for 12% than for 5%. In fact, from this point on, the decay becomes different for the two concentrations. For 5% sodium sulfate, the contour scaling turns rapidly into crumbling from cycle 8, and crumbling becomes almost the only type of decay after cycle 11, although some residual scales are found on the top of the sample (Fig. ART5-2; 5%/RoomT). The wastes turn then into a very fine powder similar to the waste of the experiments at 5°C. On the other side, at 12% sodium sulfate, contour scaling continues to be the main type of decay, and the detached parts can be up to 1 cm thick. Thus, the decay in these conditions becomes highly dependent of the heterogeneities of the stone: contour scaling seems to be initiated by flaws in the sample as opposed to crumbling which seems to be regular on the whole surface exposed to evaporation. This is remarkable to notice that under very similar experimental conditions (same salt, same stone, same cycles, same temperature, same RH) two samples show two different types of decay: crumbling and contour scaling, and it seems to depend only on the quantity of salts contained in the brine, thus in the sample.

2.2. Weight monitoring

The samples have been weighed three times during the cycles: before imbibition, after imbibition and after drying. This corresponds, as mentionned earlier, to the beginning of each step of the cycle. This means that two of the weighing are performed on dry samples (before imbibition and after drying), and the other is performed on a fully saturated sample. Figure ART5-3 presents an example of the weight monitoring. Figure ART5-3a presents the full weight evolution of a sample (A1) during the 15 cycles. The parts that fell off the samples during imbibition have also been weighed.

The difference between the weights at 16h and 18h (before and after imbibition; cf. 1.2.) corresponds to the increase due to the water and salt supply minus the parts that fell off the sample. The difference between 18h and 10h (before and after drying in the oven; cf. 1.2.) corresponds to the loss of water and the loss of material (negligible during this stage). The difference between the weighing at 10h and 16h (before and after cooling at room temperature; cf. 1.2.) corresponds only to the change in environmental conditions, hence in the water equilibrium in the sample. These two weighing have been performed in order to evaluate the weight modification due to the cooling at room temperature (around 25°C) and

room RH (35-55%). The detailed weight variation during one cycle are presented on figure ART5-3b. Figure ART5-4 presents the weight evolution of the samples during the cycles. The noticeable curves that have been plotted are the evolution of normalized dry weight (Fig. ART5-4a), normalized collected wastes (Fig. ART5-4b), and the sum of normalized dry weight and normalized collected wastes (Fig. ART5-4c).

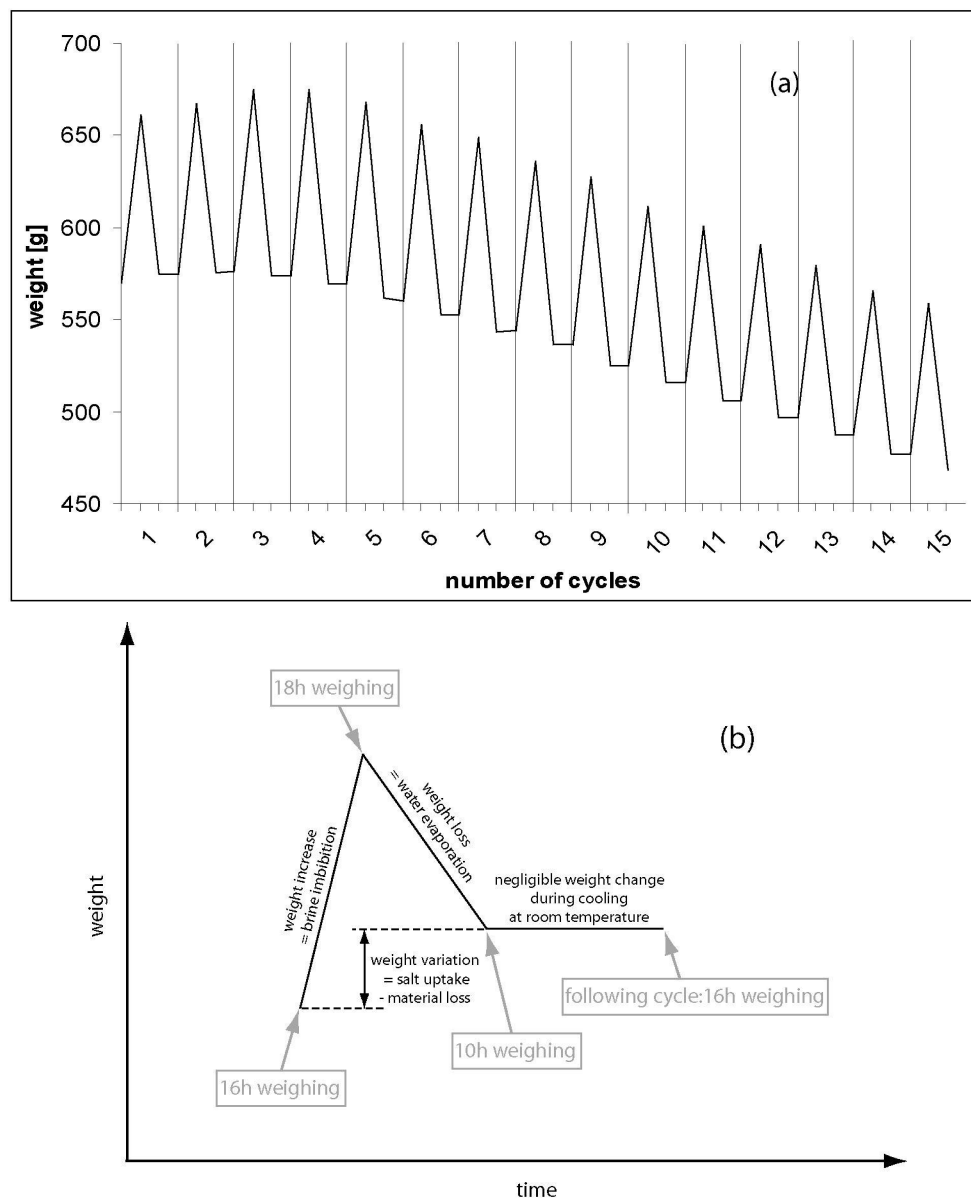


Figure ART5-3. (a) Example weighings performed during the weathering cycles for a sample at 5% / 5°C;

(b) Detail of the weighing performed during one cycle and of their experimental meaning.

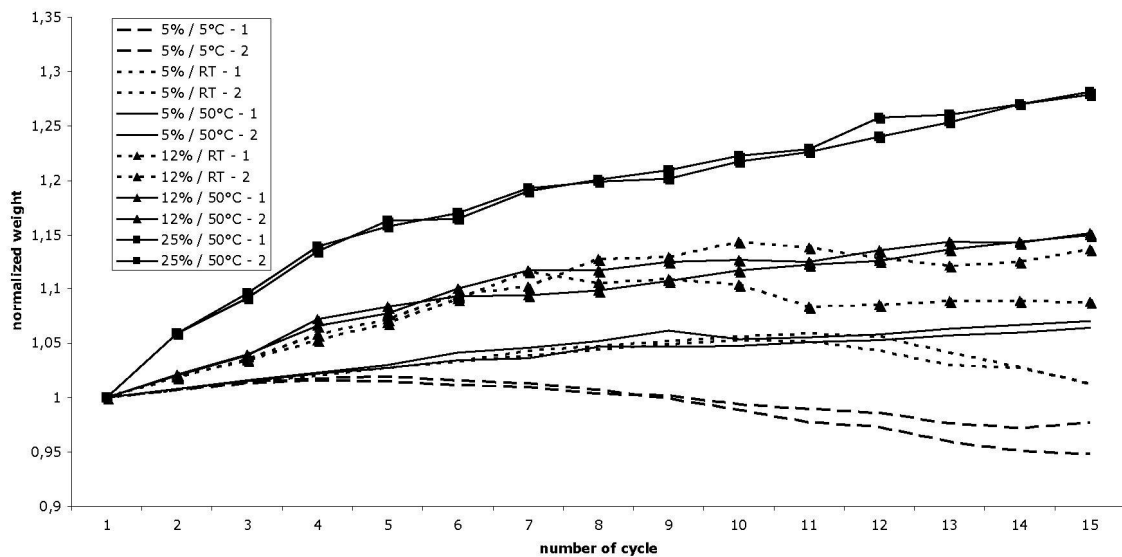


Figure ART5-4a. Weight evolution of the 12 samples in dry state.

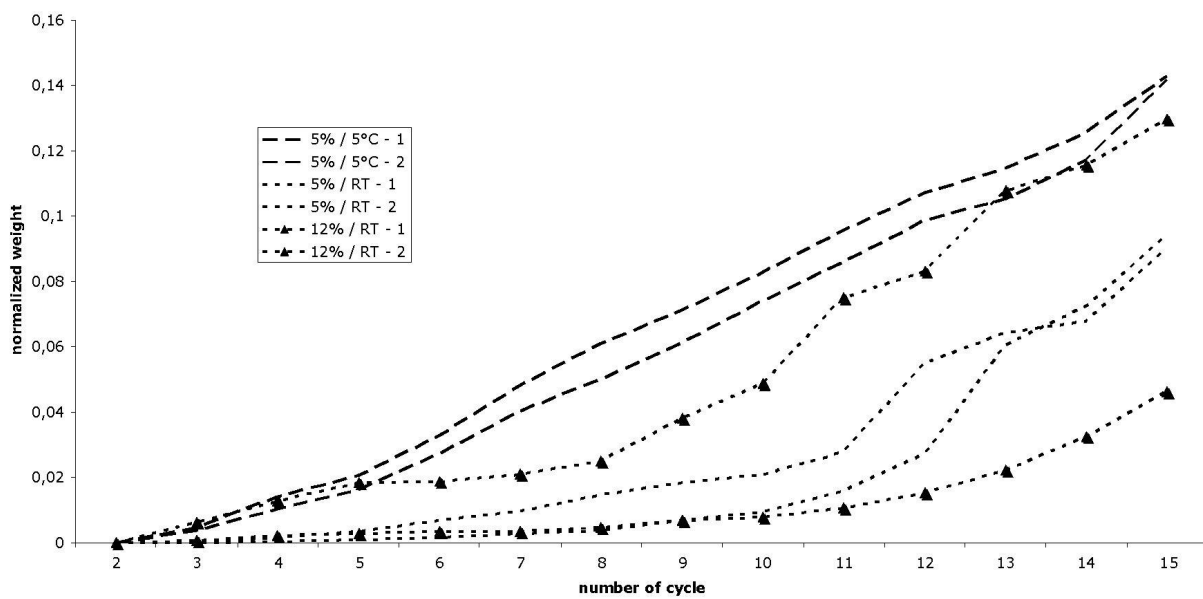


Figure ART5-4b. Weight evolution of the collected wastes. The wastes are collected only once per cycle, i.e. it is impossible to part the loss during imbibition from the loss during drying.

Since the samples at 50°C were not damaged at the end of the test, they have produced absolutely no damage.

Their weight evolution has thus not be reported on the figure.

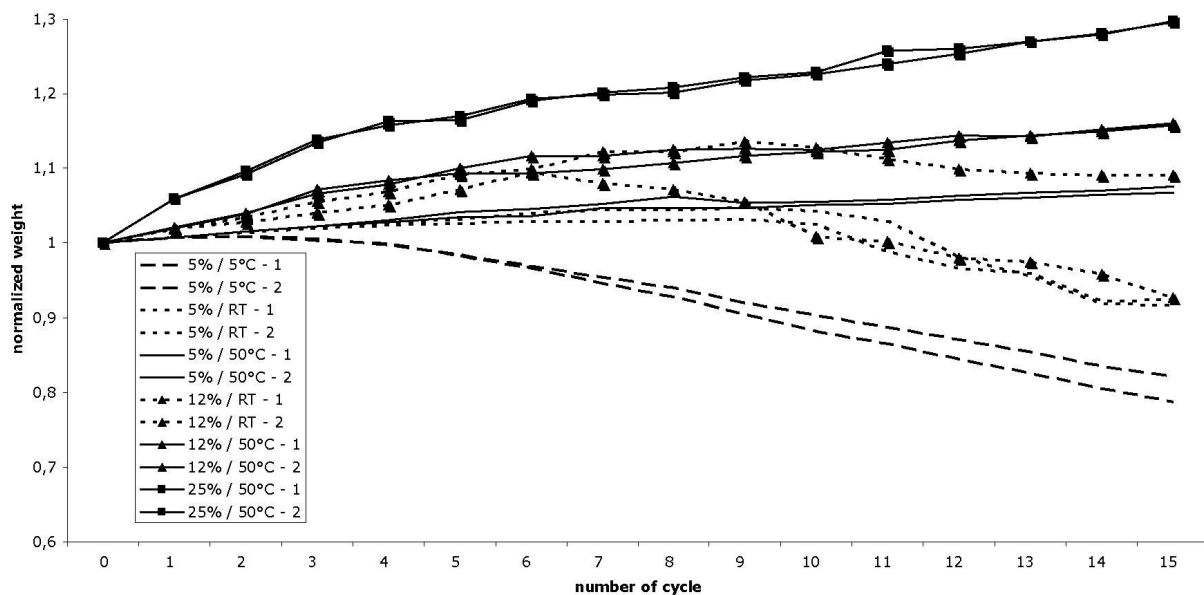


Figure ART5-4c. Weight evolution of the combined weight (dry state + collected wastes) of the 12 samples.

3. Discussion

3.1. Localization of crystallization

The most striking feature of this experiment is the decay pattern of the samples. A difference in the kinetics of damage, i.e. the apparition of the first signs of decay (alteration index AI, Angeli et al. 2007), and in the intensity was definitely suspected. Although these features have been observed during the experiments, the most unexpected feature is that the type of decay is very different from one thermodynamic condition to another. Complete values of AI and alteration velocity AV are presented in table ART5-2. Note that the alteration velocity is not exactly the same as the one defined by Angeli et al. (2007): it can normally only be calculated once the decay has become regular when salt uptake becomes negligible compared to material loss. In this experiment, it is not always the case, but the AV is used anyway to characterize the weight variations.

At 50°C, whatever the salt concentration, the samples do not suffer any damage from salt crystallization. The weight of the sample keeps increasing through the 15 cycles of the experimental ageing test. This weight increases linearly with brines at 5 and 12% sodium sulphate. For the samples filled with 25% sodium sulphate brine, the weight evolution shows

2 parts: first, until cycle 5, the weight gain is approximately constant at around 4%/cycle. Then, after cycle 5, the weight gain is still grossly linear but with a lower weight gain (approximately 1%/cycle): this is due to diffusion of ions between the saturated brine in the container and the supersaturated brine in the porous network.

		5%	12%	25%
5°C	AI	2		
	AV	2		
25°C	AI	4	3	
	AV	2	0	
50°C	AI	>15	>15	>15
	AV	-0.15	-0.8	-1

Table ART5-2. Alteration quantification of the samples in the 6 conditions (AI in cycles, AV in %/cycle).

Experimental ageing performed at 50°C by Tsui et al (2003) demonstrated that mirabilite was the damaging phase of sodium sulphate, and that crystallization of thenardite was almost not dangerous for the stones. This study clearly confirms these results, since none of the samples that suffered the test at 50°C has been damaged. But temperature is not only responsible for the presence or absence of damage. It also has an influence on the damage patterns.

At 5%/5°C, we observe almost only crumbling or granular disintegration, except for the very beginning where a very thin contour scaling seems to be initiated (cycle 2). At 5% / RT, the pattern is very similar: decay starts with very thin contour scaling and at one moment shifts to crumbling. The only difference is that this shift happens later at RT (cycle 6-7 instead of cycle 2), which is quite normal; it is now generally admitted that supersaturation of the solution is a mandatory condition to salt damage (Correns 1949). Sodium sulphate saturation is higher at 25°C (~18%) than at 5°C (~6%), thus more thenardite needs to be dissolved in the 5% Na₂SO₄ brine to reach supersaturation at RT than at 5°C. This supersaturation occurs then after more cycles of imbibition and drying (Flatt 2002; Coussy 2006). In both cases, the crystallization of sodium sulphate occurs thus close to the surface.

At 12% / RT, the decay of the samples starts after 3 cycles (table ART5-2). At first it is very similar to what happens with the 5% brine, that is to say a few efflorescences and small damage on the corners of the immersed parts. Contour scaling also occurs after cycle 6-

7, but this time with much thicker scales. These scales can have a thickness up to 1cm as observed on figure ART5-2 (12% / RT, cycles 10 and 15). This contour scaling suggests that the crystallization of sodium sulphate takes place deeper under the surface of the samples (Ioannou et al. 2005).

3.2. Weight monitoring

3.2.1. Dry samples

Figure ART5-4a presents the evolution of the dry sample weights as a function of the cycles. This evolution is normalized in order to be able to compare the weight gains as a function of the concentration of salt in the brines. An important thing to notice is that the experiments are reproducible: for each condition, the two samples have a very similar weight evolution. The only exception is the 12% / RT condition: we can clearly see a difference between the two samples from cycle 8. This difference is due to the type of decay which is at stake here: this moment corresponds to the start of a thick contour scaling. It is thus more dependent of the pre-existent heterogeneities of the samples. In this case the first sample lost a piece close to a corner at the bottom of the sample. Despite this variation, the alteration velocities of the two samples in this thermodynamic condition become similar from the tenth cycle.

The weight plots allow quantifying the observations made on the samples. It is clear on figure ART5-4a that the most damaged samples are those at 5°C, although the quantity of salt in them is lower than at the other temperatures due to a lower solubility of sodium sulphate in water at low temperature. The low temperature allows a fast supersaturation and thus a very fast apparition of decay. After 15 cycles, these samples have lost 20% of their initial weight, with a final AV of 2% per cycle. The samples in the 5% / RT conditions suffer also from crumbling from the 7th cycle: this crumbling starts later since supersaturation is reached faster at 5°C than at room temperature. The weight loss in this case becomes significant only after the 10th cycle. Once this crumbling has started, the AV becomes almost the same as in the 5% / 5°C conditions.

3.2.2. Collected wastes

Figure ART5-4b presents the weight of the wastes that are collected for each sample during the cycles. In order to compare the weight losses, these weights have been normalized to the weight of the initial clean sample. Let us remind here that all the wastes have been collected except the finest powder coming from the crumbling of the samples. An interesting thing to notice is that crumbling causes a regular loss of material at every cycle, as demonstrated by the weight of the material loss by the samples at 5% / 5°C. This is opposed to the material loss during contour scaling which is more random, as proved by the weight of the material lost by the 12% / RT samples.

3.2.3. Dry samples + collected wastes

Figure ART5-4c presents the monitoring of the dry weight plus the collected waste, which will be called later the combined waste for easier use. This plot is important since it allows us to have a precise idea of the evolution of the salt uptake. In fact this weight corresponds to the weight of the initial sample plus the weight of the salt it contains minus the fine powdery wastes that are not collected during the tests. Since there are no powdery waste (or very few) during the first four cycles, we can assume that the weight variation of this assembly during these cycles consists only in salt uptake. And this salt uptake appears to be dependant only of the concentration of the brine. In fact, whatever the temperature, the weight gain is the same for two samples filled with the same brine: 0.8%/cycle for 5% brines, 2%/cycle for the 12% brines and 4%/cycle for the 25% brines. This uptake is grossly proportional to the sodium sulphate weight fraction in the brine. This salt uptake is regular until the sample contains too much salt. From this moment on, the salt uptake is limited by ionic diffusion between the brine in the container and the brine in the pores. The 50°C weight evolution will later be used as a reference for salt uptake for each concentration. For a given condition, the difference between its weight variation and the weight variation at 50°C for the same salt concentration will give the amount of powdery wastes produced by weathering.

During the first 10 cycles, 5% / 5°C is the only condition where this combined weight decreases. It means that it is the only condition where powdery wastes are massively produced. This corresponds to the fact that it is the only condition that undergoes crumbling. Progressively, the combined weight of the 5% / RT samples starts to diminish with the same

AV as for 5% / 5°C. The AV is now approximately 0.5%/cycle for these conditions, instead of 2%/cycle if we consider only the dry sample (cf 3.2.1.). The proportion of powdery waste is thus approximately one fourth of total wastes in both cases.

However crumbling is not the only weathering pattern producing powdery waste. The diminution of the combined weight of the 12% / RT samples suggests that, although mostly producing scales, contour scaling produces also powdery wastes that have not been collected during the tests.

3.3. Variable decay at 25°C

An important fact is observed during the experiments at 25°C. The difference in the decay at 5% and 12.5% seems to be the crystallization depth. The contour scaling starting around cycle 8 is thicker at 12.5% than at 5%, this means that damage takes place deeper in the stone when the concentration of salt is higher.

Since in-depth crystallization of salts causes contour scaling (Ioannou et al. 2005), the thickness of the scales is constrained by the depth of crystallization of the salts. And this depth of crystallization depends on the evaporation speed of the brine during drying (Rijniers 2004): if drying is fast, crystallization occurs where evaporation takes place. Ruiz-Agudo et al. (2007) proved that for two brines with two different viscosities, salts will precipitate closer to the surface for the brine with the lower viscosity. They thus explained the different decay mechanisms caused by sodium and magnesium sulphate. The experimental conditions are different in Ruiz-Agudo et al. (2007) since the imbibition is continuous, but the mechanisms at stake are the same. In our experiment, supersaturation during imbibition will occur in the zone where thenardite is available for dissolution. These zones are the in-depth locations where crystallization takes place during drying. This viscosity variations can also explain why the scales are thicker at 12% / RT than at 5% / RT. The viscosity of a brine depends on the concentration of salt and of the temperature (Moore 1896). The higher concentration of salts at 12% / RT entails a higher viscosity of the brine than at 5%, and thus a deeper crystallization of the salts. This would explain the two decay mechanisms occurring in these two similar conditions.

The deceleration of drying can also be caused by a change in the thermal properties of the samples. Hebert et al. (submitted) have demonstrated that the thermal conductivity of a sample was reduced by the presence of salt in it. The sample is thus slower to heat up or cool down, and the temperature of the sample is more homogeneous from its core to its surface. Evaporation becomes slower, and thus crystallization takes place deeper in the stone. Nevertheless, the influence of this feature is certainly less important than viscosity since the variation of temperature is only of a few degrees.

Conclusion

Temperature is a decisive parameter that controls the amount and pattern of alteration in the case of sodium sulphate decay. Its importance has been previously assessed since mirabilite, which is the damaging phase, only exists under certain environmental conditions. A temperature above 32.4°C prevents the crystallization of mirabilite, and thus prevents damage (Tsui et al. 2003). This study assesses that the damage is higher at 5°C than at 25°C. The mechanisms are also different since crumbling occurs at 5°C, and contour scaling at 25°C. This implies a difference in the loss of materials during weathering: crumbling at 5°C causes the loss of fine particles composed of approximately 25% of fine powder; contour scaling at 25°C causes the loss of scales of several millimeter thickness, but also a small proportion of powder.

The concentration of salt in the brine also has an important influence on the decay. First the salt uptake in the sample is directly dependent of this concentration, whatever the temperature. Second, this concentration can directly affect the weathering pattern of samples. The concentration change can cause a switch from crumbling to contour scaling, as has been observed on the samples at room temperature. This can be explained by the variation of viscosity of the brine, which causes a variation in the crystallization depth of sodium sulphate.

References

- Angeli M, Bigas JP, Menéndez B, Hébert R, David C (2006) Influence of capillary properties and evaporation on salt weathering of sedimentary rocks – in “Heritage, Weathering and Conservation”, Edité par R. Fort, M. Alvarez de Buergo, M. Gomez-Heras & C. Vazquez-Calvo, Taylor & Francis/Balkema, AK Leiden, The Netherlands, 2006, 253-259.
- Angeli M., Bigas JP, Benavente D, Menéndez B, Hébert R. and David C. (2007) Salt crystallization in pores: quantification and estimation of damage. Environmental geology, 52:205-214.
- Correns CW (1949) Growth and dissolution of crystals under linear pressure. Discussions of the Faraday society 5: 267-271.
- Coussy O (2006) Deformation and stress from in-pore drying-induced crystallization of salt. Journal of the Mechanics and Physics of Solids 54:1517–1547.
- Flatt RJ (2002) Salt damage in porous materials: how high supersaturations are generated. Journal of Crystal Growth 242:435-454.
- Goudie AS (1986) Laboratoy simulation of “the wick effect” in salt weathering of rock. Earth surface processes and landfors 11, 275-285.
- Goudie AS (1993) Salt weathering simulation using a single-immersion technique. Earth surface processes and landforms 18, 369-376.
- Hébert R, Angeli M, Bigas JP and Benavente D (submitted) Thermal recording during experimental weathering of limestones: the role of imbibition on salt weathering and salt decay. Journal of crystal growth.
- Hougen OA, Watson KW and Ragatz RA (1954) Chemical Process Principles. Part I, 2nd ed., Wiley, New York.

Ioannou I, Hall C, Hoff WD, Pugsley VA and Jacques SDM (2005) Synchrotron radiation energy-dispersive X-ray analysis of salt distribution in Lépine limestone. *Analyst* 130:1006-1008.

Moore BE (1896) On the viscosity of certain salt solution. *The physical review* 5:312-334.

Rodriguez-Navarro C and Doehe E (1999) Salt weathering: influence of evaporation rate, supersaturation and crystallization pattern. *Earth Surface Processes and Landforms* 24: 191-209.

Ruiz-Agudo E, Mees F, Jacobs P and Rodriguez-Navarro C (2007) The role of saline solution properties on porous limestone salt weathering by magnesium and sodium sulfates. *Environmental geology* 52:269–281.

Scherer G (2004) Stress from crystallization of salt. *Cement and Concrete Research* 34:1613-1624.

Steiger M (2005a) Crystal growth in porous materials—I: the crystallization pressure of large crystals. *J Cryst Growth* 282:455–469.

Steiger M (2005b) Crystal growth in porous materials – II: Influence of crystal size on the crystallization pressure. *Journal of Crystal Growth* 282: 470-481.

Tsui N, Flatt RJ and Scherer GW (2003) Crystallization damage by sodium sulphate. *Journal of cultural heritage* 4: 109-115.

CONCLUSION AND PERSPECTIVES

Conclusion and perspectives

Conclusion

Salt damage by crystallization of salts in porous networks is a subject that deals with different fields of science. Although it has been widely studied, it is thus yet poorly understood. Several theories have been set up for soluble salts in general, but it has been clearly established that the decay mechanisms are different for each salt. The objective of this thesis was to try to specify this salt decay mechanism in the particular case of sodium sulphate crystallization, by studying the consequences and implications of salt decay on stones. In order to understand the influence of the stone properties on their durability, the study has been performed on nine sedimentary stones of various origins (two biotitic limestones, one detritic limestone, one lacustrine limestone, three quartz-rich sandstones and two layered shaly sandstones).

An experimental approach has been used to understand the sequence of sodium sulphate crystallization. This salt has two stable phases at room temperature, and the presence of these phases depends on the environmental conditions (temperature, relative humidity). It is important to constrain this crystallization sequence since it has been clearly demonstrated by Tsui et al. (2003) that one of these phases is almost harmless for the stone (the dehydrate phase, thenardite Na_2SO_4), whilst the other is very destructive (the decahydrate phase, mirabilite $\text{Na}_2\text{SO}_4 \cdot 10\text{H}_2\text{O}$). Thanks to a thermal monitoring of the weathering of samples at different temperature, a crystallization-dissolution sequence of mirabilite and thenardite during the experimental ageing cycles has been obtained. First the crystallization of mirabilite during imbibition has been highlighted: this crystallization is due to evaporative cooling. The temperature diminution during capillary imbibition of a saturated brine causes a diminution of sodium sulphate solubility, and thus crystallization of mirabilite in the sample. This explains why it has been generally observed that most damages occur during the imbibition phase of these accelerated ageing cycles. Different possible crystallization-dissolution sequences during drying are also highlighted, and they could give good constrain of the damage kinetics in the stone during drying, and moreover during the real-time exposure of actual buildings to sodium sulphate damage. This study has been completed by another round of experimental ageing tests with thermal monitoring on samples. Preliminary results of this experiment are presented in the perspectives exposed at the end of the conclusion.

Conclusion and perspectives

A new way of quantifying damage has also been proposed in this work. Generally damages are evaluated by the weight loss of a sample after a certain amount of cycles. During this study the durability of a stone has been evaluated dynamically through two parameters: the alteration index AI which corresponds to the cycle during which the first visible sign of damage appears; the alteration velocity AV which is the mean weight loss per cycle. These two parameters allow to be more precise in the evaluation of decay, by separating the first stages of alteration, which are mostly influenced by the shape of the sample or hydric properties, from the latest stages, which is the true behaviour of stones towards decay and depends on the intrinsic durability of the stone. These quantifiers have been simply estimated with intrinsic properties of the stones which are easy to measure, in order to have an indication of durability without waiting for weeks or even months of laboratory testing or in situ observations. Complementary tests have shown that the mechanical strength of the non-damaged inner parts of the samples is not affected by the weathering of external zones. Both tensile and uniaxial compressive strength remain constant throughout the test. The mechanical strength alone is thus neither a good estimator of the durability of the stone, nor of its degradation state.

The microstructural consequences of salt decay have also been studied with mercury porosimetry. It is observed that crystallization occurs in pores of almost any size, confirming the theoretic studies of crystallization during drying (Flatt 2002; Scherer 2004; Steiger 2005; Coussy 2006). It assesses also the importance of several features of the stones on salt decay, like the tortuosity or connectivity of the porous network, or the intragranular cracks that can be observed on thin sections.

Finally the influence of some parameters on the salt crystallization and on stone decay has been assessed. The evaporation possibilities have been set to conditions that are closer to the actual stones used in buildings, by isolating some faces. The results show that the damage only occur in the zones where evaporation is possible, that is to say where several cycles of imbibition and drying occur. The faces that have been isolated are totally clean after 15 cycles of imbibition and drying. The zones that are always wet do not suffer any major damage.

The influence of temperature is clearly established in the case of sodium sulphate decay: different decay patterns are obtained on the “roche fine” at different temperatures. We can notice crumbling at 5°C, contour scaling or crumbling at 25°C and no damage at 50°C.

Conclusion and perspectives

The concentration of salt in the brine also has an influence on decay: at 25°C decay can occur in two different patterns (contour scaling and crumbling) depending on the concentration of salts in the brine. This difference in the decay pattern due to temperature or salt concentration comes clearly from a modification of the fluid flow properties in the stone. This causes a difference in the sodium sulphate precipitation depth. Two hypotheses are proposed to explain this variation of crystallization depth: the variation of thermal conductivity caused by the presence of salts (Hébert et al. submitted); or the difference of viscosity of the brines at different concentrations (Ruiz-Agudo et al. 2007).

Perspectives

The results obtained leave a few questions unsolved. It could be interesting to study more precisely the changes in the pore structure at a smaller scale. For instance, the mechanism of damage at the scale of the pore has never been studied. A preliminary study has been initiated by an experiment that is described in the first part. The crystallization sequence of the couple mirabilite-thenardite is also unclear. In order to decipher it, another experiment has been recently set up: it consists in comparing the temperature evolution of samples undergoing imbibition of sodium sulphate to the temperature evolution of other samples undergoing imbibition of water or halite (which has only one stable phase at room temperature). Having a more precise knowledge of these processes could help to create new methods to cure the weathered stones or even to prevent their damage

1. Microstructural monitoring

The next step after having an image of the pores at the beginning and at the end of decay would be to try to have an image of the process during the decay. The starting point of this study is the same as for the macroscale study: experimental ageing based on the European standards. The difference lies in the shape of the sample used. In order to follow the weathering at the scale of the pores, the accelerated ageing tests had to be performed under a microscope in reflection mode. Thus a thin slice of "roche fine", the detritic limestone, has been stuck between two slices of glass. This allows having a 2D image of crystallization and prevents water from evaporating through the upper side of the sample. Fifteen cycles of imbibition and drying have been performed. The weight has been continuously monitored and pictures have been taken all along the accelerated ageing test on different spots of the thin

Conclusion and perspectives

section: recognizable fossils, corners... An acoustic emission probe has also been plugged on the thin section to follow the acoustic emission activity during imbibition and drying. Another probe has been plugged to an experimental reference consisting only of two slices of glass stuck together in the same way as before, where the same quantity of the same brine was injected at the same moment in the cycles. Figure CONCL-1 and CONCL-2 present the correlation between the weight evolution of the sample and the acoustic emissions for respectively cycle 6 (early stage with few damage) and cycle 11 (very damaging cycle). The preliminary results confirm that the evaporation kinetics are different depending on the weathering state, as observed previously (Angeli et al. 2006, submitted). The drying seems to be faster when the sample is more weathered and contains more salt. On figure CONCL-1 we can clearly notice that the recorded acoustic emissions of the sample are also very similar to those of the reference, suggesting that neither water flow nor salt phase changes are responsible for most of the acoustic emissions. On the pictures we can notice that after 6 cycles the centre of the sample is still free of salt, and that the stones contain mostly thenardite (white powder) at the beginning and the end of the cycle. On the intermediate picture we can see that both mirabilite and thenardite can be found in the sample at the same time, with thenardite in the inner parts of the sample and mirabilite in the outer parts.

Figure CONCL-2 on the opposite clearly shows a difference in the acoustic emissions of the sample and the reference. Between 3h30 and 5h30 after injection of the brine, a significant amount of acoustic emissions has been recorded on the sample. A correlation with the weight evolution suggests that this phenomenon happens at the same time than the transition between capillary and diffusive evaporation. This corresponds to the moment where the water continuity is broken in the sample, and when crystals start to grow in the pores. Nevertheless more experimental data would be necessary to correlate these acoustic emissions with cracking in the samples due to crystallization pressure.

Cycle 6

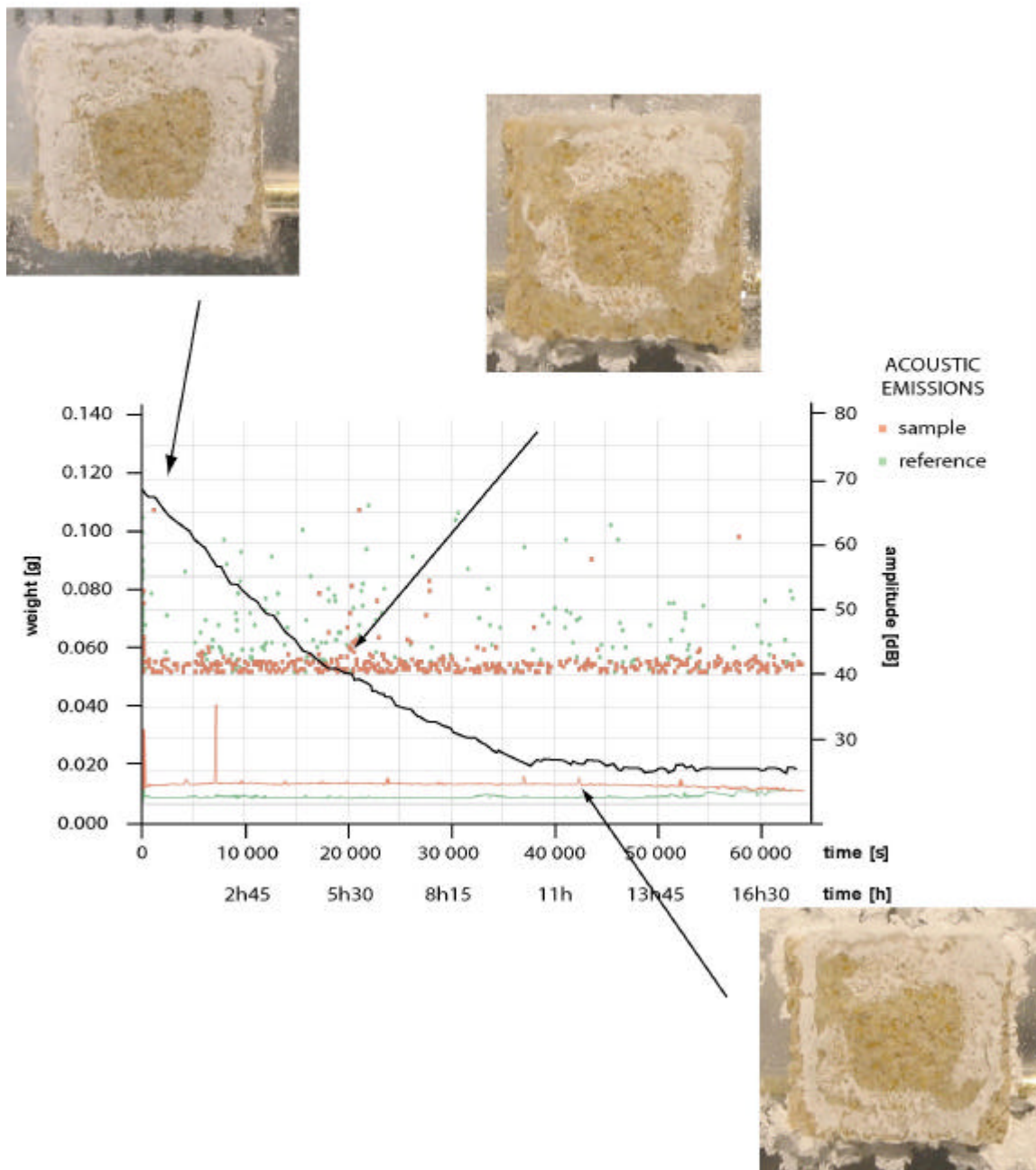


Figure CONCL-1. Monitoring of weight, acoustic emission and visual aspect of a sample of “roche fine” during cycle 6 of accelerated ageing test. The continuous red signals are due to the sound of the camera taking the picture.

Conclusion and perspectives

Cycle 11

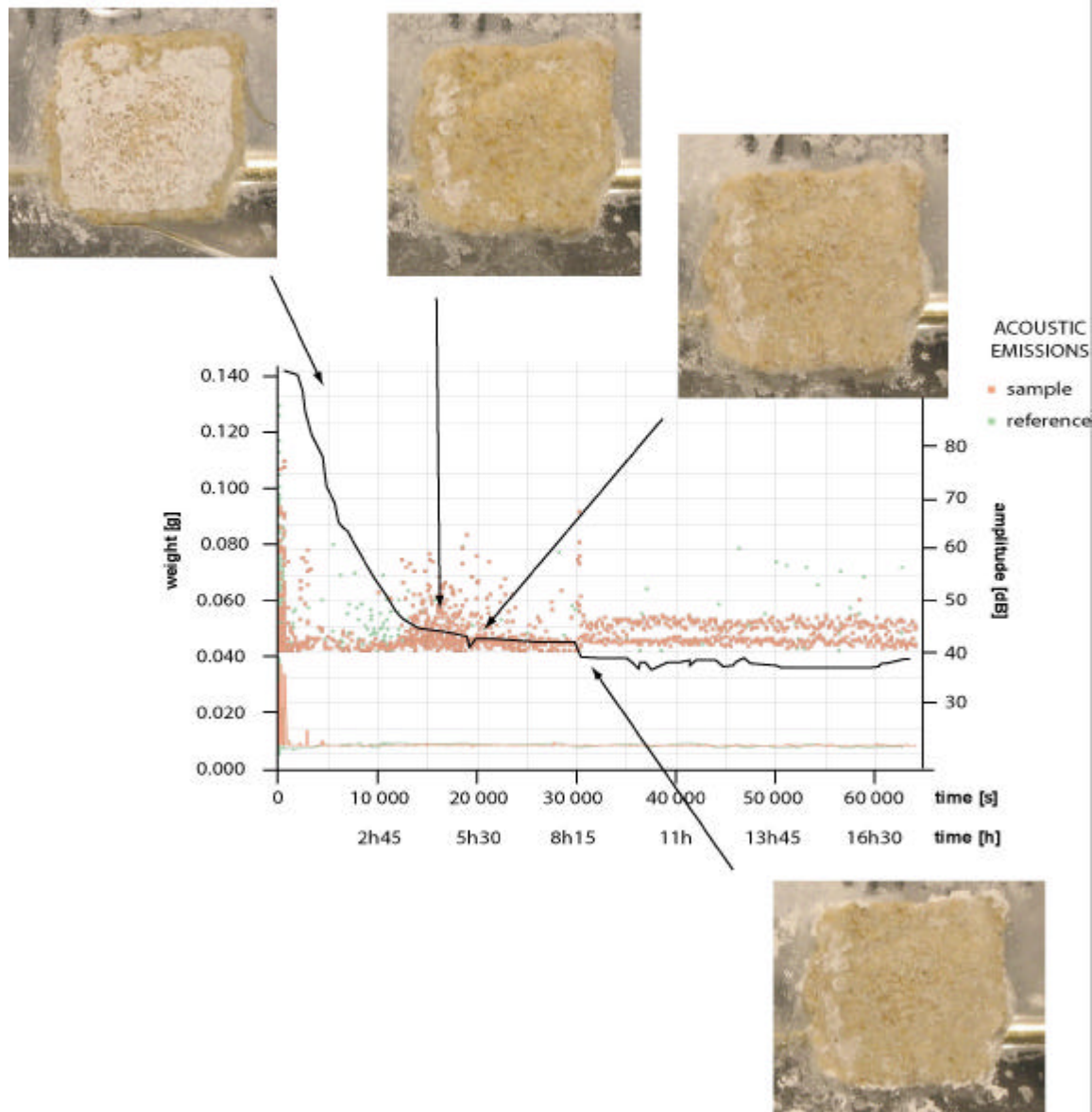


Figure CONCL-2. Monitoring of weight, acoustic emission and visual aspect of a sample of "roche fine" during cycle 6 of accelerated ageing test. The continuous red signals are due to the sound of the camera taking the picture.

2. Enhanced temperature experiment

In order to highlight the results of the first thermal monitoring experiment (Hébert et al. submitted), a second one has been performed. Several reference samples have been added to try to understand the origin of the numerous temperature variations observed during imbibition and drying. The thermal monitoring has been performed this time on samples at 5°C and room temperature RT, with only saturated brine for each condition. In fact the sample at room temperature could reach up to 29°C during the experiment. This can cause a few problems since 29°C is very close to the temperature limit of mirabilite stability as we will see later. The temperature of a reference dry sample has been monitored, as well as the temperature of a sample imbibed with only pure water. The comparison with a salt with only one stable phase at room temperature (halite NaCl) has been performed to understand the influence of the phase changes in the temperature variations. Figure CONCL-3 presents the evolution of temperature during drying at 120°C of the samples that underwent imbibition at 5°C and RT. In both figures five plots are drawn, they are called wit, eth, H₂O, NaCl and Na₂SO₄. Wit is a witness sample that is put in the oven without imbibition. Eth is a sample that has been filled by ethanol, and H₂O has been filled with deionised water. These samples act as references to locate the temperature variations that are not due to the presence of salt, and their temperature variations are presented in dashed lines. The two other samples are filled with respectively sodium chloride and sulphate during imbibition, and their temperature variations are presented in plain lines. Their main difference is that sodium chloride has only one stable phase at room temperature while sodium sulphate has two.

The temperatures variations of the references are similar at 5°C and RT for each sample: no inflexion point for the dry sample, an inflexion point around 75°C for ethanol, and two inflexion points at around 75°C and 95°C for deionised water. The origin of these sudden variations has not yet been identified. The variations at 5°C and RT for sodium chloride are very similar, with a first step at around 100°C and an inflexion point after 12h. Finally, the samples filled with sodium sulphate are the only presenting a difference between 5°C and RT. At 5°C, the samples are severely damaged and the temperature shows two inflexion points, at 80°C and 95°C. At RT, the sample has not been damaged, suggesting that the temperature was too high to allow the crystallization of mirabilite (Tsui et al. 2003; Hébert et al. submitted). The temperature evolution was very similar to the one of sodium chloride with only one inflexion point at 100°C. The exothermic processes that occurred at 80°C and 95°C

Conclusion and perspectives

for the 5°C samples could possibly be responsible for the decay of the stone, and eventually this could correspond to the crystallization of mirabilite. But these hypotheses need more analysis and experimental data to be confirmed.

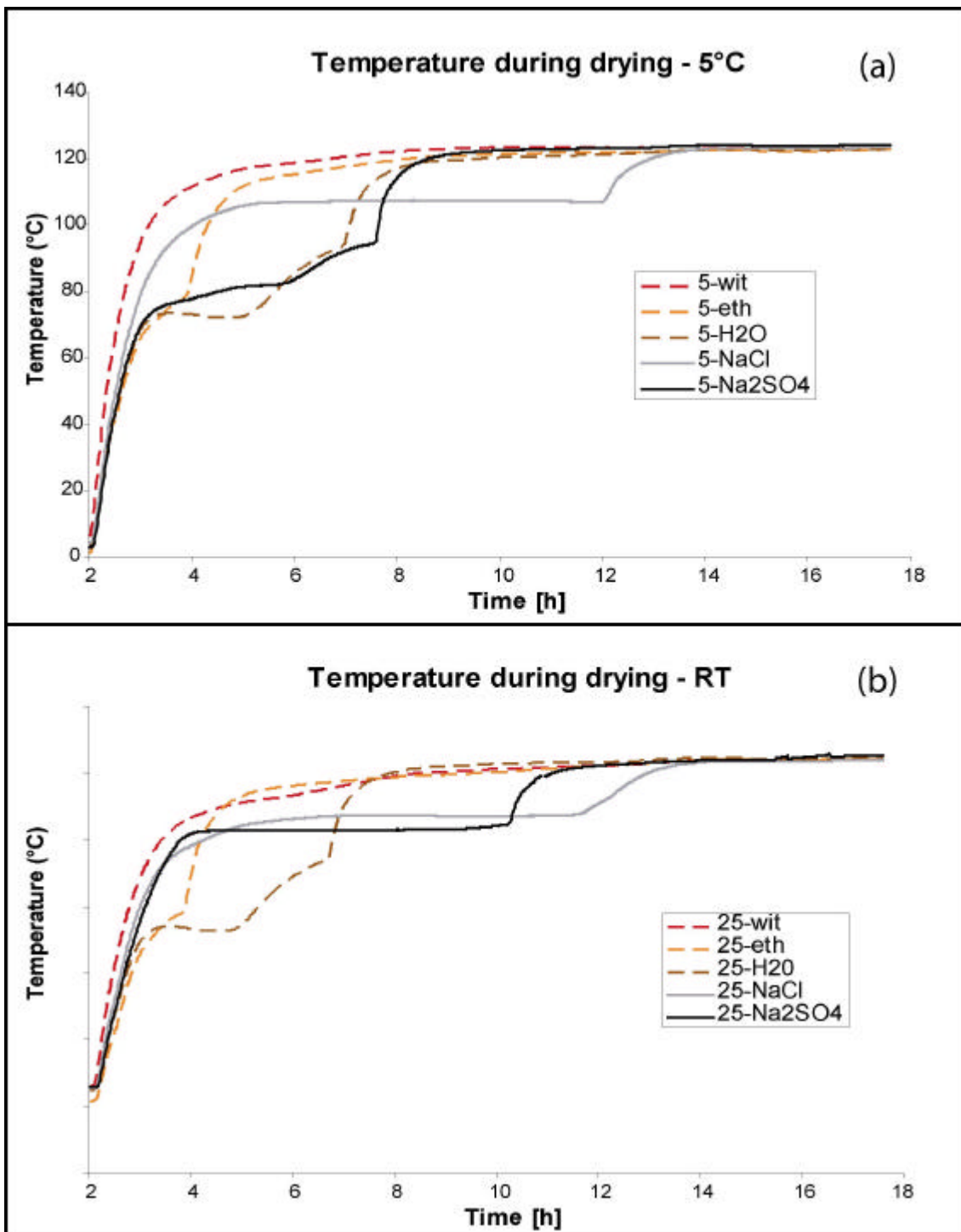


Figure CONCL-3. Temperature evolution of five samples of “roche fine” during the 120°C drying after no imbibition (wit), and imbibition of ethanol (eth), deionised water (H₂O), and brines saturated with sodium chloride (NaCl) and sodium sulphate (Na₂SO₄). The imbibition for the last four samples took place (a) at 5°C (b) at room temperature.

REFERENCES

References

References

References

Angeli M, Bigas JP, Menéndez B, Hébert R, David C (2006) *Influence of capillary properties and evaporation on salt weathering of sedimentary rocks* – in “Heritage, Weathering and Conservation”, Edité par R. Fort, M. Alvarez de Buergo, M. Gomez-Heras & C. Vazquez-Calvo, Taylor & Francis/Balkema, AK Leiden, The Netherlands, 2006, 253-259.

Angeli M., Bigas JP, Benavente D, Menéndez B, Hébert R. and David C. (2007) *Salt crystallization in pores: quantification and estimation of damage*. Environmental geology, 52:205-214.

Angeli M, Benavente D, Bigas JP, Menendez B, Hébert R and David C (in press) *Modification of the porous network by salt crystallization of experimentally weathered sedimentary stones*. Materials and structures.

Angeli M, Hébert R, Menéndez B, David C and Bigas JP (submitted) *Influence of temperature and salt content on the salt weathering of sedimentary rocks*. Geological Society of London special publication.

Ausset P, Bannery F, Del Monte M and Lefevre RA (1998) *Recording of pre-industrial atmospheric environment by ancient crusts on stone monuments*. Atmospheric environment 32:2859-2863.

Barsoum MW, Ganguly A and Hug G (2006) *Microstructural evidence of reconstructive limestone blocks in the great pyramids of Egypt*. Journal of the American Ceramic Society 89: 3788-3796.

Beaumont P (1968) *Salt weathering on the margin of the Great Kavir, Iran*. Geological society of America Bulletin 79: 1683-1684.

Beck K (2006) *Etude des propriétés hydriques et des mécanismes d'altération de pierres calcaires à forte porosité*. Thèse de doctorat, Université d'Orléans, 226p

References

- Beck K, Al-Mukhtar M, Rozenbaum O and Rautureau M (2003) *Characterization, water transfer properties and deterioration in tuffeau : building material in the Loire valley-France.* Building and Environment 38: 1151-1162.
- Becker GF and Day AL (1906) *The linear force of growing crystals.* Proceedings of the Washington Academy of Sciences 7:283-288.
- Becker G and Day AL (1916) *Note on the linear force of growing crystals.* The journal of Geology 24: 313-333.
- Benavente D, García del Cura MA, Fort R and Ordoñez S (1999) *Thermodynamic modelling of changes induced by salt pressure crystallization in porous media of stone.* Journal of Crystal Growth, 204:168-178.
- Benavente D, García del Cura MA, Bernabéu A and Ordóñez S (2001) *Quantification of salt weathering in porous stones using an experimental continuous partial immersion method.* Engineering Geology 59: 313-325.
- Benavente D, García del Cura MA, García-Guinea J, Sánchez-Moral S and Ordoñez S (2004a) *The role of pore structure in salt crystallisation in unsaturated porous stone.* Journal of Crystal Growth 260:532-544.
- Benavente D, Garcia del Cura MA, Fort R and Ordoñez S (2004b) *Durability of porous building stones from pore structure and strength.* Engineering Geology 74:113-127.
- Brunauer S, Emett PH and Teller E (1938) *Adsorption of gases in multimolecular layers.* Journal of the American chemical society 60: 309-318.
- Chatterji S and Jansen AD (1989) *Efflorescences and breakdown of building materials.* Nordic concrete research 8: 56-61.
- Correns CW (1926) *Über die Erklärung der sogenannten Kristallisationskraft.* Sitz Ber Preuss Akad Wiss, 81–88.

References

- Correns CW (1949) *Growth and dissolution of crystals under linear pressure*. Discussions of the Faraday society 5: 267-271.
- Correns CW and Steinborn W (1939) *Über die Erklärung der sogennante Kristallisationskraft*. Zeitschrift fur Kristallographie A101:117-135.
- Coussy O (2006) *Deformation and stress from in-pore drying-induced crystallization of salt*. Journal of the Mechanics and Physics of Solids 54:1517–1547.
- David C, Darot M and Jeanette D (1993) *Pore structures and transport properties of sandstone*. Transport in porous media 11: 161-177.
- Dei L, Mauro M, Baglioni P, Manganelli Del Fà C and Fratini F (1999) *Growth of Crystal Phases in Porous Media*. Langmuir, 15:8915-8922.
- Del Monte M and Lefevre RA (2001) *Particulate matter in the urban atmosphere*. In: Sciences and Technologies of the Materials and of the environment for the protection of Stained glass and Stone Monuments, European commission, Research report 14: 99-107.
- Dessandier D, Bromblet P and Mertz JD (2003) *Elaboration d'un indice de durabilité et compatibilité des pierres des monuments: essai de validation*. Comptes-rendus des rencontres de l'Association Universitaire du Génie Civil, La Rochelle : 157-158.
- De Thury H (1828) *Sur le procédé proposé par M. Brard pour reconnaître immédiatement que ne peuvent pas résister à la gelée, et que l'on désigne ordinairement par les noms de pierres gélives ou pierres gélisses*. Annales de chimie et de physique 38 :160-192.
- Dunning JD and Hulf W (1983) *The effects of aqueous chemical environments on crack and hydraulic fracture propagation and morphologies*. Journal of geophysical research 88, 6491-6499.
- EN 12370 (1999) *Natural stone test methods – Determination of resistance to salt crystallisation*. 1999-03.

References

- EN 12371 (2001) *Natural stone test methods – Determination of frost resistance*. 2001-10.
- EN 13755 (2003) *Natural stone test methods – Determination of water absorption at atmospheric pressure*. 2003-04.
- EN 14066 (2003) *Natural stone test methods – Determination of resistance to ageing by thermal shock*. 2003-04.
- EN 1925 (1999) *Natural stone test methods – Determination of water absorption coefficient by capillarity*. 1999-03.
- EN 1936 (1999) *Natural stone test methods – Determination of real density and apparent density and of total and open porosity*. 1999-03.
- Evans IS (1970) *Salt crystallization and rock weathering: a review*. Revue de geomorphologie dynamique 19: 155-177.
- Everett DM (1961) *The thermodynamics of frost damage to porous solids*. Transactions of the Faraday Society, 57:2205-2211.
- Fitzner B and Snethlage R (1982) *Über Zusammenhänge Zwischen Salzkristallisationsdruck und Porenradienverteilung*. GP Newsletter, 3:13-24.
- Fitzner B (1988) *Porosity properties of naturally or artificially weathered sandstones* – Proc VIth international Congr on Deterioration and Conservation of Stone, Torun, 12-14 Sept 1988, 236-245.
- Flatt RJ (2002) *Salt damage in porous materials: how high supersaturations are generated*. Journal of Crystal Growth 242:435-454.
- Flatt RJ, Steiger M and Scherer GW (2007) *A commented translation on the paper by CW Correns and W Steinborn on crystallization pressure*. Environmental Geology, 52:187-204.

References

- Fröhlich F and Schubnel HJ (2000) *Le lutétien, la pierre de Paris*. Booklet of the exposition « Le lutétien, la pierre de Paris » at the National Natural History Museum in Paris from Octobre to Decembre 2000.
- Genkinger S and Putnis A (2007) *Crystallization of sodium sulphate: supersaturation and metastable phases*. Environmental geology, 52:329-338.
- Gmelin L (1966) *Handbuch der anorganischen chemie*. Aufl. Natrium Erg.Bd. 3, Verlag Chemie, Weinheim.
- Good RJ, Mikhail RS (1981) *The contact angle in mercury intrusion porosimetry*. Powder Technol 29:53–62.
- Goudie AS (1986) *Laboratory simulation of “the wick effect” in salt weathering of rock*. Earth surface processes and landforms 11, 275-285.
- Goudie AS (1993) *Salt weathering simulation using a single-immersion technique*. Earth surface processes and landforms 18, 369-376.
- Goudie AS and Viles H (1997) *Salt weathering hazard*. Chapter 4, p91-122 Chichester: John Wiley & Sons.
- Hammecker C (1993) *Importance des transferts d'eau dans la dégradation des pierres en œuvre*, Ph.D. Thesis, University Louis Pasteur of Strasbourg, France.
- Hammecker C (1995) *The importance of the petrophysical properties and external factors in the stone decay of monuments*. Pageoph. 145:337-361.
- Hébert R, Angeli M, Bigas JP and Benavente D (submitted) *Thermal recording during experimental weathering of limestones: the role of imbibition on salt weathering and salt decay*. Journal of crystal growth.
- Herodotus (1972) *The histories* (translated by A. de Sélincourt). Harondsworth: Penguin books.

References

- Honeyborne DB and Harris PB (1958) *The structure of porous building stones and its relation to weathering behaviour* – in Everett D. H. and Stone F. S. (Eds), Proceedings 10th Symposium of the Colston Research Society, Butterworths Scientific Publications, London, 343-365.
- Hougen OA, Watson KW and Ragatz RA (1954) *Chemical Process Principles*. Part I, 2nd ed., Wiley, New York.
- Hrouda F (1982) *The effect of quartz on the magnetic anisotropy of quartzite*. Studia geophysica et geodaetica 30: 39-45.
- Hudson JA (1981) *Wave speeds and attenuation of elastic waves in material containing cracks* – Geophys. J. R. astr. Soc. – 64:133-150.
- Ioannou I, Hall C, Hoff WD, Pugsley VA and Jacques SDM (2005) *Synchrotron radiation energy-dispersive X-ray analysis of salt distribution in Lépine limestone*. Analyst 130:1006-1008.
- IUPAC (1972) *Manual of symbols and terminology for physicochemical quantities and units, appendix 2, definitions, terminology, and symbols in colloid and surface chemistry*. Part 1, Pure Appl. Chem. 31: 578–638.
- Jeanette D (1994) *structures de porosité, mecanismes de transfert des solutions et principales alérations des roches des monuments*, Lapierre dei monumenti in ambiente fisico et culturale, Centro universitario europeo per I beni culturali, ravello, pp94-97
- Jeffreys H. (1931) *Damping in bodily seismic waves*. Mon. Not. R. astr. Soc. Geophys. Suppl. – 3:318-323.
- Jouany C (1981) *Transfert d'eau par évaporation dans les milieux argileux*. Thèse de doctorat de l'Université Paul Sabatier, Toulouse. 102p.

References

- Kessler DW (1919) *Physical and chemical tests of the commercial marbles of the United States.* Technologic papers of the bureau standards 123, government printing office, Washington DC.
- Kracek FC (1928) *Int. Critical Tables* 3 (p. 371)
- La Iglesia A, González V, López-Acevedo V and Viedma C (1997) *Salt crystallization in porous construction materials I Estimation of crystallization pressure.* Journal of Crystal Growth 177: 111-118.
- Lavalle M (1853) *Recherches sur la formation lente des cristaux à la température ordinaire.* Compte Rendu de l Academie des Sciences 36: 493-495.
- Lefevre RA and Ausset P (2001) *Les effets de la pollution atmosphérique sur les matériaux du patrimoine bâti: la Pierre et le verre.* Pollution atmosphérique 172 : 571-588.
- Lo T-W, Coyner KB and Toksöz MN (1986) *Experimental determination of elastic anisotropy of Berea sandstones, Chicopee shale, and Chelmsford Granite.* Geophysics 51: 164-171.
- Lopez Arce P and Doehne E (2006) *Kinetics of sodium sulphate efflorescence as observed by humidity cycling with SEM* – in “Heritage, Weathering and Conservation”, Edité par R. Fort, M. Alvarez de Buergo, M. Gomez-Heras & C. Vazquez-Calvo, Taylor & Francis/Balkema, AK Leiden, The Netherlands, 2006, 285-291.
- Louis L (2003) *Anisotropies microstructurales composites dans les roches réservoir: conséquences sur les propriétés élastiques et relation à la déformation.* Thèse de l’Université Cergy-Pontoise, 240pp.
- Louis L, David C and Robion P (2003) *Comparison of the anisotropic behaviour of undeformed sandstones under dry and saturated conditions.* Tectonophysics 370: 193-212.
- Louis L, Robion P and David C (2004) *A single method for the inversion of anisotropic data sets with application to structural studies.* Journal of Structural Geology 26: 2065-2072.

References

- Louis L, David C, Metz V, Robion P, Menendez M and Kissel C (2005) *Microstructural control on the anisotropy of elastic properties in undeformed sandstones*. International Journal of Rock Mechanics and Mining Sciences 42:911-923.
- Malin MC (1974) *Salt weathering on Mars*. Journal of Geophysical Research 79: 3888-3894.
- Mc Greevy JP and Smith BJ (1984) *The possible role of clay mineral in salt weathering*. Catena 11: 1169-175.
- Mertz JD (1991) *Structures de porosité et propriétés de transport dans les grès*. Thèse de doctorat de l'Université Louis Pasteur, Starsbourg.
- Mod'd BK, Howarth RJ and Bland CH (1996) *Rapid prediction of buildong research establishment limestones durability class from porosity and saturation*. Quaterly journal of engineering geology 29: 285-297.
- Moore BE (1896) *On the viscosity of certain salt solution*. The physical review 5:312-334.
- Mottershead DN (1982) *Rapid weathering of greenschist by coastal salt spray, east Prawle, south Devon : a preliminary report*. Proceedings of the Ussher Society 5: 347-353.
- Morse JW and Arvidson RS (2002) *The dissolution kinetics of major sedimentary carbonate minerals*. Earth-science reviews 58:51-84.
- Nicholson DT (2001) *Pore properties as indicators of breakdown mechanisms in experimentally weathered limestones*. Earth Surface Processes and Landforms, 26:819–838.
- Nicholson DT and Nicholson FH (2000) *Physical deterioration of sedimentary rocks subjected to experimental freeze-thaw weathering*. Earth surface processes and landforms 25, 1295-1307.
- Ordoñez S, Fort R and Garcia del Cura MA (1997) *Pore size distribution and the durability of porous limestones*. Quaterly journal of engineering geology 30: 221-230.

References

- Partington JR (1961) *General and Inorganic Chemistry*, MacMillan & Co. Ltd., London.
- Pearse JF, Olivier TR and Newitt DM (1949) *The mechanisms of drying of solids: I. the forces giving rise to movement of water in granular beds during drying*, Tran Inst Chem Eng, London, 27:1-8.
- Pel L, Huinink HP, Kopinga K (2002) *Ion transport and crystallization in inorganic building materials as studied by nuclear magnetic resonance*. Appl Physics Letter 81:2893-2895.
- Pitzer, K. S. (1991) *Ion-interaction approach: theory and data correlation*. In K. S. Pitzer (ed.) Activity coefficients in electrolyte solutions. Boca Raton: CRC Press: chapter 3.
- Price CA (2000) *An Expert Chemical Model for Determining the Environmental Conditions Needed to Prevent Damage in Porous Materials*, Archetype Publications Ltd, London.
- Prick A (1995) *Dilatometrical behaviour of porous calcareous rock samples subjected to freeze-thaw cycles*. Catena 25: 7-20.
- Prebble MM (1967) *Cavernous weathering in the Taylor Dry Valley, Victoria Land, Antarctica*. Nature 216:1194-1195.
- Punuru AR, Chowdhury AN, Kulshreshtha NP and Gauri KL (1990) *Control of porosity on durability of limestones at the Great Sphinx, Egypt*. Environmental Geology and Water Sciences, 15:225-232.
- Remy JM (1993) *Influence de la structure du milieu poreux carbonaté sur les transferts d'eau et des changements de phase eau-glace. Application à la durabilité au gel de roches calcaires de Lorraine*. Thèse de doctorat de l institut national polytechnique de Lorraine.
- Robinson DA and Williams RBG (2000) *Experimental weathering of sandstone by combinations of salts*. Earth surface processes and landforms 25, 1309-1315.

References

- Rodriguez-Navarro C and Sebastian E (1996) *Role of particulate matter from vehicle exhaust on porous building stones (limestone) sulphation*. The Science of the Total Environment 187: 79-91.
- Rodriguez-Navarro C (1998) *Evidence of Honeycomb weathering on Mars*. Geophysical Research Letters 25:3249-3252.
- Rodriguez-Navarro C and Doehe E (1999) *Salt weathering: influence of evaporation rate, supersaturation and crystallization pattern*. Earth Surface Processes and Landforms 24: 191-209.
- Rodriguez-Navarro C, Doehe E and Sebastian E (2000) *How does sodium sulphate crystallize? Implications for the decay and testing of building materials*. Cement and Concrete research 30: 1527-1534.
- Rose DA (1963) *Water movement in porous materials – II: the separation of the components of water movement*. Br J Appl Phys 14: 491-496.
- Rousset Tournier B (2001) *Transferts par capillarité et évaporation dans les roches: rôles des structures poreuses*. Thèse de doctorat de l'université Louis Pasteur, Strasbourg, 204pp.
- Ruiz-Agudo E, Mees F, Jacobs P and Rodriguez-Navarro C (2007) *The role of saline solution properties on porous limestone salt weathering by magnesium and sodium sulfates*. Environmental geology 52:269–281.
- Russell SA (1927) *Stone preservation committee report. Appendix 1*. H.M. Stationary Office, London.
- Schaffer RJ (1932) *The weathering of natural building stones*. DSIR, Building Research Special Report 18, Stationery Office, London, 34 pp.
- Scherer G (1999) *Crystallization in pores*. Cement and Concrete Research 29:1347-1358.

References

- Scherer G (2004) *Stress from crystallization of salt*. Cement and Concrete Research 34:1613-1624.
- Steiger M (2005a) *Crystal growth in porous materials—I: the crystallization pressure of large crystals*. J Cryst Growth 282:455–469.
- Steiger M (2005b) *Crystal growth in porous materials – II: Influence of crystal size on the crystallization pressure*. Journal of Crystal Growth 282: 470-481.
- Sperling CHB and Cooke RU (1985) *Laboratory simulation of rock weathering by salt crystallization and hydration processes in hot, arid environment*. Earth Surface Processes and Landforms 10, 541-555.
- Sunagawa I (1981) *Characteristics of crystal growth in nature as seen from the morphology of mineral crystals*. Bulletin Mineralogie 104:81-87.
- Takarli M and Prince W (2006) *Etude expérimentale de l'endommagement thermique du granite*. Comptes-rendus des rencontres de l'Association Universitaire du Génie Civil, La grande Motte :157-158.
- Tarling D and Hrouda F (1993) *The magnetic anisotropy of rocks*. Chapman and Hall, London.
- Theoulakis P and Moropolou A (1997) *Microstructural and mechanical parameters determining the susceptibility of porous building stones to salt decay*. Construction and building materials 11:65-71.
- Thomachot C (2002) *Modification des propriétés pétrophysiques de grès soumis au gel ou recouverts d'encroûtement noirs vernissés*. Thèse de doctorat, Université Louis Pasteur, Strasbourg, 263p.
- Thomas WN (1938) *Experiments on the freezing if certain buildings materials*. Building research, technical paper n°17.

References

- Tiller WA (1991) *The science of crystallization: microscopic interfacial phenomena*, Cambridge University Press, Cambridge, 391pp.
- Tsui N, Flatt RJ and Scherer GW (2003) *Crystallization damage by sodium sulphate*. Journal of cultural heritage 4: 109-115.
- Turner E (1833) *Report on a lecture on the chemistry of geology*. London and Edinburgh Philosophical magazine, Journal of Science 3, 21.
- Vergès-Belmin V (2001) *Altération des pierres mises en œuvre*. In B. Schrefler & P. Delage (eds) Géomécanique environnementale, risques naturels et patrimoine. Paris: HERMES Science.
- Vickers BL and Thill RE (1969) *A new technique for preparing rock spheres*. Journal of Scientific Instrumentation 2: 901-902.
- Wellman HW and Wilson AT (1965) *Salt weathering, a neglected geological erosive agent in costal and arid environment*. Nature 205, 1097-1098.
- Wellman HW and Wilson AT (1968) *Salt weathering of fretting, in Fairbridge, RW. Eds, The encyclopedia of geomorphology*, Stroudsburg, Pennsylvania, 968-970.
- Weyl PK (1959) *Pressure solution and the force of crystallization – a phenomenological theory*. Journal of Geophysical Research 64: 2001-2025.
- Widhalm C, Tschegg E and Eppensteiner W. (1996) *Anisotropic thermal extension causes deformation of marble cladding*. Journal of performance of constructed facilities 10, 5-10.
- Williams RBG and Robinson DA (2001) *Experimental frost weathering of sandstone by various combination of salts*. Earth surface processes and landforms 26, 811-818.
- Winkler EM (1997) *Stone in Architecture* . Springer Verlag, Berlin, 313 pp.

References

Winkler EM and Singer PC (1972) *Crystallization of salt in stone and concrete*. Geological society of America bulletin 83: 3509-3514.

Zeisig A, Siegesmund S and Weiss T (2002) *Thermal expansion and its control on the durability of marbles*. Natural stone, Weathering Phenomena, Conservation strategies and case studies. Edited by: Siegesmund S., Weiss T and Vollbrecht A. Geological society of London, special publication 205, 65-80.

References

Multiscale study of stone decay by salt crystallization in porous networks

Abstract

Crystallization of soluble salts in porous networks is a major source of decay for natural stones. The objective of this thesis is to specify this salt decay mechanism in the particular case of sodium sulphate crystallization. The basis of this work is to follow the evolution of samples of nine sedimentary stones of various origins (two biotitic limestones, one detritic limestone, one lacustrine limestone, three quartz-rich sandstones and two layered shaly sandstones) during accelerated ageing tests. First, the mechanism of sodium sulfate crystallization is studied thanks to thermal monitoring of the samples. Different crystallization sequences are proposed to explain the decay during the cycles. Then a new way of quantifying salt decay in the long term is proposed, taking into account the hydromechanical properties of the stones. The importance of the microstructures on decay (porous network tortuosity or connectivity, intragrain cracks) is also assessed thanks to a mercury porosimetry study. Finally, the influence of the environmental conditions on decay is also evaluated: evaporation and temperature directs both the location and amplitude of salt decay.

Keywords

Stone decay; Salt crystallization; Sodium sulphate; Microstructures

Etude multiéchelle de la dégradation des roches par la cristallisation de sels dans les réseaux poreux

Résumé

La cristallisation de sels solubles dans les réseaux poreux est une source majeure de détérioration pour les pierres naturelles. L'objectif de cette thèse est de préciser ce mécanisme de détérioration par le sel dans le cas du sulfate de sodium. Le point de départ de cette étude est de suivre l'évolution d'échantillons de neuf roches sédimentaires d'origines différentes (deux calcaires biodétritiques, un calcaire détritique, un calcaire lacustre, trois grès riches en quartz et deux grès argileux lités) au cours des tests de dégradation accélérée. Tout d'abord, le mécanisme de cristallisation du sulfate de sodium est étudié grâce à un suivi thermique des échantillons. Différentes séquences de cristallisation sont proposées pour expliquer la détérioration au cours des cycles. Ensuite une nouvelle manière de quantifier l'altération à long terme par le sel est proposée, tenant compte des propriétés hydromécaniques des roches. L'importance des microstructures sur l'altération (connectivité et tortuosité du réseau poreux, fractures intra-grains) est aussi déterminée par une étude par porosimétrie au mercure. Enfin, l'influence des conditions environnementales sur l'altération est aussi évaluée : l'évaporation et la température influencent tous les deux à la fois la localisation mais aussi l'amplitude des dégâts causés par le sel.

Mots clés

Dégénération des roches ; Cristallisation de sels; Sulfate de sodium; Microstructures